NASA Contractor Report 198506

Analysis of New Composite Architectures

John D. Whitcomb
Texas A&M University
College Station, Texas

July 1996

Prepared for
Lewis Research Center
Under Grant NAG3–1270

National Aeronautics and
Space Administration

ANALYSIS OF NEW COMPOSITE ARCHITECTURES

(Final Report NAG3-1270)

John D. Whitcomb

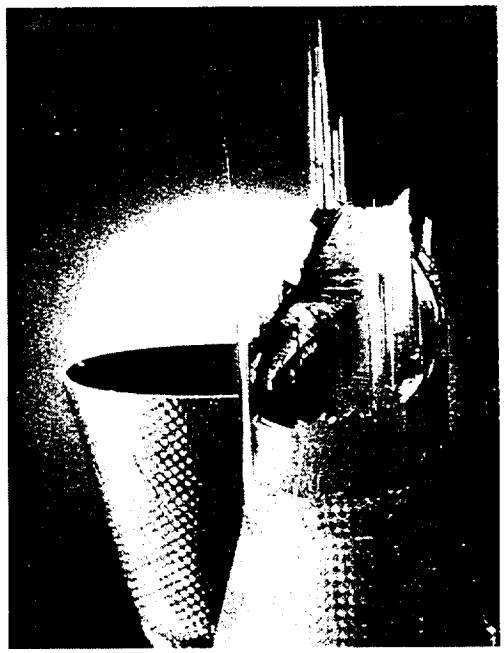

Center for Mechanics of Composites
Texas Engineering Experiment Station
The Texas A&M University System

Acknowledgement

This report documents the results and deliverables from NASA Grant NAG3-1270, which began May 1, 1991 and ended August 31, 1995. The technical monitor was Dr. Christos C. Chamis. Research results have also been published in journal articles and conference proceedings papers.

The research was leveraged by research on related projects: "Failure Analysis of 2-D and 3-D Woven Composites" (funded by NASA Langley Research Center), "Thermomechanical Analysis of Carbon-Carbon Composites" (funded by AFOSR) and "Development of Numerical Models for Carbon-Carbon Composites" (funded by AFOSR). The integration of the efforts in these projects expedited and complemented the research in these four grant efforts.

Abstract

Efficient and accurate specialty finite elements methods to analyze textile composites were developed and are described. Textile composites present unique challenges to the analyst because of the large, complex "microstructure". The geometry of the microstructure is difficult to model and it introduces unusual free surface effects. The size of the microstructure complicates the use of traditional homogenization methods. The methods developed constitute considerable progress in addressing the modeling difficulties. The details of the methods and attended results obtained therefrom, are described in the various chapters included in Part I of the report. Specific conclusions and computer codes generated are included in Part II of the report.

Table of Contents

PART I.

PART II.

Part I

Chapter: 1

Macro Finite Element for Analysis of Textile Composites

ABSTRACT: The analysis of textile composites is complicated by the complex microstructure. It is not practical to account for this microstructure directly using traditional finite elements. A new type of finite element was developed to efficiently account for microstructure within a single element. These new elements, which are referred to herein as macro elements, performed well in initial tests.

INTRODUCTION

TWO OF THE major obstacles to widespread use of laminated composites in high performance primary structures are the low strengths normal to the lamina and the labor intensive fabrication processes currently used. There has been considerable research aimed at developing tougher resin systems to enhance the through the thickness strength. Also, robotics are being developed to reduce the labor costs. Of course, there remains the question of whether laminated construction is the optimal form.

Several alternatives which are receiving attention are weaving, braiding, stitching, knitting, and combinations of these. These various forms are referred to as textile composites. Approximate analyses have been developed for predicting moduli, but these analyses are far too crude to predict details of the local stress field [1–3]. Very little detailed three-dimensional analysis has been performed. These studies, which used 3-D finite elements [4–8], required tedious modeling, many simplifying assumptions about the material microstructure, and only considered very simple loading. The computational challenge is obvious when one examines the schematic of a simple plain weave in Figure 1. The resin pockets are removed to show the fiber tow architecture. This tiny piece of material, which is only about .28 mm thick and about 1.4 mm wide, is in fact, a fairly complicated

structure. If four mats are stacked to obtain a thicker composite (still only about 1.1 mm thick), it is obvious that the number of elements required becomes intolerable very quickly even for a coarse mesh (see Figure 2). A variationally consistent and organizationally (and computationally) tolerable procedure is needed for analyzing textile composites.

The objective of this paper is to describe a displacement based finite element which accounts for the spatial variation of material properties within a single element. This is in contrast to the usual choices of either adding more elements to account for microstructure or using averaged material properties within each element. The performance of this element is very similar to that in Reference [9], but the formulation is totally different. The formulation of this new element will be discussed first. Then several configurations will be analyzed to evaulate the performance. For simplicity in the discussion, only two-dimensional configurations will be considered. However, the approach is general and can be extended easily to three dimensions.

THEORY

To simplify the discussion, a rectangular element with multiple layers of materials will be discussed first. Such an element might be used where the tows are straight or for ordinary laminated composites when there are too many lamina to model each individually. Then, microstructure of arbitrary shape will be considered.

Consider the four node rectangular element in Figure 3 which contains three lamina of composite material. To facilitate the following discussion, the element will be referred to as a macro element and the subregions (lamina) will be referred to as subelements. The displacement field within the macro element is assumed to take the form

$$\begin{aligned} u(x,y) &= N_i(x,y)u_i \\ v(x,y) &= N_i(x,y)v_i \end{aligned} \tag{1}$$

where $N_i(x,y)$ are interpolation functions and u_i and v_i are macro element nodal displacements. In Equation (1) and subsequent equations Cartesian index notation is used. In particular, a repeated subscript indicates summation. In Equation (1) the summation is for the range $i = 1$ to 4 since there are four interpolation functions for a four node element. The assumed displacement field is referred to herein as single field because a single approximation is used through the entire macro element. In contrast, a multi-field approximation would use approximations which are defined within a single subelement. The stiffness matrix can be calculated using the familiar formula

$$K_{ij} = \iint B_{mi} D_{mn} B_{nj} dxdy \tag{2}$$

where B_{ni} and D_{mn} are the strain-displacement and constitutive matrices, respectively. They are defined by the following equations

$$\begin{aligned} \epsilon_n &= B_{nj} q_j \\ \sigma_m &= D_{mn} \epsilon_n \end{aligned} \tag{3}$$

where q_j = list of the element nodal displacements.

The complication that we have is that the constitutive matrix D_{mn} is now a discontinuous function of position. However, because of the simple geometry, one can perform the required integrations in closed form for each subelement and add the contributions. The details were described in Reference [7] for a four node element. It was shown in Reference [10] that the closed form expressions for the K_{ij} are quite simple for a four node element.

Rectangular macro elements with rectangular subelements cannot accurately model wavy regions like that shown in Figure 4. For such microstructure one needs to use distorted subelements. In the more general case, such as when the interface between woven mats is not straight, the macro element will also be distorted. Figure 5 shows a distorted quadrilateral macro element with distorted subelements. The large numbers (1–4) are the macro element node numbers. The smaller numbers are the subelement node and element numbers. For simplicity the resin pockets are not modeled.

To obtain a single field approximation, the subelement degrees of freedom (dof) must be expressed in terms of the macro element dof. There are several ways in which we can proceed. Two procedures will be discussed herein. Before proceeding it should be pointed out that in general the single field character is only exactly satisfied at the subelement nodes. The first procedure is to consider the subelement mesh to be an ordinary finite element mesh. The only difference is that after the subelement stiffness matrix and equivalent nodal load vector are determined, they are not immediately assembled, but are first transformed. This transformation can be expressed in matrix notation as

$$K_{ij} = T_{mi} K^s_{mn} T_{nj}$$
$$F_i = T_{mi} F^s_m \tag{4}$$

where T_{im} is defined by $q^s_i = T_{im} q_m$ and

q^s_i = nodal displacements for subelement
q_m = nodal displacements for macro element
K^s_{mn} = stiffness matrix for subelement
K_{ij} = subelement contribution to stiffness matrix for macro element

The transformation matrix T_{im} is calculated using the macro element interpolation functions (which are defined in terms of local coordinates ξ and η) evaluated at the subelement nodes. For example, for a four-node macro element and a three-node subelement the transformation is

$$\begin{bmatrix} u^s_1 \\ v^s_1 \\ \vdots \\ u^s_3 \\ v^s_3 \end{bmatrix} = \begin{bmatrix} t_{11} & t_{12} & t_{13} & t_{14} \\ t_{21} & t_{22} & t_{23} & t_{24} \\ t_{31} & t_{32} & t_{33} & t_{34} \end{bmatrix} \begin{bmatrix} u_1 \\ v_1 \\ \vdots \\ u_4 \\ v_4 \end{bmatrix} \tag{5}$$

where $t_{ij} = \begin{bmatrix} N_j(\xi_i, \eta_i) & 0 \\ 0 & N_j(\xi_i, \eta_i) \end{bmatrix}$

Another possibility involves transforming the interpolation functions. This alternative is much more efficient unless there are a very large number of integration points. This procedure will be illustrated by considering the interpolation for the displacement in the x-direction, u. A few more definitions are required before proceeding.

u = macro element displacement in x-direction
u_i = macro element nodal displacements in x-direction
u^s = subelement displacement in x-direction
u^s_i = subelement nodal displacements in x-direction
N_i = interpolation functions for macro element
N^s_i = interpolation functions for subelement

Within a subelement the x-displacement is approximated as

$$u' = N'_i u'_i \tag{6}$$

But the subelement nodal displacements are slaves to the macro element nodal displacements, as described earlier. This can be expressed as

$$u'_i = N_j(\zeta_i, \eta_i) u_j \tag{7}$$

where ζ_i, η_i = coordinates of subelement node i. Combining Equations (6) and (7) gives

$$u' = N'_i N_j(\zeta_i, \eta_i) u_j \tag{8}$$

or

$$u' = N'_i T_{ij} u_j \tag{9}$$

where $T_{ij} = N_j(\zeta_i, \eta_i)$. Note that this transformation matrix T_{ij} is similar to that in Equation (4). The approximation for u can also be expressed in terms of modified interpolation functions,

$$u' = \bar{N}_j u_j \tag{10}$$

where $\bar{N}_j = N'_i T_{ij}$.

Since the range of i in Equation (10) is 1 — (number of nodes in the subelement) and the range of j is 1 — (number of nodes in the macro element), the "modified" interpolation functions can be different in number than the original functions. These modified interpolation functions are used when calculating the subelement stiffness matrices. Recall that the B matrix contains derivatives of the interpolation functions $\bar{N}_j$. This presents no problem since the T_{ij} contains only constants. For example,

$$\frac{\partial \bar{N}_j}{\partial x} = \frac{\partial N'_i}{\partial x} T_{ij} \tag{11}$$

These modified interpolation functions are used in evaluating the terms related to the displacement interpolation. The unmodified interpolation functions are used to determine the determinant of the Jacobian for use in mapping the differential area $d\zeta d\eta$ from the subelement local coordinate system to a global coordinate system. Since the subelement displacements are slaved to the macro element displacements, there is considerable freedom in defining the subelements. For example, there is no need to prevent "dangling" nodes like that shown in Figure 5. In fact, one can even define the stiffness matrix for a macro element to be a summation of some very unlikely looking subelements. This is shown schematically in Figure 6. This is probably of little practical utility for two-

dimensional models, but for three-dimensional models this represents a major simplification.

The single field approximation gives very poor results for some configurations. For example, if the lamina in Figure 3 have large differences in E_y, it is very difficult to approximate the stiffness in the y-direction using a single field approximation. This is because the single field assumption results in continuity of strains, which causes a discontinuity of stresses which should be continuous at the lamina interfaces. A numerical example of this poor performance will be given in the "Results and Discussion" section. However, as will be illustrated later, there are realistic configurations with significant inhomogeneity for which a single field approximation performs well. Also, the macro elements described herein cannot be evaluated using the usual mesh refinement convergence methods. As the mesh becomes more refined, the inhomogeneity within an element disappears and the macro element becomes an ordinary element.

RESULTS AND DISCUSSION

Results for two basic configurations will be presented. The first is a one-dimensional bimaterial rod and the second is a 2D idealization of a woven textile. The material properties for the woven textile were assumed to be

$E_{11} = 100$ GPa $\quad E_{22} = 10$ GPa $\quad E_{33} = 10$ GPa

$\nu_{12} = 0.35 \quad \nu_{13} = 0.35 \quad \nu_{23} = 0.3$

$G_{12} = 5$ GPa $\quad G_{13} = 5$ GPa $\quad G_{23} = 3.845$ GPa

These material properties are meant to represent those for a transversely isotropic tow. They do not correspond to any particular material system. Two-dimensional material properties were obtained by imposing plane strain conditions. The material properties were transformed to account for the inclination of the fiber bundle.

The bimaterial rod (shown schematically in Figure 7) was used to evaluate the accuracy of a single field approximation when two materials are loaded in series. The axial displacement was assumed to vary as $\Sigma_{i=1}^{n} a_i x^i$, where n equals the order of the polynomial. Figure 7 shows the error in predicted stiffness verus the ratio E_b/E_a. As expected, the error increases with the ratio E_b/E_a. Perhaps surprising is the inability of an eighth order polynomial to adequately predict the re-

sponse when E_x/E_z is larger than about 2. Obviously, the single field approximation is not very useful when two very different materials are loaded in series. However, most realistic configurations involving dissimilar materials have load paths which are a combination of series and parallel. The example of primary concern in this paper is a textile composite, which will be discussed next.

Two-dimensional idealizations of textile composites were analyzed using single field macro elements. The tow path was assumed to be sinusoidal. The thickness of the tow, $b/2$, was kept constant along the path. Waviness ratios b/a (see sketch in Figure 8) were varied from .083 to .333. It should be noted that a woven composite is inherently three-dimensional. There is no typical cross section. Concomitantly, results from any two-dimensional textile model must be used with caution. Consequently, the results presented should only be interpreted as an evaluation of the effectiveness of the macro elements for handling microstructure. Figure 8 shows the variation of extensional stiffness with waviness. Two symmetrically stacked mats were considered. Only one mat was modeled. Symmetry conditions were imposed on the lower surface of the mat. Results were obtained using 60 eight-node traditional finite elements (reference solution) and 2 eight-node macro elements. The macro elements predict the stiffness variation quite well, except for very large waviness ratios.

Figure 9 shows undeformed and deformed finite element meshes for a single textile mat using 8-node traditional and 12-node macro elements. This configuration is different from that in Figure 8, which had symmetry on the lower surface of the mat. The absence of symmetry constraints results in large bending deformation. The deformed meshes are also shown overlaid to compare the predicted shapes. The macro elements predict the deformed shape very well.

Figures 8 and 9 showed the good performance of the macro element for predicting global response. This does not imply that stresses or strains within the element can be calculated accurately. In fact, the errors can be quite large. Figures 10 and 11 show the variations of σ_x along the lower boundary of the axial tow for two symmetrically stacked mats. Results are included for both traditional and macroelement analyses. The sample points are labeled in the figures as points 1–6. Figure 10 shows σ_x for a waviness ratio of .333. The actual σ_x variations, i.e., that calculated using conventional finite elements) is not complicated, but the single-field approximation is quite inaccurate. A waviness ratio of .333 is fairly large. For a smaller waviness ratio of .166 (Figure 11) the accuracy of the single-field approximation is much better. However, the use of single-field finite elements to calculate local stresses and strains is not recommended. Much better estimates for local stresses and strains can be obtained using a global/local strategy. Single-field macro elements can be very useful for the global analysis. A refined traditional finite element analysis can then be used for the local analysis.

CONCLUSIONS

A new type of finite element was developed for analysis of textile composites. This new element (referred to herein as a macro element) accounts for the spatial variation of material properties within a single element. Tests of the macro elements showed good performance for modeling the global deformation behavior of textile composites. Because of the single field assumption, the stresses calculated inside the macro element are not accurate. To obtain these stresses a global/local strategy should be used in which macro elements are used for the global analysis and conventional finite elements are used for the local analysis.

Although only two-dimensional elements were evaluated, the formulation is valid for three dimensions. However, there are challenges in 3D modeling, which are not so apparent or do not exist for 2D models. For example, in 3D one could imagine mats which are oriented at other than 0° or 90° relative to the macro element axes. Such an off-axis mat is much more difficult to model, particularly if it is combined with mats with other orientations. There is obviously still much work required to develop a general textile composite analysis.

REFERENCES

1. Halpin, J. C., K. Jerine and J. M. Whitney. 1971. "The Laminate Analogy for 2 and 3 Dimensional Composite Materials," *Journal of Composite Materials*, 5:36–49.
2. Ishikawa, T. 1981. "Anti-Symmetric Elastic Properties of Composite Plates of Satin Weave Cloth," *Fibre Science and Technology*, 15:127–145.
3. Ishikawa, T. and T. W. Choul. 1982. "Stiffness and Strength Behavior of Woven Fabric Composites," *Journal of Material Science*, 17:3211–3220.
4. Whitcomb, J. D. 1991. "Three-Dimensional Stress Analysis of Plain Weave Composites," in *Composite Materials: Fatigue and Fracture, Volume 3*, T. K. O'Brien, ed., *ASTM STP 1110*, Philadelphia: American Society for Testing and Materials, pp. 417–438.
5. Blackketter, D. M., D. E. Walrath and A. C. Hansen. 1989. "The Study of Woven Fabric Reinforced Composite Materials," University of Wyoming Composite Materials Research Group Report UW-CMRG-R-89-102.
6. Guedes, J. M. and N. Kikuchi. 1990. "Preprocessing and Postprocessing for Materials Based on the Homogenization Method with Adaptive Finite Element Methods," *Computer Methods in Applied Mechanics and Engineering 83*, Elsevier Science Publishers, pp. 143–198.
7. Paumelle, P., A. Hassim and F. Léné. 1990. "Composites with Woven Reinforcements: Calculation and Parametric Analysis of the Properties of the Homogeneous Equivalent," *La Recherche Aérospatiale*, 1:1–12.
8. Paumelle, P., A. Hassim and F. Léné. 1991. "Microstress Analysis in Woven Composite Structures," *La Recherche Aérospatiale*, 6:47–62.
9. Woo, K. and J. D. Whitcomb. "Macro Finite Element Using Subdomain Integration," Offshore Technology Research Center Report 03/92-A-29-100, Texas A&M University.
10. Whitcomb, J. D. 1986. "A Simple Rectangular Element for Two-Dimensional Analysis of Laminated Composites," *Computer and Structures*, 22(3):387–393.

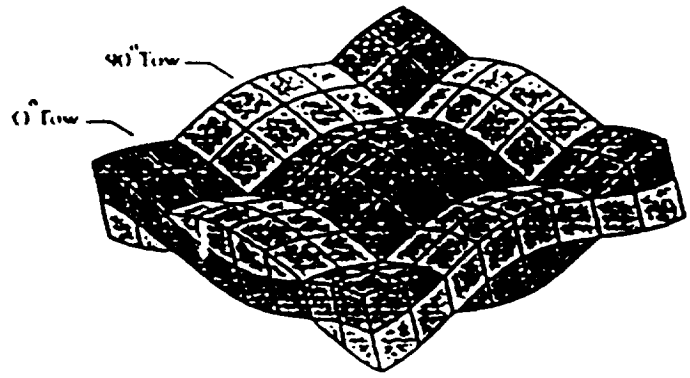

Figure 1. Schematic of plain weave composite.

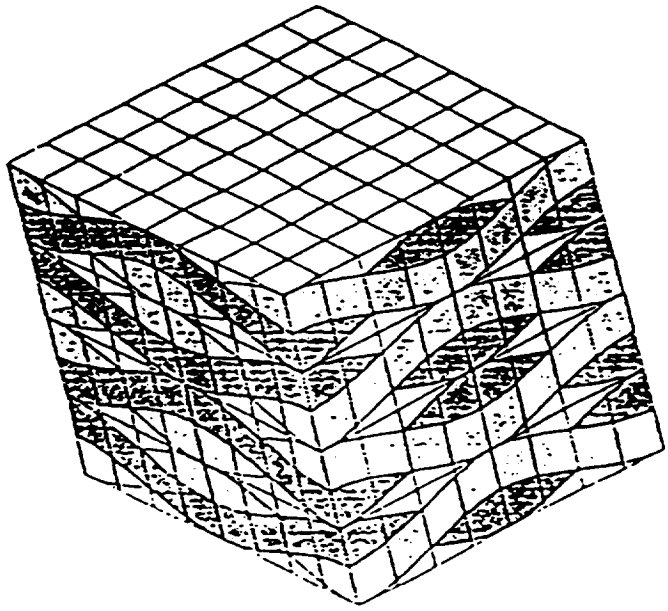

Figure 2. Schematic of symmetrically stacked plain weave composite.

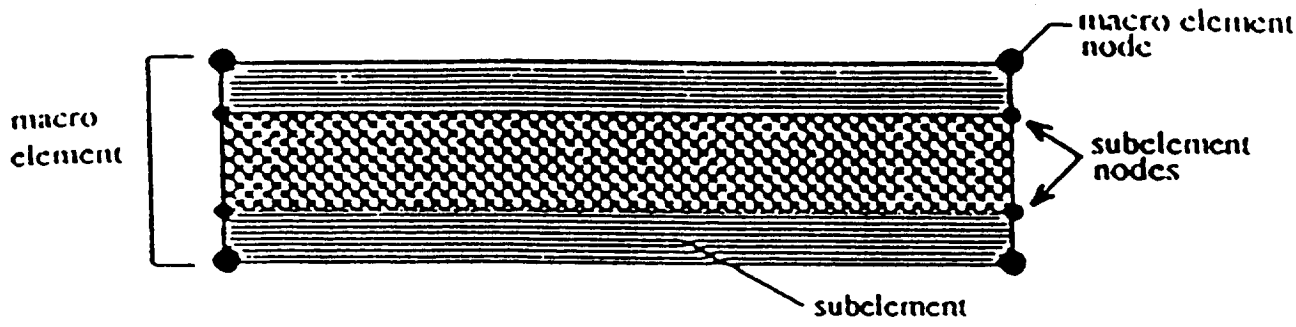

Figure 3. Macro element with layered microstructure.

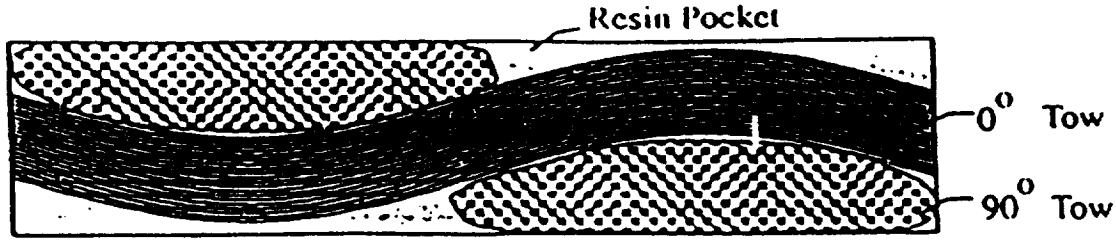

Figure 4. Schematic of plain weave cross section.

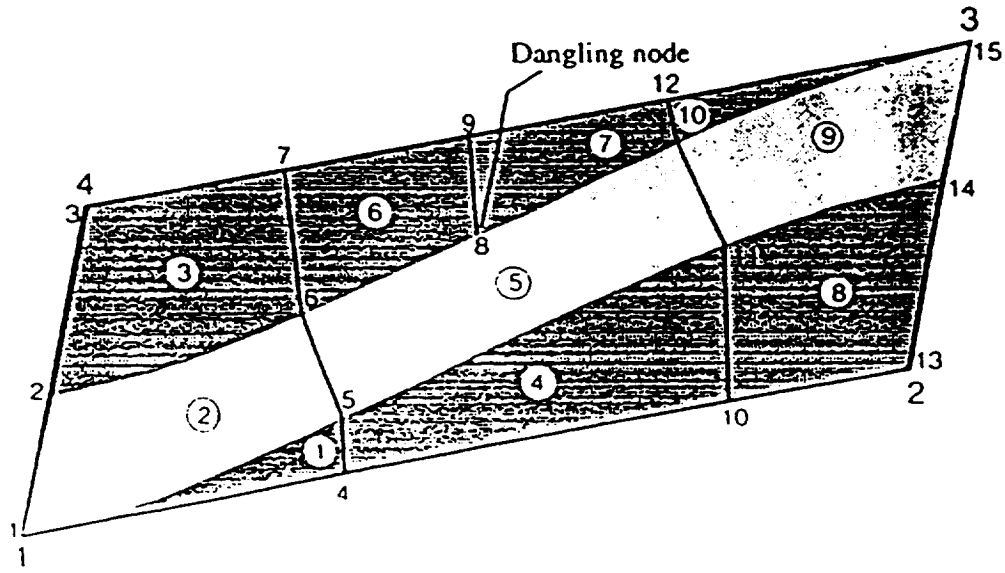

Figure 5. Distorted quadrilateral macro element with distorted subelements.

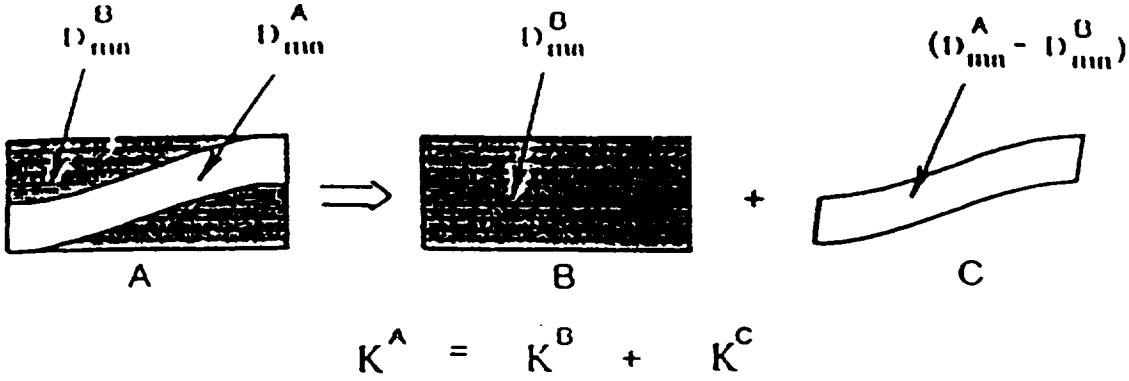

Figure 6. Alternate calculation of macro element stiffness matrix for two-dimensional configuration (D_{mn} = constitutive coefficients).

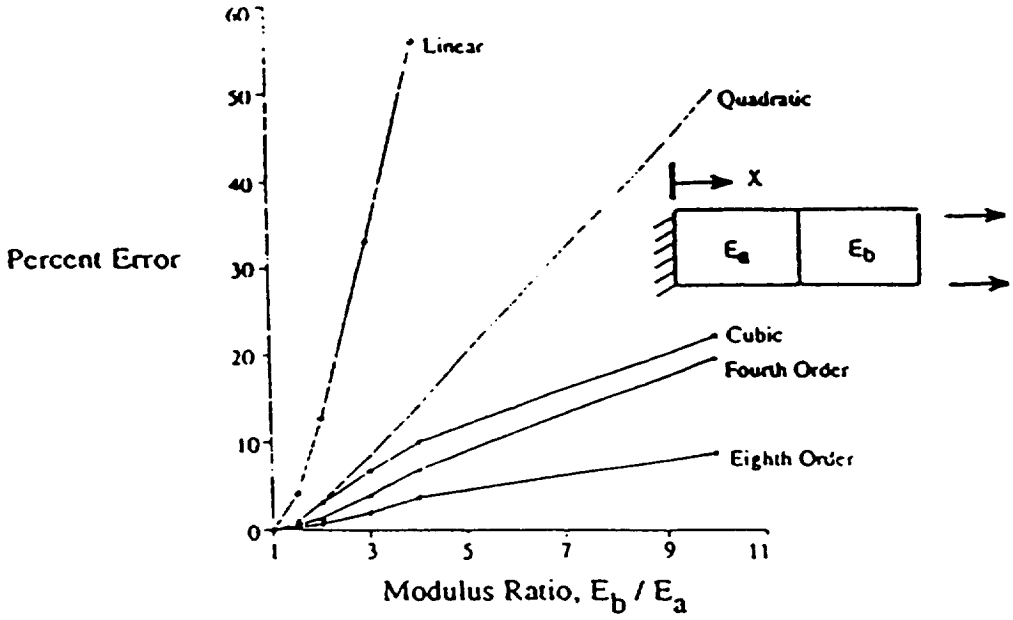

Figure 7. Error in calculated stiffness using single field approximation.

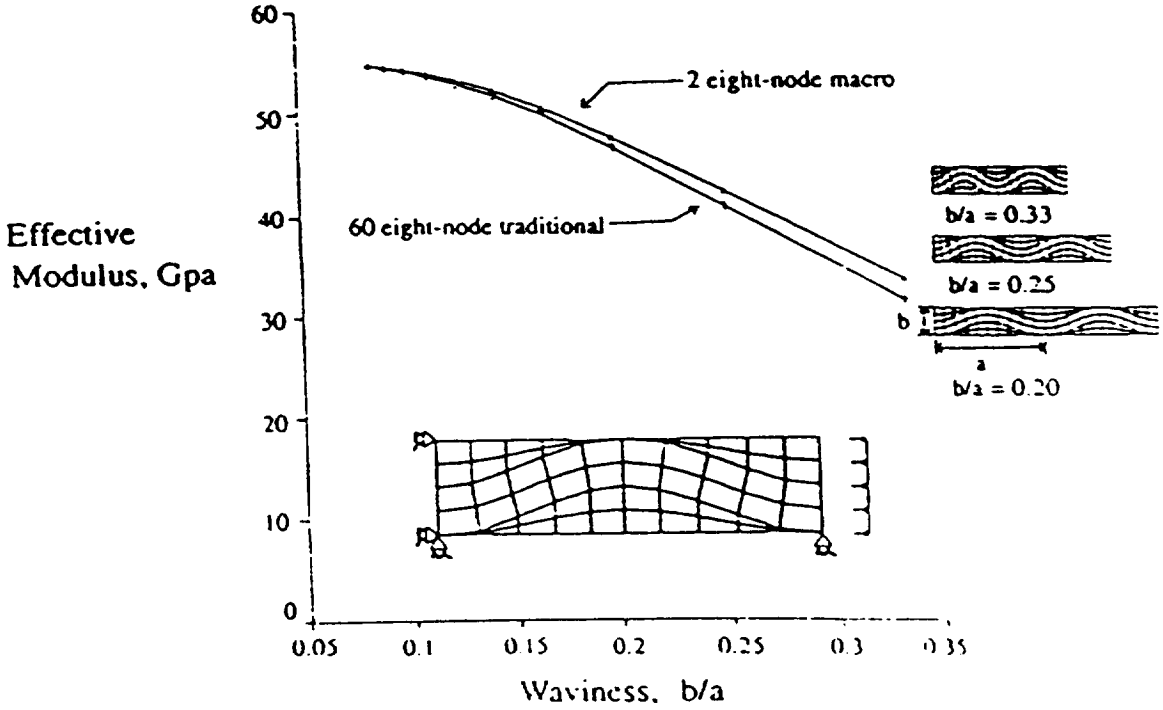

Figure 8. Extensional modulus versus waviness.

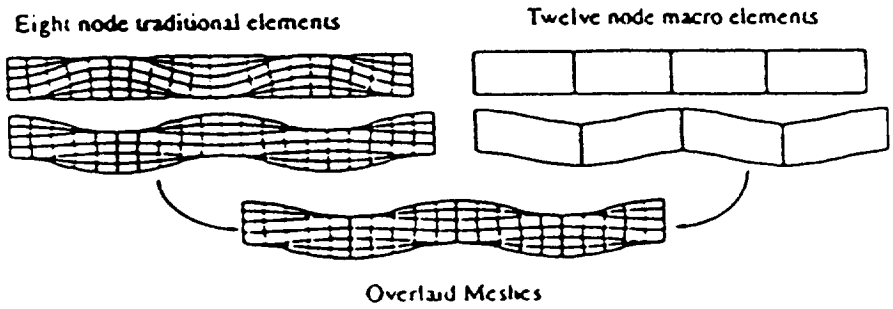

Figure 9. Comparison of deformed traditional and macro element meshes.

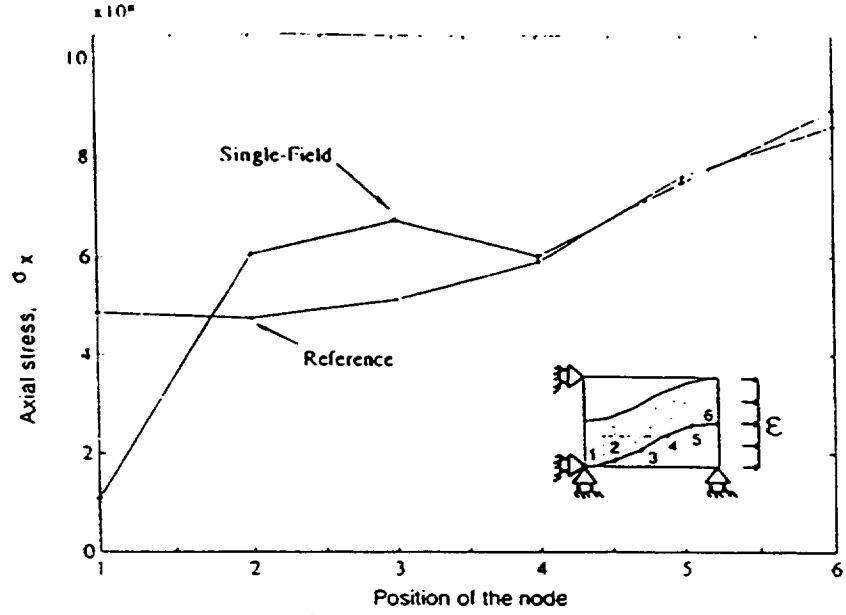

Figure 10. Variation of σ_x along the lower interface for double mat composite (waviness ratio = 0.333, axial strain = 0.01).

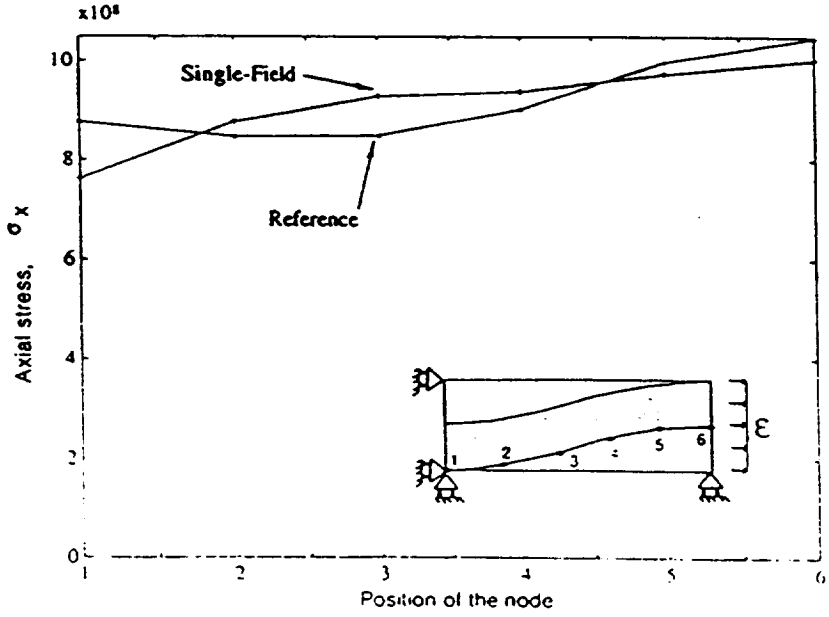

Figure 11. Variation of σ_x along the lower interface for double mat composite (waviness ratio = 0.166, axial strain = 0.01).

Chapter: 2

MACRO FINITE ELEMENT USING SUBDOMAIN INTEGRATION

SUMMARY

For some heterogeneous materials, it is not practical to model the microstructure directly using traditional finite elements. Furthermore, it is not always accurate to use homogenized properties. Macro elements have been developed which permit microstructure within a single element. These macro elements performed well in initial tests.

INTRODUCTION

In traditional 2D and 3D finite-element analysis, the material properties are assumed to be constant or at least to vary smoothly within a single element. This is valid for most engineering applications because the microstructural scale (e.g. grain size in a metal) is very small compared with the element size. However, some materials exhibit a very coarse 'microstructure', such as laminated or textile composites. Figure 1 shows a schematic diagram of a cross-section of a textile composite. Owing to the complicated geometry, textile composite structures are very difficult to analyse. To use the traditional finite-element method to solve this kind of problem, finite elements have to be defined such that the material properties vary smoothly in each finite element. This results in a very large number of elements. For laminated composites, the geometry is simpler, but if there are many laminae (for example, 50 laminae for a 6·25 mm laminate), modelling of individual layers becomes impractical because of the large number of elements.

Material homogenization is one way of treating inhomogeneous materials. In this procedure, the spatially variable material properties are replaced by some 'effective' homogeneous properties. The effectiveness of material homogenization, however, depends on the problem to be analysed. Material homogenization theories[1-3] assume that the applied loading on the boundary of the representative volume element (RVE) is spatially homogeneous. This assumption is good as long as the characteristic scale of the microstructure is much smaller than that of the macrostructure. For example, volume averaging in laminated composites works well for in-plane loads. However, it gives large errors for bending loads unless there are many plies and the different plies are highly dispersed through the thickness. Higher-order theories such as classical laminate theory (CLT)[4] account for the geometric details of the microstructure for the laminated composite plates in terms of 1st and 2nd area moments of inertia. CLT works well for in-plane and bending problems in thin laminated plates. But CLT ignores out-of-plane strains, which is unacceptable for relatively thick plates. There are many other ways of homogenization, but none of them are problem-independent. When there are

material property discontinuities, it is most accurate to model each material group discretely. However, this approach requires large computer memory and CPU resources.

Some work has been done in dealing with specific problems to overcome this difficulty. Steven[5] developed a quadratic triangular and a quadratic isoparametric element with an internal interface modelled by a straight line. In his work, trian ;ular subregions were used to perform numerical integration. He also suggested the possibility of using a second isoparametric mapping to simplify the integration, but he neither described any details nor implemented the method. The concept of splitting the integration limit was also discussed by Panda *et al.*[6] In his finite-element formulation for laminated plates, the integration limit through the thickness was divided to define material properties of each individual layer. Foye[7] studied material properties of fabric-reinforced composites using subcell analysis. The unit cell was divided into rectangular paralellepiped subcells. Since the subcell boundaries do not match the material interfaces, averaged material properties were used in each subcell.

The present paper describes a 'macro' finite element which can account for the details of microstructure within an element. A macroelement is defined to be an element consisting of several subdomains. Figure 2 shows a macro element that has four subdomains. Macro elements can have material discontinuities inside the element, but in each subdomain the material properties are smooth functions of the spatial co-ordinates. The macro element is identical to a traditional finite element when it has only one subdomain. When there are material discontinuities, the subdomainss are used to define the material boundaries and to facilitate the numerical integrations.

It should be noted that since the present study was based on a displacement formulation, even with very high-order interpolation, significant stress errors are expected near the region where geometric or material discontinuities occur. Local stress distributions for regions of special interest can be achieved by global/local analysis.[8-10] The proposed macro elements are best suited for use in the global analysis.

In the following Sections, the finite-element stiffness matrix formulation is explained in detail. Then examples for several configurations are discussed to illustrate the performance of the macro elements.

CALCULATION OF MACRO ELEMENT STIFFNESS MATRIX

This section describes the finite-element stiffness matrix formulation for a macro element for two-dimensional elasticity analysis. The extension to three dimensions is trivial and will be discussed briefly at the end of this Section.

In a traditional displacement-based finite-element method, the element stiffness matrix has the form

$$[K] = \int_{\Omega} [B]^T [D] [B] \, dx \, dy \tag{1}$$

where [D] and [B] are defined by

$$\{\sigma\} = [D]\{\varepsilon\}$$

$$\{\varepsilon\} = [B]\{q\}$$

and $\{q\}$ is the nodal displacement vector. Supposing that there are material property inhomogeneities within the integration domain Ω (i.e. the [D] matrix is a piece-wise-continuous function of spatial co-ordinates within a macro element), the macro element is divided into subdomains. Within each subdomain, the material properties vary smoothly (see Figure 2).

Consider an element that has n subdomains Ω_i where

$$\sum_{i=1}^{n} \Omega_i = \Omega \tag{2}$$

The element stiffness matrix becomes

$$[K] = \sum_{i=1}^{n} \int_{\Omega_i} [B]^T [D]_i [B] \, dx \, dy \tag{3}$$

A robust procedure is needed to evaluate the contribution of the ith subdomain

$$[K]_i = \int_{\Omega_i} [B]^T [D]_i [B] \, dx \, dy \tag{4}$$

The procedure developed herein involves the use of three co-ordinate systems. Figure 3 shows the three co-ordinate systems. The use of three co-ordinate systems differs from conventional finite elements, which use a global and a local co-ordinate system. (In Figure 3, these are the (x, y) and (ξ, η) systems.) The mapping of co-ordinate systems in conventional finite elements permits integration over a simple square region even when the actual finite element is quite distorted. If the material properties vary discontinuously within an element, subdomains must be defined in which the material properties vary continuously. In general, these subdomains are distorted such as the one indicated by the shaded region (*ijkl*) in Figure 3(a). When this distorted subdomain is mapped into the (ξ, η) co-ordinate system, it is still distorted (shaded region in Figure 3(b)) and concomitantly the integrations would not be simple. If this subdomain is mapped again into a third co-ordinate system (r, s), the integrations are again quite simple. The remaining task is to describe how to perform the integrations in the (r, s) co-ordinate system.

There are two primary concerns. The first is defining the differential element $dx\,dy$ in terms of $dr\,ds$. Figure 3 shows that

$$dx\,dy = |J| \, d\xi \, d\eta \tag{5}$$

where J is the Jacobian matrix defined by

$$J = \frac{\partial(x, y)}{\partial(\xi, \eta)}$$

However,

$$d\xi \, d\eta = |\bar{J}| \, dr \, ds \tag{6}$$

where

$$\bar{J} = \frac{\partial(\xi, \eta)}{\partial(r, s)}$$

Therefore, the net result is

$$dx\,dy = |\mathbf{J}|\,|\bar{\mathbf{J}}|\,dr\,ds \tag{7}$$

The second concern is defining the integrand in terms of the (r,s) co-ordinates. That is, $[\mathbf{B}]^T[\mathbf{D}]_i[\mathbf{B}]$ involves derivatives of the interpolation functions. These interpolation functions are defined in terms of ξ and η, not r and s. For example,

$$\begin{bmatrix} \dfrac{\partial N_i}{\partial x} \\ \dfrac{\partial N_i}{\partial x} \end{bmatrix} = \mathbf{J}^{-1} \begin{bmatrix} \dfrac{\partial N_i}{\partial \xi} \\ \dfrac{\partial N_i}{\partial \eta} \end{bmatrix} \tag{8}$$

Note that the calculation of the derivatives involves $\mathbf{J}$ but not $\bar{\mathbf{J}}$. This is because the N_i's are defined in terms of ξ and η alone. It is necessary to evaluate the integrand $[\mathbf{B}]^T[\mathbf{D}]_i[\mathbf{B}]$ at particular values of r and s. As part of the mapping between the (ξ,η) and (r,s) co-ordinate systems, ξ and η are approximated as

$$\begin{aligned} \xi &= \bar{N}_i(r,s)\xi_i \\ \eta &= \bar{N}_i(r,s)\eta_i \end{aligned} \tag{9}$$

When performing numerical integration in the (r,s) co-ordinate systems, ξ and η are determined using equation (9). These values are then used to evaluate the integrand.

With equations (4) and (7), the contribution of the ith subdomain stiffness matrix becomes

$$[\mathbf{K}]_i = \int_{-1}^{1}\int_{-1}^{1} [\mathbf{B}]^T[\mathbf{D}]_i[\mathbf{B}]\,|\mathbf{J}|\,|\bar{\mathbf{J}}|\,dr\,ds \tag{10}$$

In Figure 2, both the macro element and the subdomains are quadrilaterals. This is not necessary. The interpolation for the solution is defined in the (ξ,η) co-ordinate system. The subdomain, which is mapped into the (r,s) system, is needed only to simplify the numerical integrations. The type of subdomain does not affect the solution except that it should adequately describe the geometry of the microstructure.

The extension to three dimensions is simple. The three co-ordinate systems would be (x,y,z), (ξ,η,ζ) and (r,s,t). The form of equations (1)–(10) is unchanged except to account for an additional co-ordinate direction. The contribution of the ith subdomain to the macro element stiffness matrix would be

$$[\mathbf{K}]_i = \int_{-1}^{1}\int_{-1}^{1}\int_{-1}^{1} [\mathbf{B}]^T[\mathbf{D}]_i[\mathbf{B}]\,|\mathbf{J}|\,|\bar{\mathbf{J}}|\,dr\,ds\,dt \tag{11}$$

RESULTS AND DISCUSSIONS

This section discusses the use and performance of the macro elements for two-dimensional elasticity. Three basic configurations were studied: (1) square and distorted 4-node elements, (2) $(0/90_2/0)$ and $(90/0_2/90)$ laminated beams with end moment and shear force loadings, and (3) a single and double plain weave textile composite under tension. Four-, 8- and 12-node macro elements were evaluated. The following material properties were used:

$E_{11} = 100$ GPa	$E_{22} = 10$ GPa	$E_{33} = 10$ GPa
$\nu_{12} = 0{\cdot}35$	$\nu_{13} = 0{\cdot}35$	$\nu_{23} = 0{\cdot}3$
$G_{12} = 5$ GPa	$G_{13} = 5$ GPa	$G_{23} = 3{\cdot}845$ GPa

Two-dimensional material properties were obtained by imposing plane strain conditions. For textile composites, the material properties were transformed to account for the inclination of the fibre bundle.

The first use of the macro element was to demonstrate that the mapping is correct. Square and distorted 4-node macro elements were subdivided into four subdomains (Figure 4). All four subdomains were assigned the same material properties. The macro element stiffness matrices should be the same as that for 4-node traditional elements. Tables I and II list the eigenvalues of the traditional and macro element stiffness matrices for different orders of integration. For the square element shown in Figure 4(a), both traditional and macro elements produce exactly the same results when (2 × 2) Gaussian integration is used. Note that since there are four subdomains, the actual number of integration points for a macro element is four times the number of subdomain integration points. For the distorted element shown in Figure 4(b), results for the traditional finite element using (2 × 2) integration differ from the exact solutions. Table II shows that (3 × 3) integration for the traditional element and (2 × 2) integration for the macro element are nearly exact. As the integration points increase, both elements converge to the same results.

Figure 5 shows the moment resultants for two laminated beams. Tip displacements were applied to produce a maximum strain of 0·1%. Homogenized material properties were obtained by the rule of mixtures.[4] The reference solutions are from traditional finite-element analysis with four 8-node traditional elements. Four-node and 8-node macro elements were evaluated. A single macro element with four subdomains (one subdomain per lamina) was used. For the 4-node macro element, selective 'reduced' integrations[11] with 17 integration points were performed. Results show that for both $(0/90_2/0)$ and $(90/0_2/90)$ stacking sequences, one 4-node or 8-node macro element predicts the bending stiffness very well. Of course, an 8-node traditional element with the volume-averaged homogenized material properties cannot distinguish differences in the stacking sequence. Hence, the errors are large for the volume-averaged homogenized material model, as expected. The percentage errors are shown in Table III. Note that accuracy depends on stacking sequence.

Figure 6 shows the tip displacement comparisons for a short (3 × 1) cantilever beam for two stacking sequences. A unit shear force was applied at the right end of the beam. Four subdomains were used to account for the inhomogeneous material properties. Single 4-node, 8-node and 12-node macro elements were used. The reference solutions were obtained with a refined mesh (64 eight-node elements). As expected, the traditional finite-element analysis using the refined mesh with volume-averaged homogenized material properties does not predict the deformation behaviour. The 8-node macro element predicted the displacements fairly well. The 12-node macro element showed excellent performance. The 4-node macro element did not perform well. This was expected since the assumed displacement fields for the 4-node element are too simple for this problem. Table IV shows the percent errors for each case. For all three macro elements, the error was larger for the $(90/0_2/90)$ laminates.

The 'effective' extensional modulus E_x against waviness of plain weave textile composites was calculated using traditional and macro elements. Figure 7 shows the configuration studied: two symmetrically stacked layers. Thick and thin lines in the upper mat indicate the macro elements and subdomains, respectively. Only the upper mat was modelled because of symmetry. The models have a length which is the same as the fibre bundle wavelength. For simplicity, the textile composites were assumed not to have any pure matrix regions. Displacements were applied to produce a 0·1 per cent nominal strain $\langle \varepsilon \rangle$ in the x-direction. The effective E_x was defined to be

$$E_x = \frac{\langle \sigma \rangle}{\langle \varepsilon \rangle}$$

where

$$\langle \sigma \rangle = \frac{\text{Axial force}}{\text{Area}}, \qquad \langle \varepsilon \rangle = \frac{\Delta u}{a}$$

The waviness was defined to be $w = b/a$, where the centreline of the wavy fibre bundle is assumed to have a sinusoidal shape given by

$$y = \frac{b}{4} \sin\left(\frac{2\pi x}{a}\right)$$

Two 4-, 8- and 12-node macro elements were used. Each macro element consisted of 15 subdomains and models a half-wavelength. For the reference solution, a mesh with 60 traditional eight-node elements was used. Figure 8 shows several of the traditional finite-element models. (The wavy fibre bundles are indicated by the shaded region.) Figure 9 shows the effective E_x against waviness. The error increased with increased waviness. Both 8-node and 12-node elements performed fairly well. The 4-node element was not very accurate except for small waviness.

Deformed meshes for macro element and traditional models are shown in Figure 10. These models are for a single plain weave mat (i.e. no symmetry). The Figure shows quite graphically the effect of the microstructure on the predicted deformation of a single mat. The Figure also shows that the macro element predicts the deformed shape very well. It should be noted that only linear analysis was performed in the present study. The deformation shown in Figure 10 is larger than would be expected from a non-linear analysis.

CONCLUSION

A displacement-based macro element was developed to expedite elasticity analysis of heterogeneous materials. Two-dimensional macro elements with four, eight and 12 nodes were implemented and evaluated for several realistic configurations. Since the macro elements used a continuous strain field approximation, it is obvious that there is violation of equilibrium at the material interfaces and the stress distributions near the interfaces would not be very accurate. However, the macro elements performed well in terms of global response for the configurations considered. To obtain detailed local stress distributions, a global/local strategy is needed. The proposed macro elements should be very useful for expediting the global analysis.

REFERENCES

1. C. Stolz, 'General relationships between micro and macro scales for the non-linear behaviour of heterogeneous media', in *Modelling Small Deformations of Polycrystals*, J. Gittus and J. Zarka (Eds.) Elsevier Applied Science Publishers Ltd., 1986.
2. M. Guedes and N. Kikuchi, 'Preprocessing and postprocessing for materials based on the homogenization method with adaptive finite element methods', *Comput. Methods Appl. Mech. Eng.*, 83 (1990).
3. T. Mura, *Micromechanics of Defects in Solids*, 2nd revised edn, Martinus Nijhoff Publishers, Dordrecht, 1987.
4. R. M. Jones, *Mechanics of Composite Materials*, Scripta Book Company, 1975.
5. G. P. Steven, 'Internally discontinuous finite elements for moving interface problems', *Int. j. numer. methods eng.*, 18, 569–582 (1982).
6. S. C. Panda and R. Natarajan, 'Finite element analysis of laminated composite plates', *Int. j. numer. methods eng.*, 14, 69–79 (1979).
7. R. L. Foye, 'Finite element analysis of the stiffness of fabric reinforced composites', NASA Contractor Report 189597, February 1992.
8. J. Fish and S. Markolefas, 'The *s*-version of the finite element method for multilayer laminates', *Int. j. numer. methods eng.*, 33, 1081–1105 (1992).
9. S. McCormick and J. Thomas, 'The fast adaptive composite grid (FAC) method for elliptic equations', *Math. Comput.*, 46 (1986).
10. J. D. Whitcomb and K. Woo, 'Global/local analysis for geometrically nonlinear structures', Submitted to *Commun. numer. methods eng.*
11. O. C. Zienkiewicz and R. L. Taylor, *The Finite Element Methods*, 4 edn, Vol. 1: *Basic Formulation and Linear Problems*, McGraw Hill Book Company, 1989.

Table I. Eigenvalues against Gauss integration points for square elements (Figure 4(a))

	Eigenvalues ($\times 10^9$)	
Integration	1 × 1	2 × 2
4-node traditional:	0·00000	0·00000
	0·00000	0·00000
	0·00000	0·00000
	0·00000	5·76923
	0·00000	5·76923
	7·69230	7·69230
	7·69230	7·69230
	19·23076	19·23076
4-node macro:	0·00000	0·00000
	0·00000	0·00000
	0·00000	0·00000
	4·32692	5·76923
	4·32692	5·76923
	7·69230	7·69230
	7·69230	7·69230
	19·23076	19·23076

Table II. Eigenvalues against Gauss integration points for distorted elements (Figure 4(b))

	Eigenvalues ($\times 10^9$)				
Integration	1 × 1	2 × 2	3 × 3	4 × 4	5 × 5
4-node traditional:	0·00000	0·00000	0·00000	0·00000	0·00000
	0·00000	0·00000	0·00000	0·00000	0·00000
	0·00000	0·00000	0·00000	0·00000	0·00000
	0·00000	4·55397	4·61494	4·61621	4·61624
	0·00000	6·19357	6·25265	6·25377	6·25379
	7·18992	8·56256	8·62312	8·62441	8·62444
	7·93269	9·38271	9·46246	9·46405	9·46409
	20·57450	20·87012	20·87916	20·87935	20·87935
4-node macro:	0·00000	0·00000	0·00000	0·00000	0·00000
	0·00000	0·00000	0·00000	0·00000	0·00000
	0·00000	0·00000	0·00000	0·00000	0·00000
	7·93509	4·61146	4·61621	4·61624	4·61624
	8·59403	6·24930	6·25377	6·25379	6·25379
	3·63243	8·61957	8·62441	8·62444	8·62444
	5·06974	9·45776	9·46405	9·46409	9·46409
	20·76932	20·87863	20·87935	20·87935	20·87935

Table III. Percentage error for moment resultants

	$(0/90_2/0)$	$(90/0_2/90)$
4-node macro	2·451	5·832
8-node macro	0·001	0·000
12-node macro	–	–
Homogenized	37·61	160·3

Table IV. Percentage error for tip displacements

$(0/90_2/0)$	$(90/0_2/90)$
23·78	29·45
9·873	12·87
2·857	4·777
33·11	54·64

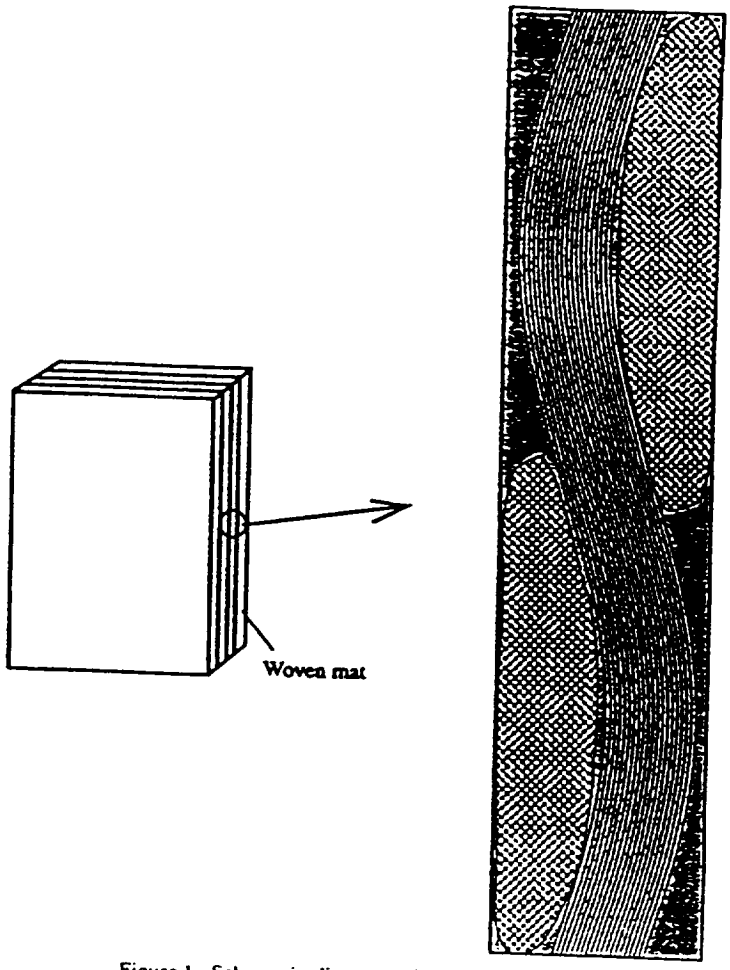

Figure 1. Schematic diagram of woven composite

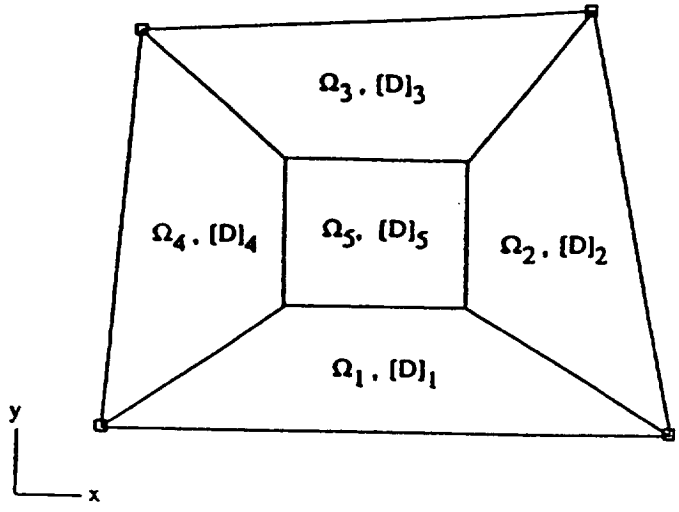

Figure 2. Typical 4-node macro element

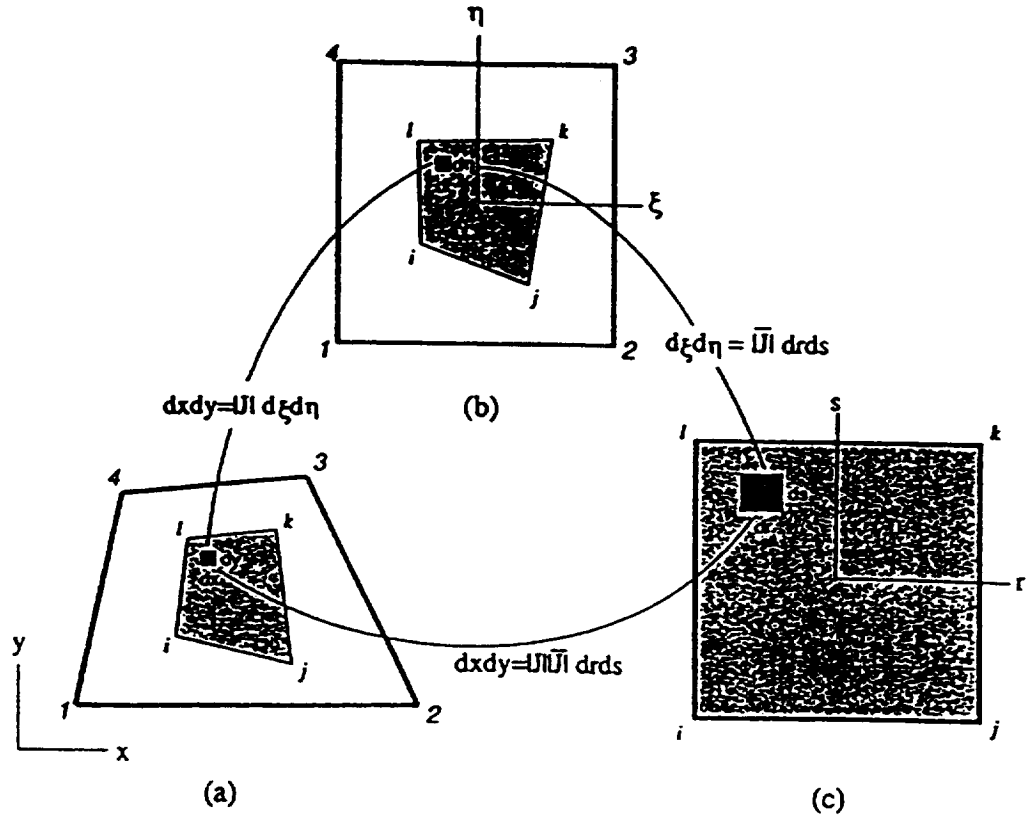

Figure 3. Mapping between three co-ordinate systems

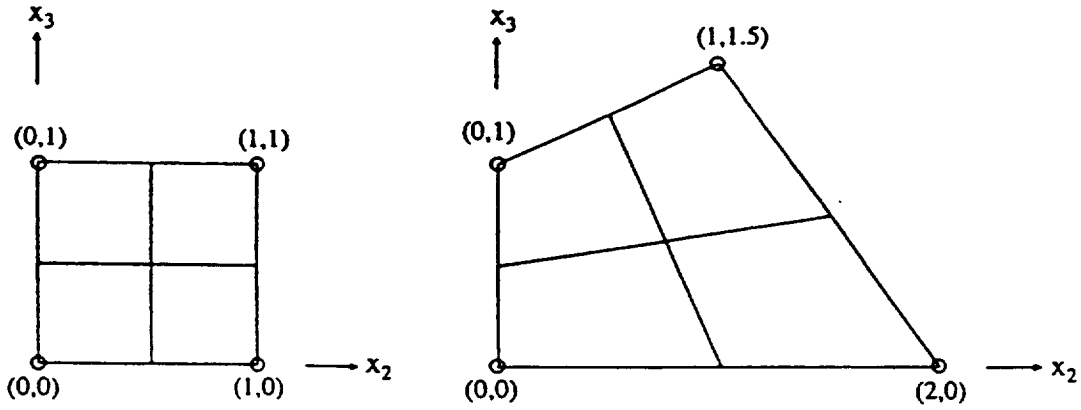

Figure 4. Macro elements for test of mapping

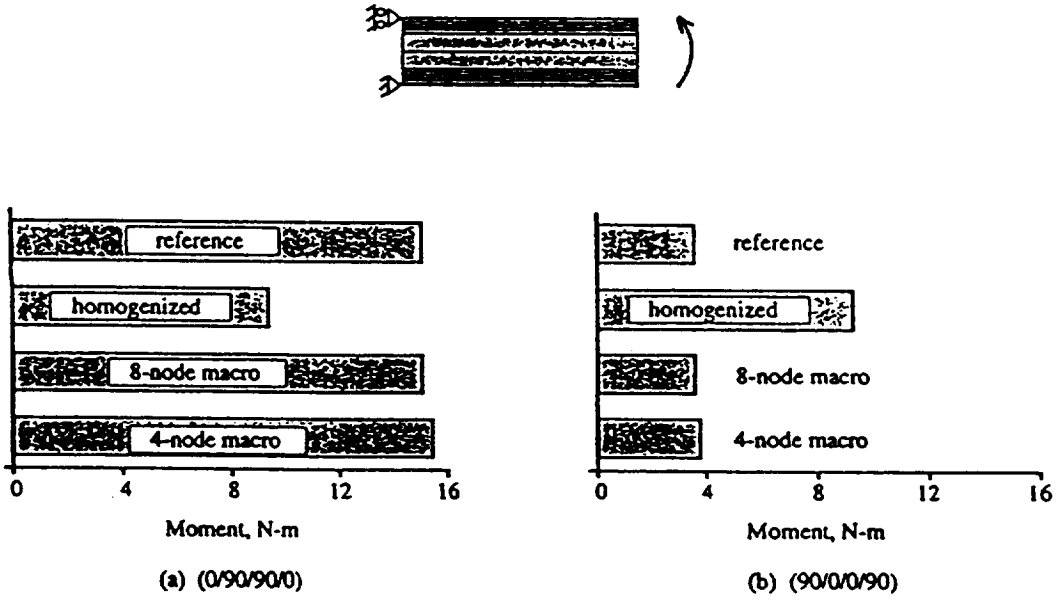

Figure 5. Moment resultants for two stacking sequences

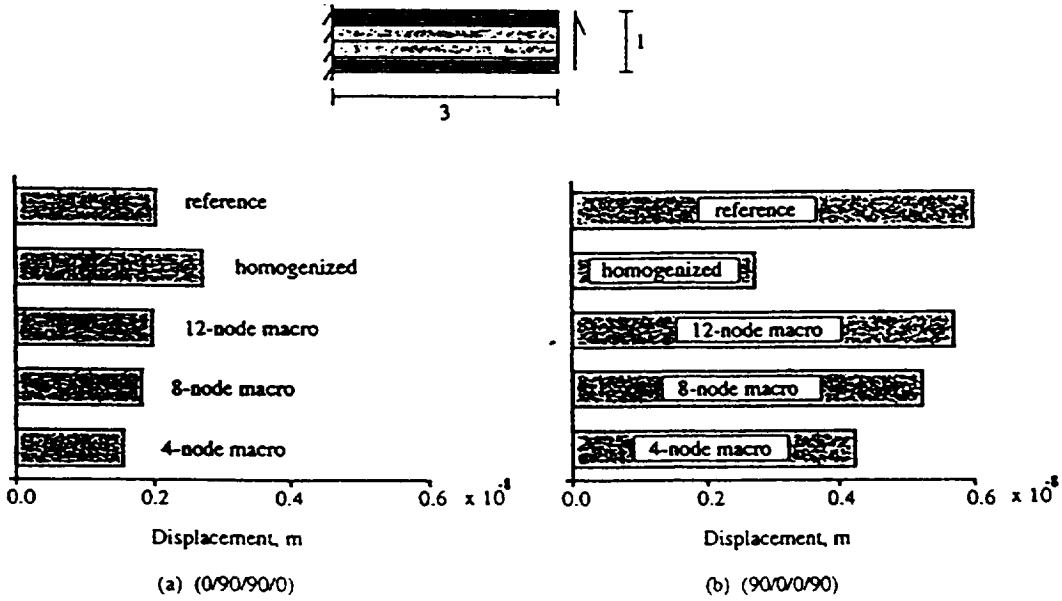

Figure 6. Tip displacements of (3 × 1) cantilever beams of two stacking sequences

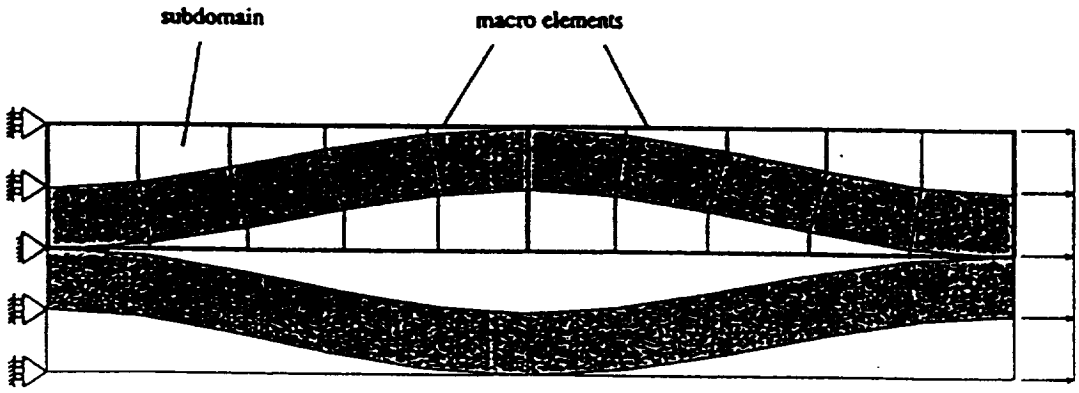

Figure 7. Two symmetrically stacked plain weave mats

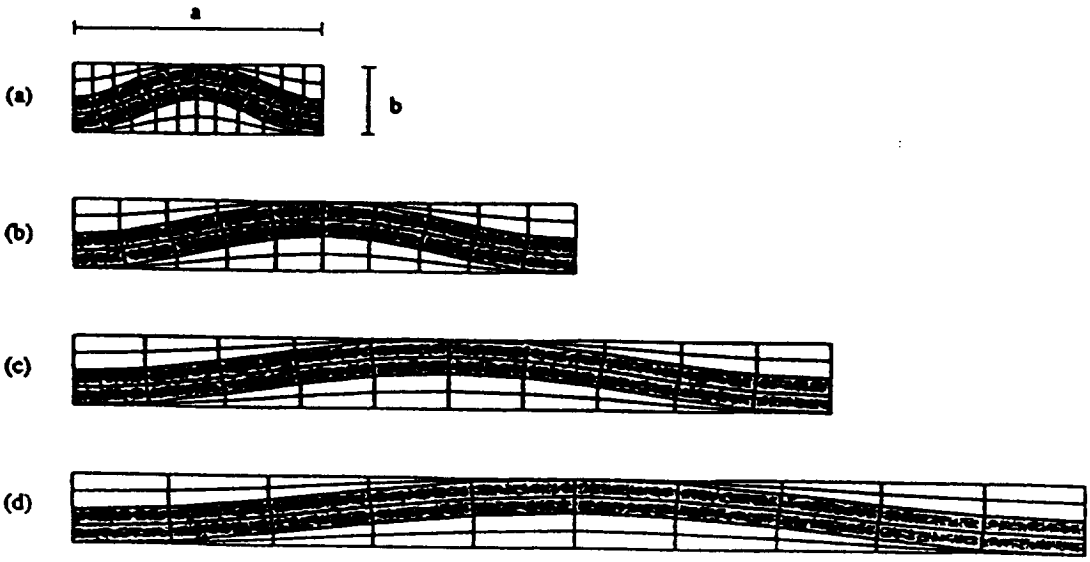

Figure 8. Several traditional meshes: (a) $b/a = 0{\cdot}333$, (b) $b/a = 0{\cdot}167$, (c) $b/a = 0{\cdot}111$, (d) $b/a = 0{\cdot}083$

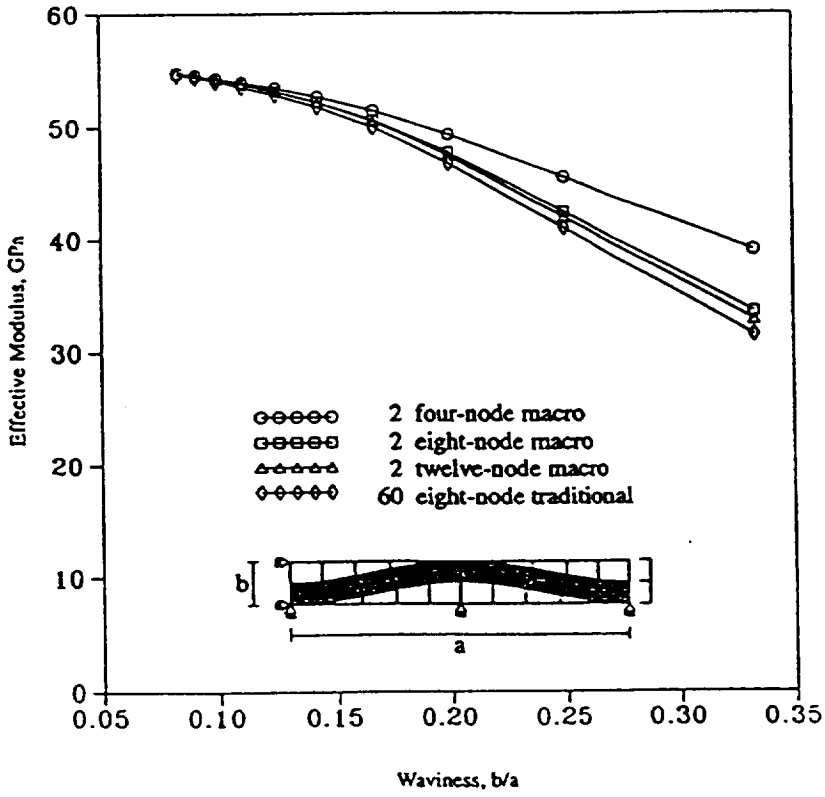

Figure 9. Extensional modulus against waviness

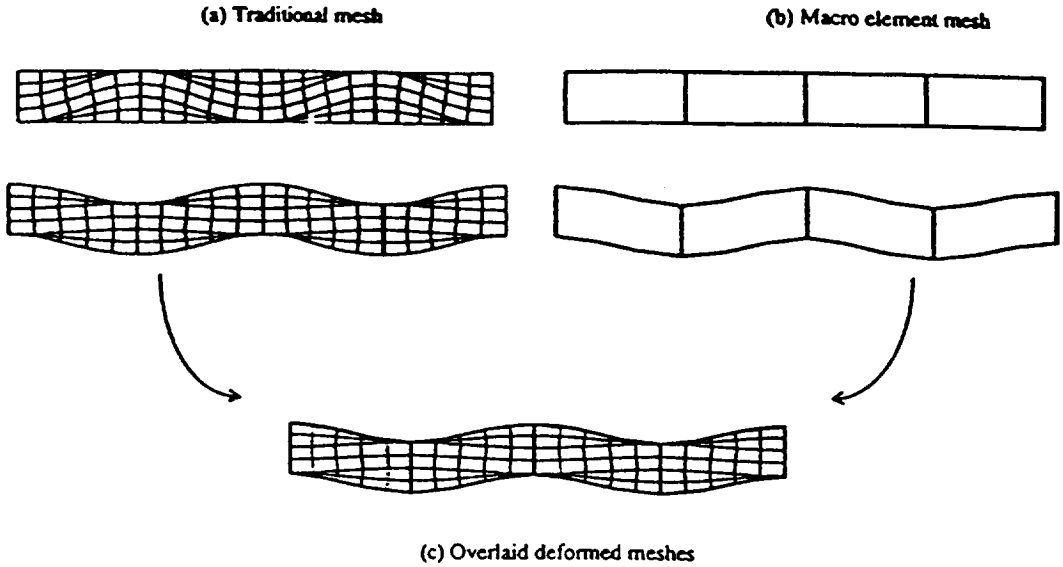

Figure 10. Deformed meshes for a single plain weave mat (120 eight-node traditional elements and 4 twelve-node macro elements are used; waviness $b/a = 0{\cdot}167$; nominal strain = 0·05)

Chapter: 3

ENHANCED DIRECT STIFFNESS METHOD FOR FINITE ELEMENT ANALYSIS OF TEXTILE COMPOSITES

ABSTRACT

Traditional homogenization techniques are not useful when the microstructural scale of a material is of the same order of magnitude as the structural scale of a component. Such is the case for many textile composites. Since discrete modeling of the microstructure throughout a component is prohibitively expensive, continuum finite elements are needed which account for microstructure within a single element. This paper describes a simple substructuring technique for formulating these special elements.

INTRODUCTION

By changing stacking sequence, fiber orientation, and materials, traditional composite laminates can be tailored for specific applications. With the introduction of advanced textile composites, there are even greater opportunities to tailor composite properties. Not only are there many textile forms (eg. weaves, braids, knits, etc.), but there are many unique varieties of each form.

Accurate predictive analyses are essential for designing high performance composites. In contrast to traditional tape laminates, verified analyses are not in place for textiles. Figure 1 illustrates the complexity of the task of developing an accurate textile analysis. The figure shows schematics of a traditional laminate and a woven material. For the traditional laminate one can define a unit cell of dimensions approximately .007 mm. This unit cell can be analyzed to determine effective engineering properties for the much larger individual lamina. Then each

lamina can be treated as a homogeneous orthotropic layer. For a woven composite the unit cell can be larger than 1mm. For the woven composite one can use homogenized engineering moduli to describe the tow properties (a tow contains on the order of 6000 filaments), but there is a much larger microstructural scale related to the interlocking of the tows.

Description of the material properties for a weave requires different strategies at different microstructural scales. Figure 2 illustrates different microstructural scales. Actually all of the schematics were generated from the same basic unit cell labeled "coarse microstructure." The term "coarse" refers to the very distinct phases at this level of observation. In contrast, if a very large number of unit cells are considered, the material appears almost homogeneous (schematic labeled fine microstructure). At the extremes of microstructural scale the choices for material modeling are obvious. For coarse microstructure the individual tows and matrix pockets are modeled discretely both in terms of geometry and the abrupt changes in properties at the interfaces. For fine microstructure effective homogenized engineering properties can be used. Traditional finite element methods are appropriate at these two scales. Between these two extremes (labeled "transitional microstructure") traditional finite elements are not appropriate. In this range there are too many microstructural features to model them all discretely, but there are too few to use homogenized material properties. In the transitional range of microstructure, special finite elements are needed which permit material variation within an element. Of course, this is routine for layered plate and shell elements.

Recently, continuum elements have been developed for accounting for textile type microstructure within a single element [1,2]. The elements described in these references are based on a single assumed displacement field throughout the entire element. A more general element formulation is presented herein that includes the single field approximation as a degenerate case. This more general formulation is an example of reduced substructuring [3]. In brief, the implementation begins with the development of an ordinary finite mesh for the basic textile unit cell. Then interior degrees of freedom are statically condensed out. Next the number and location of desired boundary degrees of freedom are selected. Finally, the original boundary degrees of freedom are expressed in terms of the desired boundary degrees of freedom. One objective of this paper is to describe a very simple technique for calculating the stiffness matrix for a reduced substructure. The other objective is to show a few results which illustrate the effectiveness of this type of element.

In the discussion that follows, the term "macro element" will be used to indicate an element which allows for internal microstructure. Accordingly, the elements described in [1,2] are single-field macro elements. Similarly, the reduced substructure elements will be referred to as multi-field macro elements, since the displacement field inside the macro element is defined piecewise.

THEORY FOR REDUCED SUBSTRUCTURING

In multi-field elements the internal dof are eliminated using the equivalent of static condensation. Also, boundary degrees of freedom (dof) which are not to be part of the macro element dof are expressed in terms of the substructure dof using multipoint constraints.

Theoretically, this is all very simple. Con ider the 4-node macro element in Figure 3.

Assume the governing equations are partitioned as follows

$$\begin{bmatrix} K_{AA} & K_{AB} \\ K_{AB}^T & K_{BB} \end{bmatrix} \begin{bmatrix} q_A \\ q_B \end{bmatrix} = \begin{bmatrix} F_A \\ F_B \end{bmatrix} \tag{1}$$

and q_A is the list of unknowns to be condensed out (see Figure 3).

Before imposing the multipoint constraints on the excess boundary dof, the reduced stiffness matrix and load vector can be expressed as

$$\begin{aligned} \bar{K}_{BB} &= K_{BB} - K_{AB}^T K_{AA}^{-1} K_{AB} \\ \bar{F}_B &= F_B - K_{AB}^T K_{AA}^{-1} F_A \end{aligned} \tag{2}$$

This procedure often is not practical as stated because of the matrix inversion which eliminates sparsity in K_{AA} and the large matrix multiplications. The elimination of internal dof can also be accomplished using Gaussian elimination if the dof to be eliminated are grouped together at either the beginning or the end of the list of unknowns. This procedure is well known, so it will not be discussed herein. See [4] for details. After eliminating the interior dof, multipoint constraints can be applied to the remaining dof to eliminate unwanted boundary dof. This can be expressed in matrix form (assuming the four node macro element in Figure 3) as

$$q_B = T q_{macro} \qquad \text{where } q_{macro} = \begin{bmatrix} u_{11} \\ v_{11} \\ \vdots \\ u_{14} \\ v_{14} \end{bmatrix} \tag{3}$$

The transformation matrix T expresses how the excess boundary dof are slaved to the macro element dof. It should be noted that if the internal dof are also slaved to the macro element dof (rather than statically condensed), a single-field approximation is obtained. Of course, a formulation like that in [1] is much more efficient for single-field elements. However, the current formulation permits great flexibility for evaluating various approximations.

It is not always efficient to order the dof such that Gaussian elimination can be used to obtain the reduced stiffness matrix and load vector, since such ordering might result in large bandwidths. An alternative is to use the formal definition of the stiffness coefficient K_{ij}.

K_{ij} = force at dof i due to unit displacement at dof j

Using this definition we would simply solve a series of problems in which one dof is set equal to 1 and the rest of the boundary dof would be constrained to zero. The restraint forces at all the boundary dof constitute one column of the reduced stiffness matrix.

This process is repeated for each boundary dof to obtain the entire reduced stiffness matrix. The reduced load vector is obtained by solving one additional problem in which all boundary dof are constrained to be zero and the internal loads are applied. The negative of the boundary restraint forces constitute the reduced load vector contribution for the internal loads. Once the reduced set of equation is obtained, the multipoint constraints can be imposed to eliminate unwanted boundary dof. This alternative is not new. It can be considered a numerical application of the direct stiffness method for calculating stiffness matrices. It also may not be very efficient when there are a large number of boundary dof to be eliminated. Consider a case in which there are 32 boundary dof, but only 8 are to be retained in the macro element. The procedure described above requires the solution of 32 unit displacement cases. A new procedure is discussed next which would only require 8 unit displacement solutions.

ENHANCED DIRECT STIFFNESS METHOD

The enhanced direct stiffness method is derived starting with a consideration of the work performed by the boundary nodal forces during deformation. To simplify the discussion only linear configurations will be considered herein. Figure 3 show a schematic of a typical mesh for a macro element. There are four interior nodes (nodes 1, 2, 3, 4), four boundary nodes to be retained (nodes 11, 12, 13, 14; dof $\equiv q_i$), and six boundary nodes (nodes 5, 6, 7, 8, 9, 10; dof $\equiv \bar{q}_\beta$) which are slaved to the q_i through multi-point constraints. The nodal forces corresponding to q_i and $\bar{q}_\beta$ are defined to be F_i and $\bar{F}_\beta$, respectively. For the particular mesh in Figure 3, the range of i and β are 1-8 and 1-12, respectively. Assuming linear elasticity, the work performed by the boundary nodal forces is

$$W = \frac{1}{2}\left(F_i q_i + \bar{F}_\beta \bar{q}_\beta\right) \quad , \qquad i = 1, \text{number of retained dof}, \quad \beta = 1, \text{number of slaved dof} \tag{4}$$

The $\bar{q}_\beta$ are slaved to the q_i, which can be expressed as

$$\bar{q}_\beta = T_{\beta i} q_i \tag{5}$$

where $T_{\beta i} = N_i(\zeta_\beta, n_\beta)$ is calculated using interpolation functions for the boundary. Combining equations 4 and 5 yields

$$W = \frac{1}{2}\left(F_i q_i + \bar{F}_\beta T_{\beta i} q_i\right) \tag{6}$$

It is well known that the stiffness matrix can be expressed as [5]

$$K_{mn} = \frac{\partial^2 U}{\partial q_m \partial q_n} \tag{7}$$

But U = W for linear configurations so that

$$K_{mn} = \frac{\partial^2 W}{\partial q_m \partial q_n} \tag{8}$$

Combining eqns. 6 and 8 yields

$$K_{nm} = \frac{1}{2}\left[\frac{\partial F_n}{\partial q_m} + \frac{\partial F_m}{\partial q_n} + \frac{\partial \bar{F}_\beta}{\partial q_m} T_{\beta n} + \frac{\partial \bar{F}_\beta}{\partial q_n} T_{\beta m}\right] \tag{9}$$

From the Maxwell-Betti reciprocity theorem we know that $\frac{\partial F_n}{\partial q_m} = \frac{\partial F_m}{\partial q_n}$. The third and fourth terms in equation 9 are also equal for the same reason, but it is not obvious in the present form. To make the equivalence more obvious, first, equate the work of the forces $\bar{F}_\beta$ with that of the equivalent forces $\bar{f}_i$ in terms of the retained dof

$$\frac{1}{2}\bar{F}_\beta \bar{q}_\beta = \frac{1}{2}\bar{f}_i q_i \tag{10}$$

Combine equations 5 and 10 to obtain

$$\bar{F}_\beta T_{\beta i} q_i = \bar{f}_i q_i \tag{11}$$

Equation 11 shows that the equivalent nodal forces $\bar{f}_i$ are

$$\bar{f}_i = \bar{F}_\beta T_{\beta i} \tag{12}$$

Hence, the third and fourth terms in equation 9 become

$$\frac{\partial \bar{f}_n}{\partial q_m} + \frac{\partial \bar{f}_m}{\partial q_n} \tag{13}$$

Again, using the Maxwell-Betti theorem, these two terms are equal. Therefore, equation 9 can be expressed as

$$K_{mn} = \frac{\partial F_n}{\partial q_m} + \frac{\partial \bar{f}_n}{\partial q_m} \tag{14}$$

The implementation of equation 14 using the direct stiffness method is as follows:

1. Impose a unit displacement q_1.
2. Also impose displacements $\bar{q}_\beta$, since $\bar{q}_\beta = T_{\beta 1} q_1$.
3. Analyze model.
4. Calculate restraint forces F_n and $\bar{F}_\beta$.
5. Calculate $\bar{f}_n = \bar{F}_\beta T_{\beta n}$
6. The sum of F_n and $\bar{f}_n$ = column 1 of the reduced stiffness matrix.
7. Repeat steps 1-6 for each q_i.

CONFIGURATIONS

Plain weave composites with different waviness were analyzed. Figure 4 shows a conventional 3D finite element model of a plain weave. It has 381 nodes and 64 quadratic elements. The tow path was assumed to the sinusoidal. The waviness ratio is defined to be b/a, where b = the mat thickness and a = the wavelength for the tows. The waviness ratio was varied from .033 to .33.

This mesh was used to obtain reference solutions. It was also used to generate 20-node single-field and multi-field macro elements. Hence, there were three models: the conventional model shown in Figure 4, a one element mesh using a 20-node single field element, and a one element mesh using a 20-node multi-field element. The single-field results were obtained using the formulation in [1].

Two sets of boundary conditions were used: one for a narrow two mat composite and the other for an infinitely repeating unit cell. The boundary conditions for the narrow two mat case correspond to a specimen which is infinitely long in the x-direction, width "a" in the y-direction, and thickness $2b$ in the z-direction. The boundary conditions were as follows.

Narrow two mat composite:

$$u(0,y,z) = 0 \qquad u\left(\frac{a}{2},y,z\right) = \text{specified constant value}$$
$$v(x,0,z) = 0 \qquad (15)$$
$$w(x,y,0) = 0$$

Infinitely repeating unit cell:

Constraints listed in equation (15) and

$$v\left(x,\frac{a}{2},z\right) = \text{constant}$$

$$w(x,y,b) = \text{constant}$$

The material properties for the tows and resin pockets were assumed to be

Tows:

E_{11} = 206.9GPa	E_{22} = 5.171GPa	E_{33} = 5.171GPa
ν_{12} = .25	ν_{13} = .25	ν_{23} = .25
G_{12} = 2.386GPa	G_{13} = 2.386GPa	G_{23} = 2.386GPa

Resin:

E = 3.45GPa $\quad \nu$ = .35

RESULTS AND DISCUSSION

There are two aspects to the evaluation of the procedures outlined in this paper. First, the methodology for calculating the multi-field stiffness matrix was checked. This was accomplished by comparing the stiffness matrix with that obtained using standard Gaussian elimination followed by application of multipoint constraints. As expected, the results agreed. The second task is to evaluate the performance of the multifield elements for analysis of textile composites. This second task is only partially complete. A few results are discussed in this section which suggest that this type of element can be very useful.

Axial loading along the x-direction of a narrow strip of plain weave composite was modeled, as described in the Configuration section. Because of the complex spatial variation of materials properties, there is significant distortion, even under simple extension. Figure 5 shows the distortion of the macro element mesh and the conventional mesh. The macro element predicts the distortion quite well. (It should be noted that the elements in Figure 5 are drawn with straight lines joining the nodes. This is a limitation of the plotting software, not a characteristic of the solution.)

Figures 6 and 7 show the variation of several effective engineering properties with waviness ratio for infinitely repeating unit cells. Results are shown for conventional, single-field, and multi-field elements. Both types of macro elements predict the trends quite well. As expected, the performance of the multi-field elements is considerably better than that for the single-field elements. The accuracy of the multi-field elements is quite good except for very large waviness ratios. At small waviness ratios the single-field macro elements predict the in-plane behavior very well, but not the out-of-plane (*ie*, E_z, ν_{xz}). The single-field approximation imposes strain continuity throughout the element, which is not correct for heterogeneous regions. The error associated this approximation is more significant for out-of-plane properties than for in-plane properties.

CONCLUSIONS

A simple formulation for multi-field continuum finite elements with microstructure was developed. Initial tests showed very good performance in modeling the global response of a plain weave composite subjected to axial extension. Much more work is needed to fully evaluate the performance of these elements. Future work is needed (and is planned) to evaluate the accuracy of these elements for much more complex loadings. Also, planned is an evaluation of the accuracy of the calculated stress fields within the elements.

REFERENCES

1. Woo, K. and Whitcomb, J.D.: Macro Finite Element Using Subdomain Integration. OTRC Report 03/92-A-29-100, Texas A&M University, March 1992.

2. Foye, R.L.: The Mechanics of Fabric-Reinforced Composites. Proceedings of Fiber-Tex Conference, September 1988. NASA Conference Publication 3038, pp. 237-247.

3. Kamel, H.; Liu, D.; McCabe, M.; and Phillipopoulos, V.: Some Developments in the Analysis of Complex Ship Structures, in *Advances in Computational Methods in Structural Mechanics and Design*, J.T. Oden, et al. (eds.), U. of Alabama Press, University, Ala., 1972, pp. 703-726.

4. Cook, R.D.; Malkus, D.S.,; and Plesha, M.E.: Concepts and Applications of Finite Element Analysis, Third Edition, John Wiley & Sons, 1989.

5. Zienkiewicz, O.D. and Taylor, R.L.: The Finite Element Method, 4th ed., Vol. 1: Basic Formulation and Linear Problems, p. 232, McGraw Hill Book Company, 1989.

6. Jones, R.M.: Mechanics of Composite Materials, p. 70, Hemisphere Publishing Corporation, 1975.

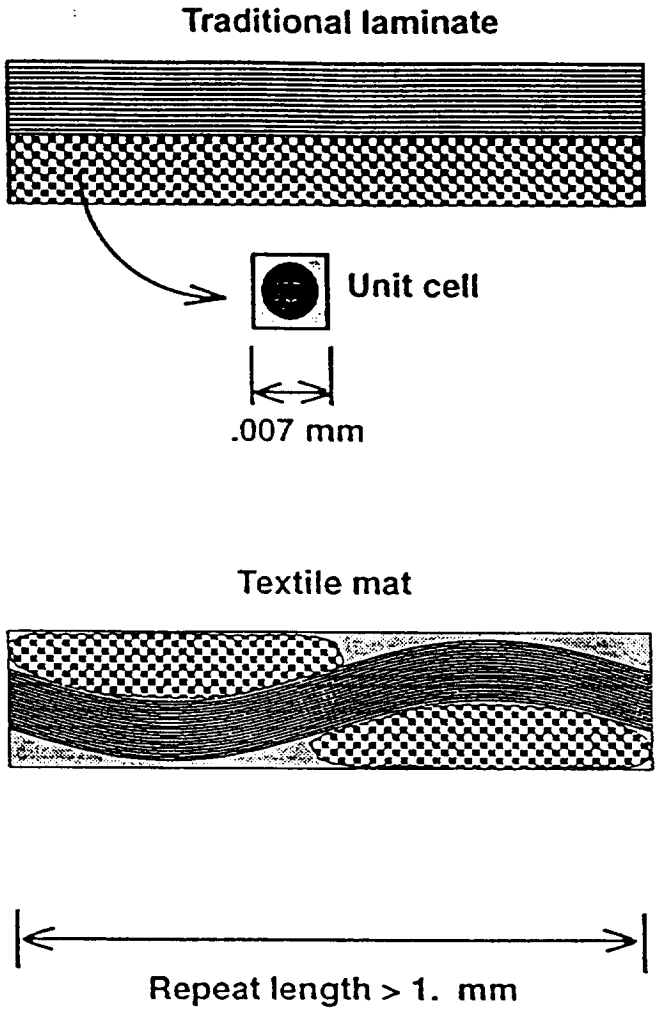

Fig. 1 Comparison of microstructural scales for traditional and textile composites.

fig1.topdraw

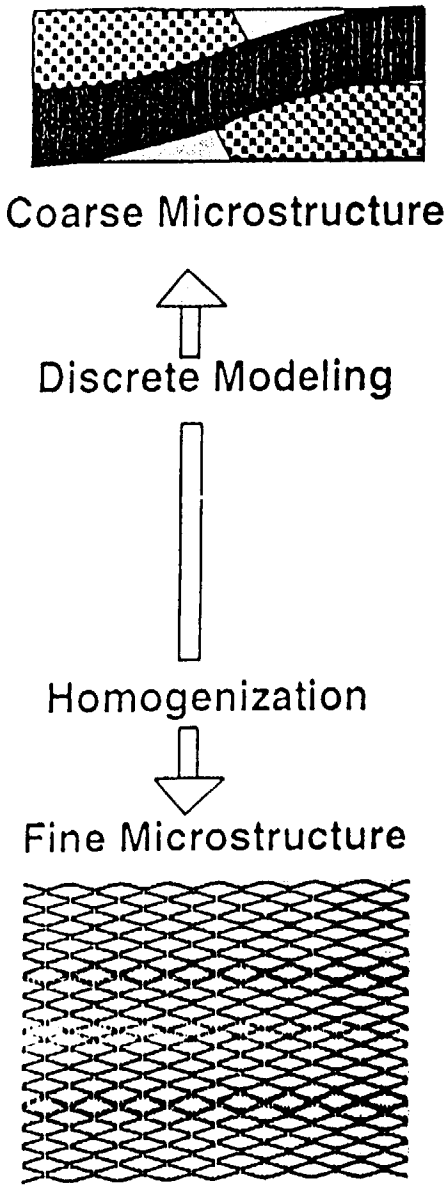

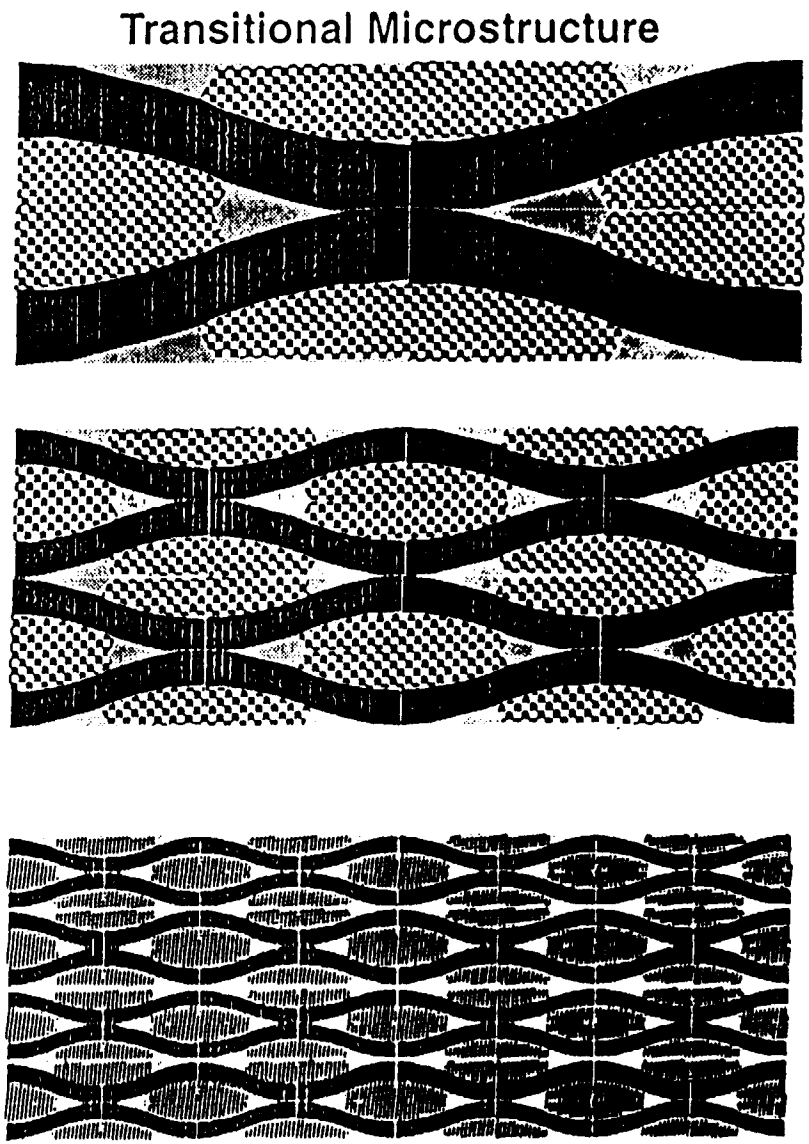

Figure 2 Range of microstructural scales.

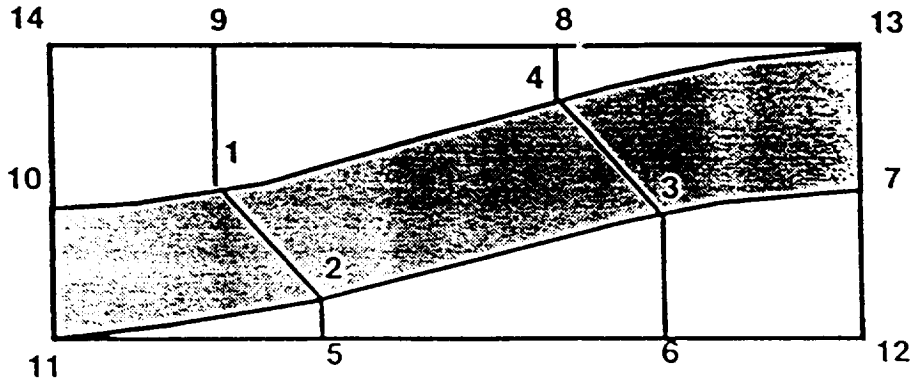

$$q_A = \begin{bmatrix} u_1 \\ v_1 \\ \vdots \\ u_4 \\ v_4 \end{bmatrix} \qquad q_B = \begin{bmatrix} u_5 \\ v_5 \\ \vdots \\ u_{14} \\ v_{14} \end{bmatrix}$$

Figure 3 Finite element mesh for substructure analysis.

fig3.topdraw

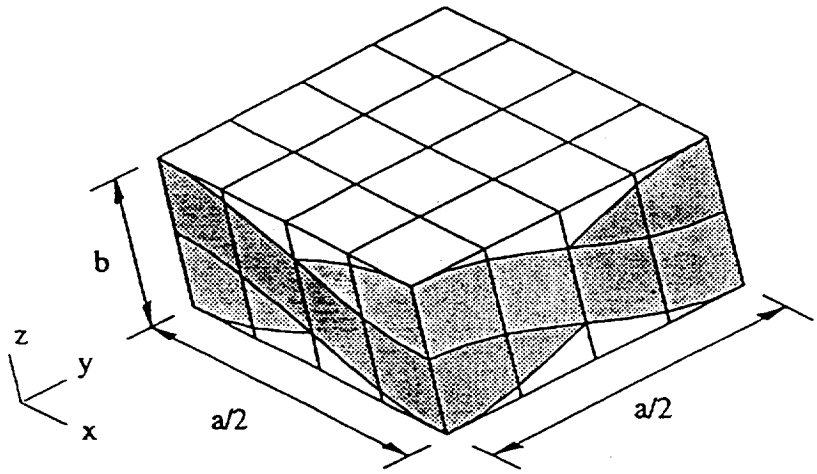

Waviness Ratio = b/a

Figure 4 Original finite element mesh for textile composites. (381 nodes, 64 elements)

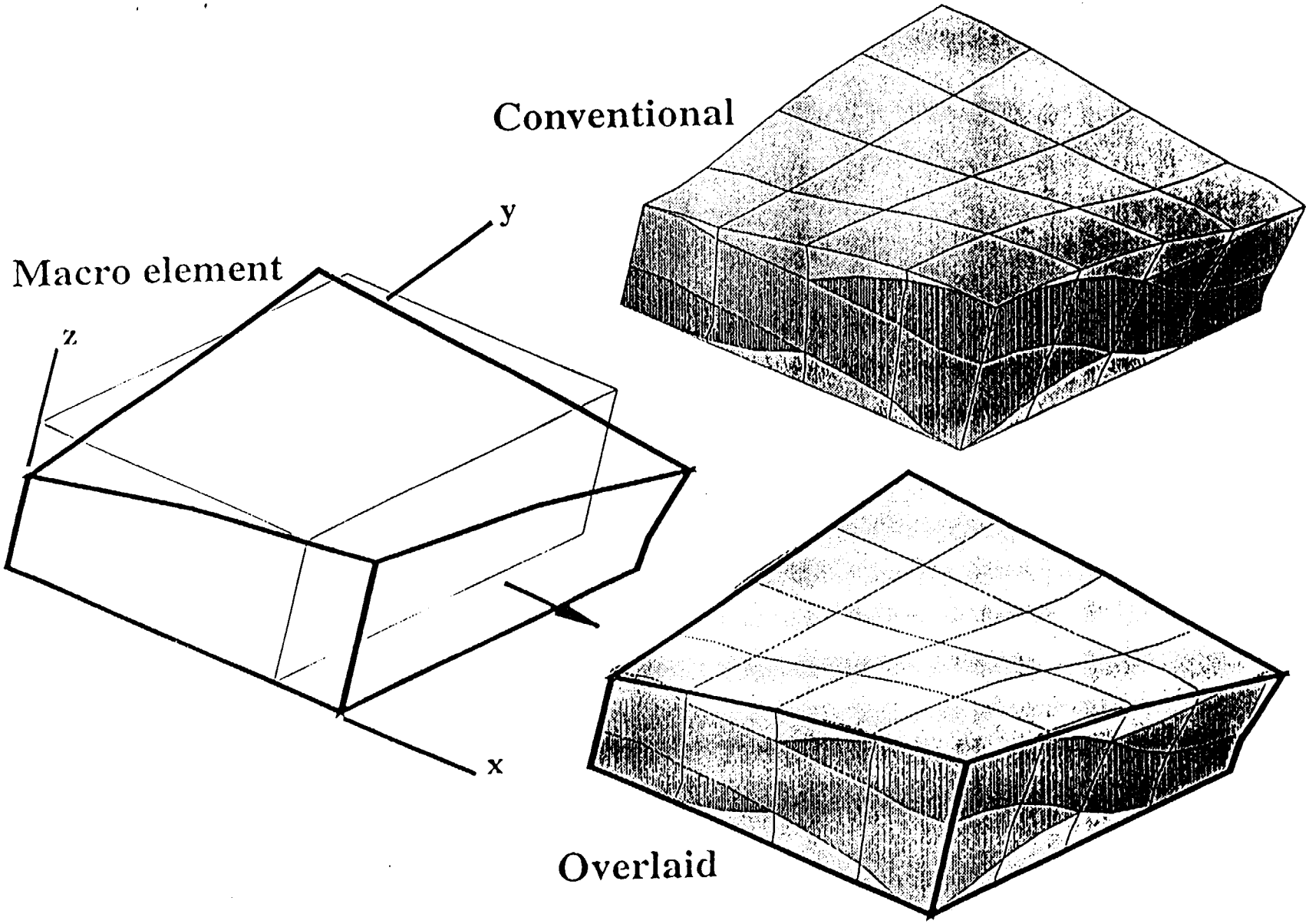

Figure 5 Deformation of multi-field macro element and conventional finite element models.

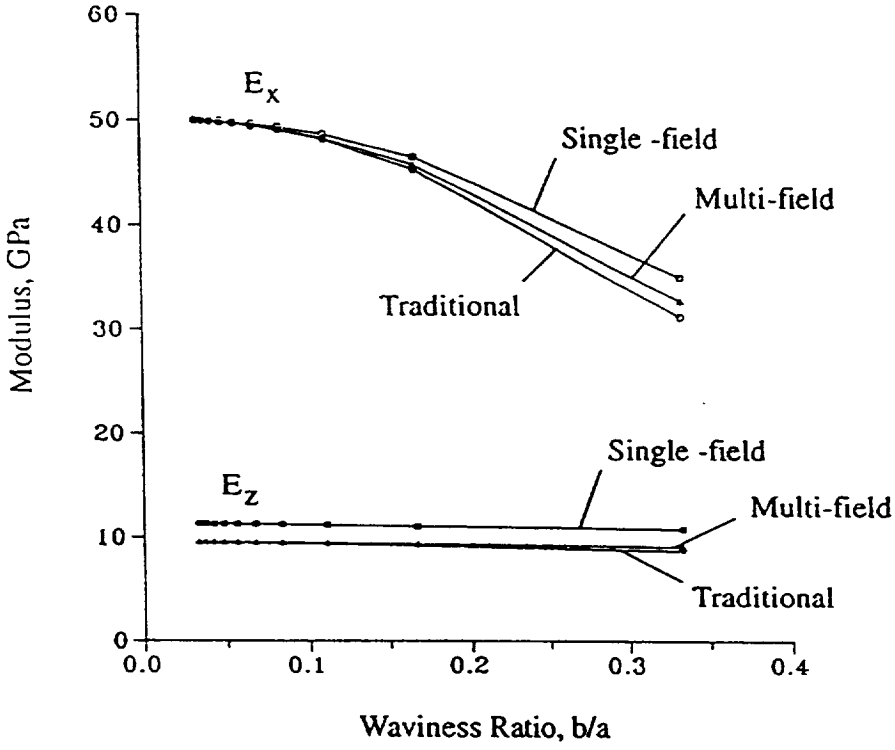

Figure 6 Extensional moduli versus waviness ratio for infinitely repeating plain weave textile composites.

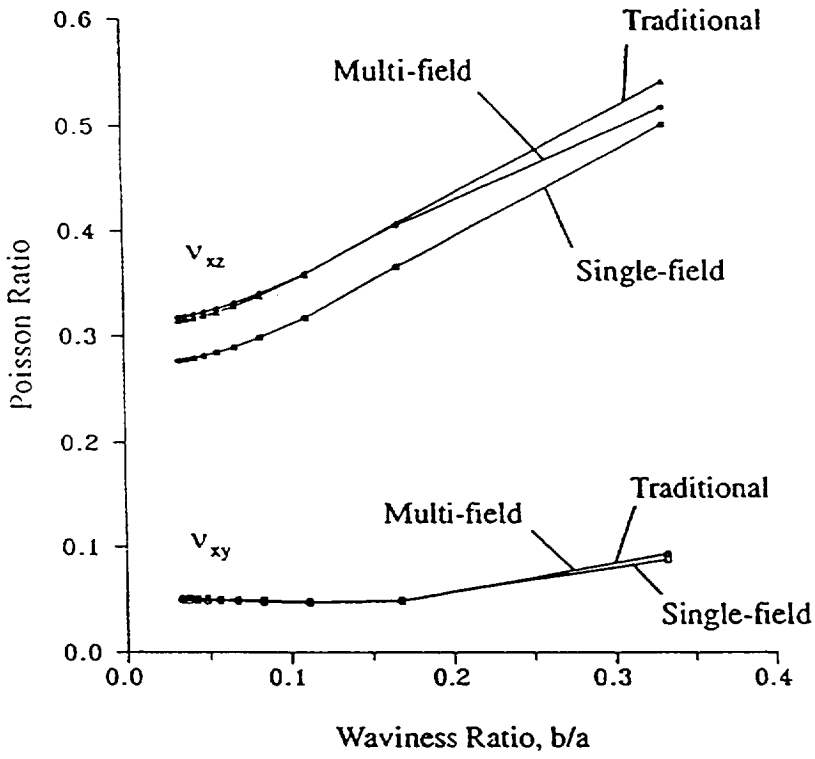

Figure 7 Poisson ratio versus waviness ratio for infinitely repeating plain weave textile composites.

Chapter: 4
Boundary Effects in Woven Composites

Abstract

Two dimensional finite elements were used to study boundary effects in plain weave composite specimens subjected to extension, shear, and flexure loads. Effective extension, shear, and flexural moduli were found to be quite sensitive to specimen size. For extension and flexure loads stress distributions were affected by a free surface, but the free surface boundary effect did not appear to propagate very far into the interior. For shear load the boundary effect appeared to propagate much further into the interior.

Key Words: textiles
woven composites
finite elements
stress analysis
boundary effects

Introduction

Fiber tows, each consisting of thousands of individual filaments, can be woven, braided, knitted, etc. to create complex fiber preforms. These preforms are then impregnated with a resin and cured to make textile composites. The interlacing of the fiber bundles provides many obstacles to damage growth. Accordingly, there is the potential for greatly improved resistance to impact damage growth. Unfortunately, there are also negative effects due to the fiber tow interlacing. The fiber tow curvature reduces the effective in-plane moduli. The curvature also

induces many local stress concentrations which can result in early diffuse damage initiation, particularly in the matrix. The fabrication process is not benign. For example, weaving involves much mechanical handling of unprotected fibers (i.e. fibers which are not embedded in matrix). Stitching of textile preforms to increase delamination resistance has the side effects of breaking fibers and inducing local fiber curvature. Optimal design requires the capability to predict both the positive and negative effects of potential textile fiber architectures. Unfortunately, the complex fiber architecture is difficult to analyze. Accurate analysis requires accurate geometric representation and constituent properties, such as fiber and matrix properties and fiber volume percentage. For textile composites there is particular difficulty in determining the actual fiber tow geometry and developing a three-dimensional model which can be analyzed. There have only been a few attempts at detailed three dimensional analysis (eg. Refs. [1-3]). Even the accuracy of these models for local stress calculation is an open question because of the uncertainties in the input data (i.e. the approximation of tow geometry and other properties). Most of the analyses to date have been similar to laminate theory in level of approximation or detailed two dimensional (2D) or quasi-three-dimensional (Q3D) numerical analyses of a "representative" cross-section (eg. Refs. [4-7]). As the schematic in Figure 1 shows, there is no such "representative" cross-section, even for a plain weave composite. While such 2D or Q3D analyses are likely insufficient for accurate prediction of local stress states, they are useful for obtaining insight about the effects of fiber tow waviness on effective moduli and strengths. In fact, the results in this paper, which are based on 2D analyses, fall into this category.

The analysis of textile composites is in its infancy as compared to laminated composites. There are many aspects of the behavior of these materials which have not even been examined, much less accurately described. The objective of this paper is to begin to address one question

about the behavior of plain weave composites: "How does the presence of a boundary affect the stiffness and stress distribution in a representative unit cell?" The boundary surfaces referred to here are those present due to finite thickness. Three nominally simple boundary conditions were considered herein: in-plane extension, transverse shear, and flexure. Configurations of different thicknesses were analyzed using 2D finite elements. The analyses were performed using conventional elements and multi-field macro elements (reference 8). Macro elements are defined to be elements which contain internal microstructure. The multi-field elements are a form of reduced substructuring. The macro elements permitted analysis of quite large models without requiring huge amounts of computer memory and cpu time. Of course, a few macro elements are not as accurate as using a huge collection of conventional elements. Accordingly, one additional objective of the paper is to evaluate the performance of macro elements for simple configurations.

The following sections will begin with a discussion of the configurations studied. Then the results will be discussed. First effective extensional, shear, and flexural moduli will be discussed. Then the effects of boundaries on stress distributions will be discussed.

Configurations

The various configurations studied are all synthesized from a single basic unit cell. This unit cell will be discussed first. Then boundary conditions for infinite and finite configurations will be discussed.

Unit Cell

The basic unit cell is shown in Figure 2 . The cell consists of tows running in the x- and z- directions. In reality there would also be pure matrix pockets, but these were filled with z-

direction tows in the model used. (Of course, in reality there is no typical cross section either, as discussed earlier.) The two dimensional approximation implies that the x- direction tow is a wavy "plate" and the z-direction tows are straight fiber bundles. Obviously these are serious approximations, so the results presented are intended to be qualitative only. The centerline of the x-direction tows follows a wavy path described by the function $\frac{\beta}{4}\sin\frac{\pi x}{\alpha}$. For the results presented herein $\alpha = 1.5\beta$. The thickness of the tow as measured along a line normal to the tow centerline was held constant. It should be noted that the unit cell selected assumes a symmetric stacking of the woven mats. There are an infinite number of other possibilities.

Two sets of two material properties were used. They are

Set I

E_{11} = 100 GPa	E_{22} = 10 GPa	E_{33} = 10 GPa
ν_{12} = 0.35	ν_{13} = 0.35	ν_{23} = 0.3
G_{12} = 5 GPa	G_{13} = 5 GPa	G_{23} = 3.845 GPa

Set II

E_{11} = 165.8 GPa	E_{22} = 11.51 GPa	E_{33} = 11.51 GPa
ν_{12} = 0.273	ν_{13} = 0.273	ν_{23} = 0.33
G_{12} = 15.4 GPa	G_{13} = 15.4 GPa	G_{23} = 4.17 GPa

These properties were transformed to account for the waviness of the x-direction tow. Plane strain conditions were imposed to obtain two dimensional properties. Two sets of properties were used. This is admittedly not optimal. The homogenization analyses were performed using Set I. The stress analysis results were obtained using Set II.

Periodic Boundary Conditions for Infinite Configurations

Figure 2 shows a typical unit cell for symmetrically stacked mats before deformation. If this cell is imbedded within an infinite array of identical cells and displacements or tractions are imposed "at infinity", then every unit cell will deform identically. The periodicity of the displacement field can be imposed on a single unit cell, thus permitting the solution for the infinite domain. The solution for an infinite domain will be useful for comparison with finite configurations subjected to nominally uniform extension or shear. Using the coordinate system in Figure 2a, the periodic conditions can be expressed as

$$u(\alpha,y) = u(-\alpha,y) + u_2 - u_1 \tag{1}$$

$$v(\alpha,y) = v(-\alpha,y) + v_2 - v_1 \tag{2}$$

$$u(x,\beta) = u(x,-\beta) + u_4 - u_1 \tag{3}$$

$$v(x,\beta) = v(x,-\beta) + v_4 - v_1 \tag{4}$$

There are no specified non-zero forces (The net forces are zero at any point inside the infinite media.). The "load" consists of the values chosen for $(u_2 - u_1)$, $(v_2 - v_1)$, etc. These values depend on the nominal strain state desired. (Specific values for the different states will be discussed later in this section. Equations 1-4 impose certain constraints which are not so obvious, but are worth mentioning, since they are exploited in the finite element analysis. These constraints are

$$u_3 - u_4 = u_2 - u_1 \tag{5}$$

$$v_3 - v_2 = v_4 - v_1 \tag{6}$$

$$u_3 - u_2 = u_4 - u_1 \tag{7}$$

$$v_3 - v_4 = v_2 - v_1 \tag{8}$$

These constraints can be obtained from equations 1-4 by substituting in specific vertex values of x and y. For example, substitute $x=\alpha$ into equation 3.

$$u(\alpha,\beta) = u(\alpha, -\beta) + u_4 - u_1$$

But $u(\alpha,\beta) = u_3$ and $u(\alpha, -\beta) = u_2$. Hence, equation 3 states that $u_3 - u_2 = u_4 - u_1$. Equations 5-8 indicate that if the nodal displacements at the four corners of the unit cell are used to calculate the displacement gradients, we find that $\left(\frac{\partial u}{\partial x}\right)_0$, $\left(\frac{\partial v}{\partial x}\right)_0$, $\left(\frac{\partial u}{\partial y}\right)_0$, and $\left(\frac{\partial v}{\partial y}\right)_0$ are constant. The subscript "0" is used to indicate that these are nominal displacement gradients. On a pointwise basis these are certainly not constant for the obviously inhomogeneous unit cells. Equations 1-4 can now be expressed as

$$u(\alpha,y) = u(-\alpha,y) + 2\alpha\left(\frac{\partial u}{\partial x}\right)_0 \tag{9}$$

$$v(\alpha,y) = v(-\alpha,y) + 2\alpha\left(\frac{\partial v}{\partial x}\right)_0 \tag{10}$$

$$u(x,\beta) = u(x, -\beta) + 2\beta\left(\frac{\partial u}{\partial y}\right)_0 \tag{11}$$

$$v(x,\beta) = v(x, -\beta) + 2\beta\left(\frac{\partial v}{\partial y}\right)_0 \tag{12}$$

Because of symmetries only part of the unit cell must be modeled. Herein the quarter unit cell shown in Figure 2(b) was modeled. If all the symmetries had been exploited, only one-eighth of the unit cell would have to be modeled. For convenience the coordinate system is shifted to the center in Figure 2(b).

For extension loading the boundary conditions are quite simple. The constraints imposed for nominal σ_x loading are

$$u\left(-\frac{\alpha}{2}, y\right) = 0 \qquad u\left(\frac{\alpha}{2}, y\right) = \text{specified constant value}$$
$$v\left(x, -\frac{\beta}{2}\right) = 0 \qquad v\left(x, \frac{\beta}{2}\right) = \text{constant, but unknown} \tag{13}$$

Nominal σ_y loading (which was not considered herein) would be very similar. For nominal σ_{xy} load the boundary conditions are

$$u\left(x, \frac{-\beta}{2}\right) = -u\left(x, \frac{\beta}{2}\right) = \text{specified constant value}$$

$$v\left(\frac{-\alpha}{2}, y\right) = -v\left(\frac{\alpha}{2}, y\right) = \text{specified constant value} \tag{14}$$

$$u\left(\frac{-\alpha}{2}, -y\right) = -u\left(\frac{\alpha}{2}, y\right)$$

$$v\left(-x, \frac{-\beta}{2}\right) = -v\left(x, \frac{\beta}{2}\right)$$

The boundary conditions in equations 14 state that the displacements normal to an edge are anti-symmetric (and unknown except at the vertices). The tangential displacements are constant along an edge and are specified.

Boundary Conditions for Finite Configurations

Extension, shear, and flexure loading were considered for a wide range of specimen thickness (in the y-direction). Hence, the various meshes had different numbers of unit cells. For extension loads the boundary conditions were like those in equation 13 if one considers α

and β to be the dimensions of the entire mesh, rather than just a quarter unit cell except that the top surface was traction free. Hence, the normal displacement "v" was not constrained to be constant along the top. For shear load all boundary displacements were constrained to follow the deformation u = cy and v = cx. Consequently, the boundaries remained straight after deformation for shear loading.

For flexure loads the top and bottom surfaces of the model were traction free. A linear variation of normal displacements were imposed on left and right ends of the model.

Results and Discussion

There are two types of results which will be discussed. The first will illustrate the effect of specimen thickness on effective moduli. The second will illustrate the effect of unit cell location on stress distributions.

Effective Moduli

For nominally simple deformation states, the effective engineering properties are expected to converge to constant values as the specimen thickness increases. Figure 3 shows the variation of the normalized effective E_x. Figure 3a shows the variation of the average E_x with the number of unit cells. The E_x is normalized by the E_x for an infinite array of unit cells modeled using conventional finite elements. The three curves were obtained using conventional finite elements and 8-node and 12-node multi-field macro elements. The 8-node macro element must be inherently a little too stiff, since it converges to a value approximately one percent too large. The 12-node macro element agrees very well with the conventional finite element results. For 8 unit cells through the thickness the effective E_x is within about one percent of convergence. This indicates that a specimen would need to be 8 unit cells thick to give an effective E_x within

one percent of a very thick specimen. Figure 3b shows the variation of the effective E_x with position for a configuration which has eight unit cells through the thickness. The effective E_x for each quarter unit cell was calculated based on the strain energy in the region. This is not a rigorous definition, but it does offer some insight. The figure shows that the boundary quarter unit cell is about 18 percent softer than an interior quarter unit cell. The next quarter unit cell is about 5 percent too stiff. The third quarter unit cell has almost exactly the same stiffness as cells which are much further from the boundary. There is an obvious boundary effect, but it dies out very quickly.

Figure 4 shows the effect of model size on normalized effective shear modulus G_{xy}. In contrast to E_x, the shear modulus converges from the stiff side. This difference is a consequence of the boundary conditions imposed. For E_x there were free surfaces. The traction free condition permitted warping deformation to occur more easily near the free surface than in the interior, so the boundary caused softening. In contrast, all of the finite size shear specimens had specified x- and y- displacements over the entire boundary. This fully constrained boundary deformation resulted in larger effective G_{xy} for smaller specimens. Figure 4 also shows that 8-node macro elements perform poorly in shear. The 12-node macro elements perform quite well. It is interesting to note the distribution of the strain energy in a finite size shear model. The bar chart in Fig. 5 shows the strain energy in each quarter unit cell for a 3x3 array of unit cells. The effect of the boundary on the strain energy distribution is obviously quite complex.

Figure 6 shows the variation of normalized flexural modulus with model size. The flexural modulus is defined to be (flexural stiffness)/I, where I = the second moment of the area. The flexural modulus in Figure 6 is normalized by the value for a configuration which is

ten cells thick. The flexural modulus converges more slowly than the extensional modulus. The 12-node macro element performs very well. The 8-node macro element is a little too stiff.

Stress Distributions

Figures 7-9 illustrate the effect of a free surface on stress distributions. Distributions are shown for extension, shear, and flexure. The stresses shown are evaluated with respect to the xy (global) coordinate system.

Figure 7 shows the stress distributions for extension loading for three unit cells from two different configurations. One configuration had two unit cells through the thickness. The other had six unit cells through the thickness. The locations of the unit cells considered are indicated by shading in the figures. The waviness of the x-direction tow and the inhomogeneity causes a complicated variation of all three stresses. The σ_x variation in the longitudinal tow is dominated by flexure induced by tow straightening, as shown by the locations of maximum and minimum σ_x. The σ_y is largest where the tows contact. The σ_{xy} is largest where the tow rotation is largest.

There are both striking similarities and differences in the stress distributions for the three unit cells. Figure 7 shows that the interior and exterior unit cells have very different stress distributions. There is obviously a significant free surface effect. The exterior unit cells in Figure 7 have very similar distributions for all three stress components. This suggests that for extension load the response of the exterior unit cells is not very sensitive to the total specimen thickness.

The interior unit cell exhibits almost the same symmetries that one would expect from a cell embedded inside an infinite array. Also, the interior half of the exterior unit cells has stress distributions which are very close to those for the lower half of the interior unit cell. Apparently the free surface effect does not propagate very far into the interior.

Figure 8 shows the stress distributions for shear loading. Single unit cell and 3x3 unit cell configurations were studied. Only the σ_y and σ_{xy} distributions are shown, since σ_x was quite small. In this case there are no free surfaces. (Displacements were specified along the entire boundary.) As was the case for extension, the interior and exterior response is different. The interior unit cell is located in the middle of the finite element model. Hence, the symmetries exhibited by the interior cell do not indicate the attenuation of boundary effects. In contrast to extension load, Figure 8 shows that for shear load the response of the boundary unit cells is very sensitive to total specimen size. Further studies are needed to determine the boundary layer thickness for shear loads.

Figure 9 shows stress distributions for flexure loads. Only exterior unit cells are compared. The single unit cell model was subjected to a combination of extension and flexure so that the loading would be comparable to the exterior unit cell of the thicker model. The thicker model was subjected to pure flexure. Both models have free surfaces at both the top and bottom. The maximum σ_x does not occur at the free surface. This is because local flexure of the wavy fiber tow as it tries to straighten attenuates the σ_x. The top halves of the two unit cells in Figure 9 have very similar σ_x, σ_y, and σ_{xy} distributions. The lower halves exhibit much more differences. This is not surprising since the lower surface of the single cell is traction free but the lower surface of the cell from the thicker model is not. These results further indicate that there is a free surface effect (in this case, from the lower surface of the single unit cell model), but that the boundary layer is quite small. Finally, it should be noted that the stresses were lower for the flexure case than for the extension case even though the maximum nominal axial strain was .001 for both.

Conclusions

Boundary effects were studied for woven composites subjected to in-plane extension, shear, and flexure. Effective moduli and stress distributions were calculated for configurations ranging from very thin to very thick. Only two dimensional models were studied. Since woven textiles are really three dimensional, these two dimensional results should only be interpreted qualitatively. Boundary effects were significant both in terms of stiffness and stresses. A specimen thickness of 6-8 unit cells was required to obtain moduli within about 2% of that for very thick specimens. For extension and flexure loading the stress distribution in exterior unit cells were quite insensitive to total specimen thickness. There appeared to be a characteristic response of boundary cells. Also, the boundary effect did not propagate very far into the interior. The response for shear load was more complex than for extension and flexure. Further work is needed to characterize boundary effects for shear loads.

References

1. Whitcomb, J.D. "Three-Dimensional Stress Analysis of Plain Weave Composites," in *Composite Materials: Fatigue and Fracture (Third Volume), ASTM STP 1110*, T.K. O'Brien, Ed., Philadelphia: American Society for Testing and Materials, pp. 417-438.
2. Paumell, P., A. Hassim, and F. Léné. La Recherche Aérospatiale, 1:1-12 (1990).
3. Paumell, P., A. Hassim, and F. Léné. La Recherche Aérospatiale, 6:47-62 (1991).
4. Ishikawa, T. Fiber Science Technology, 15:127-145 (1981).
5. Ishikawa, T., and T.-W. Chou, J. Material Science, 17:3211-3220 (1982).
6. Kriz, R.D., J. Composites Technology & Research, 7:55-58 (1985).

7. Avery, W.B., and C.T. Herakovich. A Study of the Mechanical Behavior of a 2D Carbon-Carbon Composite, Virginia Polytechnic Institute and State University, Interim Report 66 (1987).

8. Whitcomb, J.D., and K. Woo. "Enhanced Direct Stiffness Method for Finite Element Analysis of Textile Composites," *CMC Report No. 92-17*, Texas Engineering Experiment Station, Texas A&M University, (1992); submitted for publication in Journal of Composite Materials.

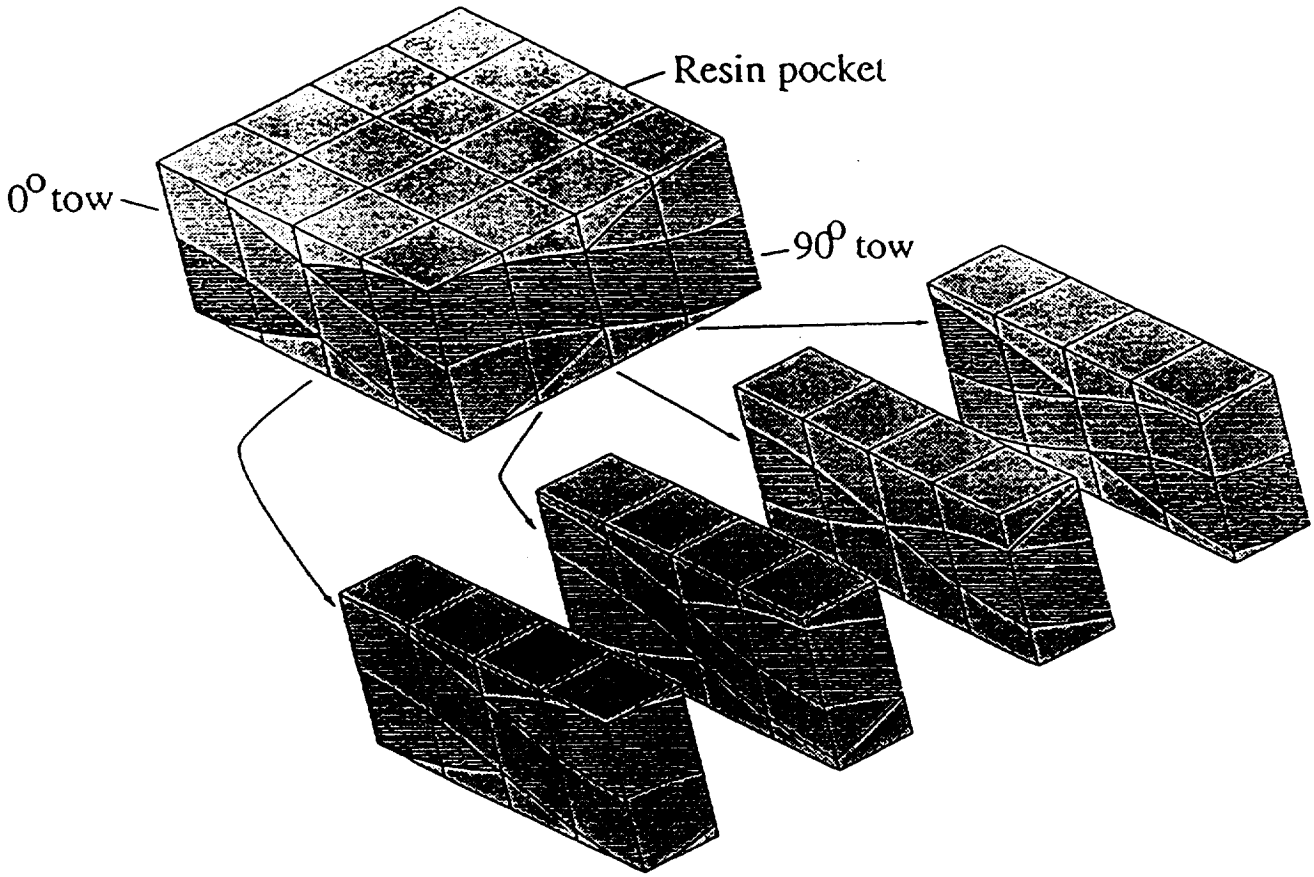

Figure 1 Variation of cross section with location.

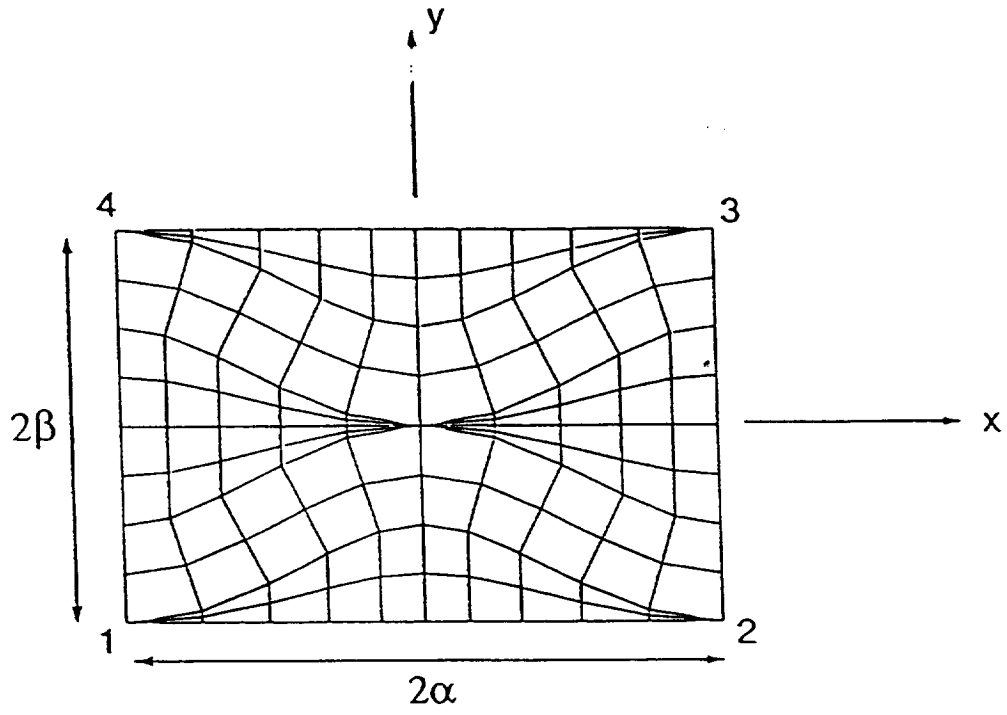

(a) Full unit cell

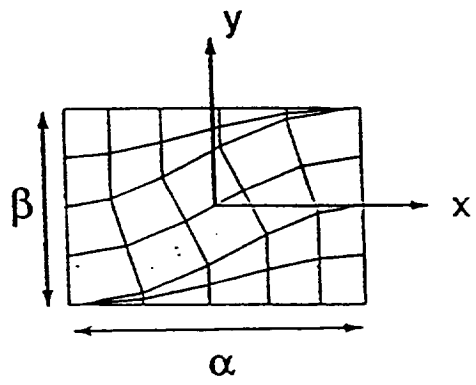

(b) Quarter unit cell

Figure 2 Basic two-dimensional unit cell models.

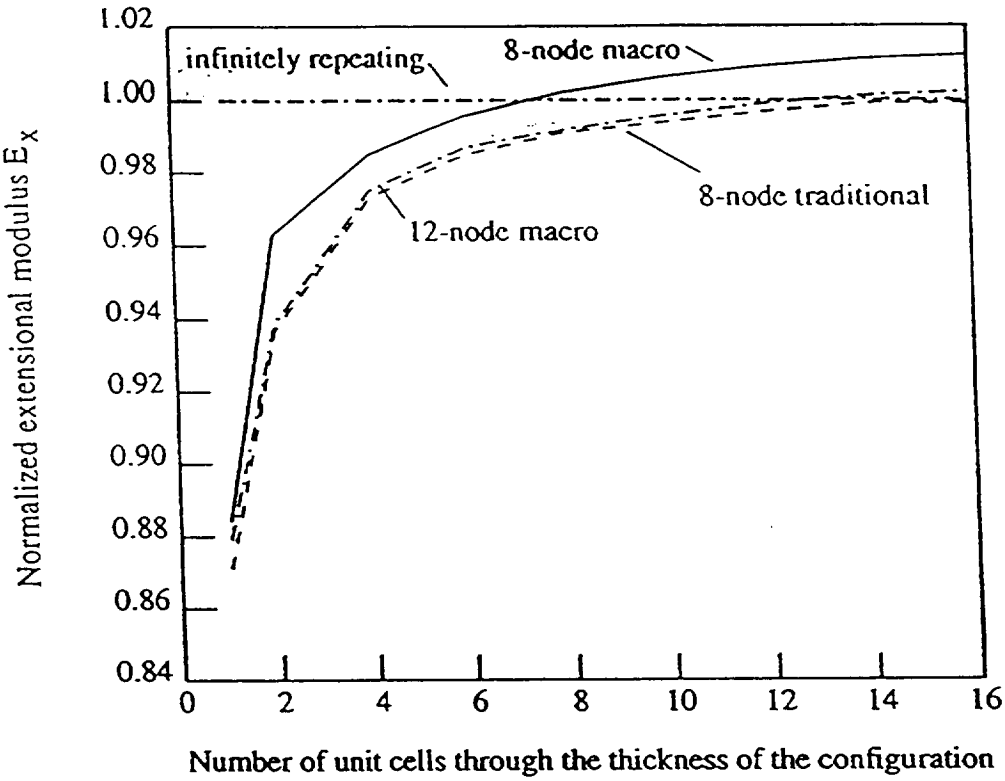

(a) Average normalized E_x vs number of unit cells through thickness.

Fig. 3 Normalized extensional modulus E_x. Eight-node traditional elements were used for the infinitely repeating unit cell case.

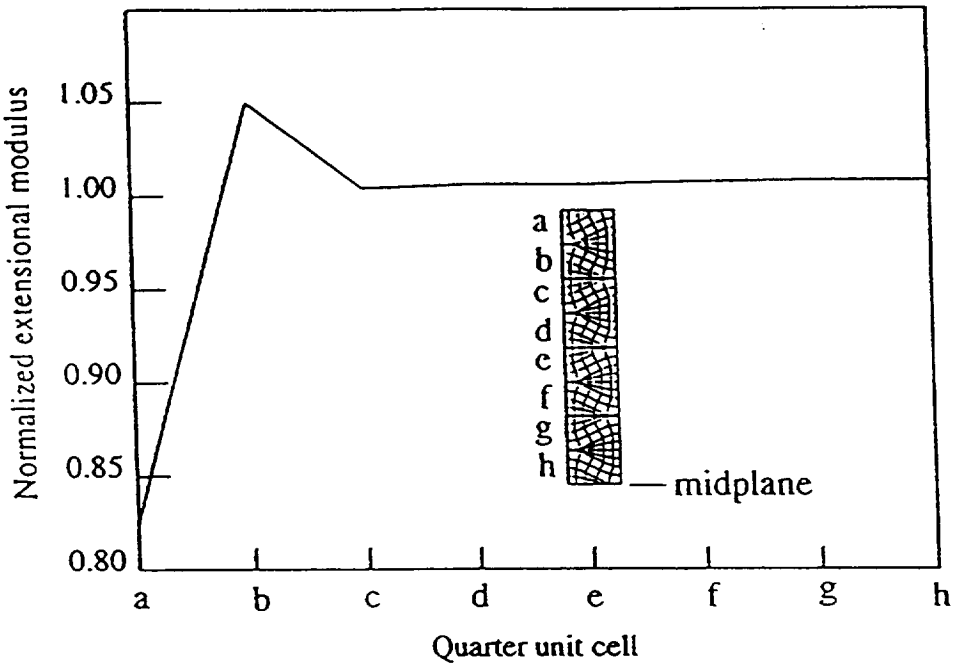

(b) Normalized extensional modulus vs. position in an 8-unit cell configuration. (The sketch only shows four unit cells, since the configuration is symmetric.)

Figure 3, completed.

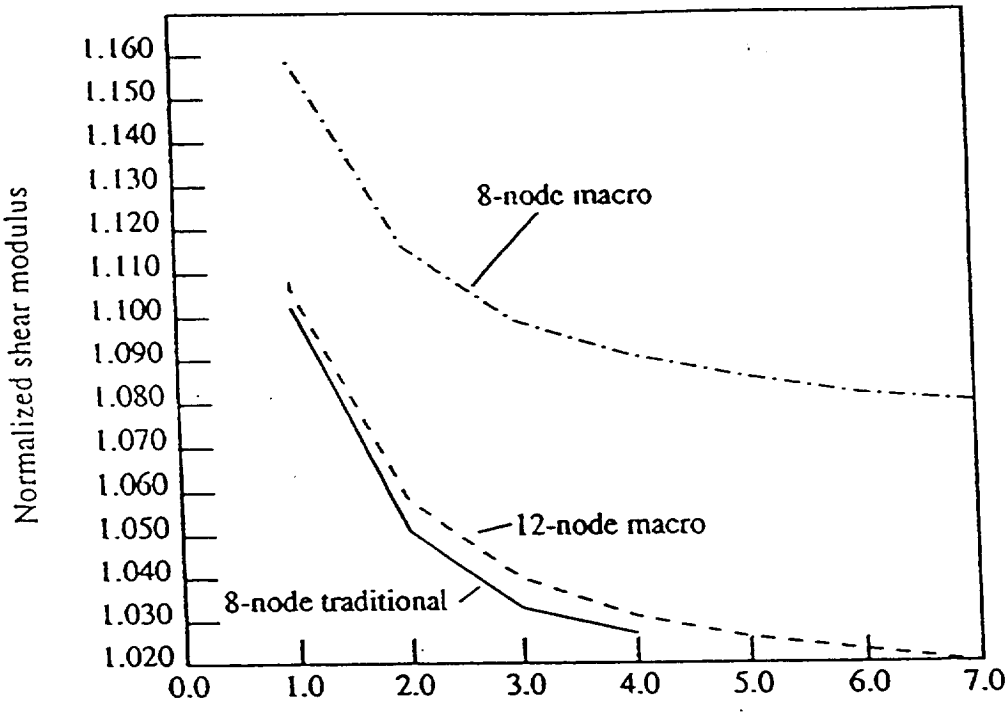

Fig. 4 Normalized shear modulus vs. number of unit cells through the thickness of the configuration.(The number of unit cells is the same in both the x- and y- directions).

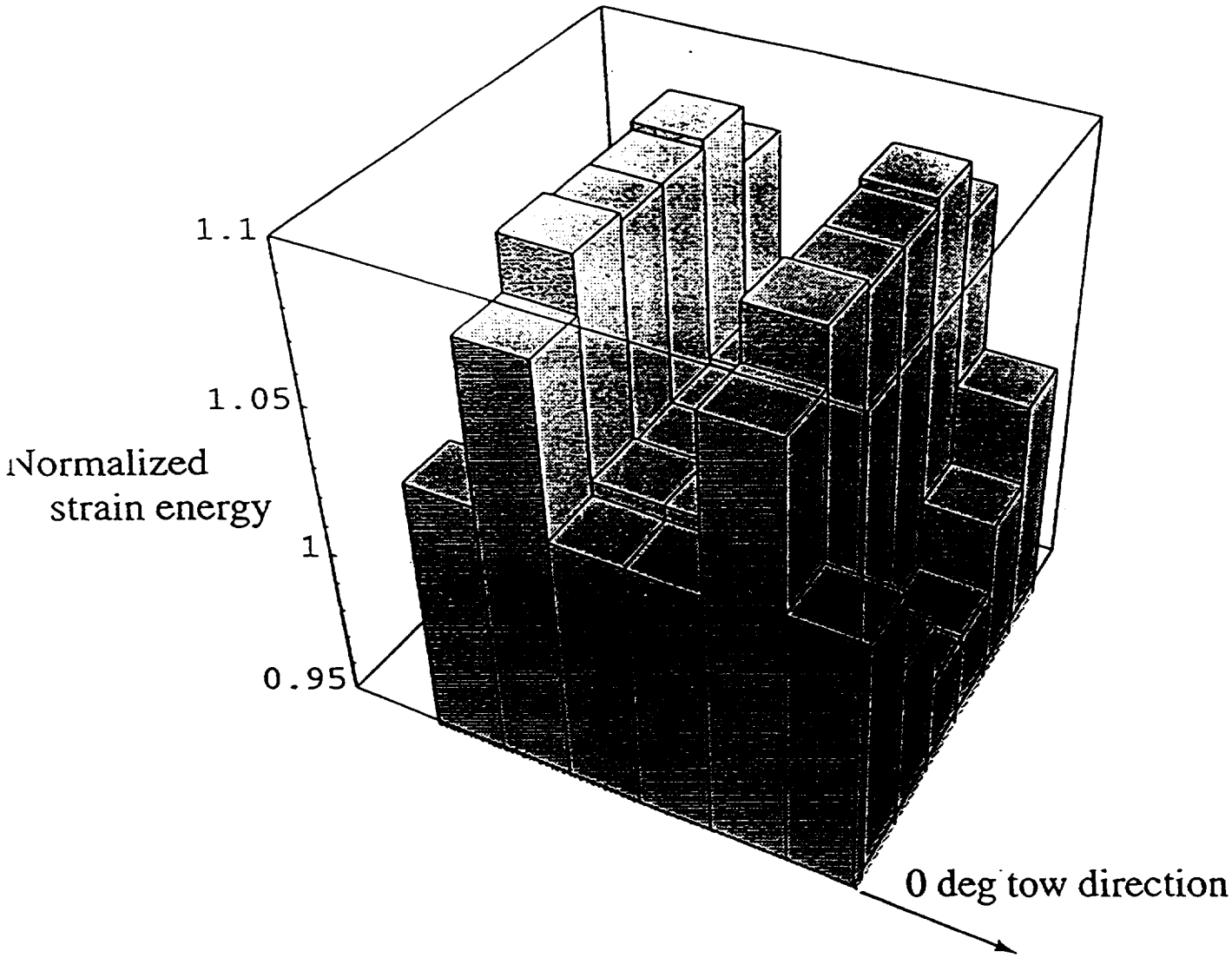

Figure 5 Normalized strain energy distribution in 3x3 unit cell model subjected to shear load. Strain energy in each quarter unit cell is normalized by that for an infinitely repeating unit cell array subjected to shear.

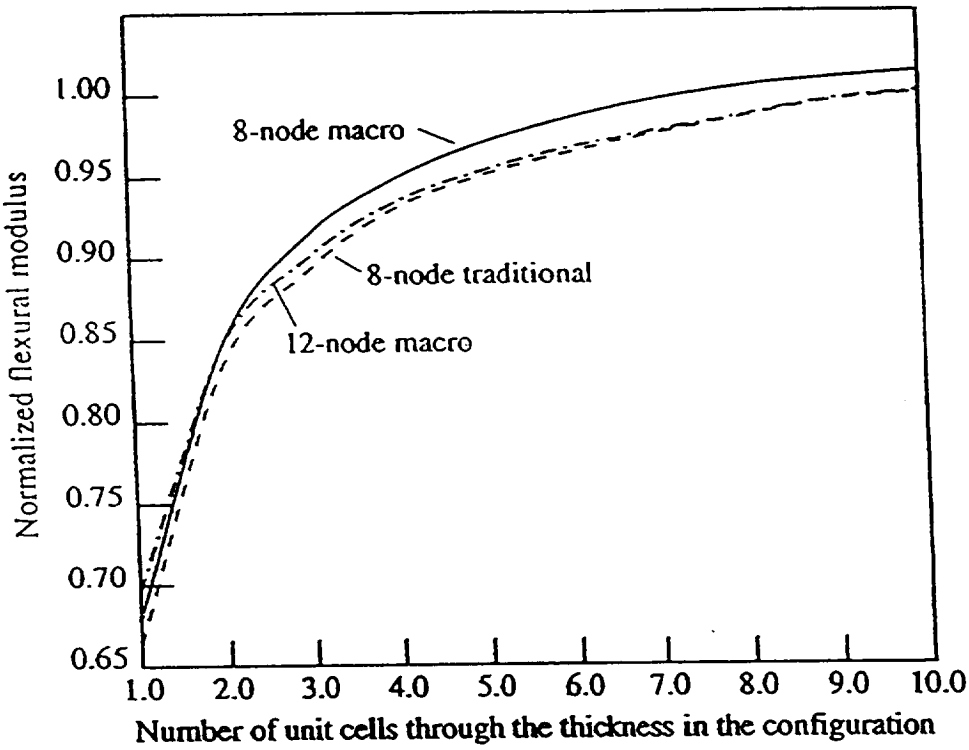

Fig. 6 Normalized flexural modulus vs. number of unit cells through the thickness of the configuration. Results were normalized with the flexural modulus for a ten unit cell model.

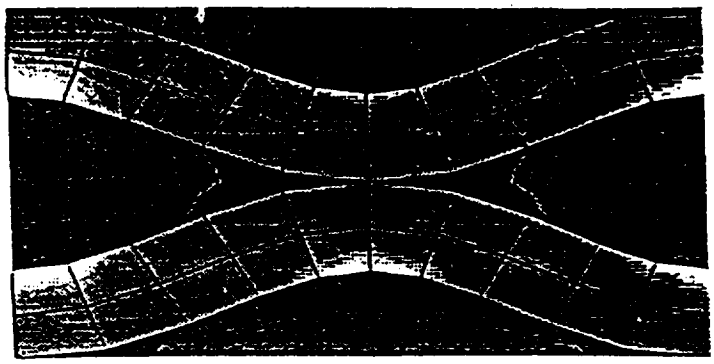

(i) Top unit cell of model with two unit cells through thickness.

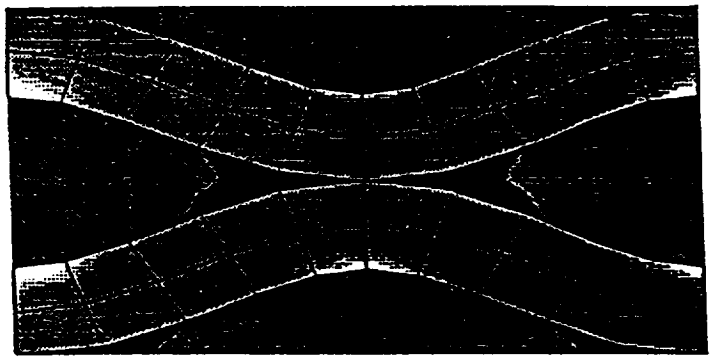

(ii) Exterior unit cell of model with six unit cells through thickness.

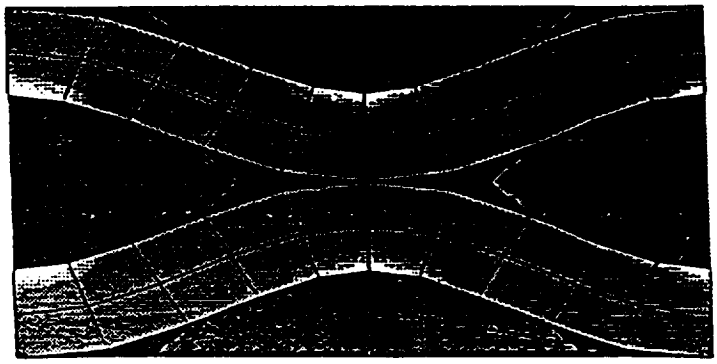

(iii) Interior unit cell of model with six unit cells through thickness.

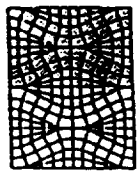

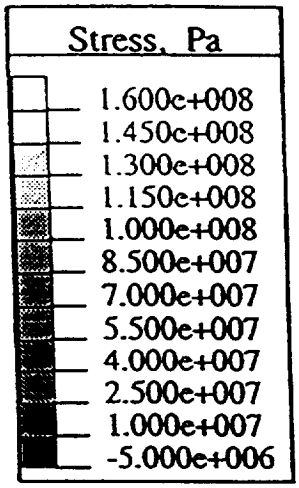

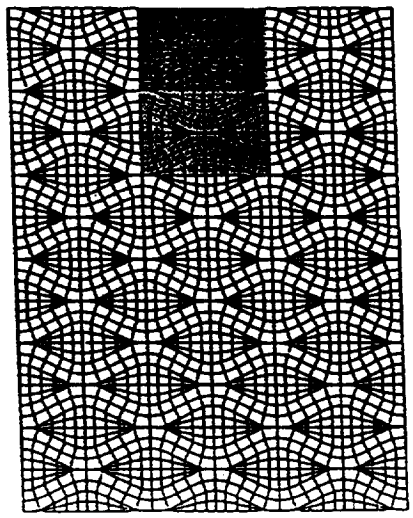

(a) Axial Stress

Figure 7 Stress contours for a two dimensional model of a plain weave composite under extension (nominal axial strain = .001).

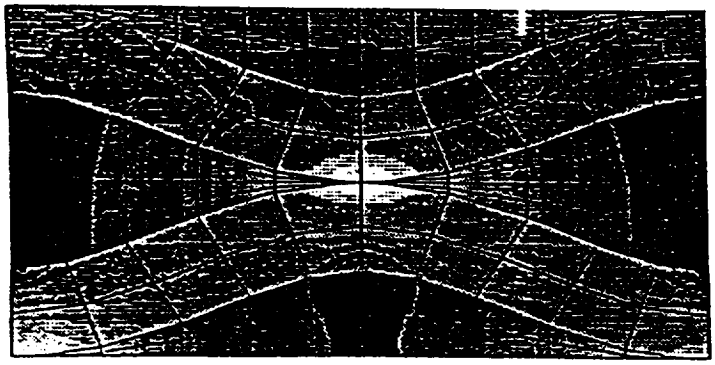

(i) Top unit cell of model with two unit cells through thickness.

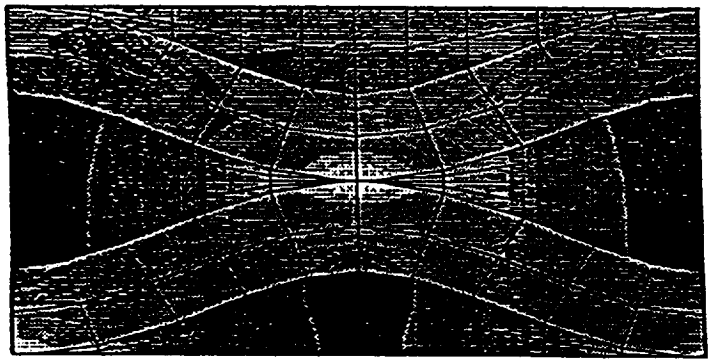

(ii) Exterior unit cell of model with six unit cells through thickness.

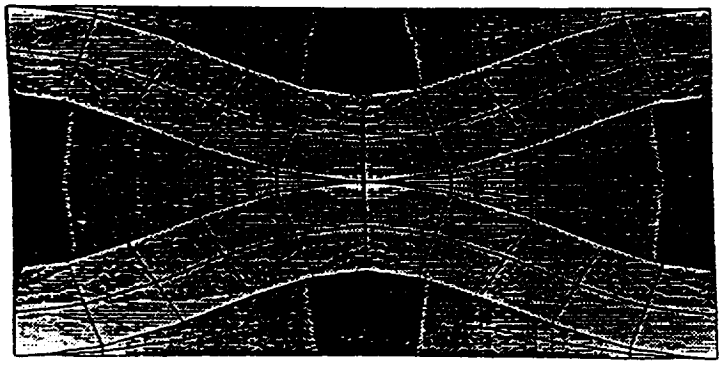

(iii) Interior unit cell of model with six unit cells through thickness.

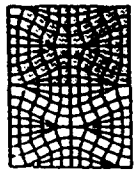

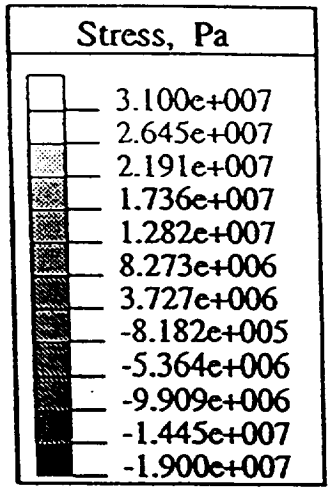

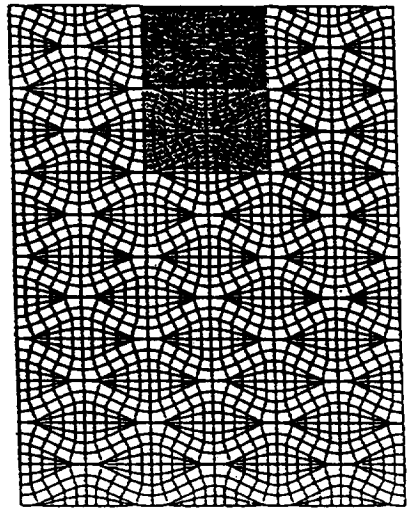

(b) Transverse Stress

Figure 7, Continued.

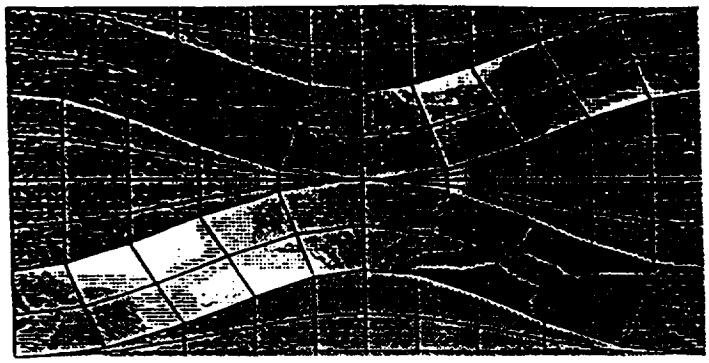

(i) Top unit cell of model with two unit cells through thickness.

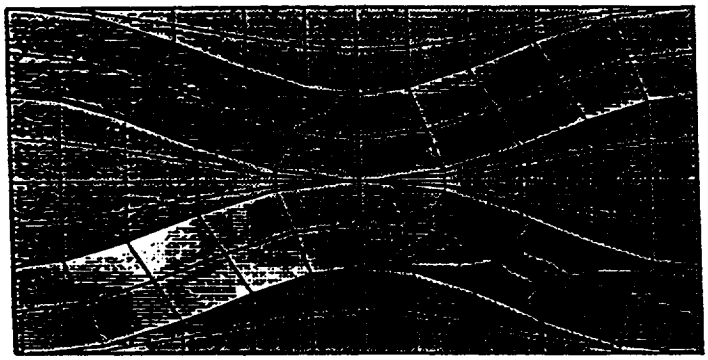

(ii) Exterior unit cell of model with six unit cells through thickness.

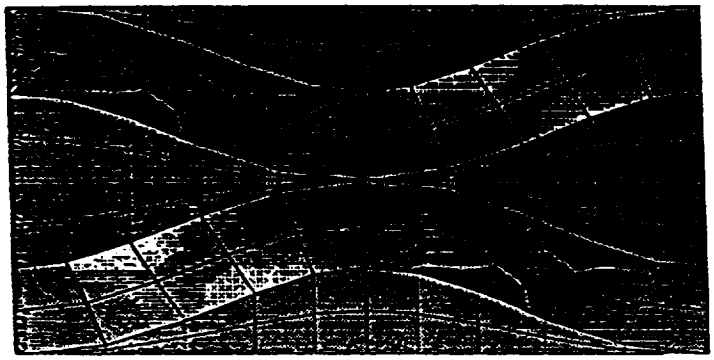

(iii) Interior unit cell of model with six unit cells through thickness.

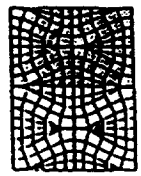

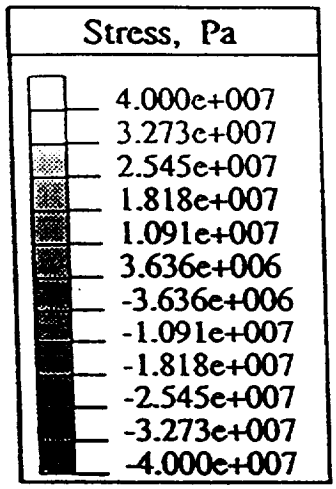

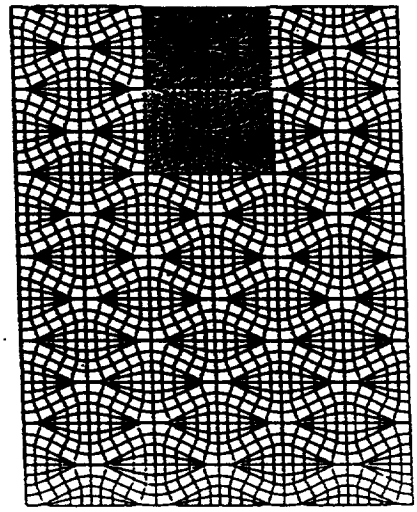

(c) Shear Stress

Figure 7. Concluded.

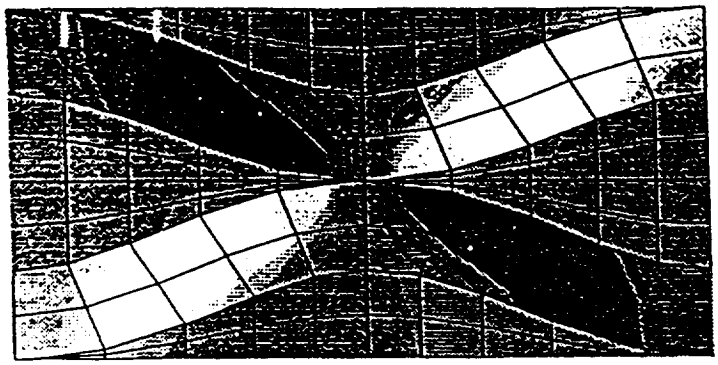

(i) Single Unit Cell

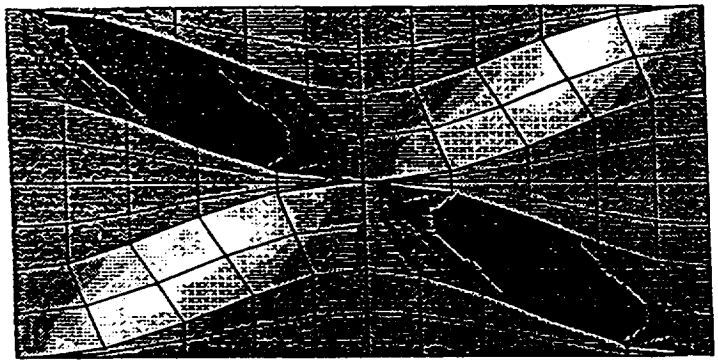

(ii) Exterior Unit Cell of a (3x3) unit cell model

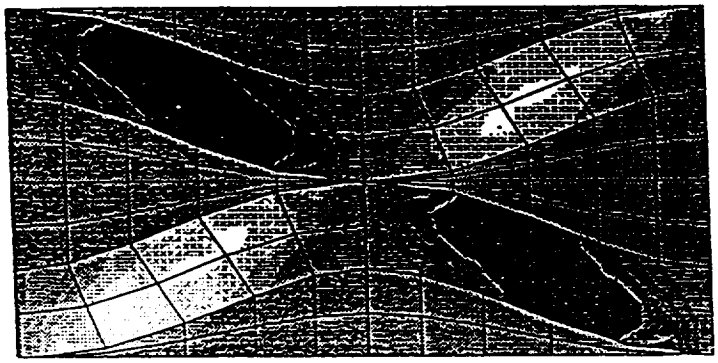

(iii) Interior Unit Cell of a (3x3) unit cell model

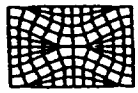

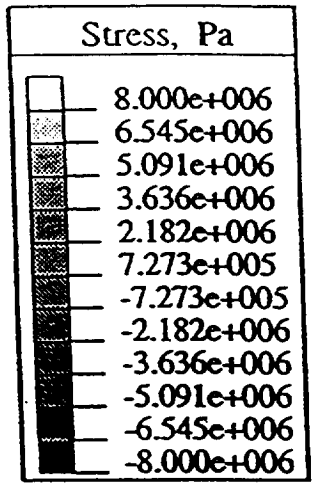

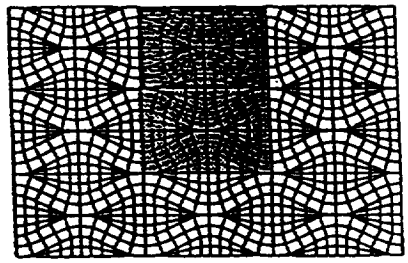

(a) Transverse Stress

Figure 8 Stress contours for a two dimensional model of a plain weave composite under shear. (nominal shear strain = .001)

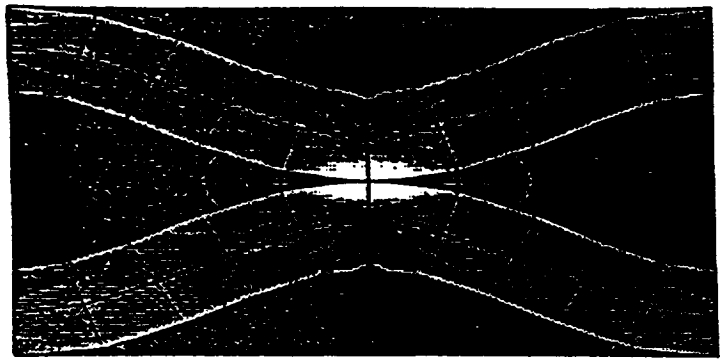

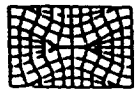

(i) Single Unit Cell

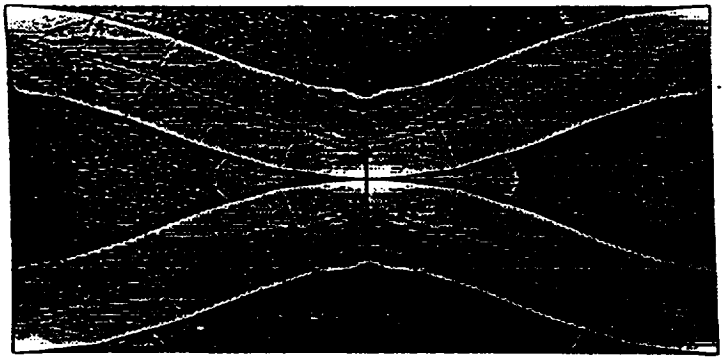

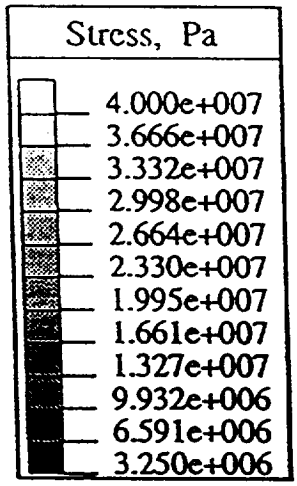

(ii) Exterior Unit Cell of a (3x3) unit cell model

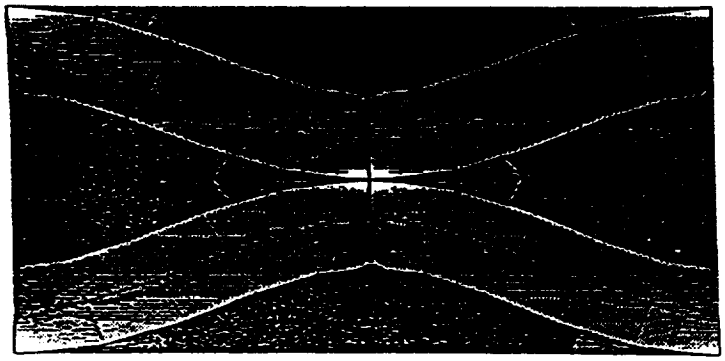

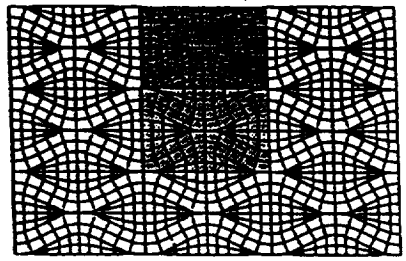

(iii) Interior Unit Cell of a (3x3) unit cell model

(b) Shear Stress

Figure 8, Concluded.

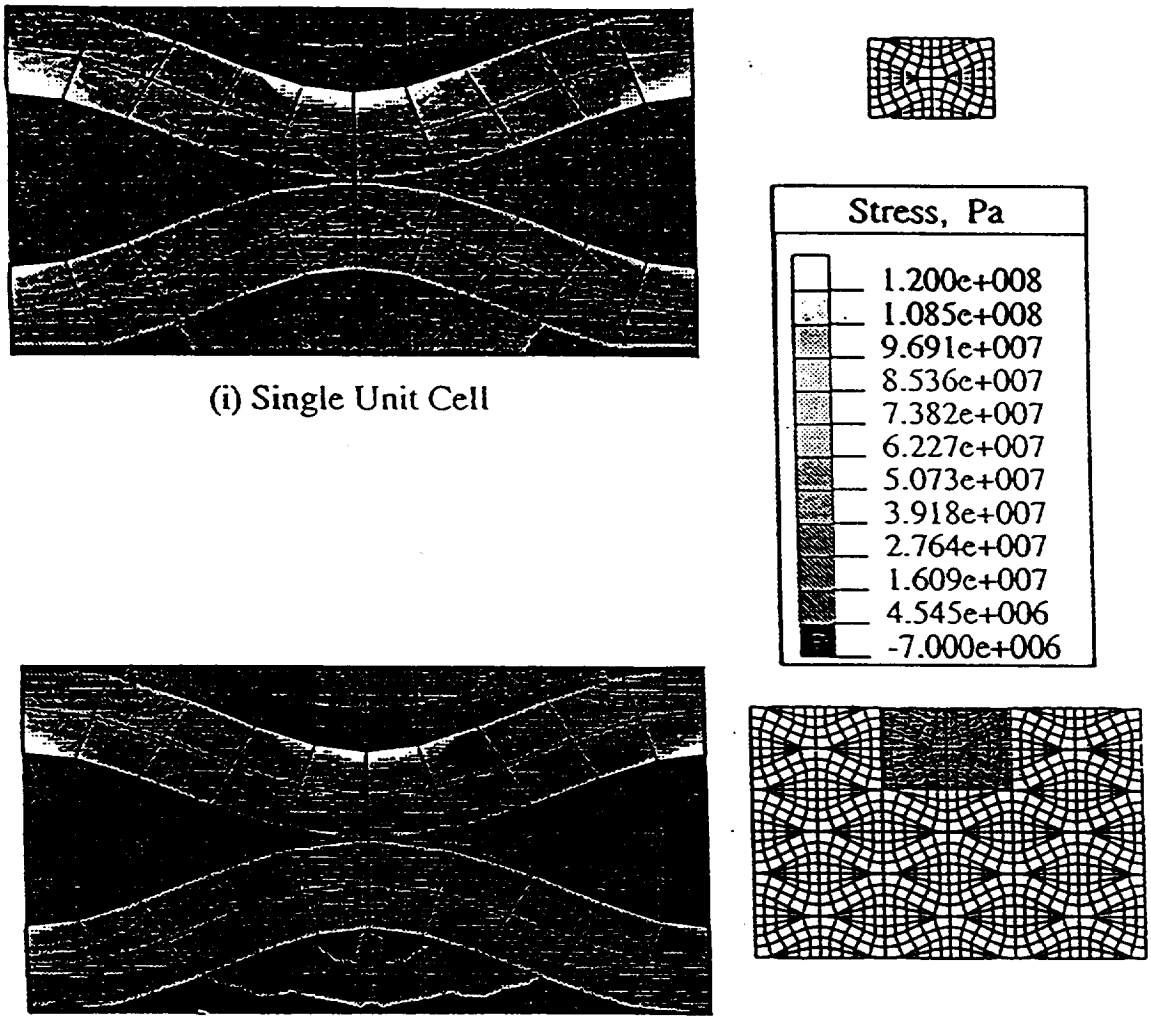

(i) Single Unit Cell

(ii) Exterior Unit Cell of a (3x3) unit cell model

(a) Axial Stress

Figure 9 Stress contours for a two dimensional model of a plain weave composite under bending. (nominal axial strain at top surface = .001)

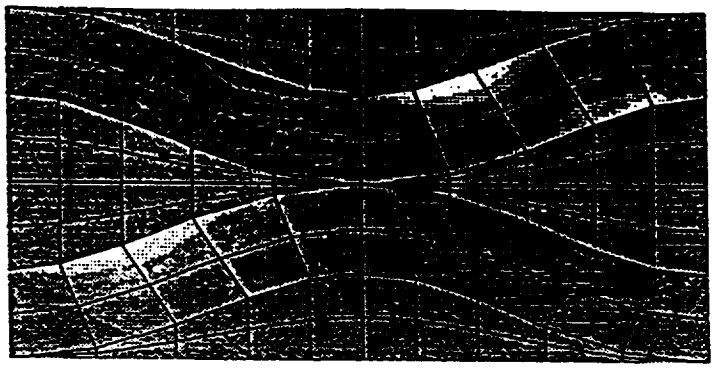

(i) Single Unit Cell

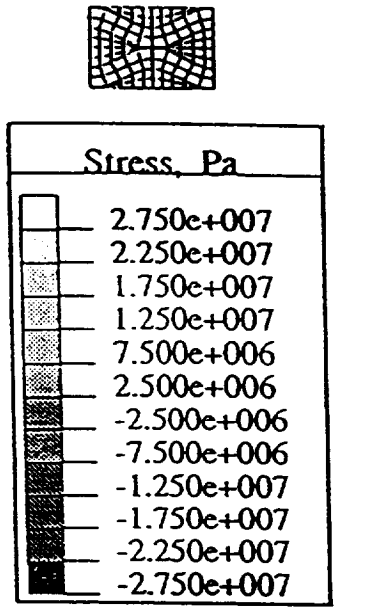

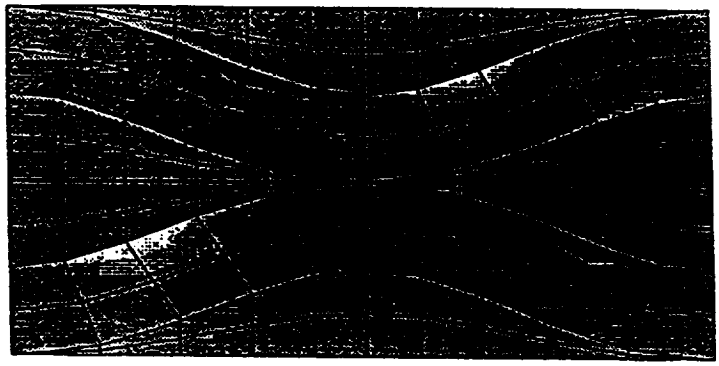

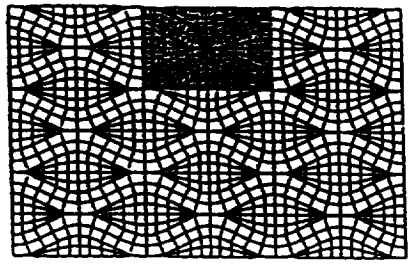

(ii) Exterior Unit Cell of a (3x3) unit cell model

(c) Shear Stress

Figure 9, Concluded.

Chapter: 5

EVALUATION OF HOMOGENIZATION FOR GLOBAL/LOCAL STRESS ANALYSIS OF TEXTILE COMPOSITES

Abstract

Global/local analysis is essential for textile composites because of their unusually large microstructure. Homogenized engineering properties were used in this study to obtain global solutions. The response of a local region was approximated by several fundamental strain or stress modes. The magnitudes of these modes, which were determined from the global solutions, were used to scale and superpose solutions from refined analyses of the fundamental modes, thus obtaining a refined local solution. Results from numerical experiments showed that the use of homogenized engineering properties often results in significant errors in prediction of global response, especially at boundaries. Also, the local predictions were very sensitive to the choice of fundamental modes.

Introduction

Recently there has been an increased interest in textile composites because of potential increases in damage tolerance and decreased cost relative to tape laminates. These composites consist of a textile preform which is impregnated with resin. The interlacing used in making a preform can be accomplished by weaving, braiding, or knitting. Figure 1 shows examples of two weave architectures: a plain weave and a 5-harness satin weave. (The resin pockets are removed in the figure so that the fiber tows can be seen.) Textile composites all have very large microstructure compared to traditional tape laminates. In fact, the "microstructure" can be of the same scale as some of the structural dimensions.

One of the techniques proposed for analyzing textile composite structures is to use homogenized engineering material properties or some other measure of effective properties for a global analysis. This avoids the impossible burden of modeling the microstructure discretely in a structural model. To determine the details of the stress and strain distributions, subsequent analyses are performed using a refined model of a representative unit cell. The boundary conditions for these subsequent analyses are determined from the results of the global analysis. Such analyses have been discussed previously (e.g., References 1-4). This multi-level procedure could be considered a global/local method and will be referred to as such herein. References 1 and 3 discussed the accuracy of this procedure if one uses special elements (referred to as macro elements) for the global analysis. However, this author is not aware of any study which evaluated the accuracy of a global/local procedure for textile composites based on using homogenized engineering properties for the global analysis.

The objective of this paper is to describe two global/local procedures which use homogenized engineering material properties to expedite global stress analysis of textile composites and to determine the errors which are inherent in such analyses. One of the key questions is whether the use of homogenized engineering properties is adequate when the microstructure is large. To simplify the discussion and numerical experiments, only two-dimensional models will be examined. Admittedly, textile composites are fully 3D in their geometry, but the trends determined from 2D models are expected to be qualitatively correct.

In the following sections the theoretical basis will be described first. Then the configurations studied will be described. Finally, the results of the numerical experiments will be discussed.

Theory

This section will describe the global/local procedures used. Figure 2 shows a schematic of the global/local analysis procedure. In this sketch the shading identifies the region which will be analyzed further using a local model. The region to be analyzed using a local model is shown isolated from the rest of the global model. After completing the global analysis, the boundary nodal displacements (u_i, v_i) and forces (F_x^i, F_y^i) are known. This boundary information is used to determine the appropriate loading conditions for a refined local model. There are many possibilities for determining these boundary conditions. In this particular study the boundary information was used to quantify the magnitudes of selected fundamental strain or stress modes. Details of the various steps are discussed in the following subsections. First, the term homogenized engineering properties will be defined. Then the fundamental macroscopic strain and stress modes will be described, including an explanation of how the magnitude of the modes were determined.

Homogenized Engineering Properties

A unit cell is the basic building block which can be used to synthesize a woven composite. In this paper the woven mats are stacked symmetrically, so the unit cell consists of one wavelength of two mats. Homogenized engineering properties for use in the global analysis were determined by analyzing an infinite array of unit cells subjected to macroscopically constant stress states. Hence, every unit cell in the array experiences the same deformation. Periodic boundary conditions were applied to a single unit cell to make it behave as though it was embedded within an infinite array. Details about the periodic boundary conditions can be found in Reference 5. The homogenized engineering properties were obtained by equating energies in the homogenized medium to that in the actual unit cell.

Fundamental Macroscopic Strain and Stress Modes

In the current study the local model consisted of a refined mesh of a unit cell. In general, the local model could be smaller or larger. The loading for this refined unit cell was determined from the nodal displacements (u^i, v^i) or forces (F_x^i, F_y^i) in the global model at the nodes which surround the region of interest. The local model typically has many more nodes along the global/local boundary than the global model. Hence, the dimensionality of the local model along the global/local boundary must be reduced. One technique to reduce the dimensionality is to

limit the response to a few macroscopic strain or stress modes. In this paper the response of the local region was characterized in terms of five strain or stress modes. These modes are:

Strain modes:

ϵ_x^0 : constant macroscopic ϵ_x
ϵ_y^0 : constant macroscopic ϵ_y
ϵ_{xy}^0 : constant macroscopic ϵ_{xy}
$\epsilon_{x,y}^0$: constant gradient of macroscopic ϵ_x with respect to y
$\epsilon_{y,x}^0$: constant gradient of macroscopic ϵ_y with respect to x

Stress modes:

σ_x^0 : constant macroscopic σ_x
σ_y^0 : constant macroscopic σ_y
σ_{xy}^0 : constant macroscopic σ_{xy}
$\sigma_{x,y}^0$: constant gradient of macroscopic σ_x with respect to y
$\sigma_{y,x}^0$: constant gradient of macroscopic σ_y with respect to x

There are interior and exterior versions of some of these modes. There are neighboring unit cells on all sides for interior modes and on only two sides for exterior modes. Figure 3 shows deformed finite element meshes which illustrate the five interior stress modes. The shaded rectangles indicate the original mesh size and shape. The interior modes were used for analyzing interior cells. A mixture of interior and exterior modes were used for analyzing exterior cells. The mix is listed below for displacement (strain modes) and force (stress modes) based superposition.

Strain Modes		Stress Modes	
Mode	Version	Mode	Version
ϵ_x^0	interior	σ_x^0	exterior
ϵ_y^0	interior	σ_y^0	interior
$\epsilon_{x,y}^0$	interior	σ_{xy}^0	interior
$\epsilon_{x,y}^0$	exterior	$\sigma_{x,y}^0$	exterior
$\epsilon_{y,x}^0$	interior	$\sigma_{y,x}^0$	interior

Only a few exterior modes were used. This is because the free surface of the exterior cell was a y = constant line. Some exterior modes, such as a σ_y^0 mode, do not exist for such a cell.

The technique for imposing boundary conditions for the various modes is described in References 5 and 6. The techniques used to determine the magnitudes of the modes is discussed in the following two sections.

Strain Mode Superposition The global/local displacement field was assumed to be describable by the following bi-linear approximation in x and y.

$$u = a + bx + cy + dxy$$
$$v = e + fx + gy + hxy \tag{1}$$

The eight constants *a-h* can be determined by requiring that equation 1 match the displacements at the corner nodes of the local region. The macroscopic strain modes can be obtained by differentiation of the equations. The equation for ε_{xy} was further simplified by evaluating it at the unit cell centroid and taking it to be constant for the entire global/local boundary. This resulted in five strain modes: ϵ^0_x, ϵ^0_y, ϵ^0_{xy}, $\epsilon^0_{x,y}$ and $\epsilon^0_{y,x}$. In particular,

$$\epsilon_x = b + dy$$
$$\epsilon_y = g + hx \tag{2}$$
$$\epsilon_{xy} = c + f$$

The coefficients *b*, *d*, *g*, *h*, and $c+f$ are the magnitudes of the five fundamental strain modes.

Stress Mode Superposition This technique is similar to the strain mode superposition method. In this case the nodal forces from the global analysis are used to determine the magnitudes of five fundamental stress modes. These fundamental modes were described earlier. This section will describe how to determine the magnitudes of these modes.

The first step is to express the tractions T_x and T_y acting along the global/local boundary in terms of the stresses.

$$T_x = \sigma_x n_x + \sigma_{yx} n_y$$
$$T_y = \sigma_{xy} n_x + \sigma_y n_y \tag{3}$$

The relationship between these tractions and the equivalent nodal forces for a single element can be derived using the principle of virtual work. The result is

$$F^i_x = \int T_x N_i(s) dS$$
$$F^i_y = \int T_y N_i(s) dS \tag{4}$$

where

i = *1, number of boundary nodes*
N_i = *interpolation functions*

In this paper the local region is rectangular and aligned with the global *xy* axes so *dS* is either *dx* or *dy*. The total nodal forces for each node along the entire boundary are obtained by

summing the contributions from each element. Next the average stresses for the entire local region are assumed to be given by

$$\sigma_x = a + by$$
$$\sigma_y = c + dx \qquad (5)$$
$$\sigma_{xy} = c$$

These expressions for stresses are used in equations 3 and 4 to determine the equivalent nodal loads. Since there are many more known nodal forces (and hence more equations) than unknown coefficients (*a-e*), a least squares procedure is used to solve for the unknowns.

Once the coefficients are determined, they are used to scale and superpose the fundamental stress modes described earlier.

Configurations

A very stubby beam was subjected to three types of loading: constant moment, distributed transverse shear at the end, and distributed transverse loading along the lower surface. More precisely, the conditions were: (see Figure 4)

Constant moment:

$u(0,0) = v(0,0) = 0$

$\frac{\partial u}{\partial y}(-4.5,y) = -.01$

$\frac{\partial u}{\partial y}(4.5,y) = .01$

Transverse end load:

$u(0,y) = v(0,y) = 0$

$T_y(4.5,y) = \text{constant}$

Distributed lateral load:

$u(0,y) = v(0,y) = 0$

$T_y(x,-3) = \text{constant}$

The beam consisted of 3x3 array of unit cells. The ratio of wavelength to mat thickness gives a measure of the waviness of the fiber tows. In this study this ratio (λ/h) was 1/3.

The following material properties were assumed:

Fiber tow [Ref. 6]

$E_x = 206.900\ GPa$
$E_y = 5.171\ GPa$
$E_z = 5.171\ GPa$
$\nu_{xy} = 0.25$
$\nu_{yz} = 0.25$
$\nu_{zx} = 0.25$
$G_{xy} = 2.386\ GPa$
$G_{yz} = 2.386\ GPa$
$G_{zx} = 2.386\ GPa$

Matrix pockets

$E_x = 3.45\ GPa$
$E_y = 3.45\ GPa$
$E_z = 3.45\ GPa$
$\nu_{xy} = 0.35$
$\nu_{yz} = 0.35$
$\nu_{zx} = 0.35$
$G_{xy} = 1.28\ GPa$
$G_{yz} = 1.28\ GPa$
$G_{zx} = 1.28\ GPa$

Homogenized properties

$E_x = 36.494\ GPa$
$E_y = 5.225\ GPa$
$E_z = 36.494\ GPa$
$\nu_{xy} = 1.078$
$\nu_{yz} = 0.154$
$\nu_{zx} = 0.154$
$G_{xy} = 3.145\ GPa$
$G_{yz} = 3.145\ GPa$
$G_{zx} = 2.000\ GPa$

Figure 4 shows typical meshes which were used in this study. The reference mesh used 5041 nodes and 1728 bi-quadratic elements to model nine unit cells. The homogenized property mesh used 217 nodes and 36 bi-cubic elements. The refined local mesh had 593 nodes and 192 bi-quadratic elements. The shading indicates the two unit cells (one interior and one exterior)

which were analyzed using global/local analysis. Obviously, there are far fewer equations involved in the global/local analysis than in the conventional analysis used to obtain a reference solution.

Results and Discussion

The errors in a global/local analysis are the cumulative result of errors at the various stages in the procedure. To improve on a procedure requires that one know where errors are being introduced. Accordingly, the following discussion will begin with an evaluation of the predicted global response and finally examine errors in the predicted local stress distributions.

To help evaluate the accuracy of the global analysis, the deformation of the reference and homogenized property meshes were compared. Figure 5 shows deformed finite element meshes for the three load cases. The meshes are overlaid to aid the comparison. The inhomogeneity in the reference mesh causes local distortions which should not (and do not) occur when homogenized properties are used. In Figure 5a (for a constant moment) the agreement appears excellent, except for the local distortion. This apparent accuracy is an artifact of the loading, which consisted of specified normal displacements on the left and right sides. The strain energy (and required moment) in the homogenized property mesh is 40% too large. In Figures 5b and 5c the loading consisted of specified forces. The agreement between the meshes is fair for these cases. Comparison of the strain energies in the reference and homogenized property models gives a scalar measure of the agreement in the predictions. The error in strain energy for the entire model was quite small (-6.6% for the transverse end load case and 2.6% for the distributed lateral load case). Also shown are magnified views of one interior and one exterior unit cell for each load case. (See Figure 4 for the location of the cells.) To expedite the comparisons, the rigid body motion of the unit cells was subtracted before plotting. Removing the rigid body rotation permits the unit cells to be aligned for comparison. When removing the rigid body rotation, it is important that the linear definition of rotation (i.e. rotation $= \frac{\partial u}{\partial y} - \frac{\partial v}{\partial x}$) be used. For example, consider the beam in Figure 6. The beam was subjected to a moment at the right end. Contrary to appearances, all the unit cells have the same strain distribution. If the rigid body rotation is removed using the linear rotation formula, the deformed meshes for each unit cell will also be identical.

The errors in the strain energies for the individual cells are tabulated below :

	Constant Moment		Transverse End Load		Distributed Lateral Load	
	Interior	Exterior	Interior	Exterior	Interior	Exterior
Reference	59520	415860	613764	465024	160320	68400
Homogenized	46152	599960	513120	394740	136956	66600
Error (%)	-22	44	-16	-15	-15	-3

The simplicity of the loading in some cases allows one to explain the source of the errors. The -22% error for the interior cell of a beam subjected to constant moment resulted from the

effective extensional modulus (which is what was used) being 22% smaller than the effective flexural modulus. For the interior cell of a beam subjected to transverse end load, there is both flexure and shear. The shear contribution to strain energy is calculated accurately but the flexure contribution is again low by 22%, which resulted in an net error of -16%. For the exterior cell of a beam subjected to constant moment the dominant deformation mode is extension. There is also some flexure. The 44% error in strain energy resulted from using the effective extensional modulus (which is based on infinite array analysis) throughout. In reality, the extensional and flexural modulus for exterior cells is much smaller than the effective extensional modulus for an infinite array. These errors illustrate the problems in using effective engineering properties for this class of materials.

As discussed in the theory section, the nodal displacements and forces were used to determine the magnitudes of the fundamental strain and stress modes, respectively. There is inherently some error in this approximation, regardless of the accuracy of the global analysis. This is because in general the actual behavior cannot be matched by just the modes selected. However, by calculating the magnitudes of the modes using the reference mesh, one obtains a baseline approximation which is about as good as can be expected. Table 1 summarizes the results.

For pure bending the strain modes for the interior cell are identical for the two meshes, but this is not a sign of accuracy, since the specified displacement loading required this identity. There was a -33% error in the constant ϵ_y mode for the exterior cell. The other two non-zero modes were exact, which again was due to the boundary conditions. The error in the stress modes depended on the location of the cell and the particular mode. The importance of a particular mode cannot be seen in Table 1 . The numbers in these tables are used to scale the stress distributions from the fundamental solutions, i.e., $\sigma_i = c^\alpha \sigma_i^\alpha$ where c^α = magnitudes in the table and σ_i^α = stress distribution for the "α" mode. Both the c^α and σ_i^α must be considered when determining the dominant modes for a particular load case. The dominant stress mode for the interior cell was the gradient of σ_x mode, which was off by -10%. In contrast, the dominant mode (constant σ_x) for the exterior cell was off by 30%. For the transverse end load case the dominant modes were ϵ^0_{xy}, ϵ^0_{xy}, σ^0_{xy}, and σ^0_{xy} for the interior cell and ϵ^0_x, ϵ^0_{xy}, ϵ^0_{xy}, σ^0_x, σ^0_{xy}, and σ^0_{xy} for the exterior cell. The largest errors in the dominant modes were for ϵ^0_{xy} and σ^0_{xy}. These errors tended to be quite large. For the distributed lateral load case most of the modes were significant. (The ϵ^0_{yx} and σ^0_{yx} modes were not significant.) The errors in the modes tended to be larger than for the other two load cases.

The magnitudes of the modes in Tables 1(a) and 1(b) can be used to scale and superpose displacements for the fundamental modes. These superposed displacements were determined for interior and exterior cells. The deformed meshes are shown in Figures 7 and 8 for strain and stress mode superposition, respectively. As was done in Figure 5, the rigid body components were subtracted to make the comparisons of the unit cell deformations more accurate. The thicker lines indicate the superposition results. The results labeled "Reference Superposition" were obtained by using the reference mesh to determine the magnitudes of the modes. The "Reference Superposition" results show that even if a global analysis is exact, the local deformation cannot in general be represented in terms of a few fundamental modes. Regardless of the type of loading, the interior behavior is more closely approximated than the exterior behavior. Strain mode superposition appears to be more accurate for interior cells. In contrast,

stress mode superposition appears to be more accurate for exterior cells.

The next step was to determine the accuracy of the calculated stresses. Three types of solutions were examined:

1) the reference solution
2) the global/local solution in which the global analysis used the reference mesh to determine the modal components
3) the global/local solution in which the global mesh used homogenized material properties.

The results are presented two ways. First, just the peak stresses for each load case and analysis type will be summarized in tabular form and then a few stress contour plots will be discussed.

The peak stresses are tabulated in Table 2. The errors in the global/local stress calculations varied over a wide range. The simplicity of the loading for the constant moment case eliminated one source of error... that related to determining the average strain field using five strain modes. The second potential source of error was in determining the local stresses from the fundamental strain modes. This was no problem for the interior cell; the error was essentially zero. In Reference 7 it was shown that unit cells at least one cell away from a free surface behaved very much like ones embedded in an infinite array. Since the fundamental strain modes (which included two bending modes) were based on infinite arrays, the accurate prediction is no surprise. In contrast, the errors are significant for the exterior cell. Even when the refined reference mesh was used to determine the magnitudes of the different modes, the errors were not negligible. The stress mode superposition method tended to perform better for exterior cells than the strain mode method. The response of an exterior cell is complex and hence poorly represented by the particular few strain or stress modes considered. The errors due to modal reduction increased with the complexity of the applied load. For the distributed lateral load case the errors were significant for the interior cell and intolerable for the exterior cell.

Obviously, the interior and exterior unit cells experience different loading and different modes are dominant for the two cells. Hence, the larger errors for the exterior cell could be due to errors associated with particular modes, rather than the location of the cells. This was checked in an approximate sense by adding a layer of unit cells to the top and bottom of the current global model. Global/local analysis of this thicker beam was performed for transverse end load case. The errors in the peak stresses for the unit cell which had been on the exterior for the thinner model were now much less. This suggests that the behavior of an exterior cell is inherently more complicated than that of an interior cell.

Examination of errors in predicted peak stresses gives only a limited appreciation of the accuracy (or inaccuracy) of the predictions. Figures 9 and 10 show stress contours for the transverse end load case for interior and exterior cells. The contours for the interior cell (Figure 9) for the global/local analysis match very closely with the reference solution. The contours for the exterior cell (Figure 10) are not as close, but still seem to agree fairly well, even though the errors in the peak stresses are up to 26%. Peak stresses will probably not be useful for predicting failure, since they occur at a point (or at least a very small region). A critical stress criterion will probably have to consider the average stress in some characteristic volume. The visual similarity of the contours in Figures 9 and 10 suggests that when global/local analysis is used, the errors in a practical failure criterion might not be as bad as the errors in a peak stress criterion. This visual evaluation of the similarities in the contours in Figures 9 and 10 is subjective and could be wrong. A more objective method is badly needed.

One technique which was considered was plotting the tow area which had a stress greater

than a particular value. The reasoning is that if a large stress occurs over only an extremely small region, then the stress calculation is suspect, since the scale is too close to that of the fiber diameter. Figures 11 and 12 show results for σ_x for an interior and exterior cell, respectively for the transverse end load case. Two graphs are shown in each figure : one which includes the entire stress range, and the other which zooms in on the peak stress region. Results from the four analyses agree quite well for the interior cell. Although the homogenized superposition technique has a 15 percent error in predicting the peak stress, the distribution is predicted fairly well. If the failure criteria requires that a particular volume be at a critical stress, the prediction would be in error about 15 percent for very small critical volumes, but the error would be less for larger critical volumes. Figure 12 shows analogous results for the exterior cell. The errors are larger than for the interior cell, but the trend is the same, ie. for larger critical volumes the error in failure prediction is less than for very small critical volumes.

Concluding Remarks

Global/local stress analysis techniques based on the use of homogenized properties for the global analysis were evaluated. A very stubby beam containing nine unit cells was subjected to three types of loading. Considering the strong macroscopic stress and strain gradients relative to the microstructure these were probably fairly severe tests. For force type loading the overall deformation of the beam was not always predicted very well using homogenized properties. For larger configurations with more unit cells (and hence more homogeneous microstructure) the accuracy is expected to be considerably better. The accuracy of the calculated stresses was not too bad for interior cells, but was poor for exterior cells. This is not surprising based on earlier work on free boundary effects.

Regardless of how a global solution is obtained, there is considerable difficulty in using the crude nodal force and displacement information from the global mesh to determine appropriate load conditions for the local mesh. In this paper a modal technique was used. For the constant moment and transverse end load cases this technique performed well. For the more complicated case of distributed lateral load the performance was only fair for the interior cell and poor for the exterior cell, even when a refined global mesh was used.

There are several steps (and inherent approximation at each step) in global/local analysis. This study was just a beginning. Further work is needed in several areas. Alternatives to homogenization, such as the macro elements in References 8 and 9 need to be evaluated. Other techniques for imposing the global solution on a local model also need evaluation, including additional types of fundamental modes and the use of smaller local regions. Finally, more realistic configurations need to be identified and studied. Otherwise it is difficult to assess the significance of the errors in the various global/local techniques for practical applications.

References

1. Woo, K.: Stress and Failure Analysis of Textile Composites Using a Global/Local Finite Element Method. PhD thesis, Texas A&M University, August, 1993.

2. Guedes, J.M. and Kikuchi, N.: Preprocessing and Postprocessing for Materials Based on the Homogenization Method with Adaptive Finite Element Methods. Computer Methods in Applied Mechanics and Engineering, pp. 83, 1990.

3. Woo, K. and Whitcomb, J.: Global/Local Finite Element Analysis For Textile Composites. Accepted for publication in Journal of Composite Materials.

4. Paumelle, P., Hassium, A., and Léné, F.: Composites with Woven Reinforcements: Calculation and Parametric Analysis of the Properties of the Homogeneous Equivalent. La Recherche Aérospatiale, 1:1-12, 1990.

5. Chapman, C.: Effects of Assumed Tow Architecture on the Predicted Moduli and Stresses in Woven Composites. Master's thesis, Texas A&M University, December, 1993.

6. Whitcomb, J.D., Chapman, C., and Srirengan, K.: Analysis of Woven Composites Subjected to Flexure. Manuscript in preparation.

7. Whitcomb, J. ; Kondagunta, G.; and Woo, K.: Boundary Effects in Textile Composites. Submitted for publication in Journal of Composite Materials.

8. Whitcomb, J. and Woo, K.: Enhanced Direct Stiffness Method for Analysis of Textile Composites. Accepted for publication in Composite Structures.

9. Woo, K, and Whitcomb, J.D.: Macro Finite Element Using Subdomain Integration. Communications in Numerical Methods in Engineering, Vol. 9, pp. 937-949, 1993.

10. Jones, R.M.: Mechanics of Composite Materials. Scripta Book Company, pg. 70, 1975.

Table 1 Modal magnitudes for interior and exterior unit cells from reference model and homogenized model.

(a) Strain modes

Global Analysis	Interior Cell					Exterior Cell				
	ϵ^0_x	ϵ^0_y	ϵ^0_{xy}	$\epsilon^0_{x,y}$	$\epsilon^0_{y,x}$	ϵ^0_x	ϵ^0_y	ϵ^0_{xy}	$\epsilon^0_{x,y}$	$\epsilon^0_{y,x}$
	Constant Moment									
Reference	0.00E-0	0.00E-0	0.00E-0	1.11E-3	0.00E-0	2.22E-3	-4.23E-3	0.00E-0	1.11E-3	0.00E-0
Homogenized	0.00E-0	0.00E-0	0.00E-0	1.11E-3	0.00E-0	2.22E-3	-2.83E-3	0.00E+0	1.11E-3	0.00E-0
	Transverse End Load									
Reference	0.00E-0	0.00E-0	-8.04E-3	7.71E-4	0.00E-0	1.81E-3	-3.38E-3	-3.56E-3	1.04E-3	7.45E-4
Homogenized	0.00E-0	0.00E-0	-7.34E-3	5.29E-4	0.00E-0	1.28E-3	-1.53E-3	-4.03E-3	0.75E-3	3.39E-4
	Transverse Lateral Load									
Reference	-1.60E-4	9.30E-4	-3.85E-3	3.41E-4	6.50E-5	3.20E-4	-7.21E-4	-1.84E-3	1.39E-4	3.86E-4
Homogenized	-1.87E-4	8.13E-4	-3.55E-3	2.68E-4	3.60E-5	2.18E-4	-2.55E-4	-2.12E-3	1.38E-4	1.68E-4

(b) Stress modes

Global Analysis	Interior Cell					Exterior Cell				
	σ^0_x	σ^0_y	σ^0_{xy}	$\sigma^0_{x,y}$	$\sigma^0_{y,x}$	σ^0_x	σ^0_y	σ^0_{xy}	$\sigma^0_{x,y}$	$\sigma^0_{y,x}$
	Constant Moment									
Reference	0.00E+0	0.00E+0	0.00E+0	4.60E+7	5.33E+4	6.37E+7	-3.35E+5	0.00E+0	-0.08E+7	-2.67E+4
Homogenized	0.00E+0	0.00E+0	0.00E+0	4.15E+7	0.00E+0	8.31E+7	0.00E+0	0.00E+0	4.15E+7	0.00E+0
	Transverse End Load									
Reference	0.00E+0	0.00E+0	-2.11E+7	3.21E+7	3.63E+4	5.08E+7	1.13E+5	-1.04E+7	5.58E+6	-5.61E+4
Homogenized	0.00E+0	0.00E+0	-2.20E+7	1.94E+7	0.00E+0	4.74E+7	3.60E+5	-1.14E+7	2.93E+7	3.22E+5
	Transverse Lateral Load									
Reference	-2.33E+5	4.83E+6	-1.02E+7	9.82E+6	2.99E+5	1.48E+7	1.25E+6	-5.20E+6	-1.81E+6	1.02E+5
Homogenized	-3.91E+5	5.18E+6	-1.07E+7	7.75E+6	1.88E+5	1.39E+7	1.56E+6	-5.78E+6	5.52E+6	1.92E+5

Table 2 Reference peak stresses and corresponding global/local stresses (%e = percent error)

Global/Local Analysis	Interior Cell						Exterior Cell					
	σ_x	%e	σ_y	%e	σ_{xy}	%e	σ_x	%e	σ_y	%e	σ_{xy}	%e
	Constant Moment											
Reference	1.22E+08		3.12E+07		5.02E+07		2.53E+08		5.95E+07		9.71E+07	
Reference Sup:												
Displacement Fit	1.22E+08	0	3.12E+07	0	5.02E+07	0	2.21E+08	-13	4.01E+07	-33	9.09E+07	-6
Force Fit	1.22E+08	0	3.12E+07	0	5.02E+07	0	2.81E+08	11	6.39E+07	8	8.53E+07	-12
Homogenized Sup:												
Displacement Fit	1.22E+08	0	3.12E+07	0	5.02E+07	0	2.40E+08	-5	5.66E+07	-5	9.96E+07	3
Force Fit	1.10E+08	-10	2.82E+07	-10	4.54E+07	-10	3.68E+08	45	8.60E+07	45	14.30E+07	47
	Transverse End Load											
Reference	2.47E+08		6.10E+07		-1.15E+08		3.01E+08		5.64E+07		-1.03E+08	
Reference Sup:												
Displacement Fit	2.47E+08	0	6.07E+07	-1	-1.16E+08	1	2.00E+08	-34	4.68E+07	-17	-1.03E+08	0
Force Fit	2.36E+08	-5	5.80E+07	-5	-1.11E+08	-4	2.37E+08	-21	5.96E+07	6	-1.04E+08	1
Homogenized Sup.												
Displacement Fit	2.11E+08	-15	5.13E+07	-16	-0.99E+08	-14	1.57E+08	-48	4.90E+07	-13	-0.96E+08	-7
Force Fit	2.17E+08	-12	5.24E+07	-14	-1.00E+08	-13	2.24E+08	-26	6.48E+07	15	-1.22E+08	18
	Distributed Lateral load											
Reference	1.32E+08		3.38E+07		-6.32E+07		1.14E+08		2.21E+07		-4.93E+07	
Reference Sup:												
Displacement Fit	1.17E+08	-11	3.23E+07	-4	-5.49E+07	-13	0.39E+08	-66	1.07E+07	-52	-1.99E+07	-60
Force Fit	1.05E+08	-21	2.92E+07	-14	-4.85E+07	-23	0.70E+08	-39	2.26E+07	2	-2.14E+07	-57
Homogenized Sup:												
Displacement Fit	1.01E+08	-23	2.71E+07	-20	-5.06E+07	-20	0.33E+08	-71	1.42E+07	-36	-2.31E+07	-53
Force Fit	1.05E+08	-21	2.94E+07	-13	-4.92E+07	-22	0.67E+08	-41	2.06E+07	-7	-2.35E+07	-52

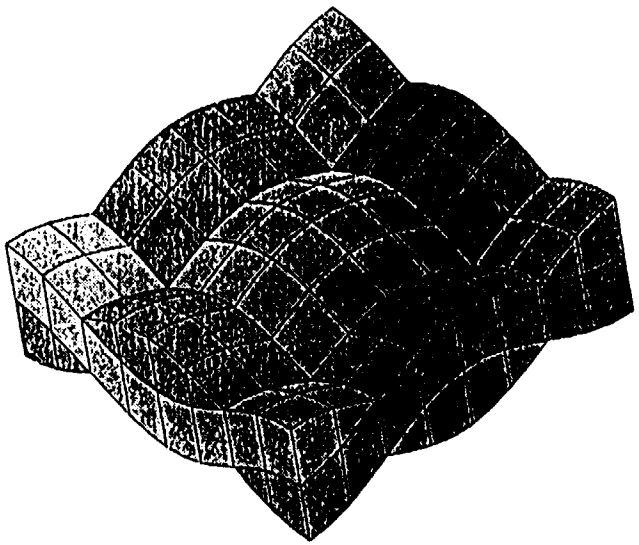

Plain weave

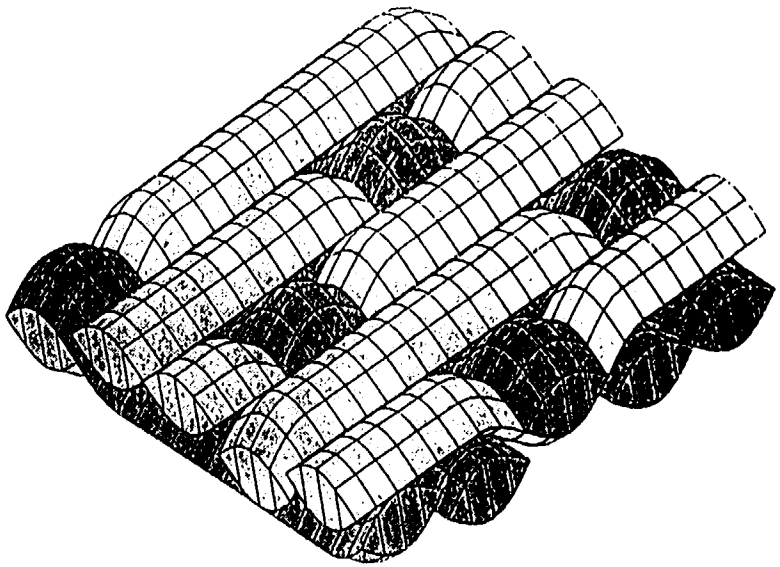

5-harness satin weave

Figure 1 Examples of textile architecture.

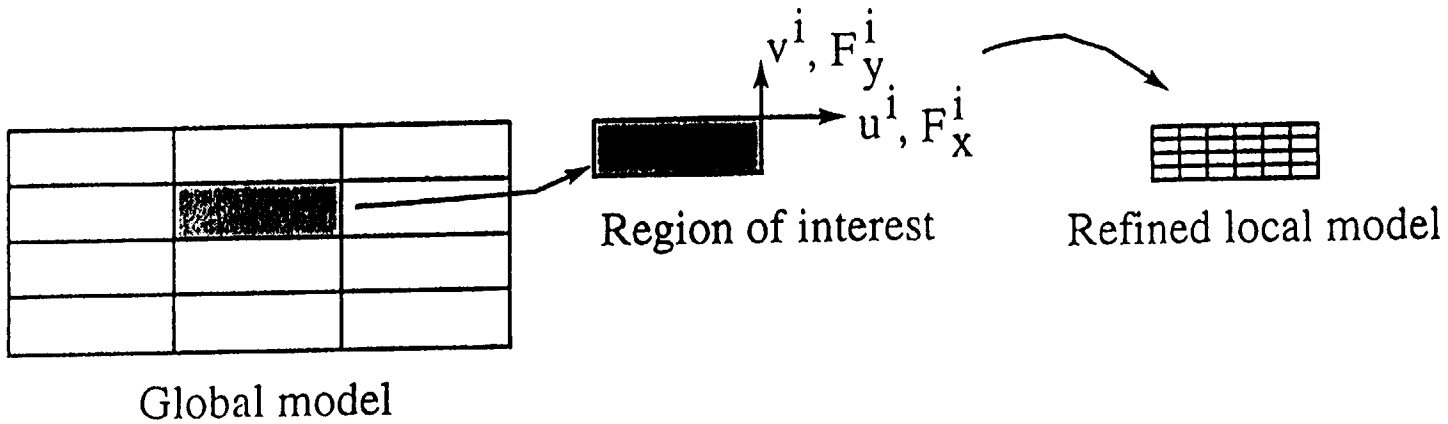

Figure 2 Boundary data.

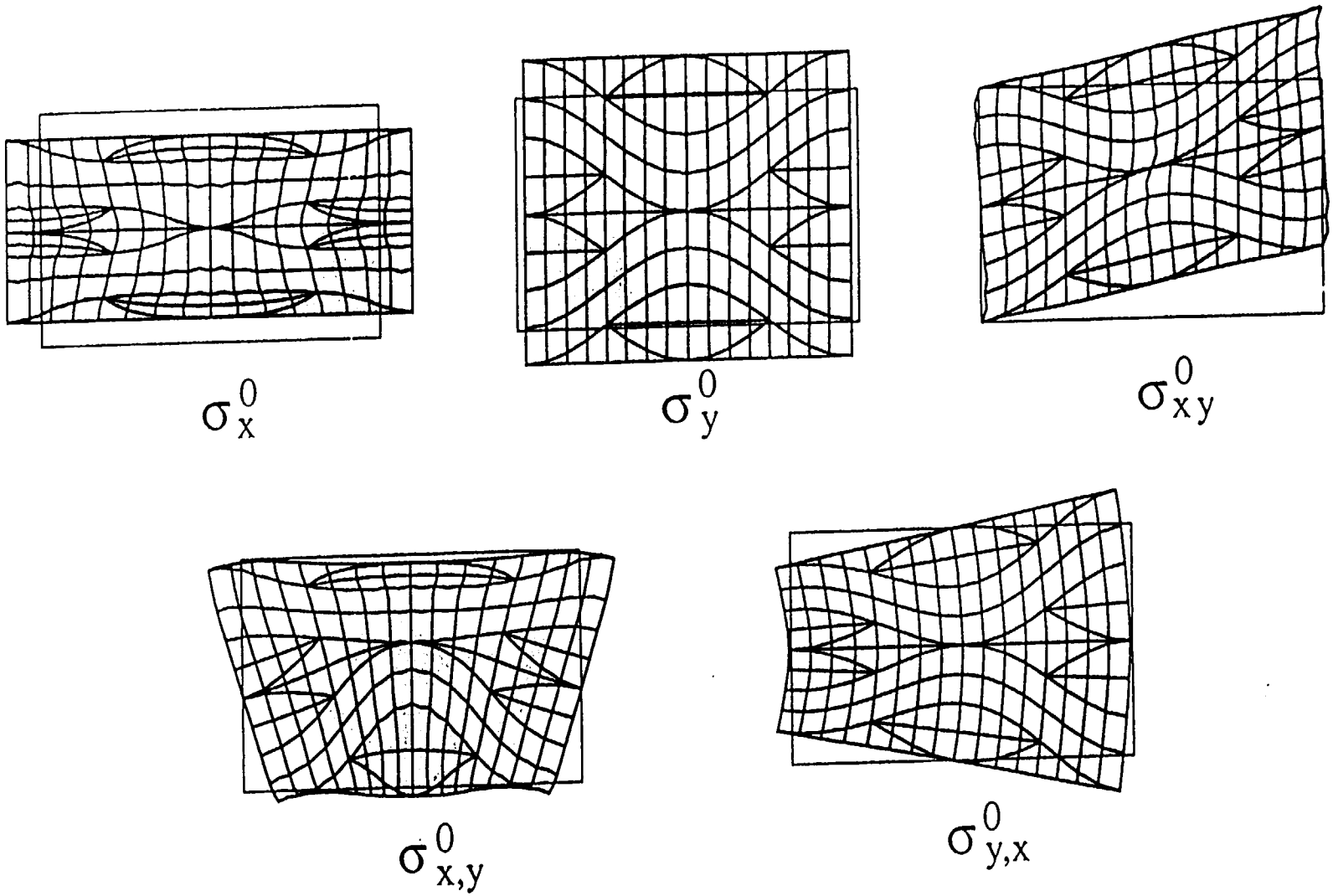

Figure 3 Deformed meshes for the five interior stress modes.

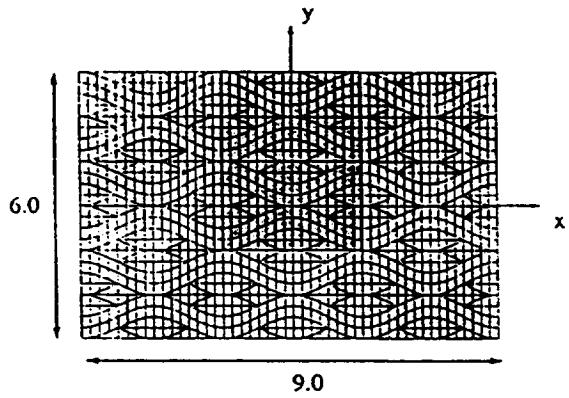

(a) Reference mesh

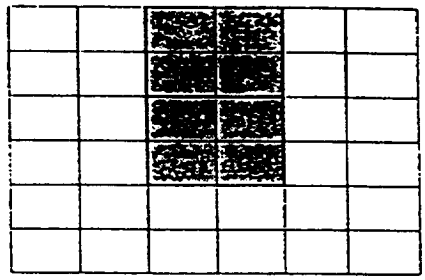

(b) Mesh used with homogenized properties

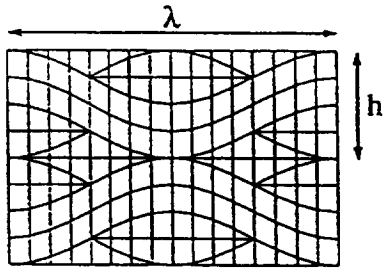

(c) Local finite element mesh

Figure 4 Finite element meshes.

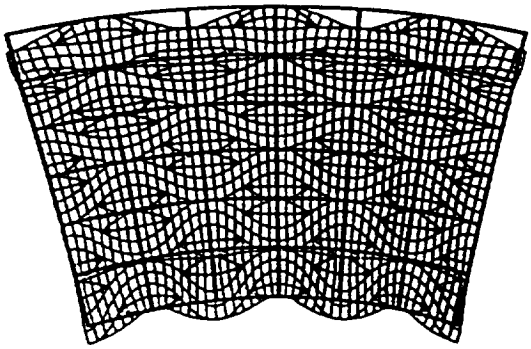

(a) Constant Moment

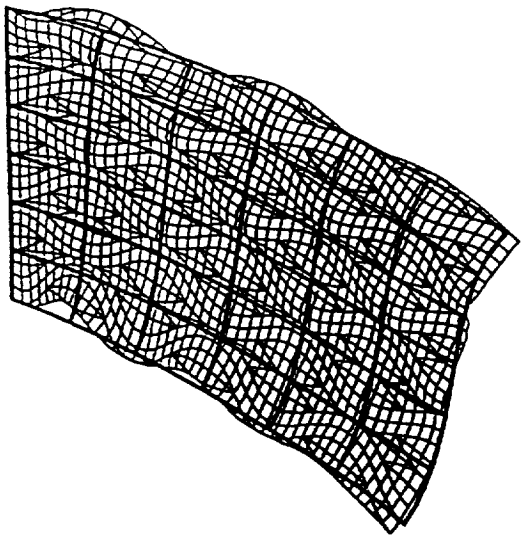

(b) Transverse End Load

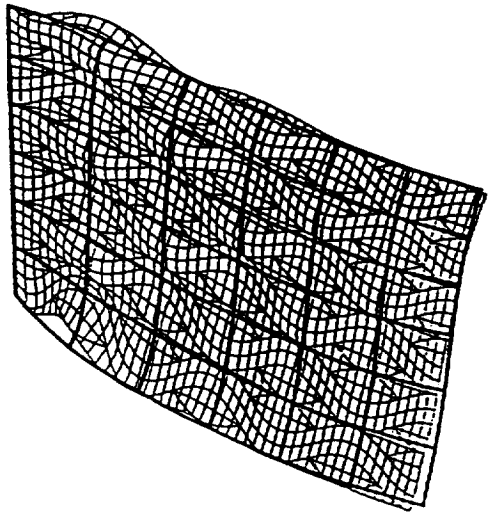

(c) Distributed Lateral Load

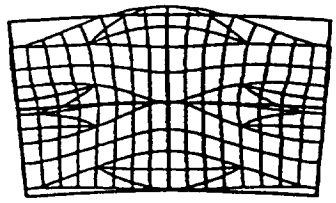

Exterior Cell

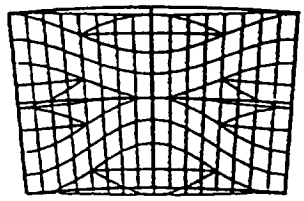

Interior Cell

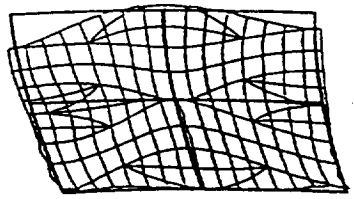

Exterior Cell

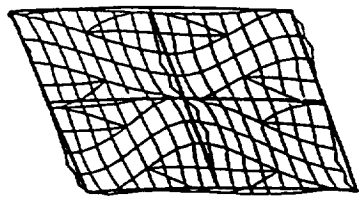

Interior Cell

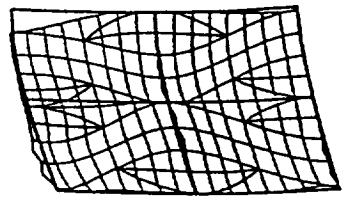

Exterior Cell

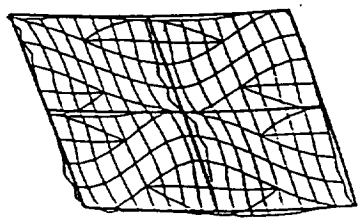

Interior Cell

Figure 5 Comparison of deformed meshes of reference model and homogenized property model.

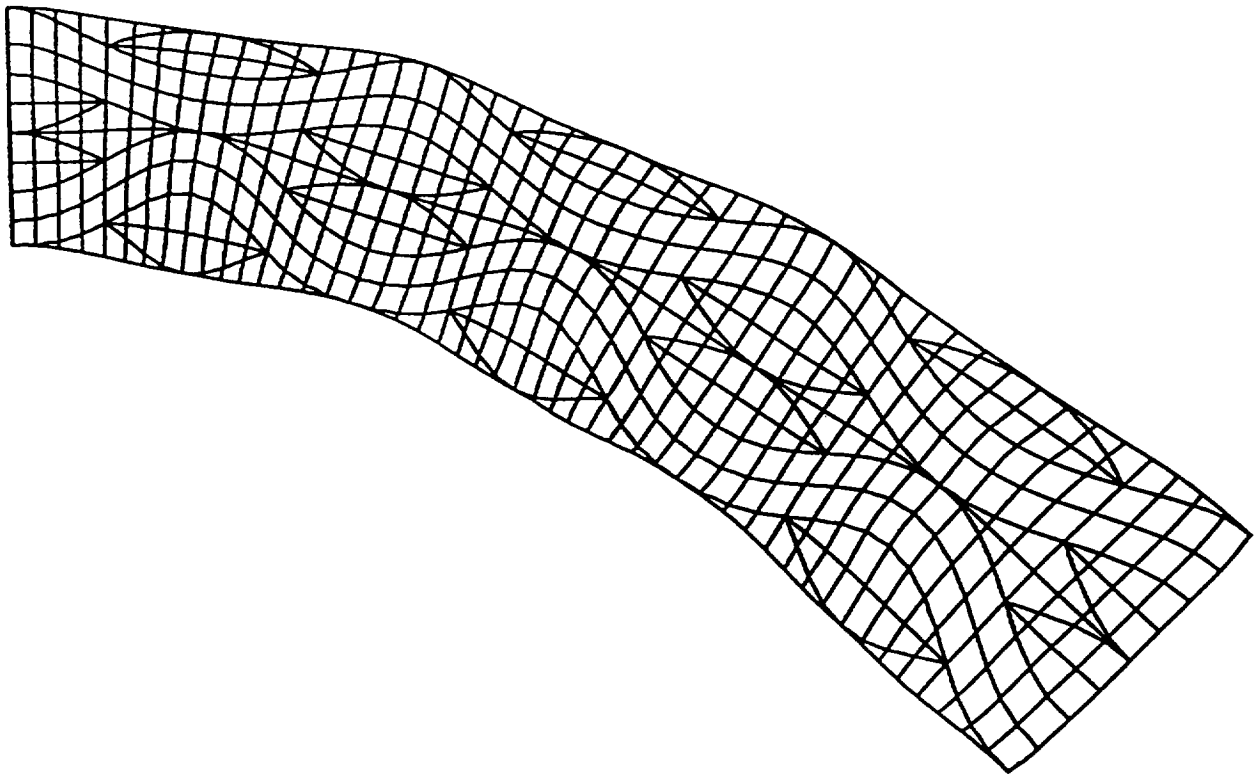

Figure 6 Artifacts due to magnification of deformation.

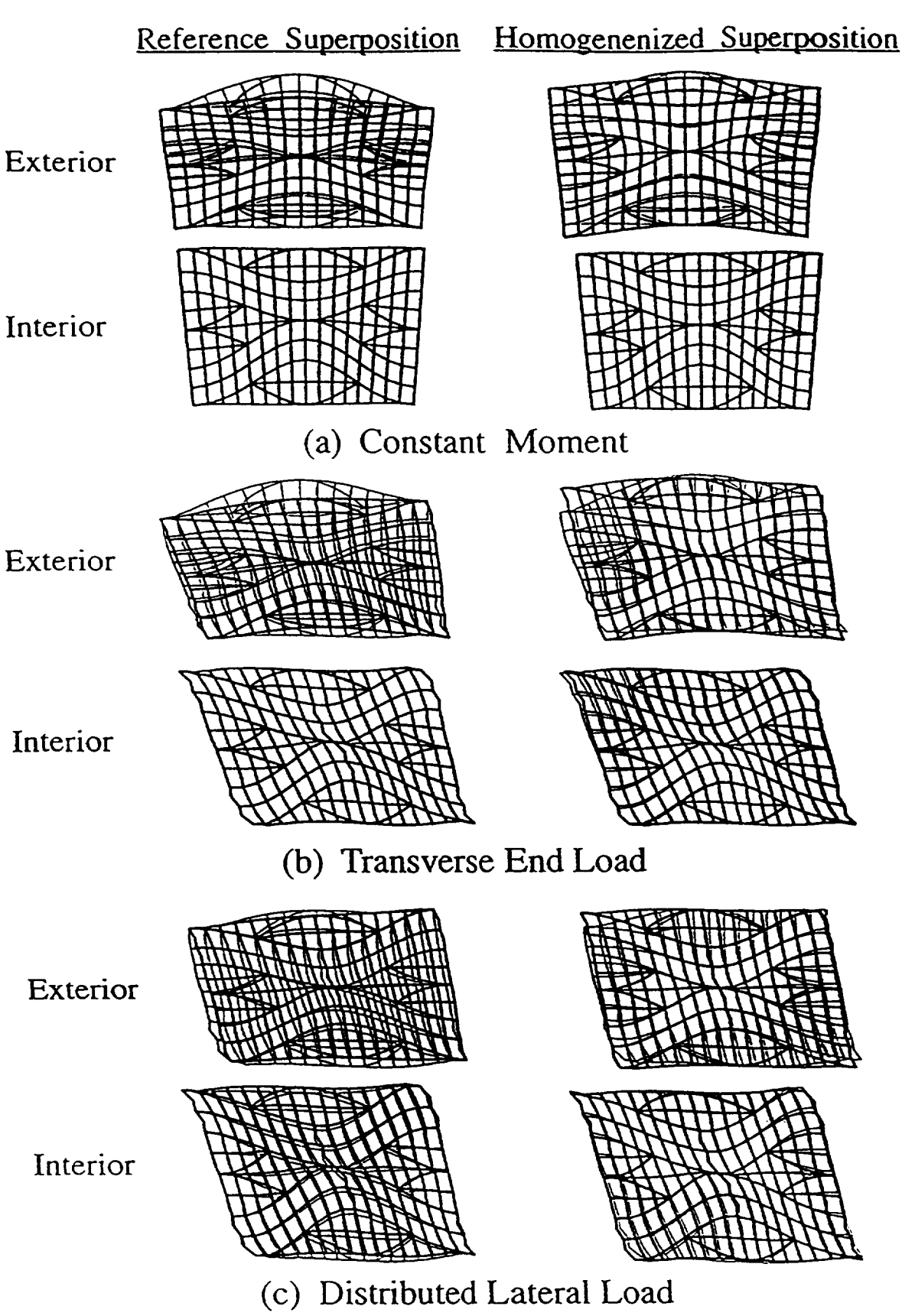

Figure 7 Comparison of deformed meshes for strain mode superposition results.

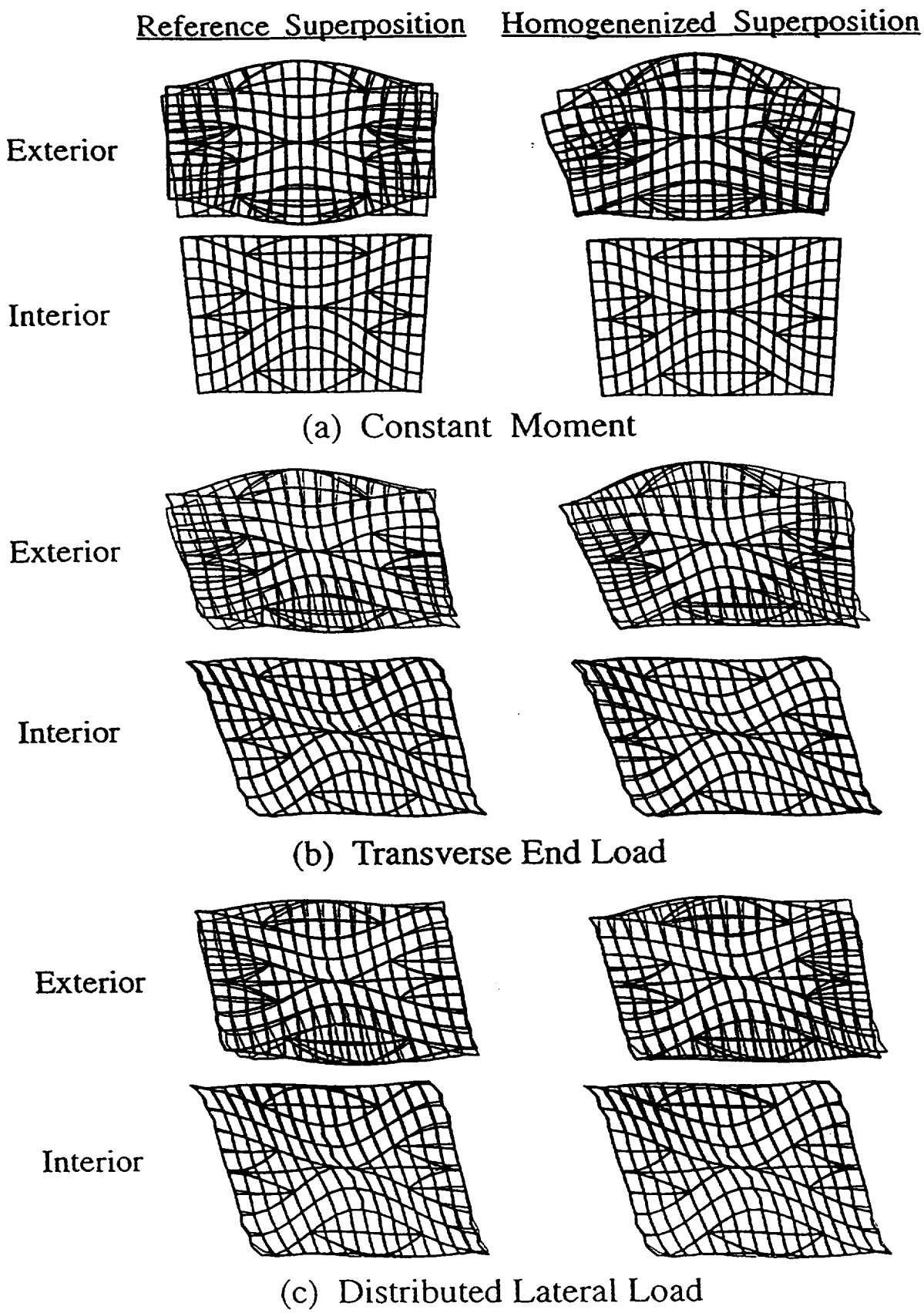

Figure 8 Comparison of deformed meshes for stress mode superposition results .

Reference solution

Homogenized superposition

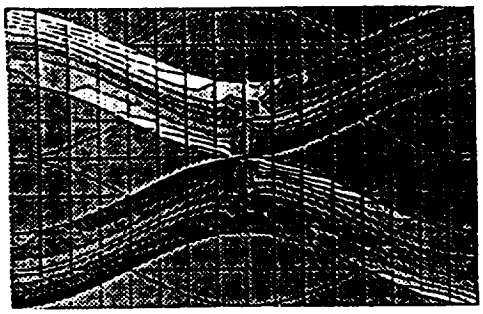

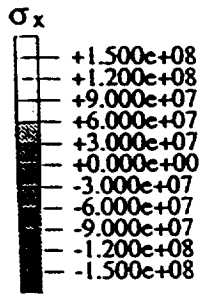

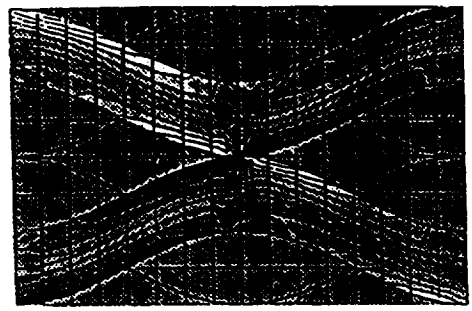

Peak magnitude : 2.47E+08

Peak magnitude : 2.11E+08
Error : -15%

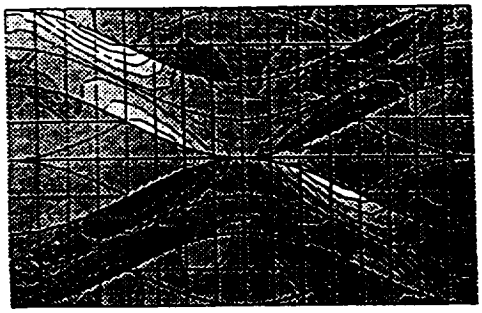

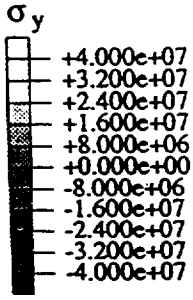

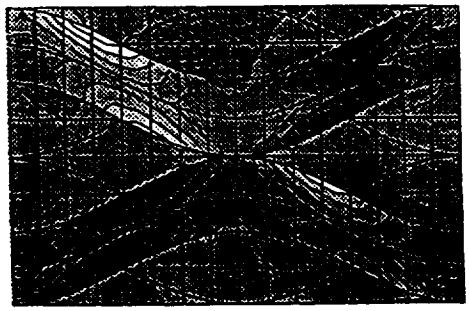

Peak magnitude : 6.10E+07

Peak magnitude : 5.13E+07
Error : -16%

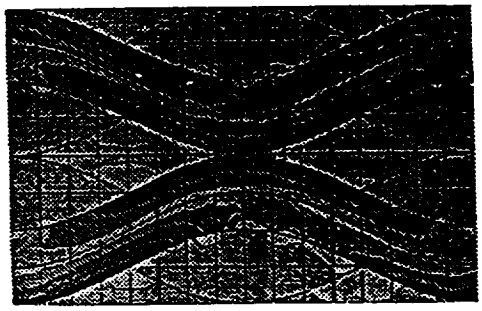

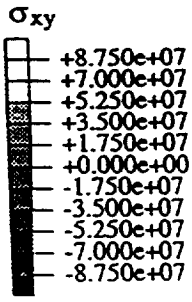

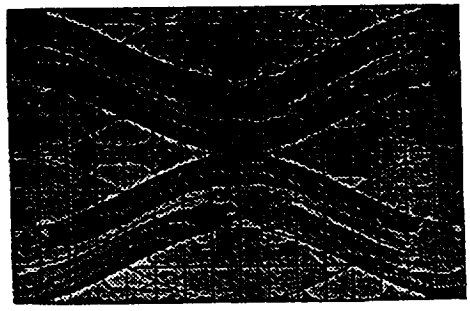

Peak magnitude : -1.15E+08

Peak magnitude : -0.99E+08
Error : -14%

Figure 9 Comparison of stress distributions of reference solution and homogenized strain mode superposition for the interior cell for transverse end load case .

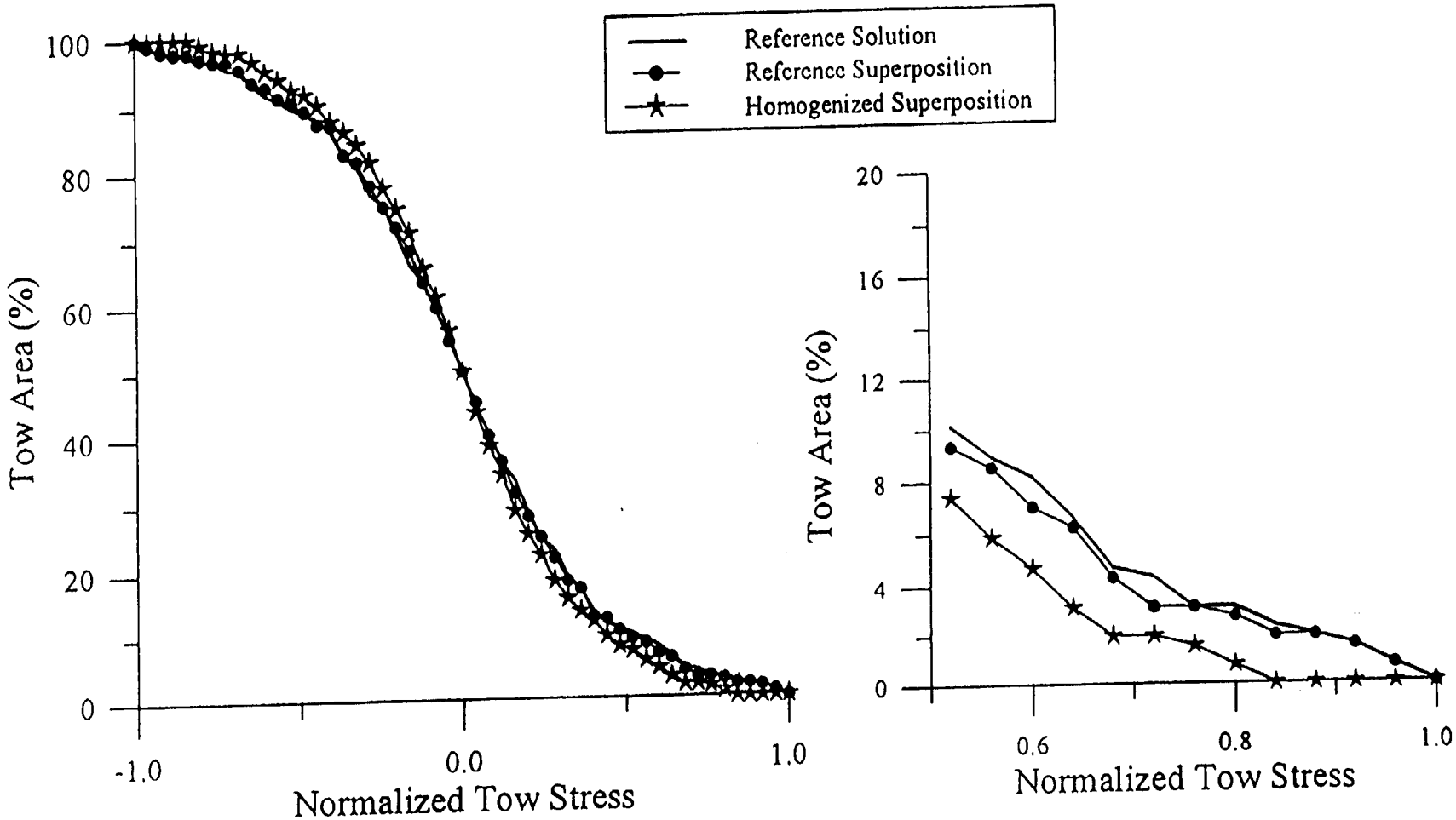

Figure 11 Tow area with σ_x greater than particular stress level.
Interior cell for transverse end load case.

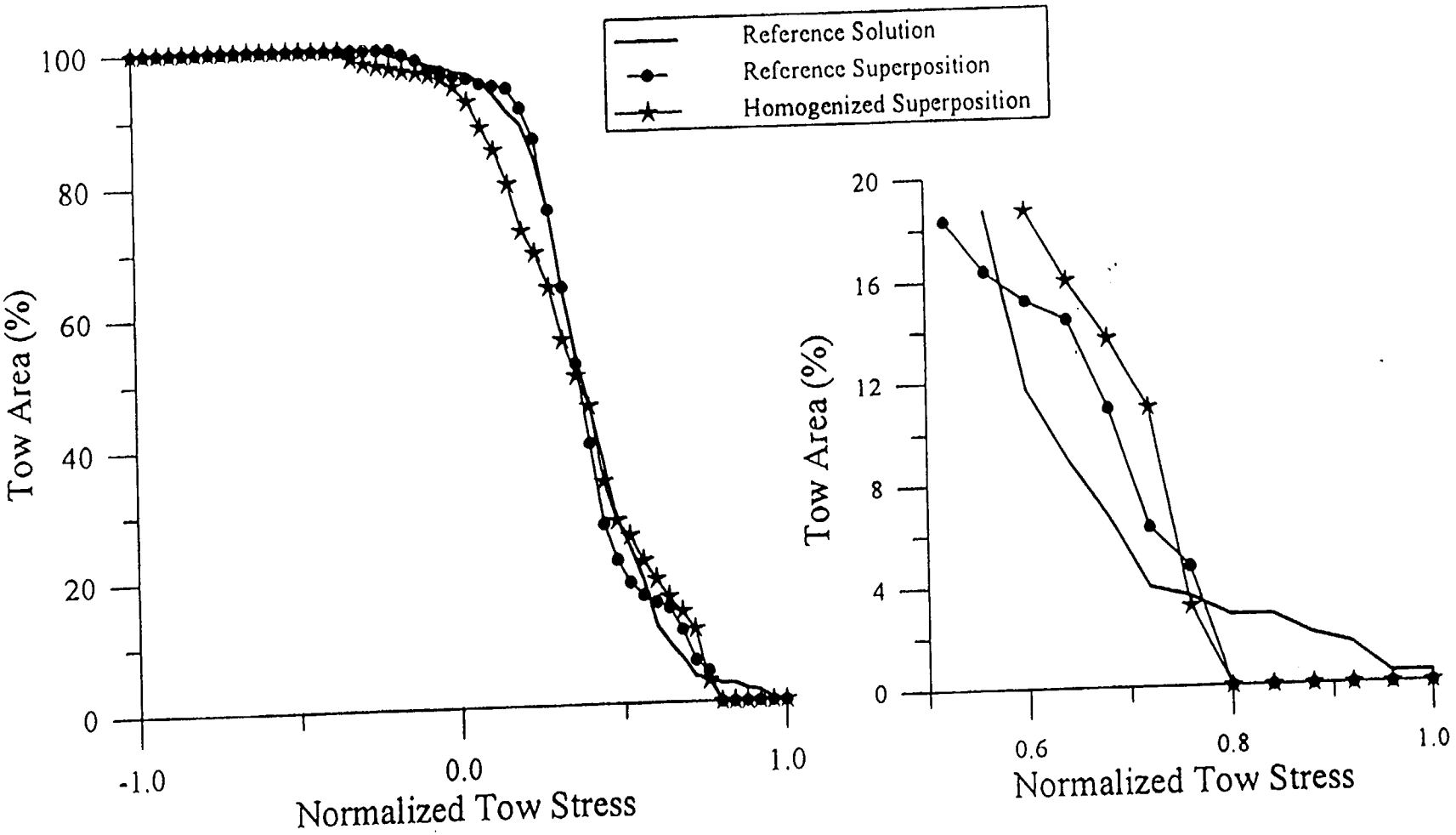

Figure 12 Tow area with σ_x greater than particular stress level.
Exterior cell for transverse end load case.

Chapter: 6

Simulation of Progressive Failure in Plain Weave Textile Composites

Abstract

Three-dimensional finite element analysis was used to simulate progressive failure of a plain weave subjected to in-plane extension. The loading was parallel to one of the tow directions. The effects of various characteristics of the finite element model on predicted behavior were examined. More numerical studies and comparisons with experimental data are needed to establish guidelines for accurate progressive failure prediction. Also the sensitivity of the predictions to the tow waviness was studied. The predicted strength decreased considerably with increased waviness.

Introduction

Textile composites consist of interlaced fiber bundles which are then impregnated with a matrix material and cured. Figure 1 illustrates the architecture for a plain weave composite. The interlacing of the fibers offers the potential for increased through-thickness strength There is also the potential for reduced fabrication costs, since fairly complicated shapes can be formed using textile machinery. One disadvantage of textiles is the difficulty in predicting their performance. The complex geometry makes detailed stress analysis quite challenging. The early analyses were based on modified laminate theory. (eg. References 1,2). In recent years there have been a few attempts to discretely model the fiber bundle architecture and predict internal stress states (eg References 3-10). Reference 10 presented a particularly interesting progressive failure analysis of a plain weave composite. The results in Reference 10 consisted of nominal stress strain curves. The response of the composite was almost linear for in-plane extension and highly nonlinear for in-plane shear. the nonlinearity was primarily a result of progressive damage. However, little information was provided on damage evolution and load redistribution within the composite during the loading process. Also, there was no indication of the sensitivity of the predictions to mesh refinement or other approximations inherent in such analyses.

This paper has two objectives. The first is to evaluate the sensitivity of predicted progressive failure to quadrature order, mesh refinement, and choice of material degradation model. The second objective is to describe the nature of the progressive failure process for two weaves with very different waviness. Loading consisted of a nominally uniaxial stress along one of the fiber tow directions. Only mechanical loads were considered in this study. To simplify the response the composite was assumed to consist of an infinite number of unit cells in all three coordinate directions.

The following sections begin with a description of the basic theory used for progressive damage modelling. Then the configurations will be described. Finally the results from the numerical simulations will be discussed.

Theory

There is no "right" way to model damage evolution that is also practical. It is not feasible to discretely model the damage, so approximation is unavoidable. Perhaps the simplest procedure to account for damage in a finite element model is to modify the constitutive matrix at the quadrature points of a numerically integrated finite element. No history effects are included, so the analysis of the loading becomes a series of elastic analyses. Of course, there are many possibilities for how to modify the constitutive matrix. Three techniques were used herein. The first method considered the material totally failed (i.e. the entire constitutive matrix was reduced to essentially zero) when any allowable stress component was exceeded. This method will be referred to as the non-selective discount method. Except as noted, this technique was used in the analyses. The second technique selectively reduced the rows and columns of the constitutive matrix according to the particular stress allowable which was exceeded. The third technique selectively reduced the engineering moduli according to the particular stress allowable which was exceeded. The scheme for this selective reduction was based on References 10.

Figure 2 gives a flowchart for the progressive failure analysis. First a linear analysis was performed. Based on the calculated stresses, the initial load was scaled back so that failure would occur only at points which were within two percent of the maximum normalized stress. (The stresses were normalized by the respective strengths.) The constitutive matrix was modified at the failure points. Residual forces were calculated and used to determine the incremental displacements required to restore equilibrium. The total displacements were updated and used to determine the new stresses. If no further failures occurred at the current nominal strain state, the nominal strain was incremented to cause failure. This procedure was repeated until there was total failure or at least loss of most of the original stiffness.

Configurations

The fiber bundles or tows in the models were generated by translating a lenticular cross-section along a sinusoidal path. The waviness ratio is defined to be the ratio of the woven mat thickness to the wavelength. Except where indicated otherwise, the results presented are for a waviness ratio of 1/3. More details about the mesh geometry can be found in Reference 8. The following subsections describe the finite element meshes, the boundary conditions, and the material properties.

Finite Element Meshes

Symmetry in the material and loading was exploited so that only 1/32 of a unit cell had to be modeled. A wide range of mesh refinements were used, as shown in Figure 3. The crude mesh had only 4 elements and 43 nodes. The most refined mesh had 192 elements and 1049 nodes.

Boundary Conditions

The periodic boundary conditions for a complete unit cell are quite simple. The appropriate boundary conditions for a 1/32 unit cell are a bit more complicated. Derivation of the periodic boundary conditions is somewhat tedious, so details will not be given here. Details can be found in Reference 8. The periodic conditions are listed below. Figure 3 shows the coordinate system assumed.

$$u(a/2,y,z) = u_0 \qquad v(x,a/2,z) = \text{constant}$$
$$u(0,y,z) = -u(0,y,-z) \qquad v(0,y,z) = v(0,y,-z)$$
$$u(x,0,z) = u(x,0,-z) \qquad v(x,0,z) = -v(x,0,-z)$$

$$w(x,y,c/2) = \text{constant}$$
$$w(0,y,z) = -w(0,y,-z)$$
$$w(x,0,z) = -w(x,0,-z)$$

The load was controlled by specifying the magnitude of u_0.

Material Properties

The unit cells contains two "types of materials: the tows and the matrix pockets. Relative to the material coordinate system, the properties of the tows are invariant (before damage occurs). Of course, the properties of the tows are needed in the global coordinate system. Fourth order tensor transformation formula were used to perform the required calculations. The rotation angles to be used in these formulas were obtained at each quadrature point by using interpolation. This procedure was shown in Reference 8 and 11 to be preferable to using a single angle for the entire element. The particular properties used are listed below. These properties are from Reference 12.

	Tow properties		Matrix properties	
	Modulus	Strength	Modulus	Strength
E_{11}	154.27 GPa	2342.0 MPa	3.45 GPa	84.85 MPa
E_{22}	10.80 GPa	56.6 MPa	3.45 GPa	84.85 MPa
E_{33}	10.80 GPa	56.6 MPa	3.45 GPa	84.85 MPa
G_{12}	7.47 GPa	48.7 MPa	1.28 GPa	101.00 MPa
G_{13}	7.47 GPa	48.7 MPa	1.28 GPa	101.00 MPa
G_{23}	3.33 GPa	48.7 MPa	1.28 GPa	101.00 MPa
ν_{12}	0.278		0.35	
ν_{13}	0.278		0.35	
ν_{23}	0.340		0.35	

Results and Discussions

Most of the results in this paper illustrate the effects of characteristic of the finite element model on the progressive failure prediction. The effects of quadrature order, mesh refinement, and material degradation strategy will be considered first. Then the effect of tow waviness on failure behavior will be discussed.

Figure 4 shows the effect of quadrature order on the stress-strain curve. The peak stress obtained using 8 quadrature points (2x2x2), is 10 percent higher than that obtained using 27 or 64 points. Although the peak stress is the same for 27 and 64 points, damage is predicted earlier when 64 points integration is used. This sensitivity is not particularly surprising for at least two reasons. First, when more quadrature points are used, the more extensive sampling is more likely to find the extremes in the stress field. Second, when failure occurs within an element and the constitutive matrix is modified, the element becomes inhomogeneous. The numerical integration effectively fits a polynomial function to the variation of material properties. Since the properties are very different in the failed and unfailed parts of the element, it is difficult to obtain a good fit. In fact, there is concern as to whether the assumed quadratic displacement functions for a 20-node element are sufficient to obtain a reasonable approximation regardless of the integration order.

Figure 5 shows the effect of mesh refinement on the predicted stress-strain curve for two waviness ratios. The 4 element model predicts the correct trends, but is quite inaccurate. The error is much worse for the large waviness ratio. For the 1/6 waviness ratio, the 32 and 192 element models agree quite well. There is a considerable difference between the 32 and 192 element models for the 1/3 waviness ratio. Although the response is quite brittle for both waviness ratios, there is no more non-catastrophic damage before collapse for the larger waviness ratio.

Figure 6 shows the effect of the discount factor on the stress-strain curve. The stiffness terms at failed quadrature points were reduced to either 01. or .0001 of the original value. Intuitively, one might expect to obtain the same results. Figure 6 shows that there was no difference in the peak stress, but the response was very different when there is considerable damage.

Figure 7 shows the stress-strain curves obtained using non-selective discount method, selective reduction of rows and columns in the constitutive matrix (the stiffness terms, not the compliance terms), and the selective method described in Reference 10. The selective method described in Reference 10 predicts about a 21 percent higher peak stress than the non-selective discount method.

Figures 8 and 9 show the effect of mesh refinement and waviness ratio on damage accumulation during loading. The black region indicates the damage zone. The stress-strain curve for a particular mesh is shown above the results for that mesh. The points labeled A,B, and C, indicate the correspondence between the strain level and the damage contours. Also indicated are the stress components which contributed to the damage contour. The 4 element mesh does not perform well at all for the waviness ratio of 1/3, but does a little better for the 1/16 waviness. The 32 element mesh performs reasonably well for obtaining qualitative results. Further numerical studies are needed to determine how close the 192 element mesh is to convergence. For the 1/3 waviness ratio the σ_{33} stress component dominates the damage development up to the point shown. For the 1/6 waviness ratio σ_{33} plays a part, but there is also significant cracking of the 90 degree tow due to σ_{22}. Reference 6 had also noted a change in initial damage mode with waviness ratio.

Concluding Remarks

Simulation of progressive failure in a plain weave composite is extremely complex. Consequently, only approximate treatment is practical at this time. One of the goals of this paper was to examine the effect of several approximations on predicted behavior. The one obvious conclusions from this study is that the predictions are quite sensitive to a number of decisions which must be made when assembling a finite element model. Further numerical experiments and comparisons with experimental data are needed to establish guidelines for accurate analysis of progressive failure. Another objective of this paper was to describe the effect of tow waviness on damage accumulation. The results suggest that the degree of waviness not only affects the stress at which damage initiates, but also the type of damage which occurs.

References

1. Ishikawa, T. and Chou, T.W: "Stiffness and Strength Behavior of Woven Fabric Composites." Journal of Material Science, 17:3211-3220, 1982.

2. Ishikawa, T. and Chou, T.W: "Elastic Behavior of Woven Hybrid Composites," Journal of Composite Materials, 16-2-19, January 1982.

3. Paumelle, P.A. Hassim, and F. LÁnÁ: "Composites with Woven Reinforcements: Calculation and Parametric Analysis of the Properties of the Homogeneous Equivalent," La Recherche AÁrospatiale, 1:1-12, 1990.

4. Paumelle, P.A. Hassim, and F. LÁnÁ: "Microstress Analysis in Woven Composite Structures," La Recherche AÁrospatiale, 6:47-62, 1991.

5. Whitcomb J.D: "Three-Dimensional Stress Analysis of Plain Weave Composite," Composite Materials: Fatigue and Fracture, ASTM STP 1110 T.K. O'Brien, Ed., Philadelphia: American Society for Testing and Materials, 3:417-438, 1991.

6. Woo, K: "Stress and Failure Analysis of Textile Composites," Ph.D. Dissertation, Department of Aerospace Engineering, Texas A&M University, 1993.

7. Dasgupta, A. and Bhandarkar, S: "Effective Thermomechanical Behavior of Plain-Weave Fabric-Reinforced Composites Using Homogenization Theory," Journal of Engineering Materials and Technology, 116:99-105, January 1994.

8. Chapman, C: "Effects of Assumed Tow Architecture on the Predicted Moduli and Stresses in Woven Composite," MS thesis Department of Aerospace Engineering, Texas A&M University, 1993.

9. Guedes, J.M. and Kikuchi N: "Preprocessing and Postprocessing for Materials Based on the Homogenization Method with Adaptive Finite Element Methods," Computer Methods in Applied Mechanics and Engineering, 83:143-198, 1990.

10. Blackketter, D, Walrath, D, and Hansen, A: "Modeling Damage in a Plain Weave Fabric-Reinforced Composite Material," Journal of Composite Technology and Research, 15:2:136-142, Summer 1993.

11. Avery, William B. and Carl T. Herakovich, 1987: "A Study of the Mechanical Behavior of a 2D Carbon-Carbon Composite," Virginia Polytechnic Institute and State University, Interim Report 66.

12. Naik, R: "Micromechanical Combined Stress Analysis-MICSTRAN, A User Manual," NASA Contractor Report 189694, October 1992.

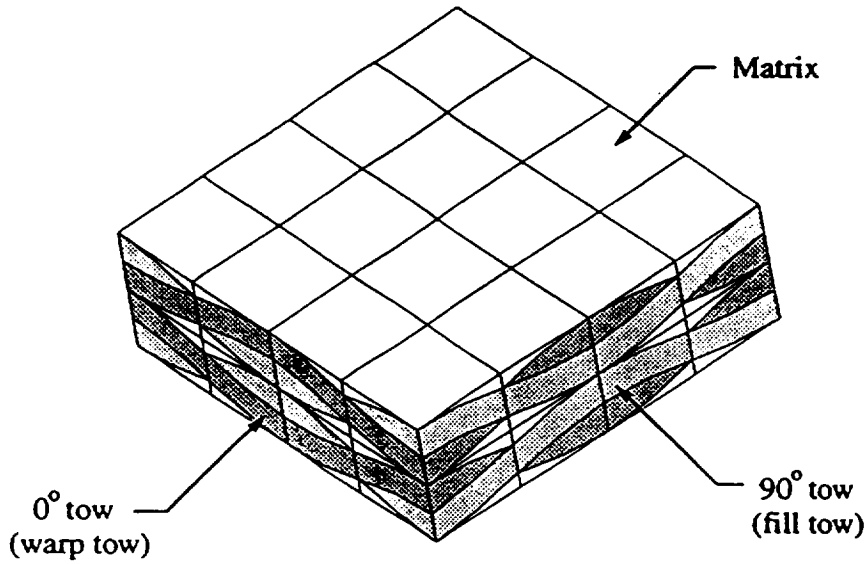

(a) A full unit cell.

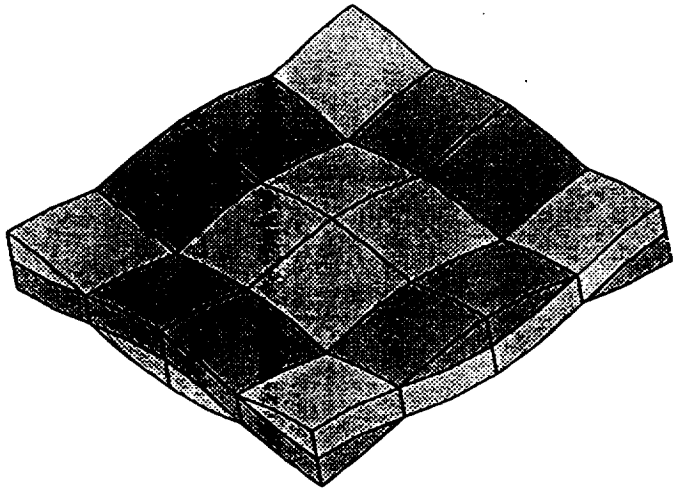

(b) A single mat with matrix pockets removed.

Figure 1 Schematic of Plain Weave composite.

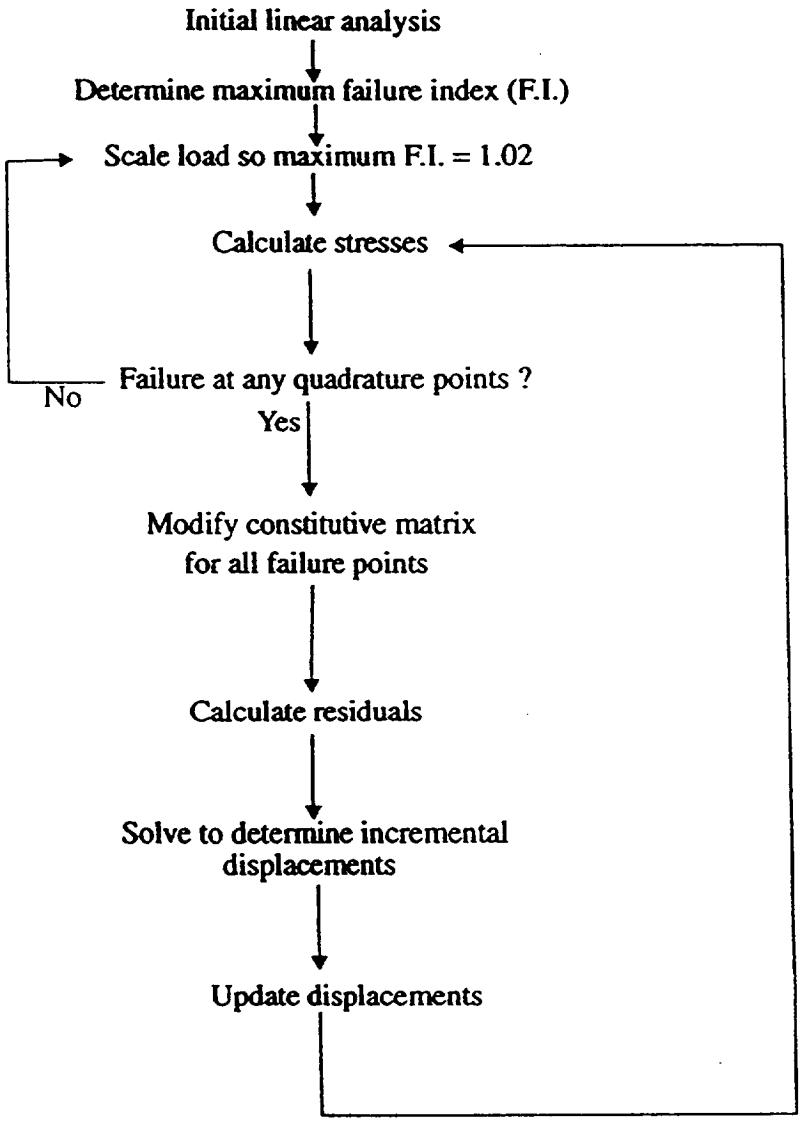

Figure 2 Flowchart of progressive failure analysis.

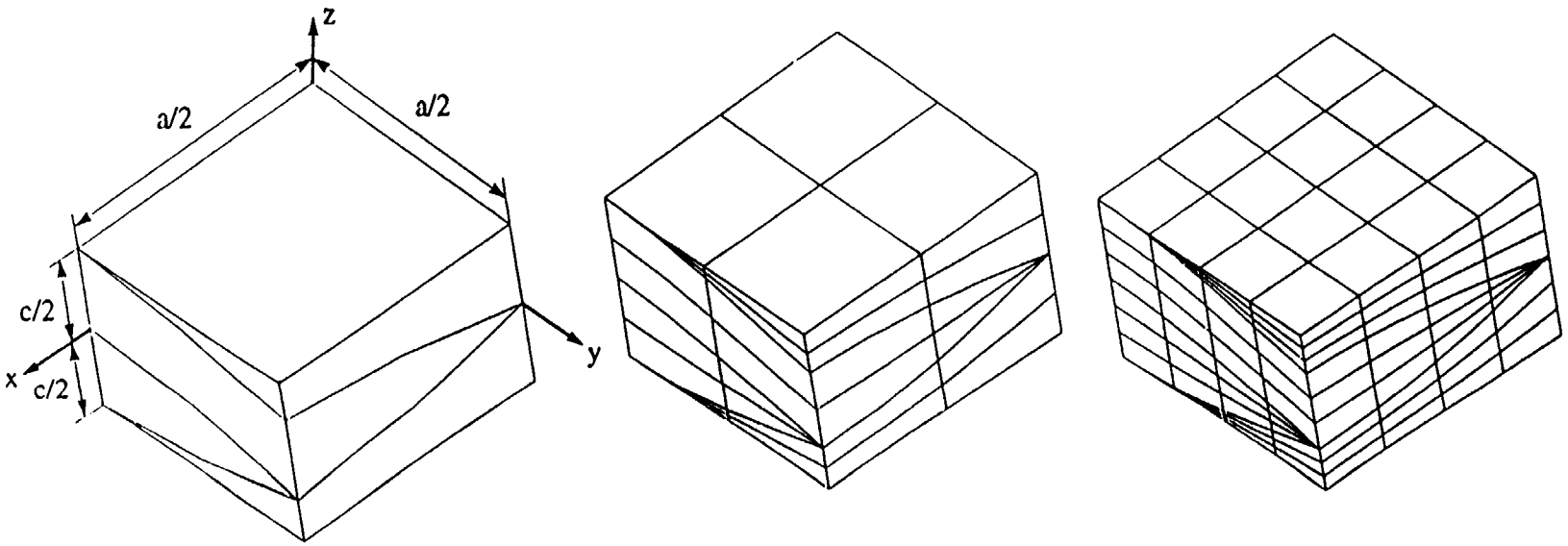

Mesh 1 :
4 elements and 42 nodes

Mesh 2 :
32 elements and 221 nodes

Mesh 3 :
192 elements and 1049 nodes

Figure 3 Finite element meshes used to determine the effect of mesh refinement on failure prediction.

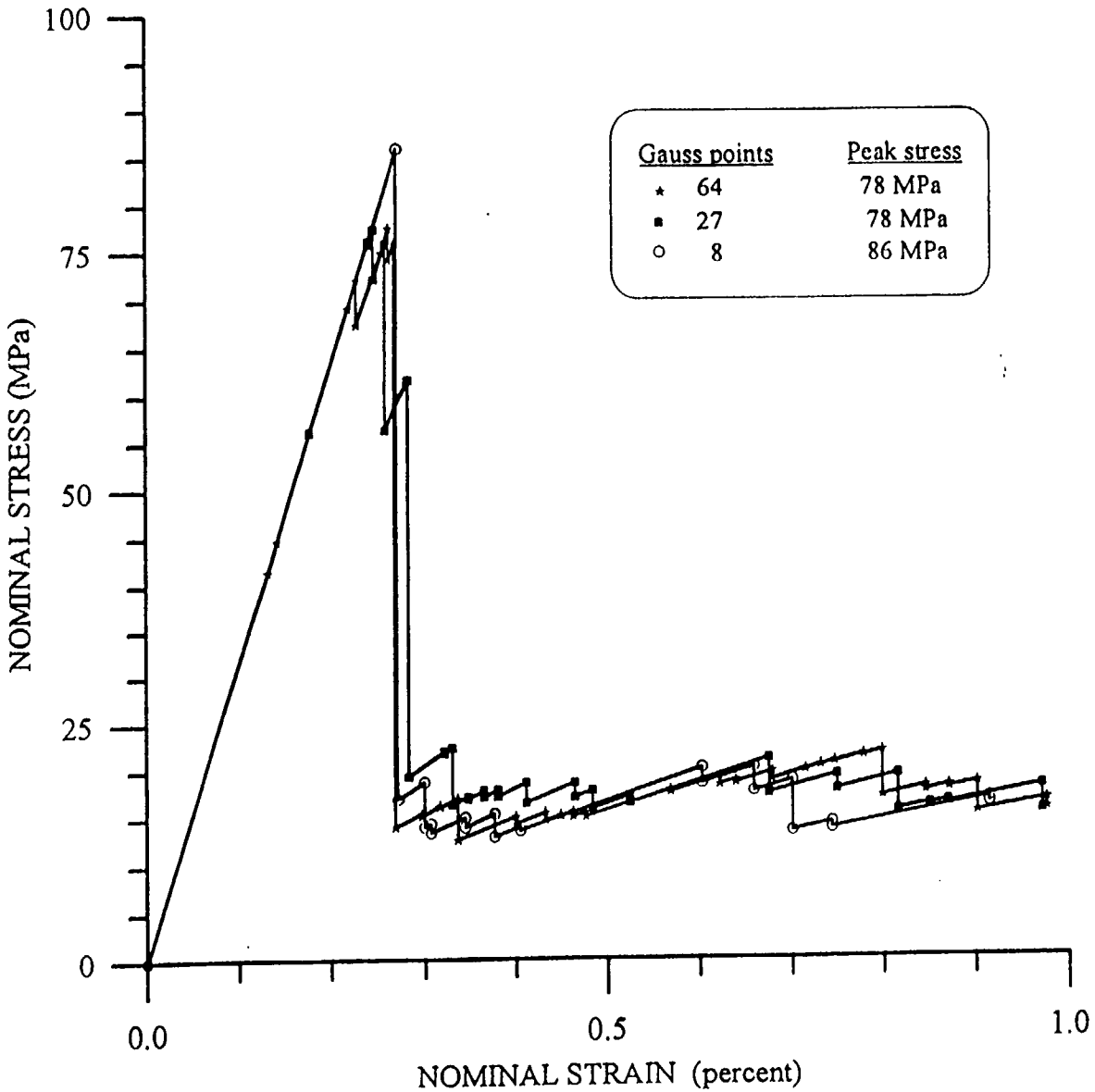

Figure 4 Effect of Gauss quadrature order on stress-strain response. Waviness ratio = 1/3. Non-selective discount method was used.

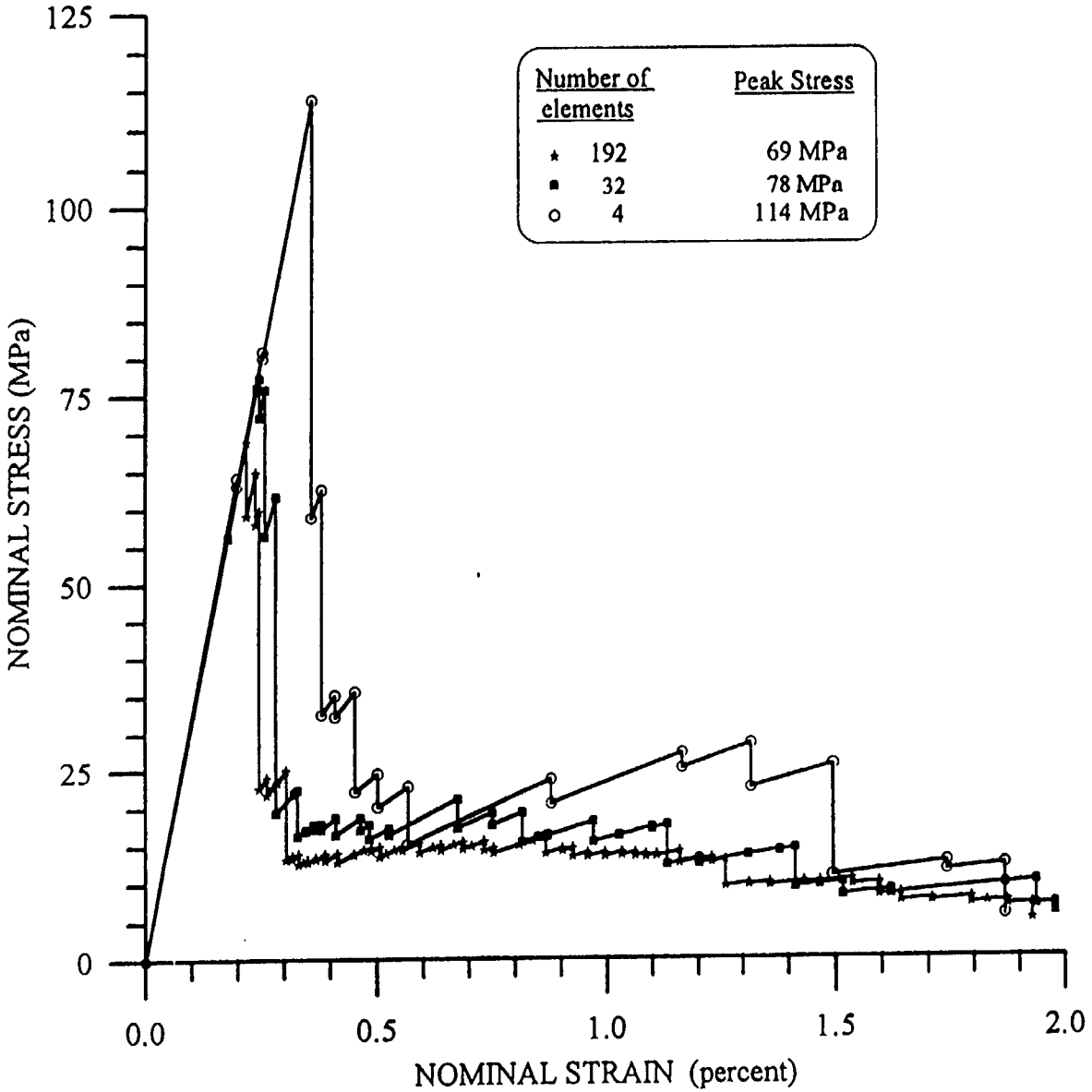

(a) Waviness ratio = 1/3

Figure 5 Effect of mesh refinement on stress-strain response. Non-selective discount method was used.

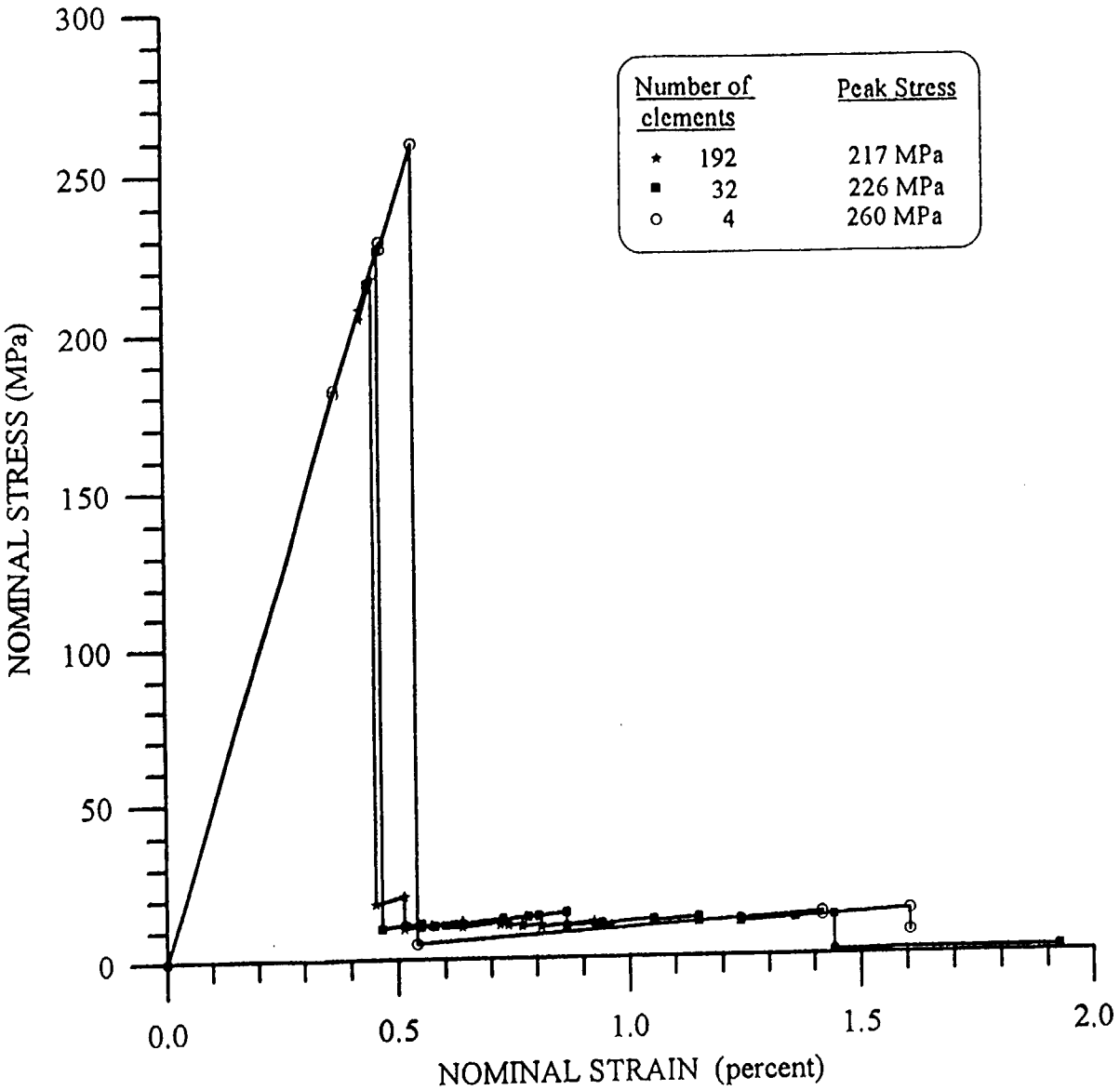

(b) Waviness ratio = 1/6

Figure 5, continued .

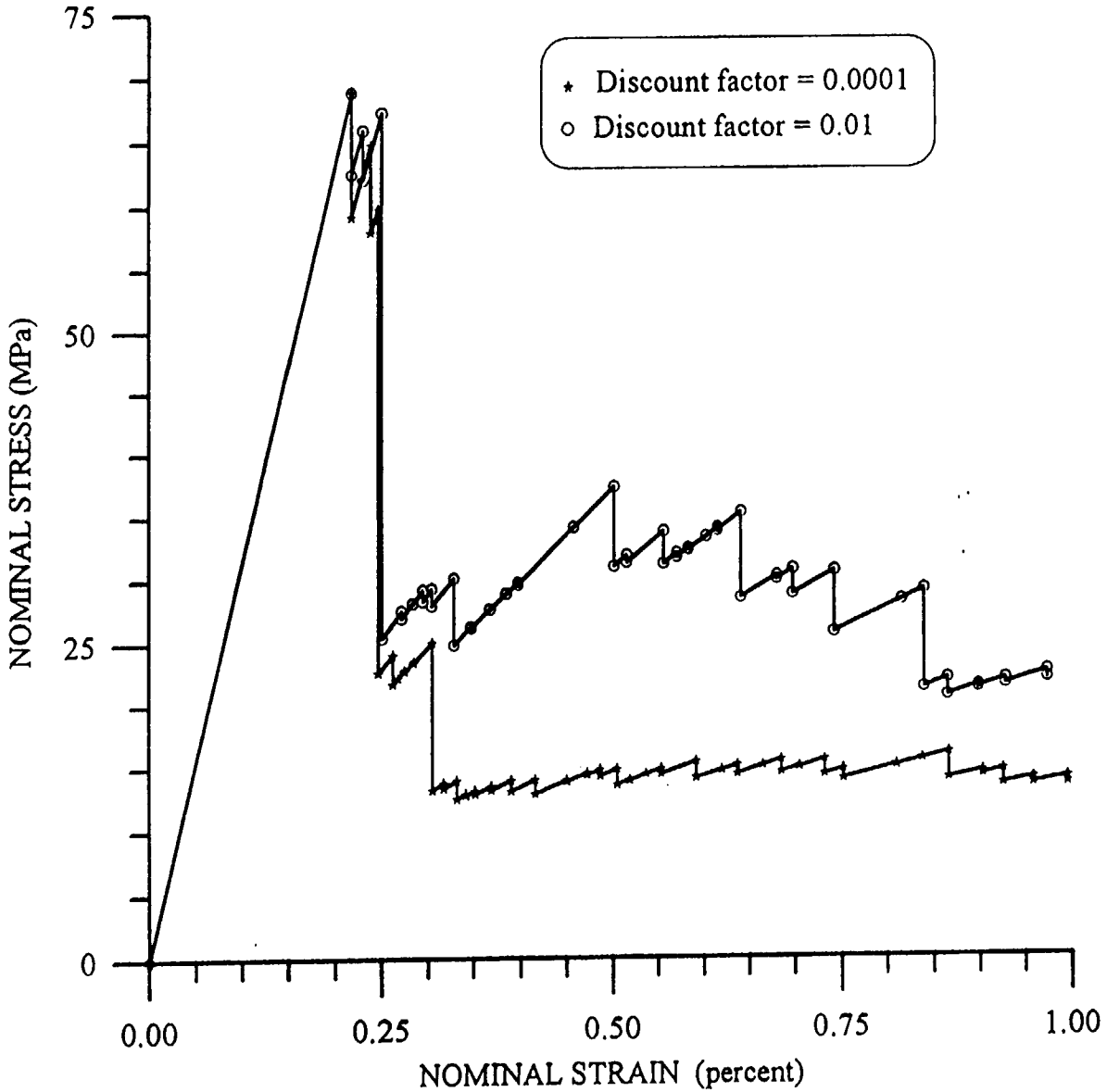

Figure 6 Effect of degradation factor on stress-strain response.
Waviness ratio = 1/3. Non-selective discount method was used.

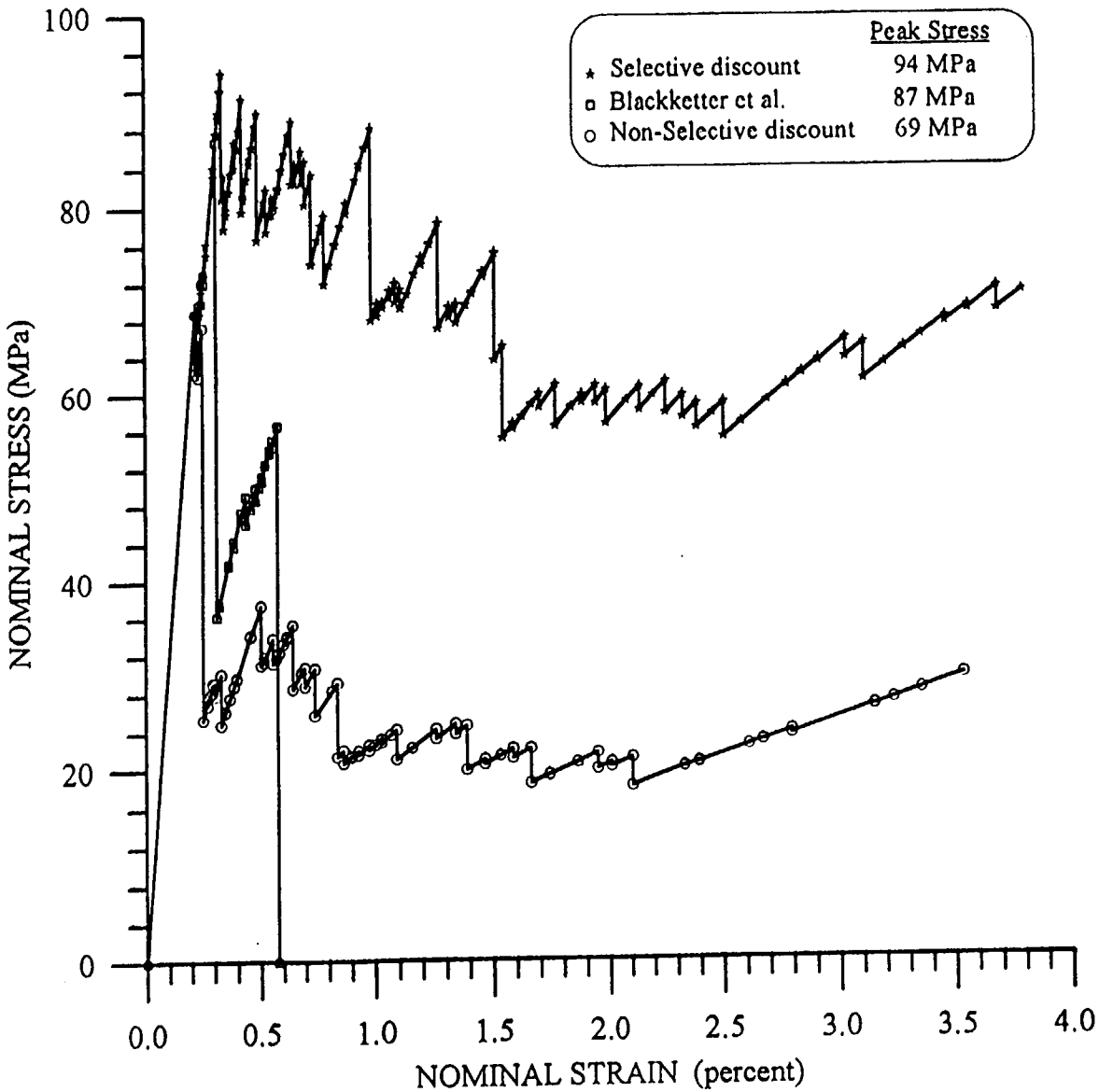

Figure 7 Effect of material degradation method on stress-strain response.

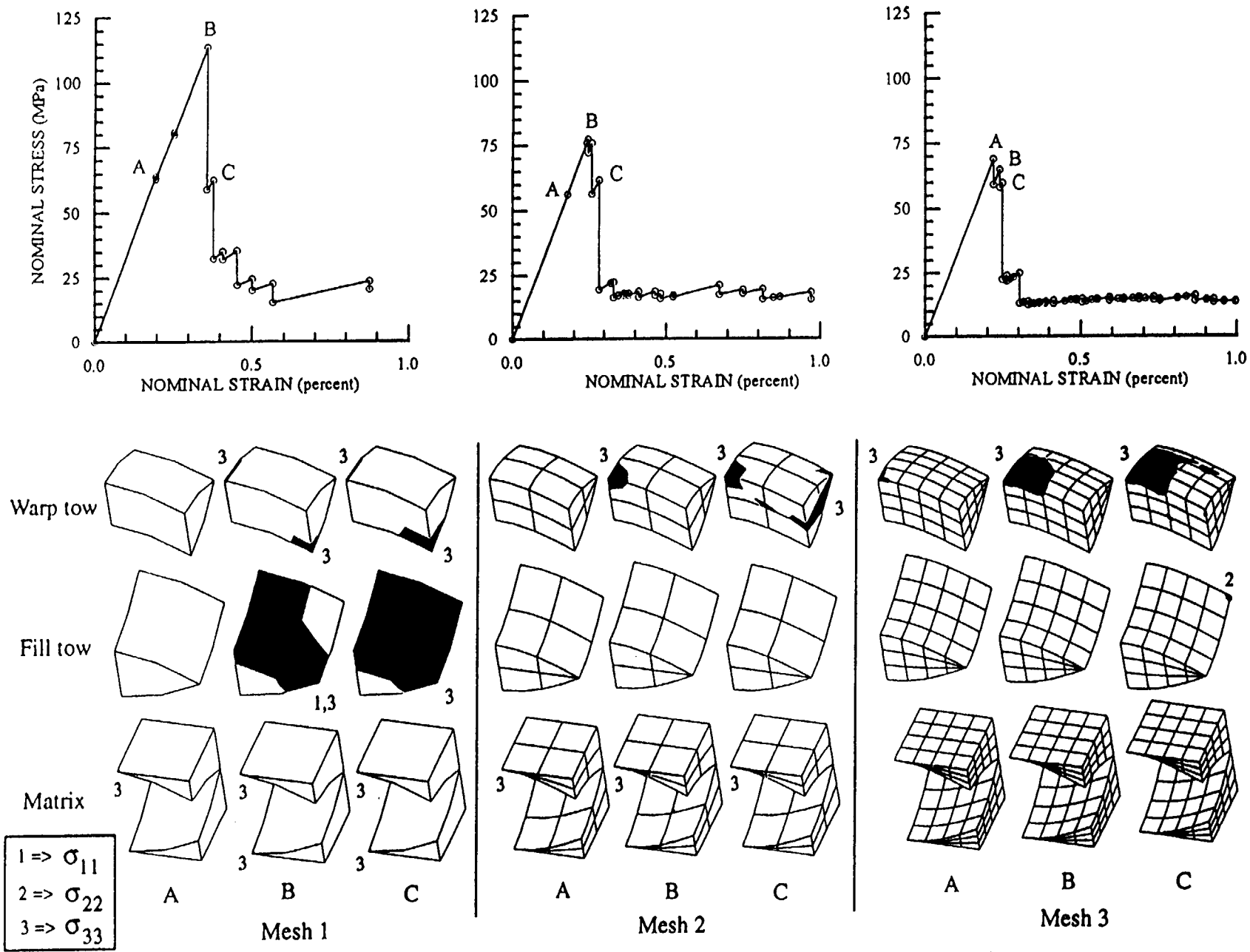

Figure 8 Effect of mesh refinement on damage development for waviness ratio = 1/3.

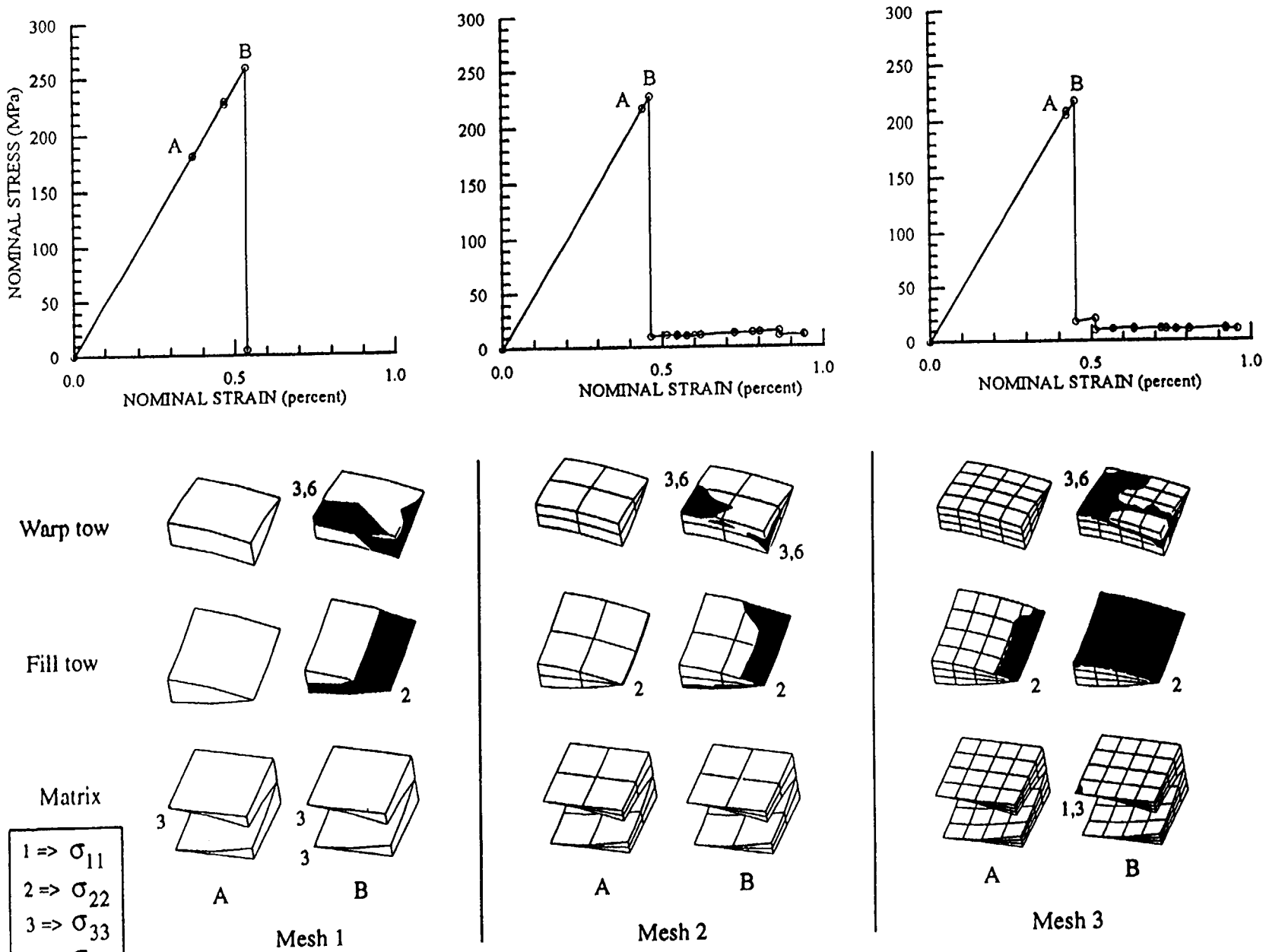

Figure 9 Effect of mesh refinement on damage development for waviness ratio = 1/6.

Chapter: 7

Effect of Assumed Tow Architecture on Predicted Moduli and Stresses in Plain Weave Composites

Abstract

This paper examines the effect of assumed tow architecture on the predicted moduli and stresses in plain weave textile composites. Two architectures are examined which have a sinusoidal tow path and a lenticular cross-section. Three-dimensional finite elements are employed to model a T300/Epoxy plain weave composite with symmetrically stacked mats. Macroscopically homogeneous in-plane extension and shear and transverse shear loadings were considered. Symmetries are exploited which permitted modeling of only 1/32nd of the unit cell. Accounting for the variation of material properties throughout each element is determined to be necessary for accurate prediction of stresses in the composite. For low waviness, the two tow architectures examined are very similar. At high waviness, the stress predictions are much more sensitive to the assumed tow geometry.

Introduction

As more demands are placed on structural materials, more complex materials must be developed in order to satisfy these demands. Fibrous composites are being employed for many of these applications. One type of fibrous composite which is receiving increased attention is the woven composite, which is constructed by grouping the fibers into bundles called tows and weaving these bundles together to make preforms. With the addition of a matrix material and curing, a woven composite is constructed. Figure 1 shows a schematic of a plain weave composite.

Woven composites have recently been receiving considerable attention due to their potential for improved properties compared with traditional laminated composites. Some of these properties include an increase in impact toughness and higher specific-strength

and specific-stiffness [1]. Other properties include the ability of *near-net-shape* manufacturing capability [2,3] and a high resistance to damage and impact [4].

Unfortunately, the microstructure of a woven composite is highly complex making it usually not cost effective to experimentally explore the effect of different weave geometries [1]. In fact, it is not currently practical to model the actual tow geometry. Idealization is mandatory. The idealization is critical, since the composite properties are very sensitive to some aspects of the tow geometry [5]. Since the stress analysis problem is too complicated for the luxury of modeling insignificant details, the obvious goal is to include just enough details in the idealized geometry to predict the most important aspects of the composite behavior. One way to determine the necessity of modeling particular details is to perform analytical studies which use various approximations of the tow geometry and observe the effects of these approximations on predicted response (eg. moduli and internal stresses). These analytical studies should be supplemented by experiments. However, this paper will focus only on the analytical task.

The objective of this paper is to determine the sensitivity of predicted moduli and internal stress distributions and failure initiation to one aspect of tow geometry: the variation of tow cross-section along the length of the tow. There are basically two categories of stress analysis methods which could be used for the study. One of these is based on a modified form of laminate theory (eg. References [4,6-11]) and the other is finite elements (eg. References [1,5,12-18]). The first category of analyses is only suitable for modulus prediction and rough estimates of stresses. To fully evaluate the accuracy of various approximations of tow geometry requires numerical analysis. Finite elements are ideal for this task and were used in this study.

In this study, only elastic behavior of mechanically loaded specimens will be considered. Residual stresses caused by differences in coefficients of thermal expansion should be included in a later study.

Although there are many types of woven composites, plain weaves will be studied in this paper because it offers sufficient complexity for the task at hand. The tows of a plain weave are woven together as shown in Figure 1. The tows which run in the x-direction are the warp tows. The tows running perpendicular to these are the fill tows. In a balanced weave the warp and fill tows have the same geometry and material properties. A balanced weave was used in this study.

The next section describes the assumed tow architectures. Next, boundary conditions used with the finite element model of the infinite periodic arrays will be described followed by a description of the material properties. Finally, the results of this study will be presented followed by conclusions.

determined for in-plane extension and shear and transverse shear. Included in this examination was a study on the specification of material properties using the single angle and multi-angle methods described earlier.

A convergence study was performed for a WR=1/3 to determine a suitable mesh for prediction of elastic properties and stress distributions for the two architectures. Twenty node isoparametric hexahedral elements were used. The meshes used are shown in Figure 5 for the translated and extruded models. Convergence of the elastic properties for translated tows is shown in Figure 6. The translated moduli are normalized with respect to the converged extruded model in order to also show the relative difference in moduli between the two architectures. This figure also compares the multi-angle and single angle methods of specifying material properties in the elements. As can be seen from the figure, convergence of most of the elastic properties was reached with just 32 elements using the multi-angle method.

Convergence of the stress distributions is shown in Figure 7 for translated tows using the multi-angle method. This figure shows the σ_{11} stress distribution in the tows after subjecting the meshes to a 1% ϵ_{xx} strain. Even using the 454 model with 400 elements convergence was not reached. However, there was only a moderate change between the 343 model with 192 elements and the 400 element 454 model. For this reason, the 454 model will be assumed to be nearly converged and will be used to study both the elastic moduli and stress distributions for the translated and extruded models.

A further comparison of the single angle and multi-angle method is shown in Figure 8. This figure shows the σ_{13} stress distributions in translated tows using single and multiple angles in the elements for a mesh subjected to a 1% ϵ_{xx} strain. Due to symmetry, the stress at the end of the tow as indicated by A should be zero, but as shown in the figure, the predicted stress is not zero for the single angle method. In fact, the highest stress in the tow using the single angle method is reported to be at A. If the mesh were refined, the incorrect stresses would disappear; however, this would be extremely costly using 3D finite elements. This indicates that the multi-angle elements are essential to an accurate analysis of the composite. Therefore only the multi-angle method will be used in for the following analyses.

The tow volume fraction vs. waviness ratio of translated and extruded tows is shown in Figure 9. (Note that this is not the fiber volume fraction.) The difference between the translated and extruded models increases with waviness. At WR=1/3, the percent difference between the tow volume fraction is approximately, 4.5%. This is significant because this alone will cause a difference in the predicted moduli of the composite. Additionally, as the waviness approaches zero, it is seen that the volume fraction for translated and extruded tows converge. Something else interesting to note is that the volume fraction of the translated tow is constant with respect to changes in WR, which seems unrealistic. The reason for this is that the volume of a wavelength of the translated tow is simply the cross-section area times the wavelength.

Figure 10 shows the differences in predicted elastic properties for weaves with translated and extruded tows. At low waviness, the figure shows that the differences between predicted elastic properties for translated and extruded tows are very small. However, at higher waviness, the difference between extruded and translated tows is more apparent. The difference is greatest for E_X. The translated model predicts a 6.8% higher moduli than the extruded model at a WR=1/3. For WR < 1/6, the difference in predicted moduli is less than 1% for all of the moduli.

Stress distributions are not as easily compared as the moduli due to the amount of data which must be presented. For this reason only stresses which contribute significantly to the predicted failure of the material will be presented. These stresses are determined by normalizing the stress in a material with respect to its material strength. Also, since the greatest difference occurs at a WR=1/3 for the three WR's studied, only stress distributions at this WR will be presented.

Three macroscopically homogenous single stress states were considered: σ_{xx}, σ_{xy}, and σ_{xz}. These three loadings were imposed on the 1/32nd sub-cells shown in Figure 5 with the boundary conditions shown in Table 1. Stresses for the 1/8th sub-cell were then generated using the appropriate factors given in Table 2.

Extension in warp direction (σ_{xx} loading)

A σ_{xx} extensional load was applied to the 454 translated and extruded meshes in Figure 5 using the boundary conditions shown in Table 1 so that a 1% ε_{xx} macroscopic strain was applied to the translated model. The same force need to apply the 1% macroscopic strain was then applied to the extruded model. Since the stiffness is different for the two architectures, the strains are different. Figure 11 shows the predicted Tsai-Hill failure criterion for the warp tows. Only the warp tows are presented because failure is predicted to initiate in the warp tows. Although the contours appear very similar, the maximum failure criteria predicted by the extruded model is 22% higher than that predicted by the translated model. This indicates that the translated model can withstand 10% more load than the extruded before initial failure occurs. By examining the maximum normalized stresses experienced by the warp tows, the stresses in the warp tow which are the main contributors to failure were determined to be the σ_{11} and σ_{33} stresses. Consequently, only these two stresses will be examined in the remainder of this sub-section.

Figure 11 also compares the normalized σ_{11} and σ_{33} stress distributions predicted in the warp tows with the translated and extruded models. As can be seen in Figure 11, σ_{11} stress distributions in the regions of failure in the warp tows are very similar and contribute little to the initial failure for the translated and extruded models. However, near the edge of the tows one can see a more significant difference in the two models. The translated model predicts a high σ_{11} stress in the cross-over region as shown in Figure 2. This is not seen in the extruded model in which parallel tows are separated by a region of resin. This difference is interesting but somewhat insignificant since failure

does not iniate in this region.

The σ_{33} stress distribution indicates that initial failure is being caused primarily by this stress. The tows are failing in the region where the warp tows in adjacent mats are closest to one another because the warp tows are wanting to straighten and pull apart from one another. This prediction should change drastically if the mats are simply stacked instead of symmetrically stacked as assumed in this study. The extruded mesh experiences a maximum σ_{33} stress 10.3% greater than the translated mesh. Other than this, there is no substantial difference in the warp tow stress distribution.

As stated earlier, the stress levels in the fill tows and resin regions of the composite are uniteresting due to the relative size of the stress exhibited in these regions. However, if thermal stresses were included in the analysis, these regions could become very interesting.

In-plane shear (σ_{xy} loading)

A σ_{xy} shear load was applied so that a 1% ε_{xy} macroscopic strain was experienced by the 454 translated model in Figure 5. This load was then applied to the 454 extruded model. Graphs of the Tsai-Hill failure criteria are shown in Figure 12 for the tows. Note that only one tow is shown because the stress state in the warp and fill tows is the same. The maximum predicted failure criterion for the translated model is 30% larger than the maximum predicted by the extruded model. This is a substantial difference. Using (14), the translated model will initiate failure at a macroscopic stress level 14% lower than the extruded model. The normalized stresses indicate that the primary contributing stresses to the initial failure in the warp tow of the composite are the shearing stresses, σ_{12} and σ_{23}. For the fill tow, the stresses are σ_{12} and σ_{13}.

The normalized σ_{12} stress distributions in the tows are also shown in Figure 12 for the translated and extruded models. The maximum stress predicted by the translated model is 8% greater than that predicted with the extruded model. This indicates that parallel tows in the composite are influencing the stresses in this region. Due to the extruded tows being separated by regions of resin in the cross-over region as shown in Figure 2, the extruded model predicts a higher strain to initial failure than that predicted by the translated model.

The comparison of the normalized σ_{23} stress distributions in the warp tows is also shown in Figure 12. This figure shows that there is a considerable difference in the predicted stresses of the two architecturess. The translated architecture predicts approximately 50% greater stress than the extruded at the cross-over region in the 1/8th sub-cell. The extruded architecture predicts its highest stress in a region away from the center of the 1/8th sub-cell as shown in the figure. The reason for this is, again, that the tows of the extruded model are seperated by regions of resin. The σ_{23} stress distribution is what causes the large difference in the predicted failure of the two architectures.

Trasverse shear (σ_{xz} loading)

A σ_{xz} shear load was applied so that a 1% ε_{xz} macroscopic strain was applied to to the 454 translated model in Figure 5. This lad was then applied to the 454 extruded model. The Tsai-Hill criteria is plotted in Figure 13 for these two models. Failure is predicted to initiate in the resin between the mats as indicated by A in the figure. The translated model predicts a failure criterion 1.37% less than that predicted by the extruded model which indicates that initial failure will occur at essentially the same macroscopic stress level in both models. The main source of initial failure is the σ_{13} stress. If the mats were assumed to be simply stacked, a much differenent prediction would be made for this load case.

Conclusions

The effect of assumed tow architecture, specifically the effect of how a cross-section is assumed to sweep out the volume of a tow, was studied for a plain weave composite with symmetrically stacked mats. Comparison of two architectures, translated and extruded, was made on the basis of predicted moduli and stress distributions. Results of the analysis show that at a high waviness ratio there is a significant difference between the two architectures.

It was determined early in this study that to provide an accurate analysis, the variation of material properties through the elements must be modelled accurately. This was shown by the convergence of the elastic properties and stress distributions of the multi-angle method compared to the single angle method. A more refined analysis was also achieved by reducing the size of the model which needed to be analyzed. It was determined that only 1/32nd of the unit cell for symmetrically stacked mats need be analyzed. Very dramatic computational savings were obtained by this reduction.

The differences in the tow architectures revealed several drawbacks and advantages of the translated and extruded models. The translated model thins at high waviness ratio which is unrealistic; however, the mesh generation of the translated model is algebraic. The extruded model does not thin at high waviness but at the cost of complicating the mesh generation. The extruded model also includes thin matrix layers between the warp and fill tows which the translated does not. The significance of this was not determined.

Of the three waviness ratios studied, the largest difference was observed at the highest waviness, WR=1/3. Very little difference between the translated and extruded architectures was observed at the other two waviness ratios. Two of the loading cases, extension in the warp direction and in-plane shear, indicate that there is a significant difference between the two architectures. Extension in the warp direction indicated a significant difference in the predicted extensional moduli, E_x, and in the load to initial failure. In-plane shearing showed a significant difference in the stress state in the cross-

over region. The third loading case, transverse shearing, showed little difference in the predicted moduli and stress distributions due to how the mats are assumed to be stacked. If the mats were assumed to be simply stacked instead of symmetrically stacked more difference might be noted in transverse shearing as well as extensional loading.

References

1. Dasgupta, A., and R. K. Agarwal. 1992. "Orthotropic thermal conductivity of plain-weave fabric composites using homogenization technique," *Journal of Composite Materials*, 26(18):2736-2758.

2. Byun, J.-H. and T.-W. Chou. 1989. "Modelling and characterization of textile structural composites: A review," *Journal of Strain Analysis*, 24:253-252.

3. Naik, N. and P. Shembekar. 1992. "Elastic behavior of woven fabric composites: I- Lamina Analysis," *Journal of Composite Materials*, 24(15):2196-2225.

4. Ishikawa, T. and T.-W. Chou. 1982. "Stiffness and strength behavior of woven fabric composites," *Journal of Material Science*, 17:3211-3220.

5. Masters, J. E., R. L. Foye, C. M. Pastore, and Y. A. Gowayed. 1992. "Mechanical properties of triaxially braided composites: Experimental and Analytical results," *NASA Contractor Report 189572*, Langley Research Center.

6. Ishikawa, T. 1981. "Anti-symmetric elastic properties of composite plates of satin weave cloth," *Fiber Science Technology*, 15:127-145.

7. Ishikawa, T. and T.-W. Chou. 1982. "Elastic behavior of woven hybrid composites," *Journal of Composite Materials*, 16:2-19.

8. Ishikawa, T. and T.-W. Chou. 1983. "In-plane thermal expansion and thermal bending coefficients of fabric composites," *Journal of Composite Materials*, 17:388-413.

9. Ishikawa, T. and T.-W. Chou. 1983. "Thermoelastic analysis of hybrid fabric composites," *Journal of Material Science*, 28:2260-2268.

10. Ishikawa, T. and T.-W. Chou. 1983. "One dimensional micro-mechanical analysis of woven fabric composites," *AIAA Journal*, 21:1714-1721.

11. Naik, N. K. and P. S. Shembekar. 1992. "Elastic behavior of woven fabric composites: II - Laminate Analysis," *Journal of Composite Materials*, 25(15):2226-2246.

12. Paumelle, P., A. Hassim, and F. Léné. 1990. "Composites with woven reinforcements: Calculation and parametric analysis of the properties of the homogeneous equivalent," *La Recherche Aérospatiale*, 1:1-12.

13. Dasgupta, A., S. M. Bhandarkar. 1994. "Effective thermomechanical behavior of plain-weave fabric-reinforced composites using homogenization theory," *Transactions of the ASME Journal of Engineering Materials and Technology*, 166(1):99-105.

14. Woo, K. 1993. *Stress and failure analysis of textile composites*. Ph.D. Dissertation, Department of Aerospace Engineering, Texas A&M University. College Station, Texas.

15. Whitcomb, J. D. 1991. "Three-dimensional stress analysis of plain weave composites," *Composite Materials: Fatique and Fracture (Third Volume), ASTM STP 1110*, T. K. O'Brien, Ed., Philadelphia: American Society for Testing and Materials, pp. 417-438.

16. Woo, K. and J. D. Whitcomb. 1992. "Macro finite element using subdomain integration," *OTRC Report 03/92-A-29-100*, Texas A&M University. College Station, Texas.

17. Avery, W. B. and C. T. Herakovich. 1987. *A study of the mechanical behavior of a 2D carbon-carbon composite*. Virginia Polytechnic Institute and State University, Interim Report 66. Blacksburg, Virginia.

18. Chapman, C. D. 1993. *Effects of assumed tow architecture on the predicted moduli and stresses in woven composites*. Master Thesis, Department of Aerospace Engineering, Texas A&M University. College Station, Texas.

Table 1: Boundary conditions for 1/32nd sub-cell for extension, transverse shear and in-plane shear loadings.

Macroscopic extension:
$u(\frac{a}{2},y,z)=u_0 \quad v(x,\frac{a}{2},z)=v_0 \quad w(x,y,\pm\frac{c}{2})=\pm w_0$ $u(0,y,z)=-u(0,y,-z) \quad v(0,y,z)=v(0,y,-z) \quad w(0,y,z)=-w(0,y,-z)$ $u(x,0,z)=u(x,0,-z) \quad v(x,0,z)=-v(x,0,-z) \quad w(x,0,z)=-w(x,0,-z)$
Transverse shear (σ_{xz} loading):
$u(x,y,\pm\frac{c}{2})=\pm u_0 \quad v(x,\frac{a}{2},z)=0 \quad w(\frac{a}{2},y,z)=w_0$ $u(0,y,z)=-u(0,y,-z) \quad v(0,y,z)=v(0,y,-z) \quad w(0,y,z)=-w(0,y,-z)$ $u(x,0,z)=u(x,0,-z) \quad v(x,0,z)=v(x,0,-z) \quad w(x,0,z)=-w(x,0,-z)$
In-plane shear (σ_{xy} loading):
$u(x,\frac{a}{2},z)=d \quad v(\frac{a}{2},y,z)=d \quad w(\frac{a}{2},y,z)=w(x,\frac{a}{2},z)=w(x,y,\pm\frac{c}{2})=0$ $u(0,y,z)=u(0,y,-z) \quad v(0,y,z)=v(0,y,-z) \quad w(0,y,z)=-w(0,y,-z)$ $u(x,0,z)=u(x,0,-z) \quad v(x,0,z)=v(x,0,-z) \quad w(x,0,z)=-w(x,0,-z)$

Table 2: Factors for synthesis of 1/8th sub-cell stresses from 1/32nd sub-cell.

Extension	σ_1	σ_2	σ_3	σ_4	σ_5	σ_6
Q1	1	1	1	1	1	1
Q2	1	1	1	-1	-1	1
Q3	1	1	1	1	-1	-1
Q4	1	1	1	-1	1	-1

xz Shear	σ_1	σ_2	σ_3	σ_4	σ_5	σ_6
Q1	1	1	1	1	1	1
Q2	1	1	1	-1	-1	1
Q3	-1	-1	-1	-1	1	1
Q4	-1	-1	-1	1	-1	1

xy Shear	σ_1	σ_2	σ_3	σ_4	σ_5	σ_6
Q1	1	1	1	1	1	1
Q2	-1	-1	-1	1	1	-1
Q3	1	1	1	1	-1	-1
Q4	-1	-1	-1	1	-1	1

Equations for formation of stresses in quadrants 2,3, and 4 in the xy plane.

$$\sigma_i^2(-x,y,-z) = \sigma_i^1(x,y,z) f_i^2$$

$$\sigma_i^3(-x,-y,z) = \sigma_i^1(x,y,z) f_i^3$$

$$\sigma_i^4(x,-y,-z) = \sigma_i^1(x,y,z) f_i^4$$

Table 3: Comparison of CPU and memory requirements for three models with same refinement. Times were determined on an IBM RISC System/6000 POWERstation 355.

Cell Size	CPU Time (min):(sec)	Elements	Memory Requirements (Words / KiloBytes)
Full Unit Cell	37:05	512	7,932K / 63,456K
1/8th Unit Cell	0:28	64	310K / 2,480K
1/32nd Unit Cell	0:10	16	38K / 304K

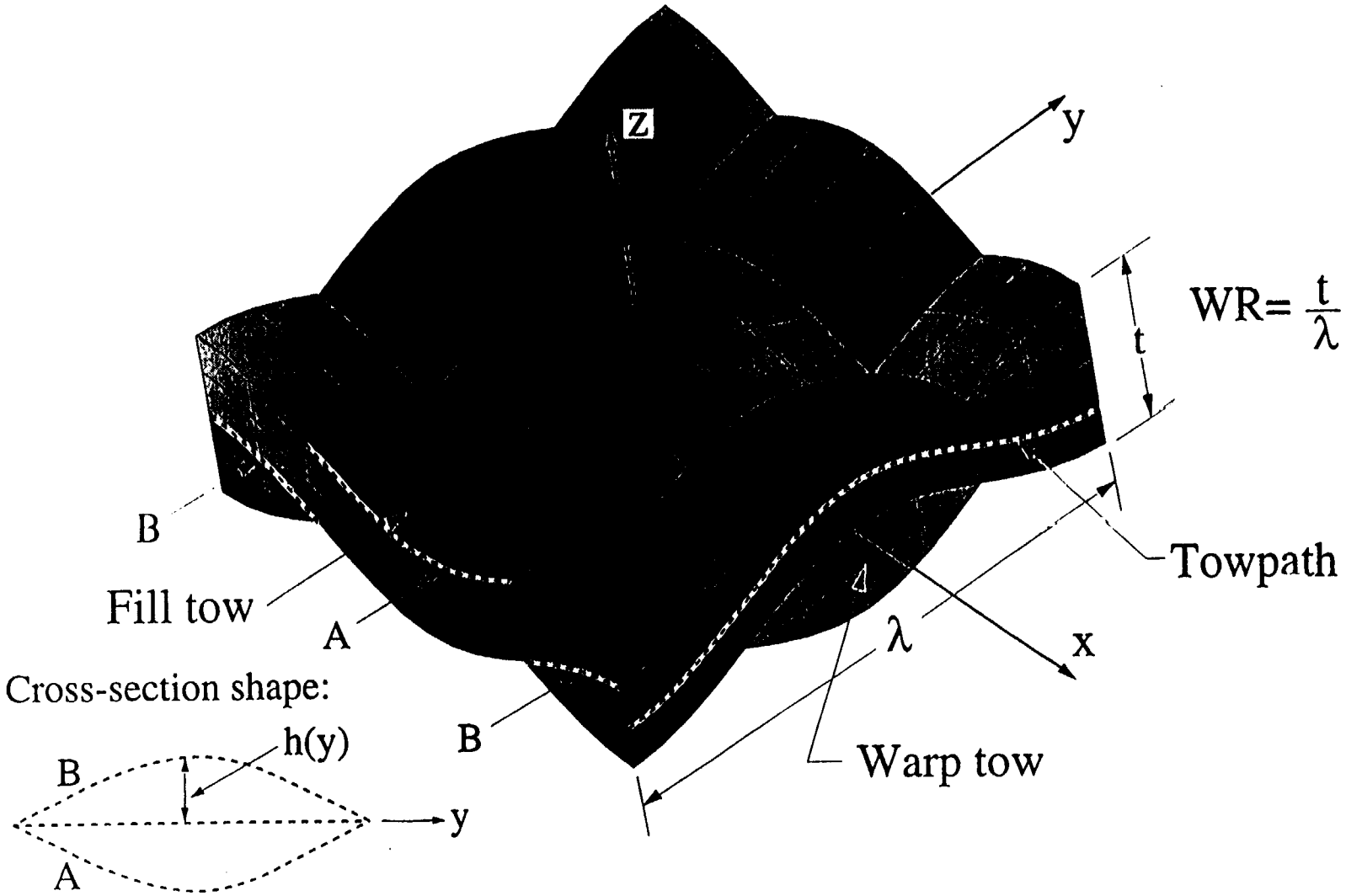

Figure 1: Tows of plain weave composite with warp and fill tows indicated as well as towpath and definition of waviness ratio, WR (resin omitted for clarity.) Cross-section shape and sections used to define cross-section also shown.

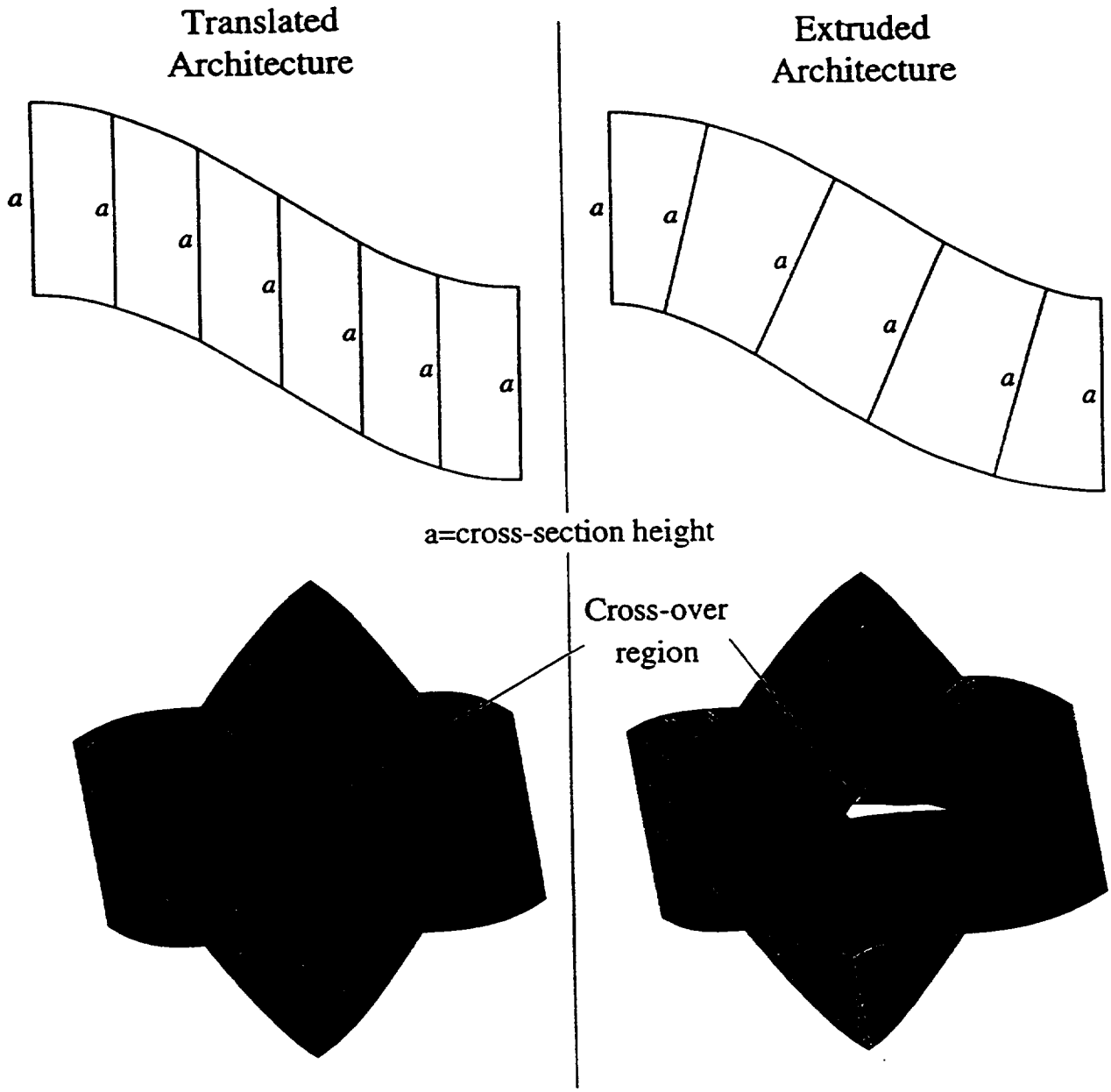

Figure 2: Comparison of translated and extruded architectures.

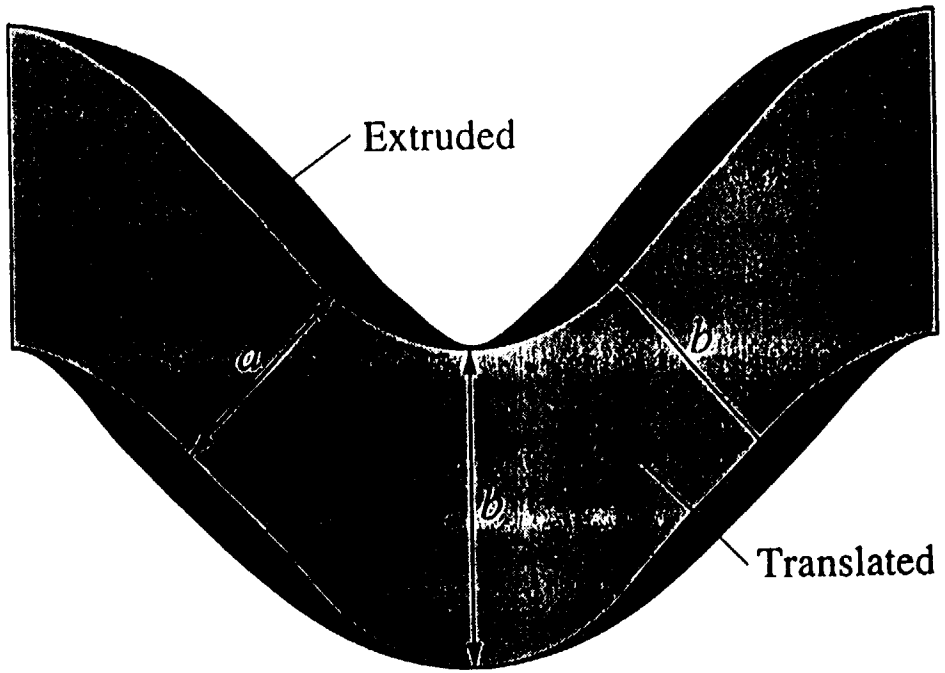

Figure 3: Translated tow at high waviness superimposed on extruded tow showing thinning across tow.

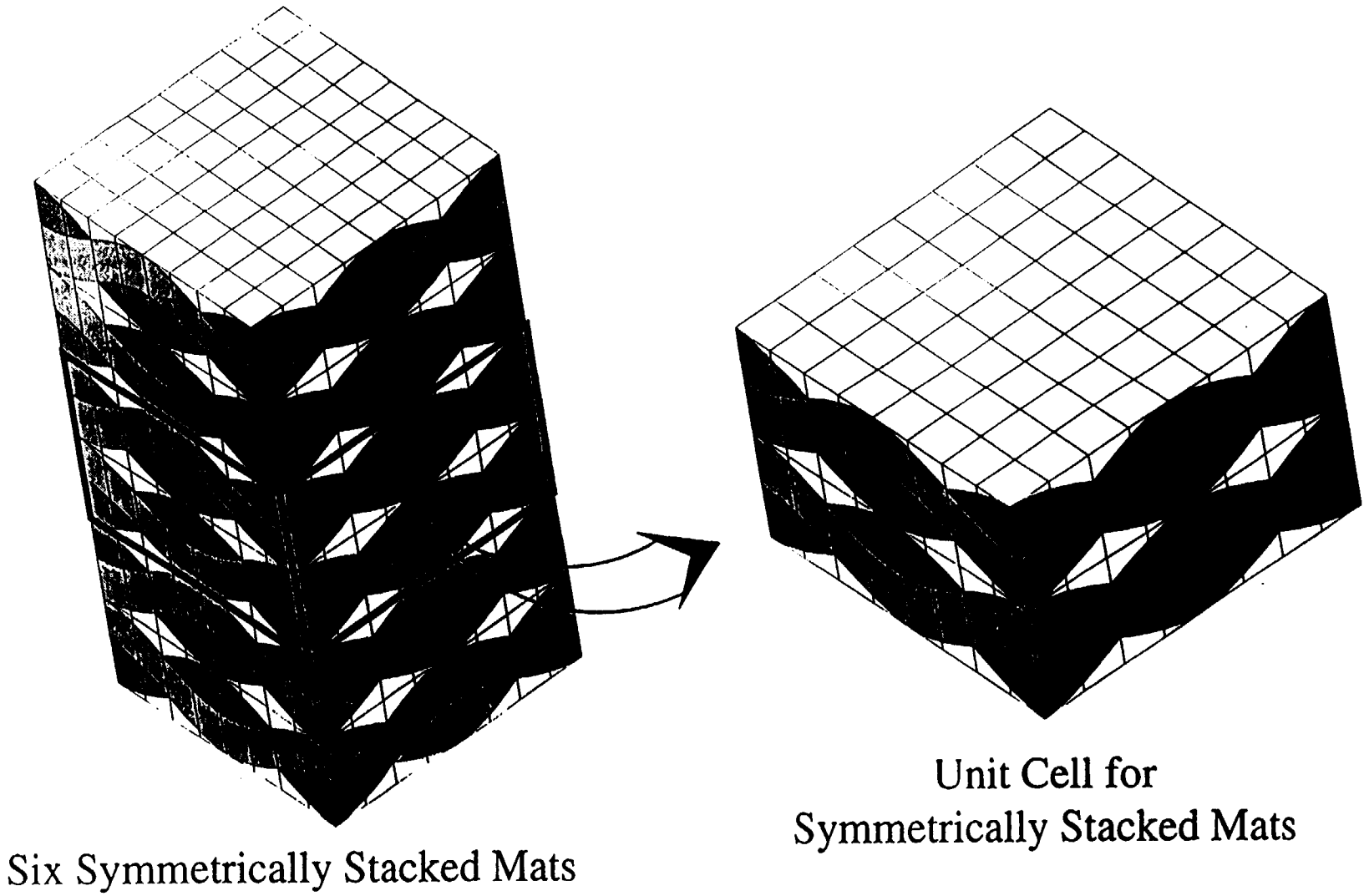

Figure 4: Assumed geometry and unit cell for symmetrically stacked mats.

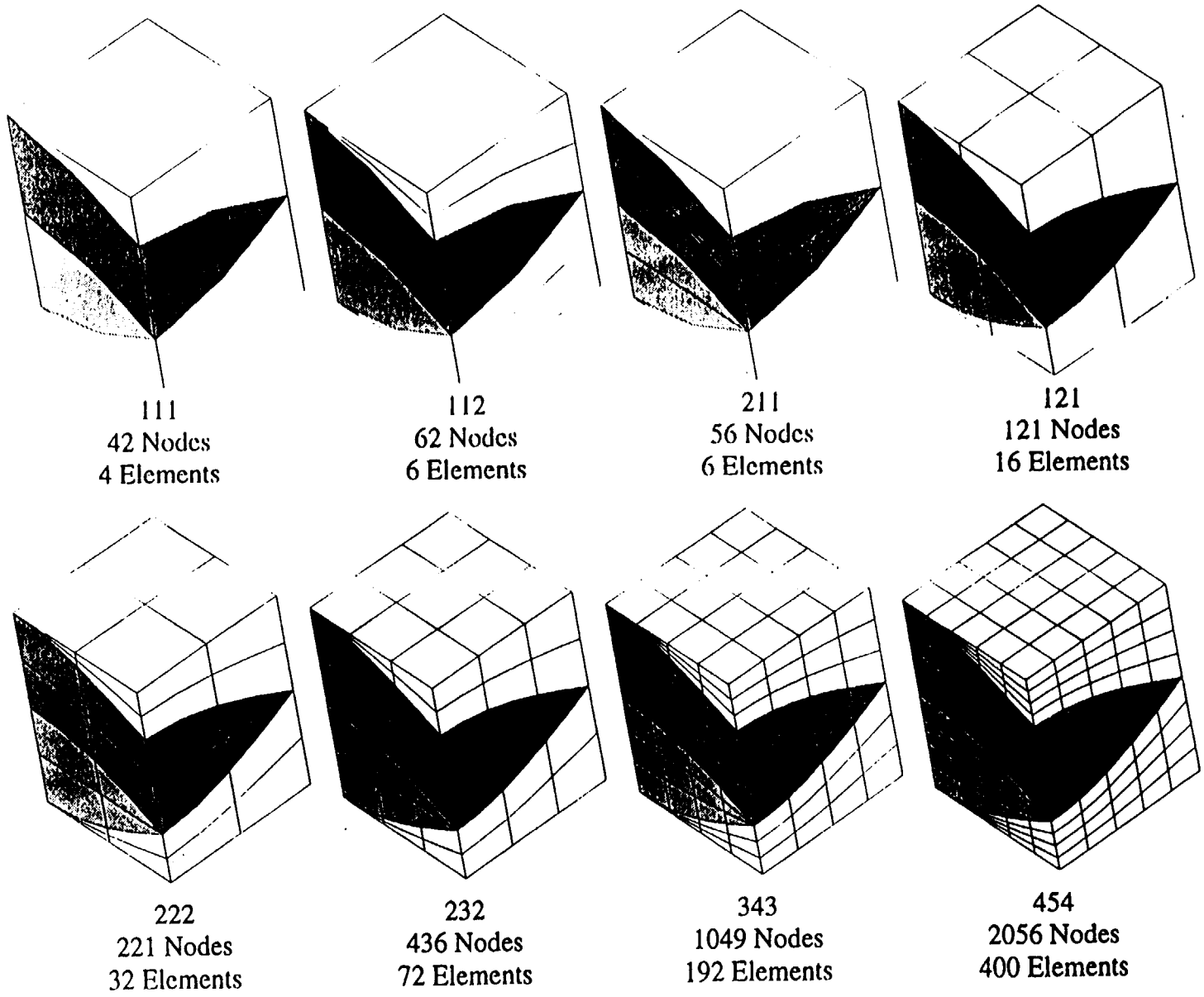

a) Translated Meshes

Figure 5: Meshes used in study of translated and extruded tows.

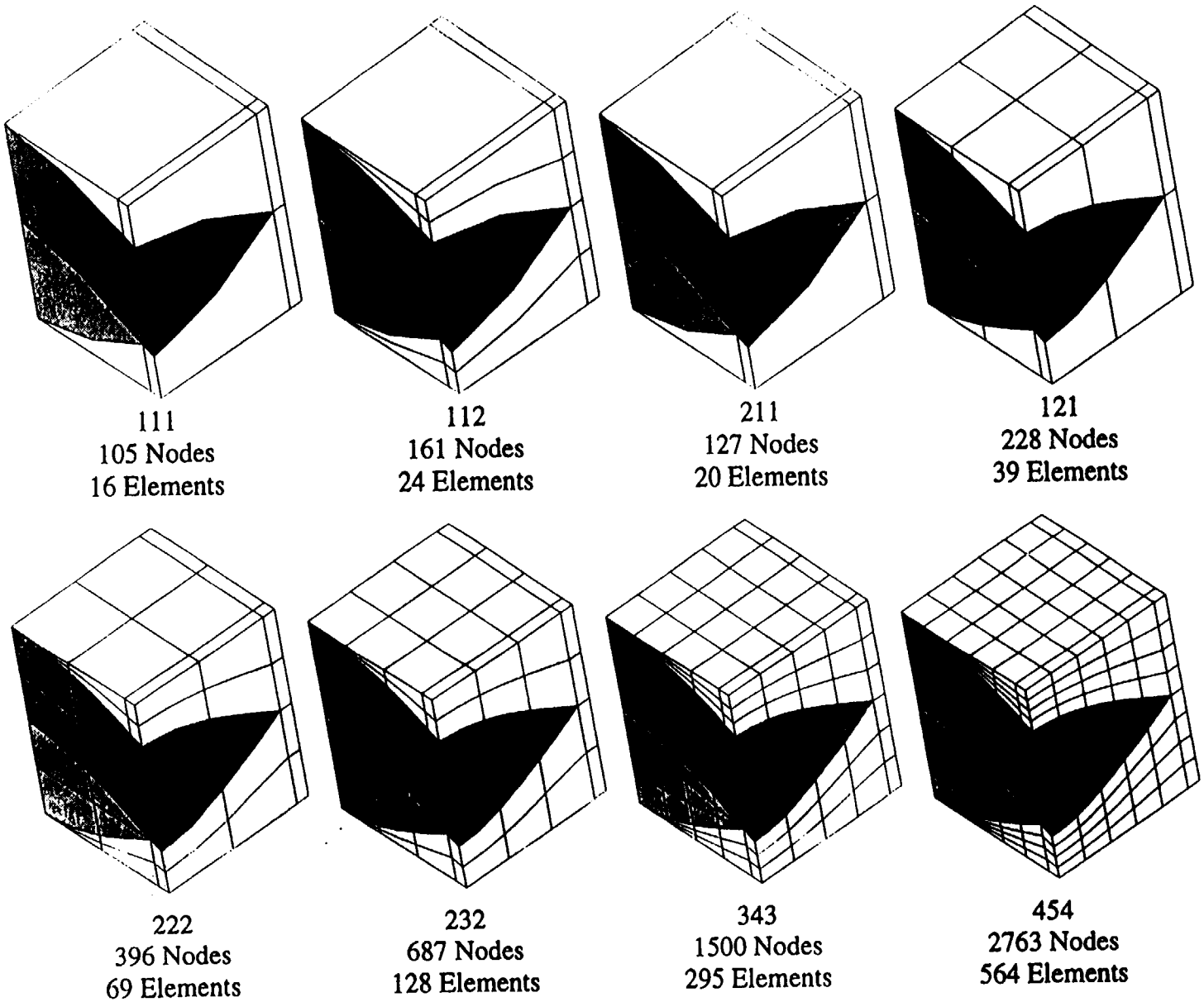

b) Extruded meshes.

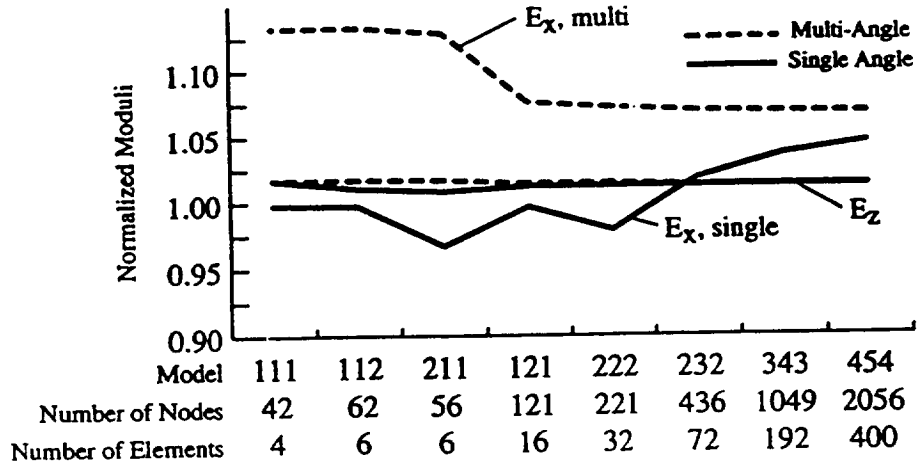

Model	111	112	211	121	222	232	343	454
Number of Nodes	42	62	56	121	221	436	1049	2056
Number of Elements	4	6	6	16	32	72	192	400

(a) Extensional Moduli

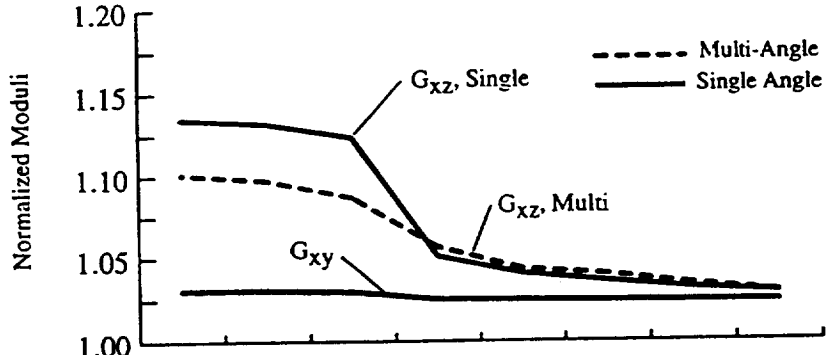

Model	111	112	211	121	222	232	343	454
Number of Nodes	42	62	56	121	221	436	1049	2056
Number of Elements	4	6	6	16	32	72	192	400

(b) Shear Moduli

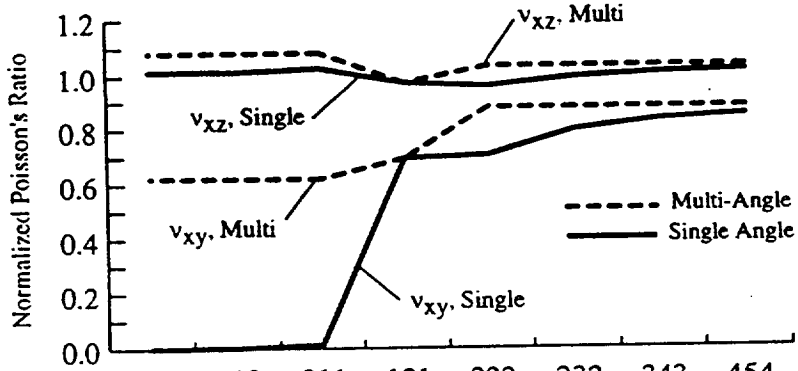

Model	111	112	211	121	222	232	343	454
Number of Nodes	42	62	56	121	221	436	1049	2056
Number of Elements	4	6	6	16	32	72	192	400

(c) Poisson's Ratios

Figure 6: Convergence of predicted moduli for translated tows normalized with respect to extruded 454 model.

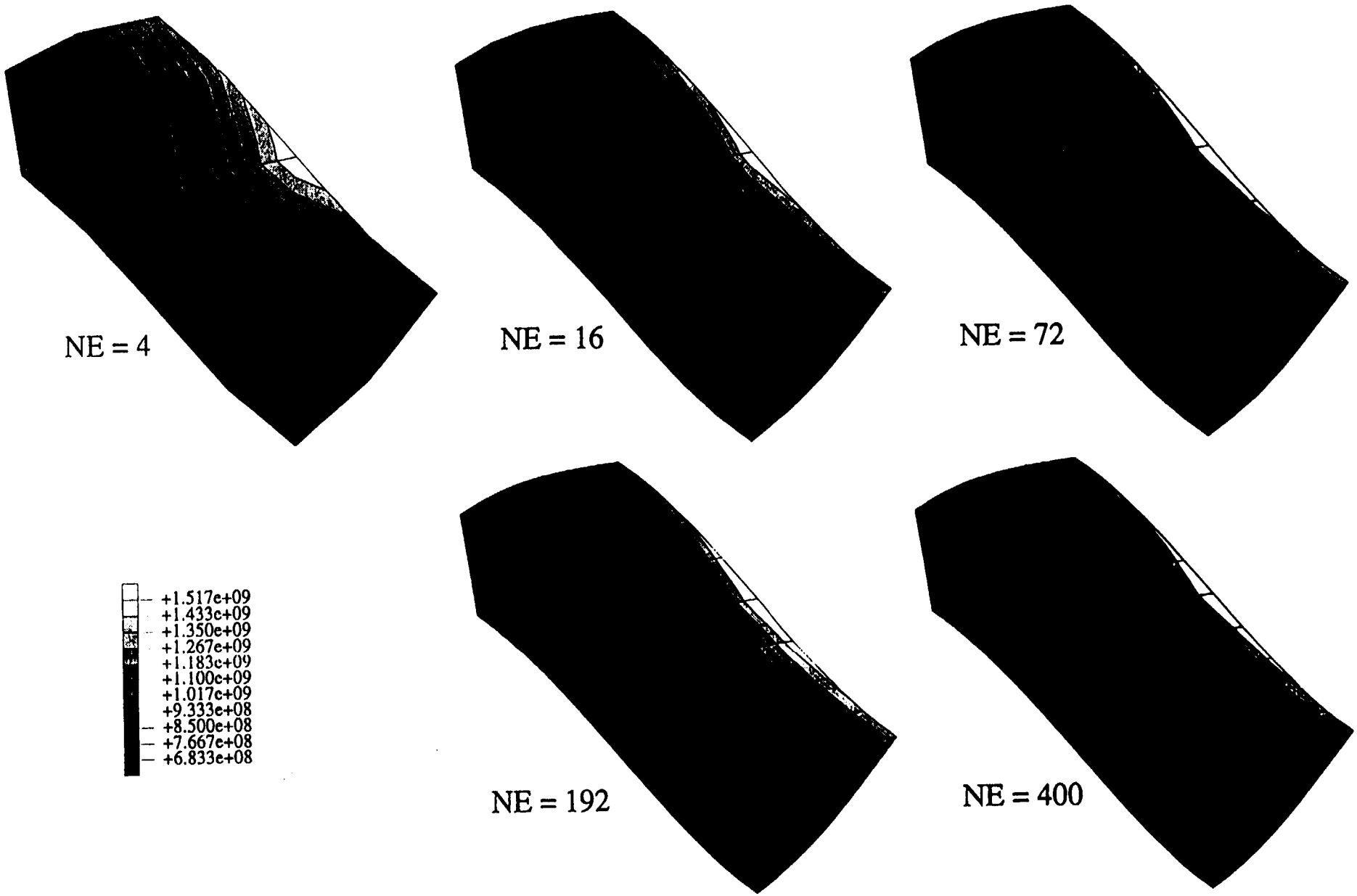

Figure 7: Convergence of σ_{11} stress distributions in warp tows of translated meshes at 1% ε_{xx}. NE refers to the number of elements in model analyzed.

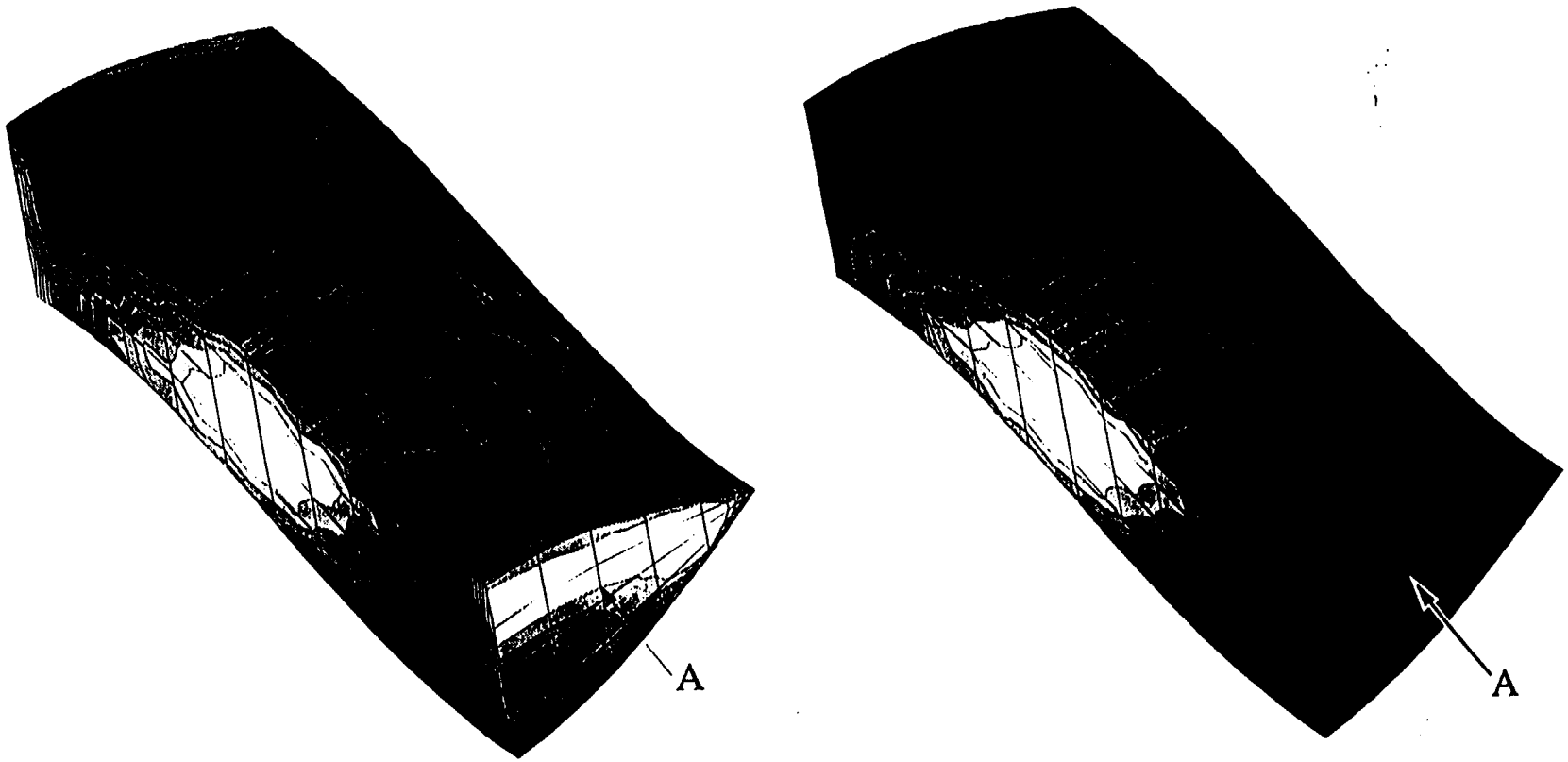

Figure 8: Comparison of single angle and multi-angle specification of material rotation angles for σ_{13} stress distributions in translated warp tows subjected to σ_x extensional loading.

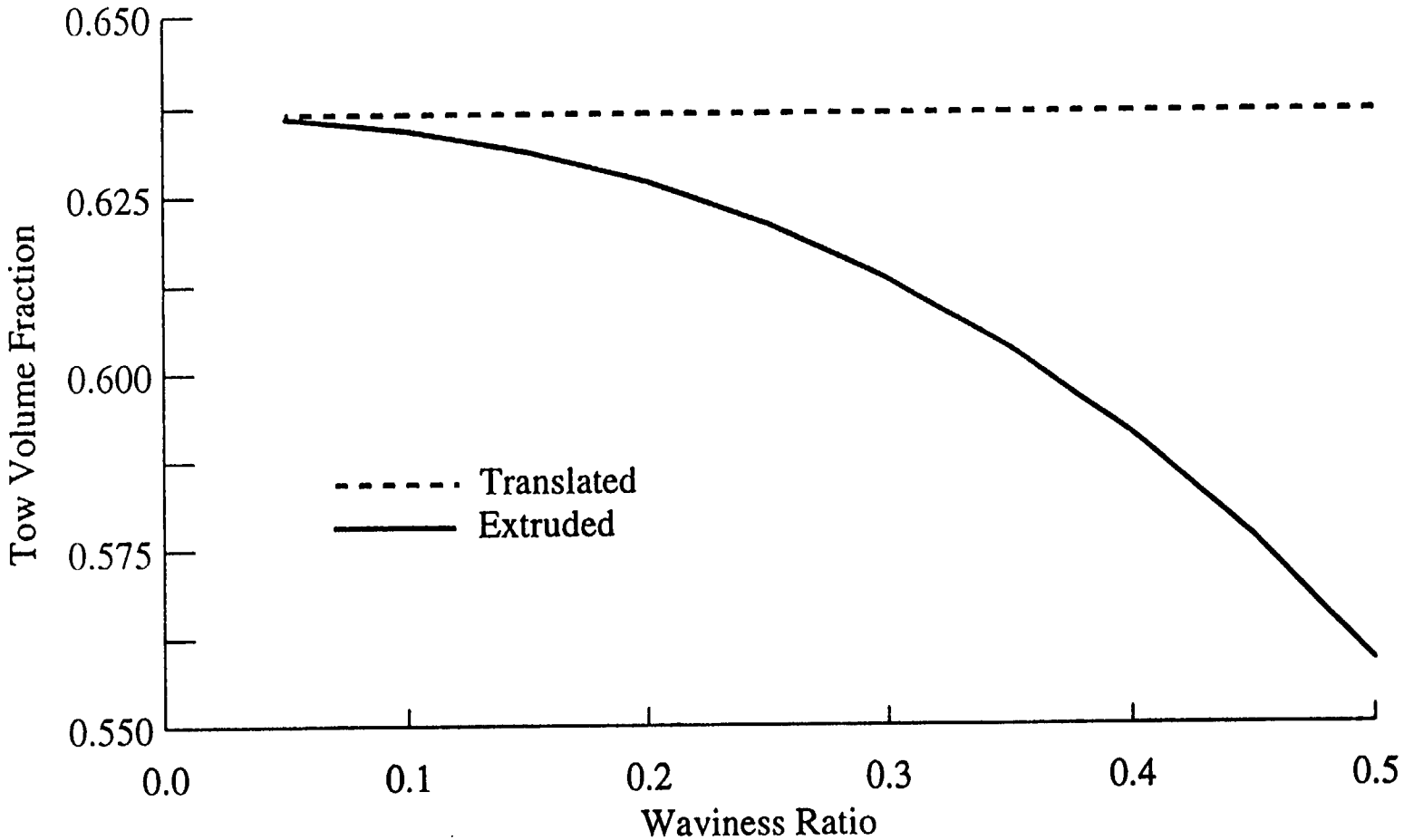

Figure 9: Variation of tow volume fraction with waviness ratio for extruded and translated models.

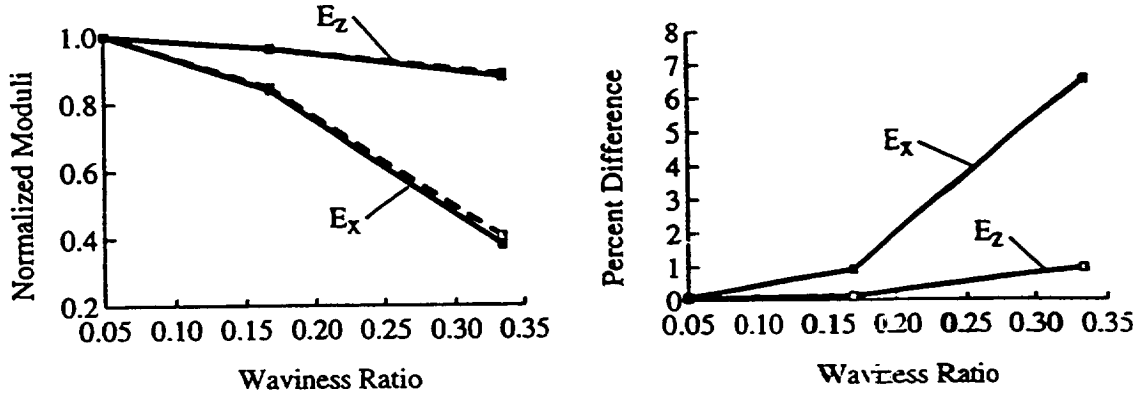

a) Extensional Moduli

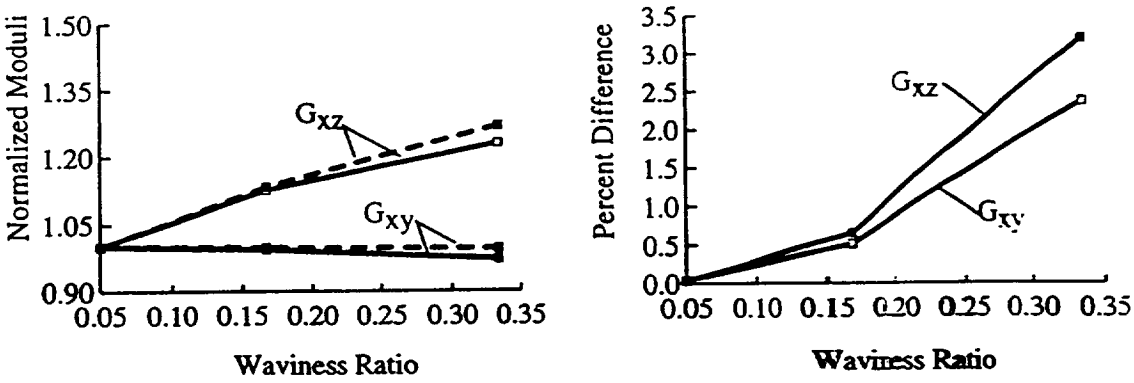

b) Shear Moduli

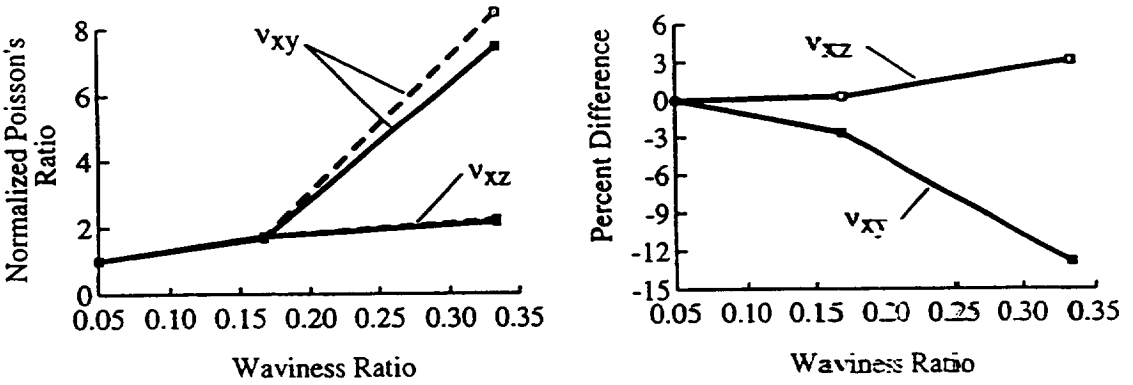

c) Poisson's Ratios

Translated - - - -
Extruded ———

Figure 10: Comparison of predicted elastic moduli using translated and extruded models. Values are normalized with respect to values predicted at WR=0.05.

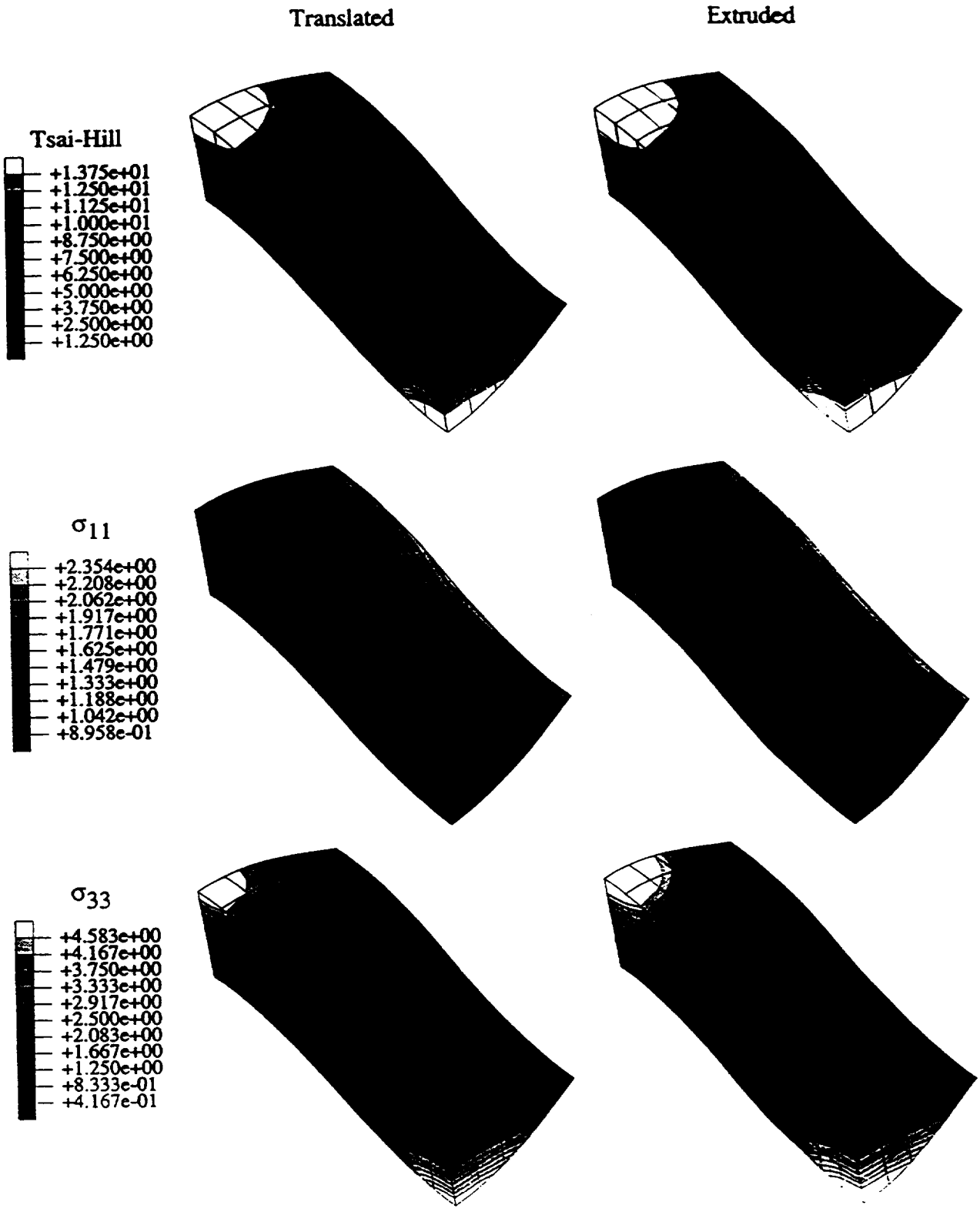

Figure 11: Comparison of predicted Tsai-Hill failure criterion, normalized σ_{11}, and normalized σ_{33} in warp tows of translated and extruded meshes subjected to load generated by 1% ε_{xx} extension of translated model.

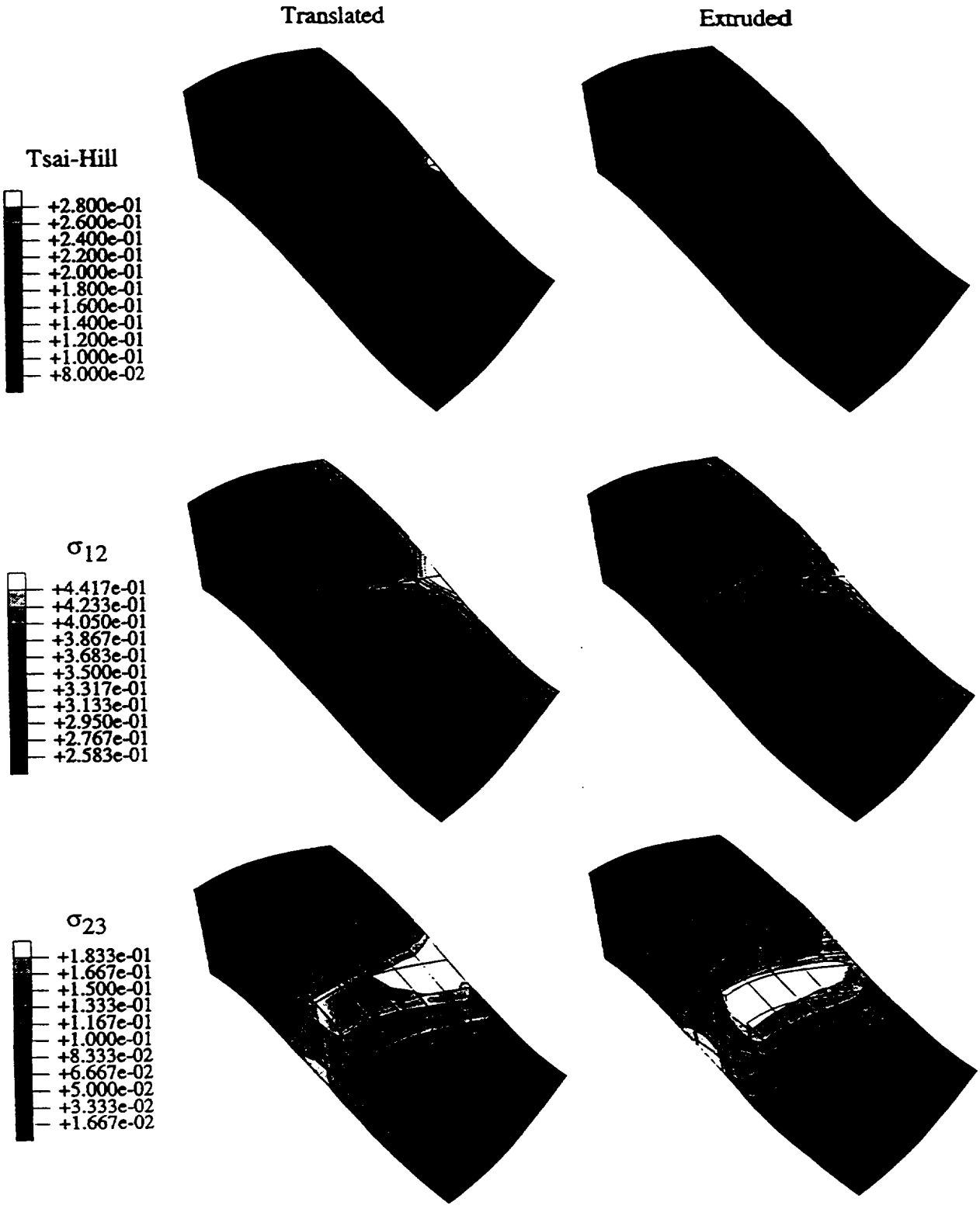

Figure 12: Comparison of predicted Tsai-Hill failure criterion, normalized σ_{12}, and normalized σ_{23} in warp tows of translated and extruded meshes subjected to load generated by 1% ε_{xy} shearing of translated model.

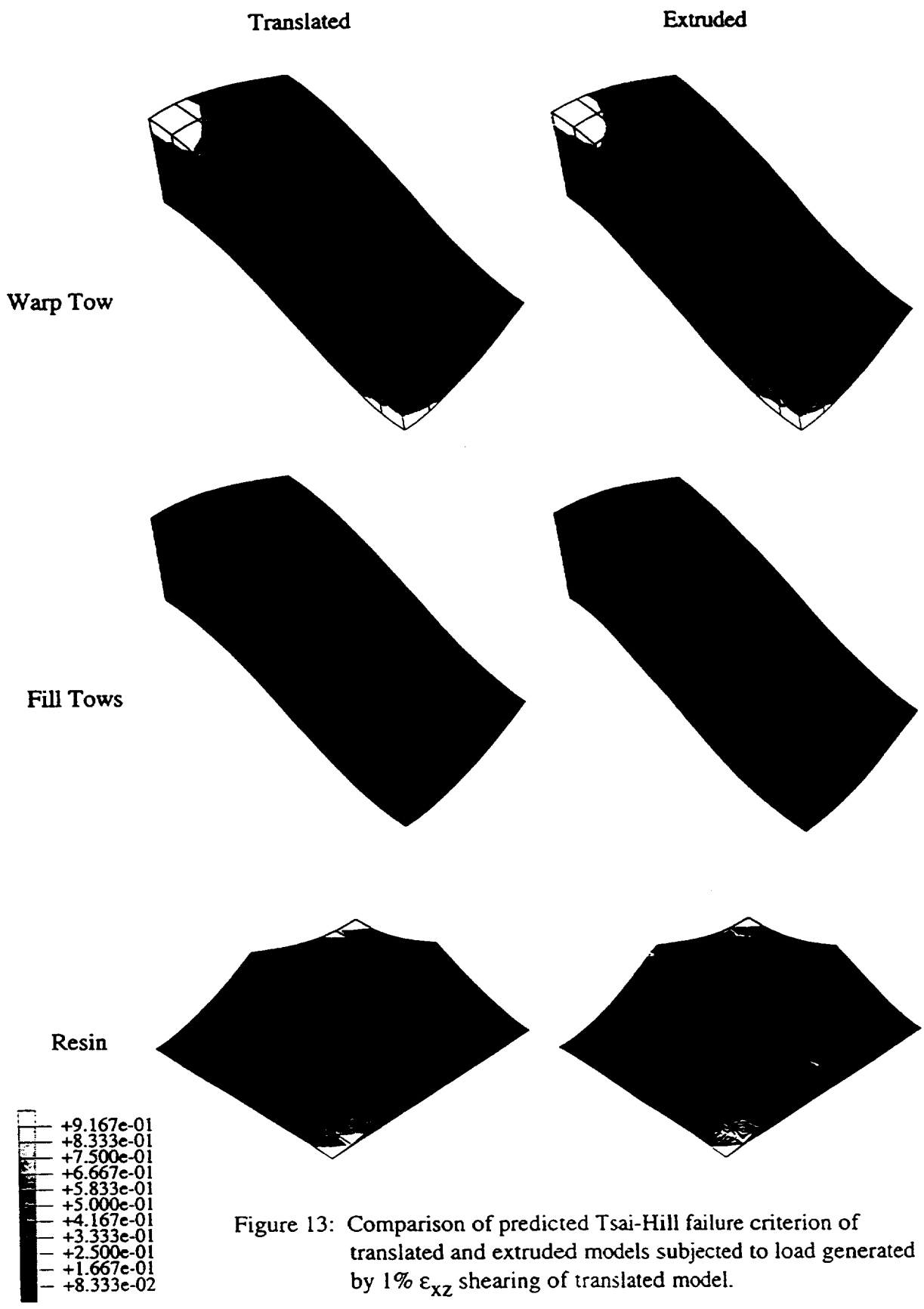

Figure 13: Comparison of predicted Tsai-Hill failure criterion of translated and extruded models subjected to load generated by 1% ε_{xz} shearing of translated model.

Chapter: 8

MODAL TECHNIQUE FOR THREE-DIMENSIONAL STRESS ANALYSIS OF PLAIN WEAVE COMPOSITES

ABSTRACT

Textile composites present a unique challenge to the stress analyst due to their large microstructure. A global/local method was developed which significantly reduces the computational challenge and retains reasonable accuracy. This method uses homogenized engineering properties for the global analysis. The nodal displacements from this global analysis are used to determine the magnitudes of a few fundamental modes. These magnitudes are used to scale and superpose refined local solutions for these fundamental modes. A stubby cantilevered plate subjected to end moment and transverse load was analyzed using the proposed method. The results were quite encouraging.

INTRODUCTION

Plain weave composites consist of interlaced fiber bundles which are impregnated with a resin and then cured. It is not practical to discretely model each fiber bundle even when analyzing a simple coupon. Instead, the analysis is divided into two stages: a global analysis and a local analysis. The global analysis uses some form of effective constitutive properties. This might take the form of homogenized engineering moduli or macro elements, which are finite elements which approximately account for the microstructure within a single element [1,2]. To obtain detailed stress information requires a subsequent local analysis which discretely models the individual fiber bundles and matrix pockets.

There are many global/local strategies [e.g. 3-6]. A critical step in all of these strategies is how to apply boundary conditions on the detailed local model based on nodal forces and displacements from a crude global model. In an earlier study, the displacements from the global model were imposed along the entire global/local boundary of the local model. [3] Compatibility is exactly satisfied by this procedure. However, this procedure resulted in excellent predictions of the stress distribution away from the global/local boundary, but large errors near the boundary. This paper describes a procedure which satisfies compatibility between the global and local models in an average sense. In particular, the magnitudes of a few basic deformation modes are determined from the global analysis and then imposed on the local model. The next section will describe the global/local method. Then the cantilevered plate configuration selected

for this evaluation and the finite element models will be described. Finally, a few results will be presented which illustrate the advantages of the technique.

DESCRIPTION OF GLOBAL/LOCAL METHOD

Fig. 1 shows a schematic of the global/local procedure. The global analysis was performed using effective engineering properties. The effective properties for interior cells were determined using periodic boundary conditions for an infinite array of unit cells. [7]. Because of free-surface effects [3], the effective properties are different for interior and exterior cells. For the exterior cells the properties E_x, E_y, ν_{yz}, and ν_{xz} were determined using a two unit cell model with free surfaces at the top and bottom (ie. $z = \pm 2$ c, where c= mat thickness).

The nodal displacements from the global analysis were used to determine the magnitudes of the selected fundamental deformation modes for the region of interest. In this study the region of interest was simply a 1/8 subcell of a unit cell (referred to herein as simply a subcell) and was modeled by one of the 20-node elements in the global model. The displacements for the 20 nodes were used to determine the 20 coefficients in a tri-quadratic polynomial fit for each displacement component. These polynomial curve fits were differentiated to obtain the magnitudes of the particular modes. In particular, for this study 12 fundamental modes were selected which were assumed to be constant for a unit cell. There were 6 constant strain modes: ϵ_x , ϵ_y, ϵ_z , ϵ_{xy} , ϵ_{yz} , and ϵ_{xz}. There were also 6 -flexure modes: $\epsilon_{x,y}$, $\epsilon_{x,z}$, $\epsilon_{y,z}$, $\epsilon_{y,x}$, $\epsilon_{z,x}$ and $\epsilon_{z,y}$. The comma in the subscript indicates differentiation. For example, the mode $\epsilon_{x,z}$ equals $\partial^2 u/\partial z \partial x$ evaluated at the centroid of the unit cell containing the subcell.

Because of symmetry and the invariance in the y-direction for the configuration studied, a maximum of only 5 were non-zero: ϵ_x, ϵ_z , ϵ_{xz} , $\epsilon_{x,z}$, and $\epsilon_{z,x}$. The refined local model was subjected to unit values of each mode. For an interior cell the modal magnitudes determined from the global analysis were then used to scale and superpose the interior unit modal solutions to obtain a refined solution for the selected region. For an exterior cell this procedure was modified, as described later in this section. This is essentially a higher order version of the traditional use of micromechanics in a structural analysis. It is not unusual to obtain a global solution using homogenized properties and then use the calculated global strains with the actual material properties or a unit cell analysis to determine local stresses. The difference is that traditionally the unit cell analysis is performed for constant strain modes only. The advantages of including the linear strain modes will be discussed in the Results and Discussion section.

It should also be noted that different boundary conditions were used to determine the interior and exterior unit modal solutions. The interior solutions were obtained from a model which assumed that the cell was buried inside an infinite array of cells. Only one exterior mode solution was used in this study: ϵ_x. The exterior ϵ_x mode solution was obtained using a model with two unit cells through the thickness (i.e. the z-direction) and an infinite number in the x- and y-directions. That is, there were traction-free surfaces at $z = \pm 2$ c. The possibility of more free surfaces was not considered in this effort. Since the exterior ϵ_x mode also contains an ϵ_z component, it was necessary to account for this contribution when determining the magnitude of the pure ϵ_z mode to superpose. If one defines ν_{xz} to be the average Poisson's ratio for an exterior cell, then the modified ϵ_z mode is (ϵ_z from the global analysis) - ν_{xz} (ϵ_x from the global analysis).

CONFIGURATION

This section describes the cantilevered plate configuration and the finite element models selected for this initial evaluation of the global/local method. A simple three dimensional configuration was selected so that reference solutions could be obtained using conventional finite element modeling. Fig. 2 shows the configuration considered. The cantilevered length (x-direction) was 1.5 times the thickness. The plate was infinite in the y-direction. The nominal curvature in the y-direction was restrained to be zero by imposing zero normal displacements on the planes $y = \pm\lambda/2$. The fiber tows were assumed to follow a sinusoidal path. The ratio of the tow wavelength to the mat thickness was 1/3.

Two load cases were considered: constant moment and transverse end load. For both cases $v(x, \pm\lambda/2, z) = 0$. The other boundary conditions are as follows:

Constant moment case: $u(0,y,z) = 0$ $\quad u(3\lambda, y, z) = .01\ z$ $\quad w(0,0,0) = 0$

Transverse end load: $u(0,y,z) = v(0,y,z) = w(0,y,z) = 0$
Traction in the z-direction on the plane $x = 3\lambda$ was -16 MPa.

Figs. 1 and 2 show the meshes used for the reference solution and the global and local models for the global/local analysis. All of the models used 20-node solid elements. The global/local analysis uses far fewer elements and degrees of freedom. The difference would be even greater if more refined models were used.

The material properties used for the fiber tows and matrix pockets are shown in the following table.

	Tow		Matrix		Homogenized properties	
	modulus	strength*	modulus	strength*	modulus(I.C.)	modulus (E.C.)
E_{11}	206.50 GPa	1034/-689.5 MPa	3.45 GPa	103.4/-241.3 MPa	29.45 GPa	24.97 GPa
E_{22}	5.17 GPa	41.37/-117.2 MPa	3.45 GPa	103.4/-241.3 MPa	29.45 GPa	24.97 GPa
E_{33}	5.17 GPa	41.37/-117.2 MPa	3.45 GPa	103.4/-241.3 MPa	4.80 GPa	4.80 GPa
ν_{12}	0.25		0.35		0.09	0.16
ν_{13}	0.25		0.35		0.94	0.99
ν_{23}	0.25		0.35		0.94	0.99
G_{12}	2.39 GPa	68.95 MPa	1.28 GPa	89.6 MPa	1.96 GPa	1.96 GPa
G_{13}	2.39 GPa	68.95 MPa	1.28 GPa	89.6 MPa	2.64 GPa	2.64 GPa
G_{23}	2.39 GPa	68.95 MPa	1.28 GPa	89.6 MPa	2.64 GPa	2.64 GPa

I.C. = interior cell * Tension/compression strength
E.C. = exterior cell

RESULTS AND DISCUSSION

Stress distributions were determined for a cantilevered beam using a traditional finite element model using the proposed global/local procedure. Two subcells were examined in detail for each load case. One was in the interior and one was on the exterior of the plate. These subcells are shown shaded in Fig. 2. The stresses were normalized by the allowable for each stress component and the locations and magnitudes of the largest normalized stresses were identified. These normalized stresses can be considered failure indices for a maximum stress failure

criterion. The table below summarizes the results for several of the larger values.

Table 1. Summary of predicted critical locations.

	interior cell (G/L prediction)					exterior cell (G/L prediction)				
	location	σ_{ij}	F.I.	%e	$\%e_1$	location	σ_{ij}	F.I.	%e	$\%e_1$
Constant Moment	warp tow	σ_{13}	0.807	0	-100	warp tow	σ_{13}	2.628	-5	-25
	warp tow	σ_{33}	0.605	0	-100	warp tow	σ_{33}	1.927	-12	-31
	matrix	σ_{33}	0.573	0	-100	fill tow	σ_{23}	1.035	-32	-26
	fill tow	σ_{23}	0.365	0	-100	matrix	σ_{33}	1.000	-9	-10
	matrix	σ_{22}	0.273	0	-100	fill tow	σ_{11}	0.607	-17	-41
Transverse End Load	warp tow	σ_{13}	1.440	5	-7	warp tow	σ_{13}	2.786	22	-3
	warp tow	σ_{33}	1.097	4	-22	warp tow	σ_{33}	2.099	16	48
	matrix	σ_{13}	1.000	-2	-4	fill tow	σ_{23}	0.778	-37	-25
	matrix	σ_{33}	0.490	-1	-76	matrix	σ_{13}	0.574	13	7
	fill tow	σ_{13}	0.368	1	1	matrix	σ_{11}	0.548	-10	-41

σ_{ij} = actual stress component
F.I. = failure index = actual stress/allowable stress.
%e = error in the G/L prediction (linear modes included) w.r.t reference solution.
$\%e_1$ = error in the G/L prediction (only constant modes) w.r.t reference solution.

In the table, the location is given as warp or fill tow or matrix pocket. Subsequent contour plots will give a more precise indication of the location of the largest failure indices. For both load conditions and subcell locations the normalized σ_{13} and σ_{33} were largest and the largest values were in the warp tows. The errors were zero for the interior subcell for the constant moment load case. This was expected. For the transverse load case the errors tended to be significantly smaller for the interior subcell that for the exterior one. The most critical failure indices were predicted very well for the interior subcell. Although the predictions were not as good for the exterior subcell, the predictions were generally much better than if only constant modes had been used.

Figs. 3 and 4 show normalized stress contours for the interior and exterior subcell warp tow for the transverse end load case. The most critical locations were in the warp tow and the critical stress components were σ_{33} and σ_{13}, so that is what is shown. The location and magnitude of the peak values are labeled. The figures show that the global/local procedure predicts the location of peak stress and the distribution quite well for the interior subcell and reasonably well for the exterior subcell.

SUMMARY

A global/local procedure was described for analyzing textile composites. The procedure would be equally applicable for other materials for which a characteristic unit cell can be identified. The initial evaluation of the method showed the technique is quite promising. It should be noted that in this study, a simple configuration was studied. Further evaluation is needed for more complex configurations. The major obstacle is obtaining reference solutions for complex

configurations. In fact, even for the current study only very coarse meshes were used for the reference and local solutions in order to limit the number of equations involved. For this reason, this paper did not discuss the significance of the stress components, but instead concentrated on showing that the proposed global/local technique predicts the same trends as a similarly refined traditional analysis. However, the global/local technique is far less costly than a traditional analysis.

REFERENCES

1. J. D. Whitcomb and K. Woo, Enhanced Direct Stiffness Method for Finite Element Analysis of Textile Composites.Proceedings of the ASME Winter Annual Meeting, Anaheim, CA, November 8-13(1992).

2. K. Woo and J. D. Whitcomb, Macro Finite Element Using Subdomain Integration. Communications in Numerical Methods in Engineering 9,937-949(1993).

3. K. Woo, Stress and Failure Analysis of Textile Composites Using a Global/Local Finite Element Method. Ph.D. thesis, Texas A&M University, August(1993).

4. N. Kikuchi and J. M. Guedes, Preprocessing and Postprocessing for Materials Based on the Homogenization Method with Adaptive Finite Element Methods.Computer Method in Applied Mechanics and Engineering 83,143-198(1990).

5. I. Hirai, T. Uchiyama, Y. Mizuta and W. Pilkey, An Exact Zooming Method, Finite Elements in Analysis and Design I. Elsevier Science Publishers,61-69(1985).

6. J. D. Whitcomb and K. Woo, Application of Iterative Global/Local Finite Element Analysis,Part II: Geometrically Non-Linear Analysis., Communications of Numerical Methods in Engineering 9,757-766(1993).

7. C. D. Chapman, Effects of Assumed Tow Architecture on the Predicted Moduli ans Stresses in Woven Composites, M.S. thesis, Texas A&M University, December(1993).

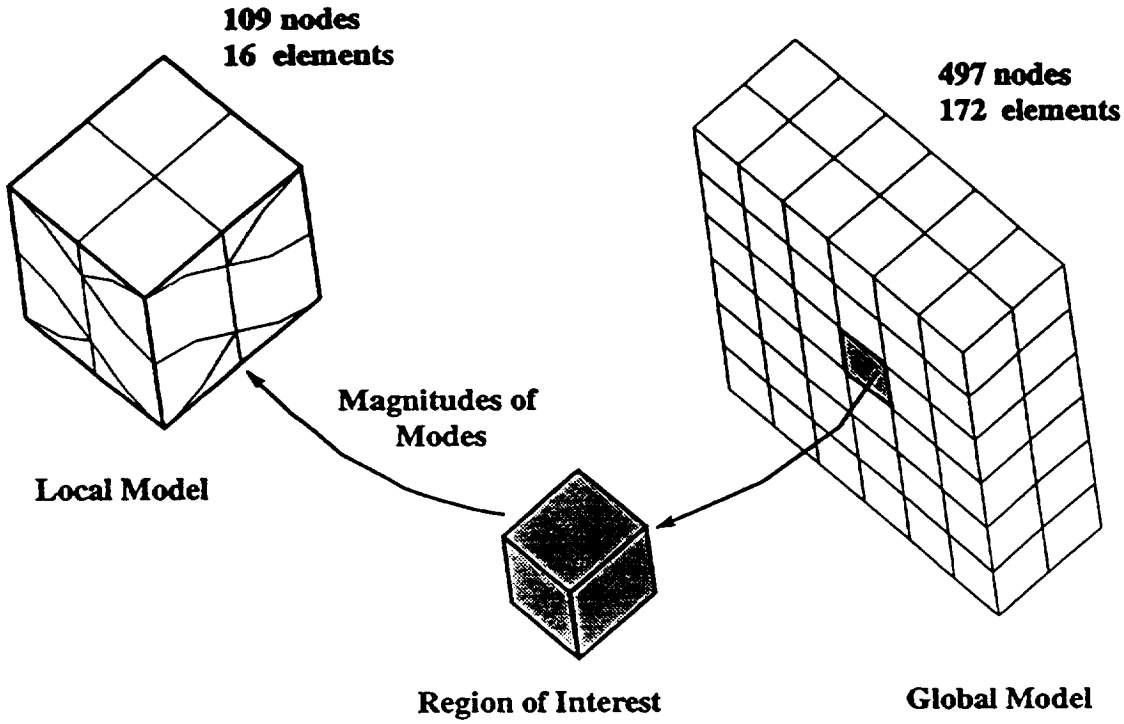

Figure 1 Modal superposition technique using strain modes.

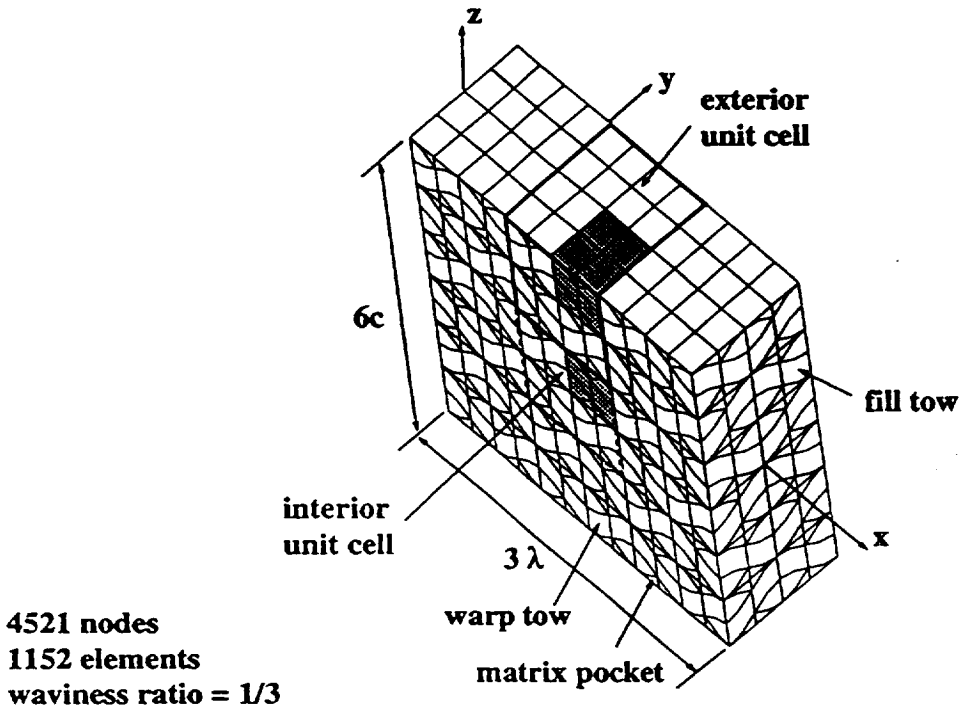

Figure 2 Schematic of woven composite plate.

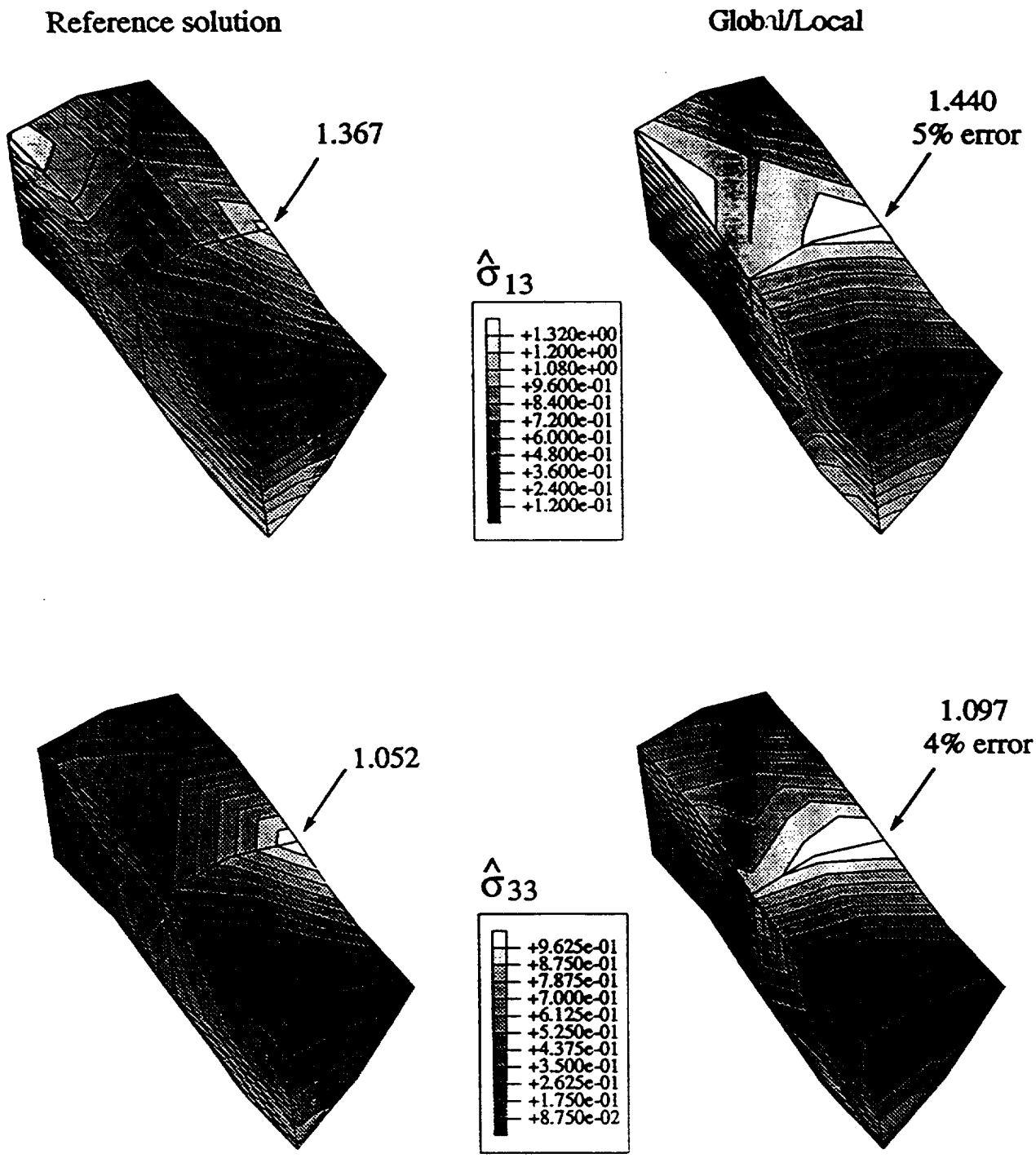

Figure 3 Comparison of predicted normalized stresses for warp tow in interior subcell for transverse end load case.

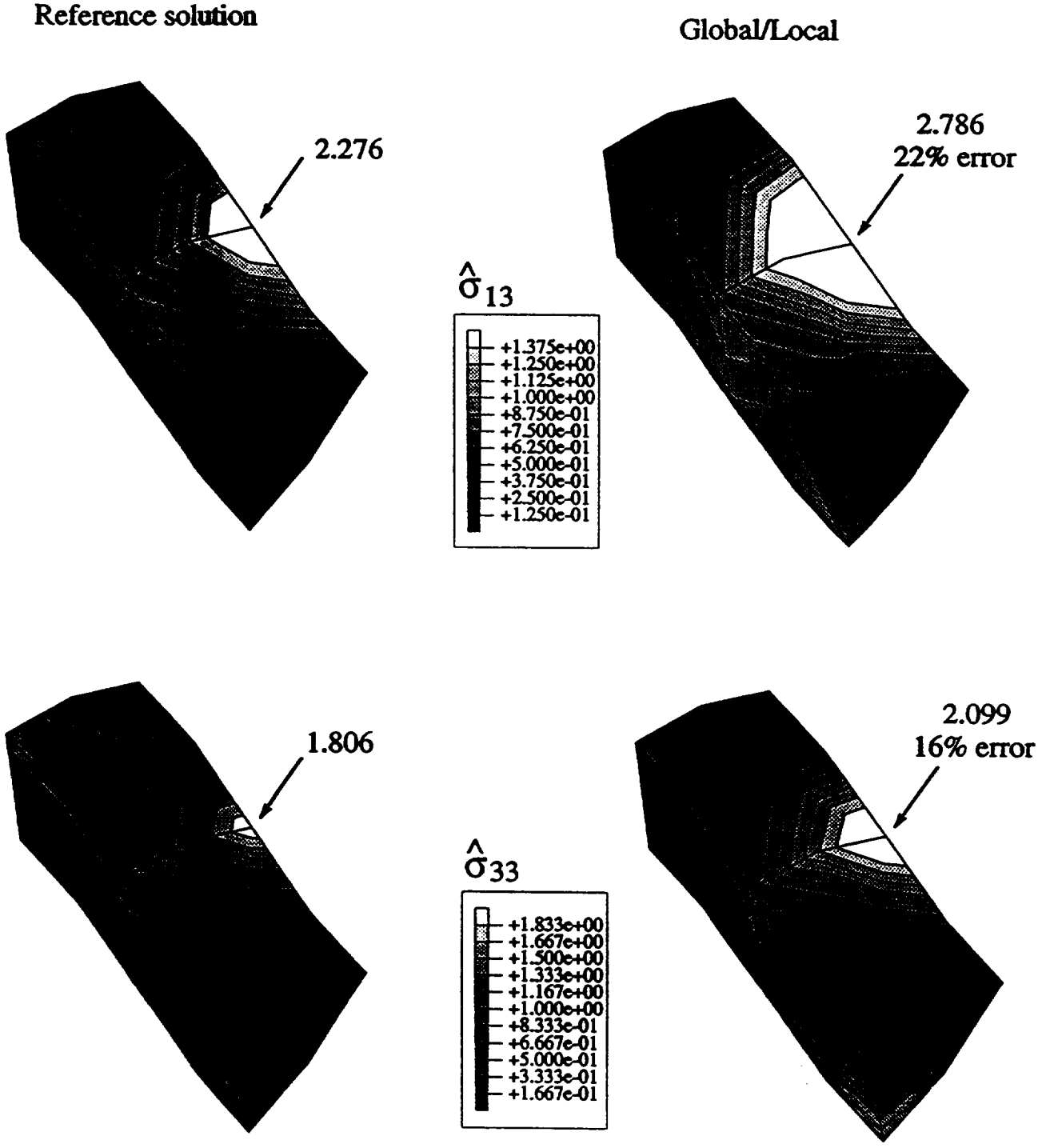

Figure 4 Comparison of predicted normalized stresses for warp tow in exterior subcell for transverse end load case.

Chapter: 9

Effect of Various Approximations on Predicted Progressive Failure in Plain Weave Composites

Abstract

Three-dimensional finite element analysis was used to simulate progressive failure of a plain weave composite subjected to in-plane extension. The loading was parallel to one of the tow directions. The effects of various characteristics of the finite element model on predicted behaviour were examined. The predicted behavior was found to be sensitive to quadrature order, mesh refinement and the material degradation model. Also the sensitivity of the predictions to the tow waviness was studied. The predicted strength decreased considerably with increased waviness. More numerical studies and comparisions with experimental data are needed to establish reliable guidelines for accurate progressive failure prediction.

Introduction

Textile composites consist of interlaced tows (fiber bundles) which are then impregnated with a matrix material and cured. Figure 1 illustrates the architecture for a plain weave composite. The interlacing of the tows offers the potential for increased through-thickness strength. There is also the potential for reduced fabrication costs, since fairly complicated shapes can be formed using textile machinery. One disadvantage of textiles is the difficulty in predicting their performance. The complex geometry makes detailed stress analysis quite challenging. The early analyses were based on modified laminate theory. (e.g. References 1,2) In recent years there have been a few attempts to discretely model the fiber bundle architecture and predict internal stress states. (eg. References 3-11) Reference 11 presented a particularly interesting progressive failure analysis of a plain weave composite. The results in Reference 11 consisted of nominal stress-strain curves. The response of the composite was almost linear for in-plane extension and highly nonlinear for in-plane shear. The nonlinearity was primarily a result of progressive damage. However, little information was provided on damage evolution and load redistribution within the composite during the loading process. Also, there was no indication of the sensitivity of the predictions to

mesh refinement or other approximations inherent in such analyses.

This paper has two objectives. The first is to evaluate the sensitivity of predicted progressive failure to quadrature order, mesh refinement, and choice of material degradation model. The second objective is to describe the nature of the progressive failure process for two weaves with very different waviness. Loading consisted of a nominally uniaxial stress along one of the fiber tow directions. Only mechanical loads were considered in this study. To simplify the response the composite was assumed to consist of an infinite number of identical unit cells in all three coordinate directions.

The following sections begin with a description of the basic theory used for progressive damage modelling. Then the configurations will be described. Finally the results from the numerical simulations will be discussed.

Theory

There is no "right" way to model damage evolution in a textile composite that is also practical. It is not feasible to discretely model all of the damage, so approximation is unavoidable. Perhaps the simplest procedure to account for damage in a finite element model is to modify the constitutive matrix at the quadrature points of a numerically integrated finite element. If history effects are not included, the analysis of the loading becomes a series of elastic analyses. Of course, there are many possibilities for how to modify the constitutive matrix. Three techniques were used herein. The first method considered the material totally failed (ie. the entire constitutive matrix was reduced by 3 orders of magnitude) when any allowable stress component was exceeded. This method will be referred to as the non-selective discount method. The second technique selectively reduced the rows and columns of the constitutive matrix C (where $\sigma=C\varepsilon$) according to the particular stress allowable which was exceeded. For example, if the third stress component exceeded the allowable, the third row of C was set to essentially zero (reduced by 3 orders of magnitude) to eliminate that stress component. To keep the constitutive matrix symmetric, the third column would also be set to zero. Zeroing the column has the undesirable side effect of stiffening the material with respect to the other stresses. This degradation method based on setting rows and columns of C equal to zero will be referred to as the selective RC method. The third technique selectively reduced the engineering moduli according to the particular stress allowable which was exceeded. Except as noted, this technique was used in the analyses. This technique will be referred to as the Blackketter method.(see Reference 11)

The progressive failure analysis begins with a linear analysis of the undamaged configuration. Based on the calculated stresses, the initial load was scaled back so that failure would occur only at points which were within two percent of the maximum normalized stress. (The stresses were normalized by the respective strengths.) The constitutive matrix was modified at the failure points. Residual forces were calculated and used to determine the incremental displacements. The total displacements were updated and used to determine the new stresses, which were then used to predict further failure. If no further failures occurred at the current nominal strain state, the nominal strain was incremented to cause failure. This procedure was repeated until the nominal strain exceeded one percent.

Configurations

The fiber bundles or tows in the models were generated by translating a lenticular cross-section along a sinusoidal path. The waviness ratio is defined to be the ratio of the woven mat thickness to the wavelength. The weave consists of warp and fill tows oriented perpendicular to

each other. In general, the warp and fill tows could be different in terms of material and shape. In this study they were assumed to be identical. More details about the mesh geometry can be found in Reference 9. The following subsections describe the finite element meshes, the boundary conditions, and the material properties.

Finite Element Meshes

Symmetry in the material and loading was exploited so that only 1/32 of a unit cell had to be modeled. A wide range of mesh refinements were used, as shown in Figure 2. The crude mesh had only 4 elements and 42 nodes. The most refined mesh had 192 elements and 1049 nodes. The elements were 20-node hexahedral elements. Since only 1/32 of the unit cell was modeled, these refinements correspond to full cell models with 128 to 6144 elements.

Boundary Conditions

The periodic boundary conditions for a complete unit cell are quite simple. The appropriate boundary conditions for a 1/32 unit cell are a bit more complicated. Derivation of the periodic boundary conditions is somewhat tedious, so details will not be given here. Details can be found in Reference 9. The periodic conditions are listed below. Figure 2 shows the coordinate system assumed.

$u(a/2,y,z) = u_0$	$v(x,a/2,z) = \text{constant}$	$w(x,y,c/2) = \text{constant}$
$u(0,y,z) = -u(0,y,-z)$	$v(0,y,z) = v(0,y,-z)$	$w(0,y,z) = -w(0,y,-z)$
$u(x,0,z) = u(x,0,-z)$	$v(x,0,z) = -v(x,0,-z)$	$w(0,y,z) = -w(0,y,-z)$

The load was controlled by specifying the magnitude of u_0. This corresponds to uniform uniaxial extension in the warp tow direction.

Material Properties

The unit cell contains two "types" of materials: the tows and the matrix pockets. Relative to the material coordinate system, the properties of the tows are invariant (before damage occurs). Of course, the properties of the tows are needed in the global coordinate system. Fourth order tensor transformation formulas were used to perform the required calculations. The rotation angles to be used in these formulas were specified at each quadrature point by using interpolation. This procedure was shown in References 8 and 9 to be preferable to using a single angle for the entire element. The particular properties used are listed below. These properties, which are

representative of AS4/3501-6 graphite/epoxy, are from Reference 13.

	Tow properties		Matrix properties	
	Modulus	Strength	Modulus	Strength
E_{11}	154.27 GPa	2342.0 MPa	3.45 GPa	84.85 MPa
E_{22}	10.80 GPa	56.6 MPa	3.45 GPa	84.85 MPa
E_{33}	10.80 GPa	56.6 MPa	3.45 GPa	84.85 MPa
G_{12}	7.47 GPa	48.7 MPa	1.28 GPa	101.00 MPa
G_{13}	7.47 GPa	48.7 MPa	1.28 GPa	101.00 MPa
G_{23}	3.33 GPa	48.7 MPa	1.28 GPa	101.00 MPa
ν_{12}	0.28		0.35	
ν_{13}	0.28		0.35	
ν_{23}	0.34		0.35	

Results and Discussions

Most of the results in this paper illustrate the effects of characteristics of the finite element model on the progressive failure prediction. The effects of quadrature order, mesh refinement, and material degradation strategy will be considered first. Then the effect of the tow waviness on failure behavior will be discussed. Except where indicated otherwise, the results will be presented for a waviness ratio of 1/3 and for the material degradation strategy in Reference 11, (the "Blackketter method").

Figure 3 shows the effect of quadrature order on the stress-strain curve. The peak stress obtained using 8 quadrature points (2x2x2) is 3 percent higher than that obtained using 64 points. The peak stresses obtained using 27 and 64 quadrature points differ by 1 percent. Damage initiation is predicted 3 percent earlier when 64 points are used. After the large stiffness loss which occurs at about 0.3 percent strain, there are even larger differences in the predictions. In Reference 12, non-selective discount was used for the same configuration. The difference in the peak stress obtained using 8 and 64 point quadratures was 10 percent. Hence, the sensitivity of the predictions to quadrature depends on the degradation model. The sensitivity to quadrature order is not suprising. For example, when more quadrature points are used, the more extensive sampling is more likely to find the extremes in the stress field. One might expect a refined mesh to exhibit less sensitivity to quadrature order than a coarse mesh. For the meshes considered in this study, this was the case. Also, when failure occurs within an element, and the constitutive matrix is modified, the element becomes inhomogeneous. The numerical integration effectively fits a polynomial function to the variation of the material properties. Since the material properties are very different in the failed and unfailed parts of the element, it is difficult to obtain a good fit. In fact, there is a concern as to whether the assumed quadratic displacement functions for a 20-node element are sufficient to obtain a reasonable approximation regardless of the integration order.

Figure 4 shows the effect of mesh refinement on the predicted stress-strain curve for the two waviness ratios. The four-element model predicts the correct trends, but is quite inaccurate. The error in the peak stress is much worse for larger waviness ratio. The peak stress and corresponding strain for a coarse mesh is larger than for a refined mesh, but the peak stress and corresponding strain for a moderately refined mesh are not necessarily bound by the extreme cases of mesh refinement. (see Figure 4b) The peak stress and the corresponding strain decrease with increased waviness. The ratio of the initial damage stress to the peak stress and the corresponding ratio of strains increase with decrease in waviness ratio. That is, not only is the strength reduced by increased waviness, but there is also earlier damage initiation relative to the

peak stress. After the peak stress is reached, there is a precipitious drop in stress with little change in strain. For the 1/3 waviness ratio and a coarse mesh, this "collapse" actually occured in stages, with a small strain increase between the stages. For the most refined model the collapse occurred in a single stage. For the 1/6 waviness ratio the collapse occured in a single stage for all three mesh refinements. It should be noted that in real specimens there would be a distribution of strength in the various cells. Accordingly, the nominal stress-strain curves would not be expected to have such deep jogs. Also, it would not be possible to impose displacement or load control for the individual cells. Load redistribution and the stability of the damage growth would determine whether the nominal stress-strain curve would appear brittle or there would be significant nonlinearity before total fracture.

Figure 5 shows damage volume versus the nominal strain for the warp and fill tows for four mesh refinements. Damage volume for the resin is not shown since there is almost no damage. The curves are quite close for the 108 and 192 element meshes, which suggests that the curves might be close to convergence. As the mesh is refined, the increments in damage volume become smaller , but more numerous. The damage volume just after collapse tends to decrease with mesh refinement for both warp and fill tows. This is not surprising since the corresponding strain is also smaller. The curve for the 192 element mesh in Figure 5a has points labeled A and B. From A to B the damage initiation and growth was dominated by the inter-tow normal stress σ_{33}. The sudden increase in damage at point B was due to the stress component σ_{13} (the x_1 direction is parallel to the fibers).

The damage volumes just after the peak stress is reached is as follows

Waviness Ratio	Warp	Fill	Percent Stiffness Loss
1/6	.76	.88	41
1/3	.41	.21	45

Interestingly, the damage volume is larger for the 1/6 waviness ratio, but the percentage stiffness loss is less.

Figures 6 and 7 show the effect of mesh refinement and waviness ratio on damage accumulation during loading. To plot the damage zones accurately, each element is sub-divided into 27 blocks, where each block represents the volume associated with a quadrature point. The black region indicates the damage zone. The stress-strain curve for a particular mesh is shown above that mesh. The points labeled A,B and C indicate the correspondence between the strain level and the damage zone. The damage zone corresponding to point A indicates the initial damage. The damage zones corresponding to points B and C indicate the pre- and post- collapse damage states. Also indicated are the stress components which contributed to the damage. The four-element mesh does not model the initial failure well for the two waviness ratios of 1/3 and 1/6. The 32 element model performs reasonably well for obtaining qualitative results. Further numerical studies are needed to determine how close the 192 element results are to convergence. For the 1/3 waviness ratio σ_{33} dominates the initial failure. This initial failure appears to be an inter-tow failure resembling delamination in laminated composites. The collapse is characterized by σ_{13} failure in the warp tows. For the 1/6 waviness ratio, the collapse is due to a significant failure of the warp tow due to σ_{13} and cracking of the fill tow due to σ_{22}.

Figure 8 shows the stress-strain curves obtained using the three degradation models described earlier: non-selective, selective RC, and the Blackketter method. The non-selective method predicts 22% lower peak stress than the Blackketter method. Selective reduction of rows and

columns in the constitutive matrix results in a much larger residual stiffness just after the peak stress than the other two methods. Selective reduction of rows and columns in the constitutive matrix also does not result in a large sudden drop in the stress after the peak stress is reached. Concomitantly, for the selective RC method there is also no sudden increase in the damage volume after the peak stress is reached. (This is not shown on the plot.)

Concluding Remarks

Simulation of progressive failure in a plain weave composite is extremely complex. Consequently, only approximate treatment is practical at this time. One of the goals of this paper was to examine the effect of several approximations on predicted behaviour. One obvious conclusion from this study is that the predictions are quite sensitive to a number of decisions which must be made when assembling a finite element model. Further numerical experiments and comparisons with experimental data are needed to establish guidelines for accurate analysis of progressive failure.

Another objective of this paper was to describe the effect of tow waviness on damage accumulation. The results suggest that the degree of waviness not only affects the stress at which damage initiates, but also the type of damage which occurs. Also, the stress component responsible for damage changed during the progressive failure process.

References

1. Ishikawa, T. and Chou,T.W.: "Stiffness and Strength Behavior of Woven Fabric Composites," Journal of Material Science, 17:3211-3220, 1982.

2. Ishikawa,T. and Chou,T.W.: "Elastic Behavior of Woven Hybrid Composites," Journal of Composite Materials, 16:2-19, January 1982.

3. Paumelle, P., Hassim.,A. and LÁnÁ,F.: "Composites with Woven Reinforcements: Calculation and Parametric Analysis of the Properties of the Homogeneous Equivalent," La Recherche AÁrospatiale, 1:1-12, 1990.

4. Paumelle, P., A. Hassim, and F. LÁnÁ.: "Microstress Analysis in Woven Composite Structures," La Recherche AÁrospatiale, 6:47-62., 1991.

5. Whitcomb, J. D.: "Three-Dimensional Stress Analysis of Plain Weave Composites." Composite Materials: Fatigue and Fracture , ASTM STP 1110, T. K. O'Brien. Ed., Philadelphia: American Society for Testing and Materials, 3:417-438., 1991.

6. Woo, K.: "Stress and Failure Analysis of Textile Composites," Ph.D. Dissertation, Department of Aerospace Engineering, Texas A&M University, 1993.

7. Dasgupta, A. and Bhandarkar, S.: "Effective Thermomechanical Behavior of Plain-Weave

Fabric-Reinforced Composites Using Homogenization Theory," Journal of Engineering Materials and Technology, 116 :99-105, January 1994.

8. Avery, W.B. and Herakovich,C.T. 1987. "A Study of the Mechanical Behavior of a 2D Carbon-Carbon Composite," Virginia Polytechnic Institute and State University, Interim Report 66.

9. Chapman, C.: "Effects of Assumed Tow architecture on the Predicted Moduli and Stresses in Woven Composite," MS thesis, Department of Aerospace Engineering, Texas A&M University, 1993.

10. Guedes, J.M. and Kikuchi N.,"Preprocessing and Postprocessing for Materials Based on the Homogenization Method with Adaptive Finite Element Methods," Computer Methods in Applied Mechanics and Engineering, 83 :143-198, 1990.

11. Blackketter, D.; Walrath, D.; and Hansen, A.: "Modeling Damage in a Plain Weave Fabric-Reinforced Composite Material," Journal of Composites Technology and Research, 15 :2 : 136-142, Summer 1993.

12. Whitcomb, J.D. and Srirengan, K.: Simulation of Progressive Failure in Plain Weave Composites. Proceedings of the Symposium on Mechanics of Textile Composites at the ASME International ME'94 Congress & Exposition, Chicago,Il.,November, 1994.

13. Naik, R.: "Micromechanical Combined Stress Analysis-MICSTRAN, A User Manual NASA Contractor Report 189694, Oct. 1992.

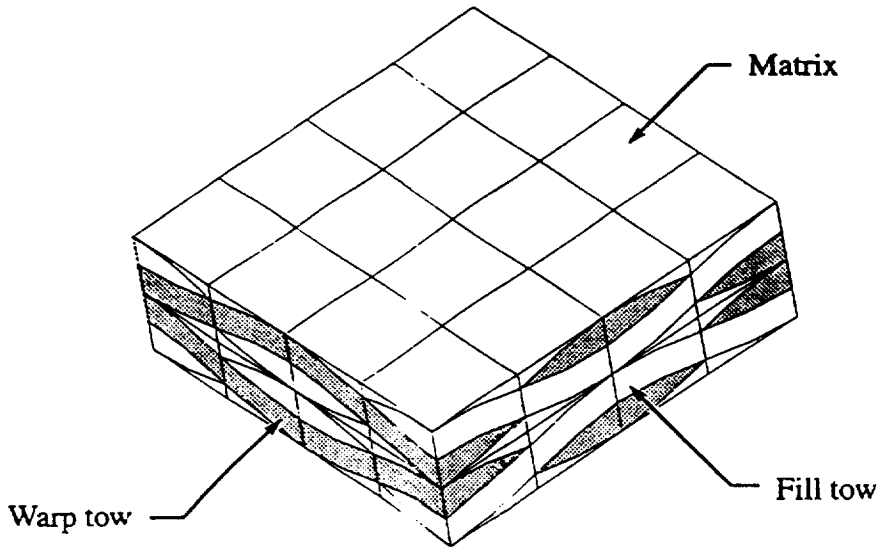

(a) Full unit cell.

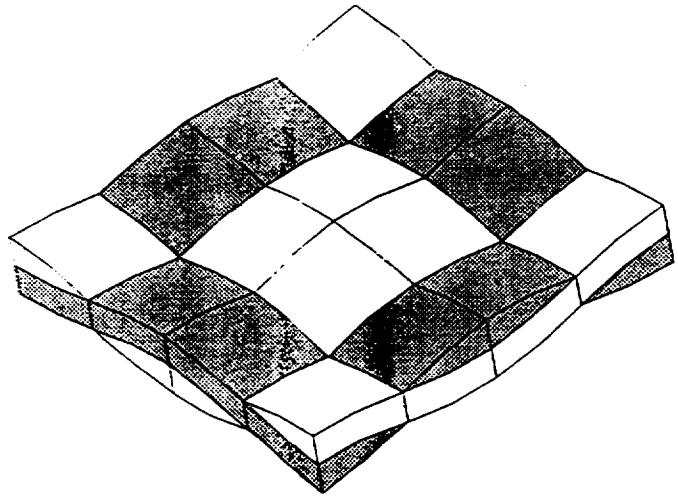

(b) Single mat with matrix pockets removed.

Figure 1 Schematics of plain weave composite.

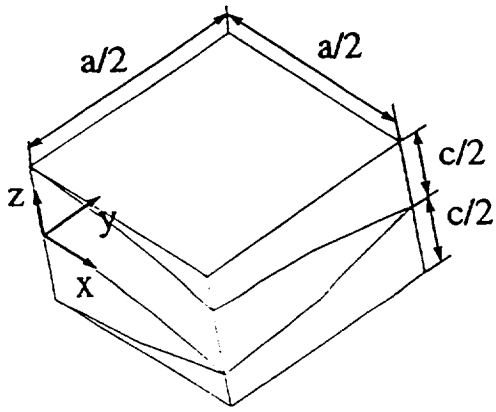

Mesh 1 :
4 elements and 42 nodes

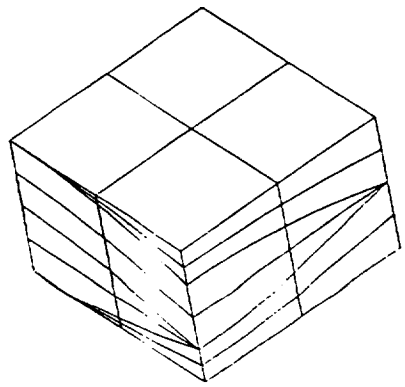

Mesh 2 :
32 elements and 221 nodes

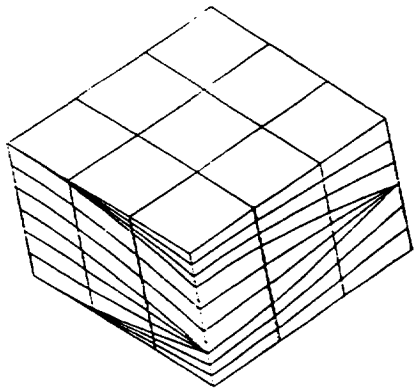

Mesh 3 :
108 elements and 634 nodes

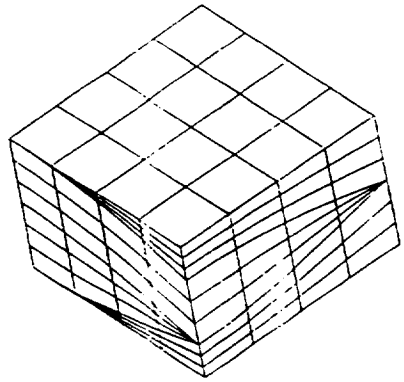

Mesh 4 :
192 elements and 1049 nodes

Figure 2 Finite element meshes used to determine the effect of mesh refinement on failure prediction.

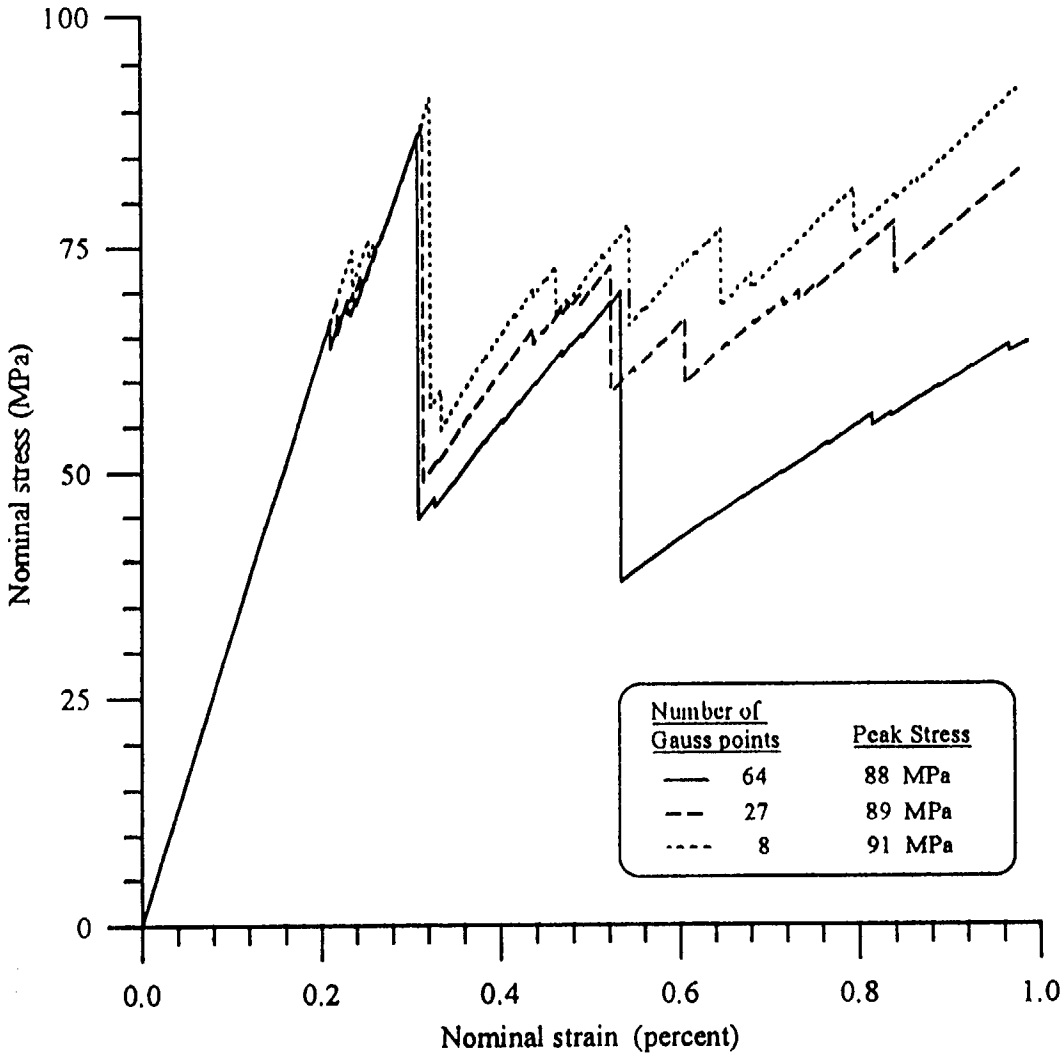

Figure 3 Effect of quadrature order on nominal stress-strain curve. Waviness ratio = 1/3. Blackketter discount method was used. The model had 192 elements and 1049 nodes.

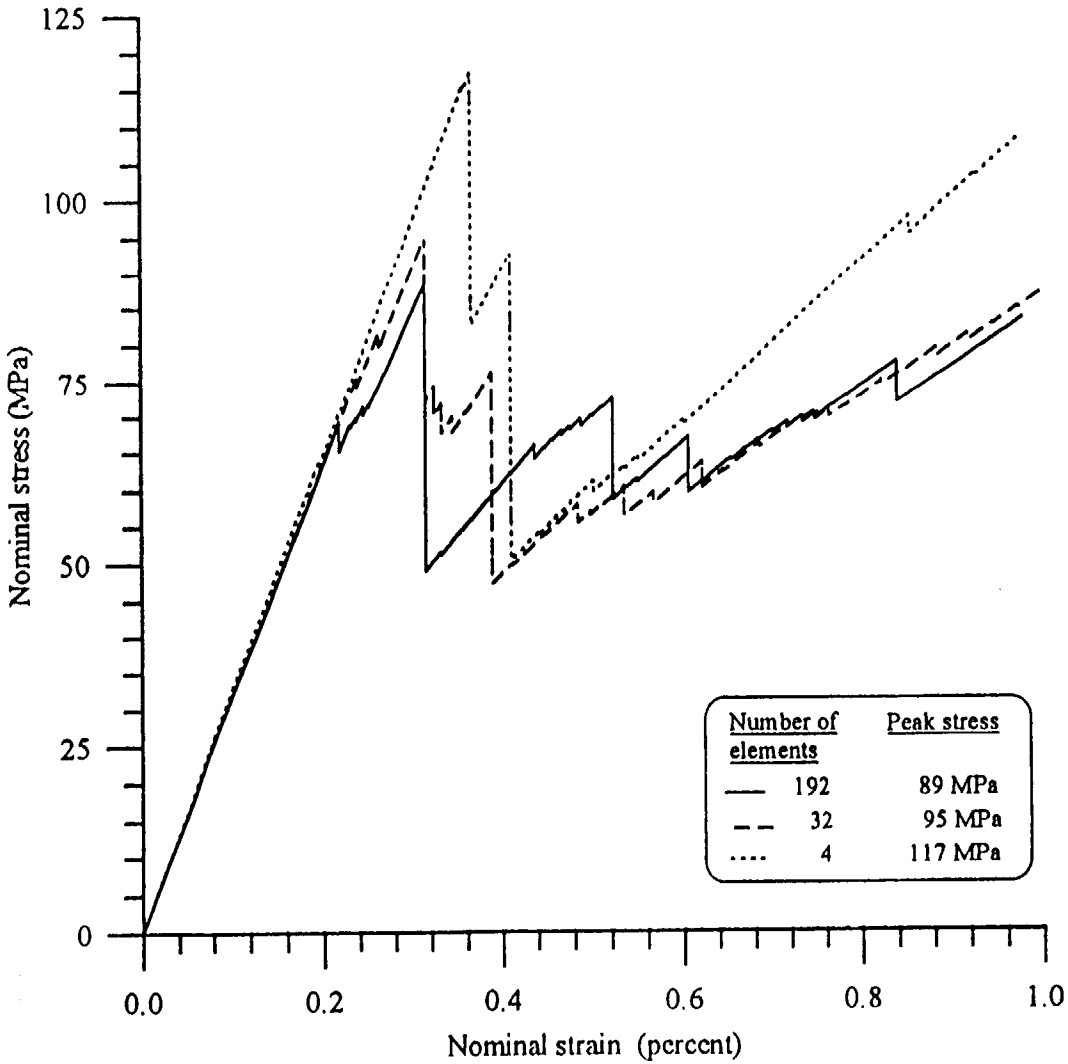

(a) Waviness ratio = 1/3

Figure 4 Effect of mesh refinement on nominal stress-strain curve. Blackketter discount method was used.

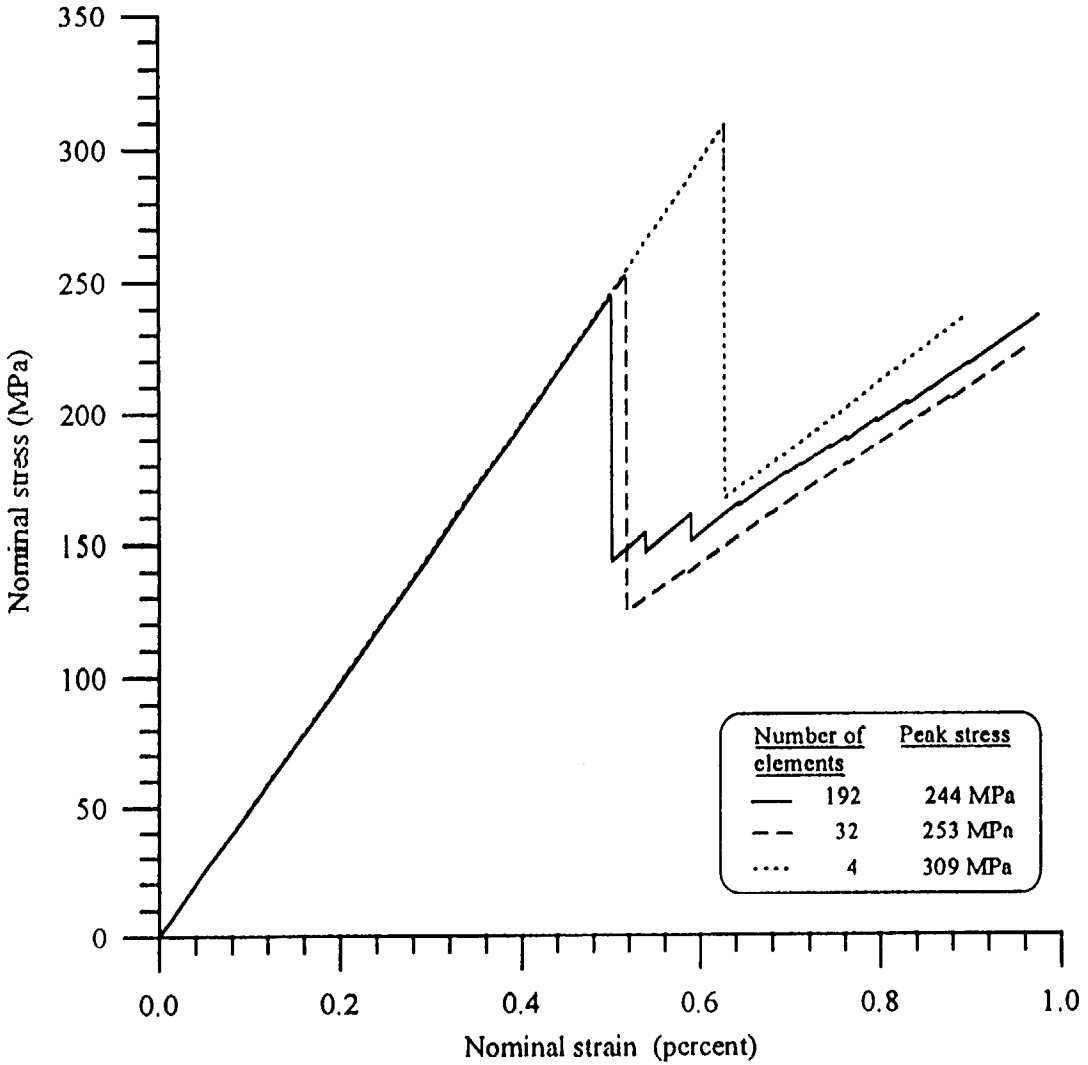

(b) Waviness ratio = 1/6

Figure 4, Cont'd.

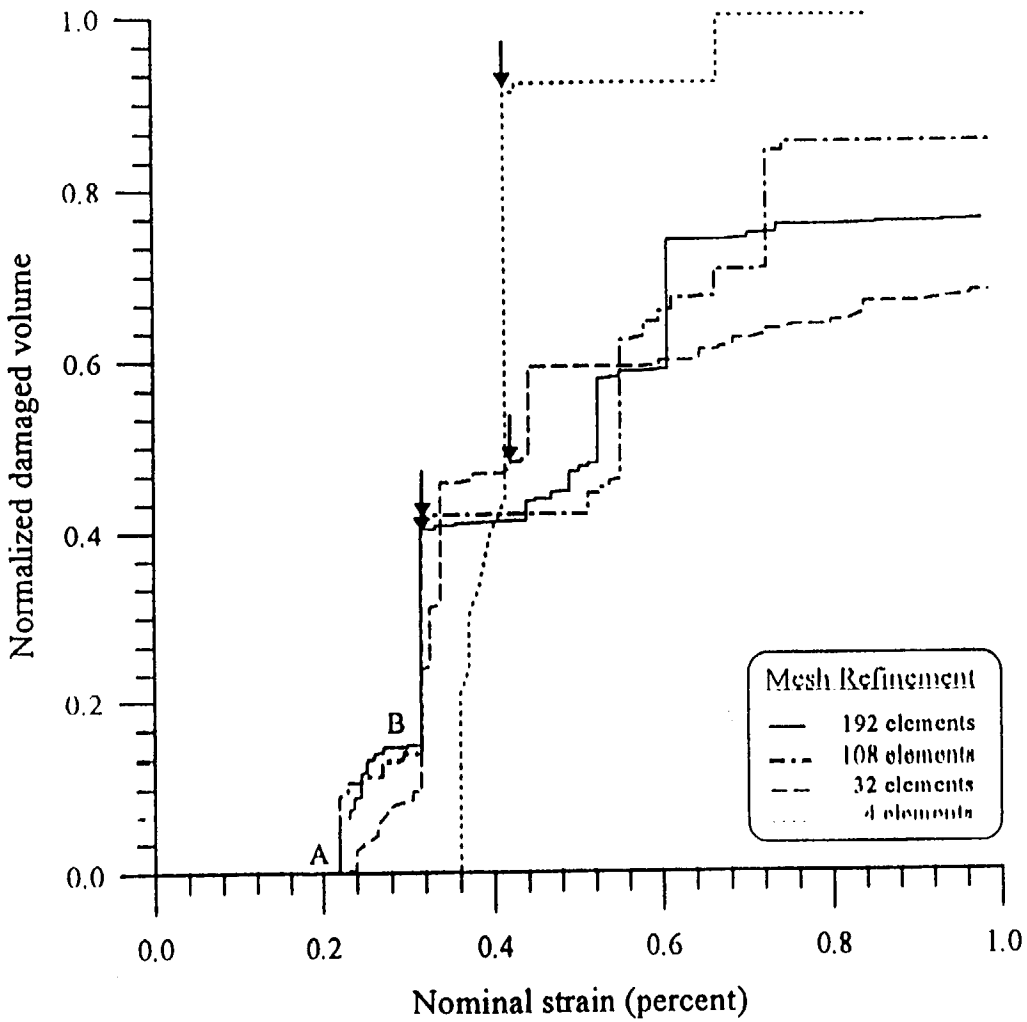

(a) Warp tow

Figure 5 Effect of mesh refinement on damage volume.
Waviness ratio = 1/3. Blackketter discount method was used.
↓ indicates strain at which collapse occured.

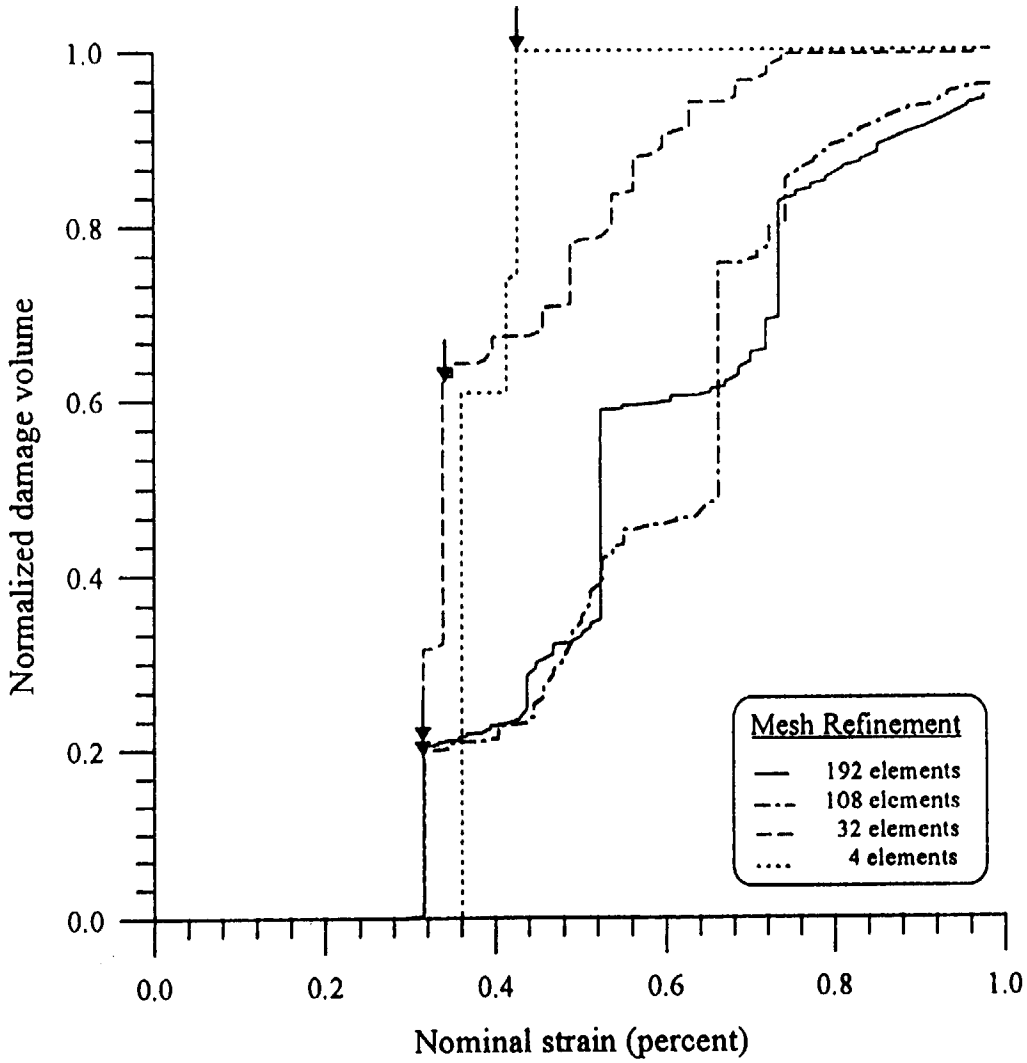

(b) Fill tow

Figure 5, Cont'd.

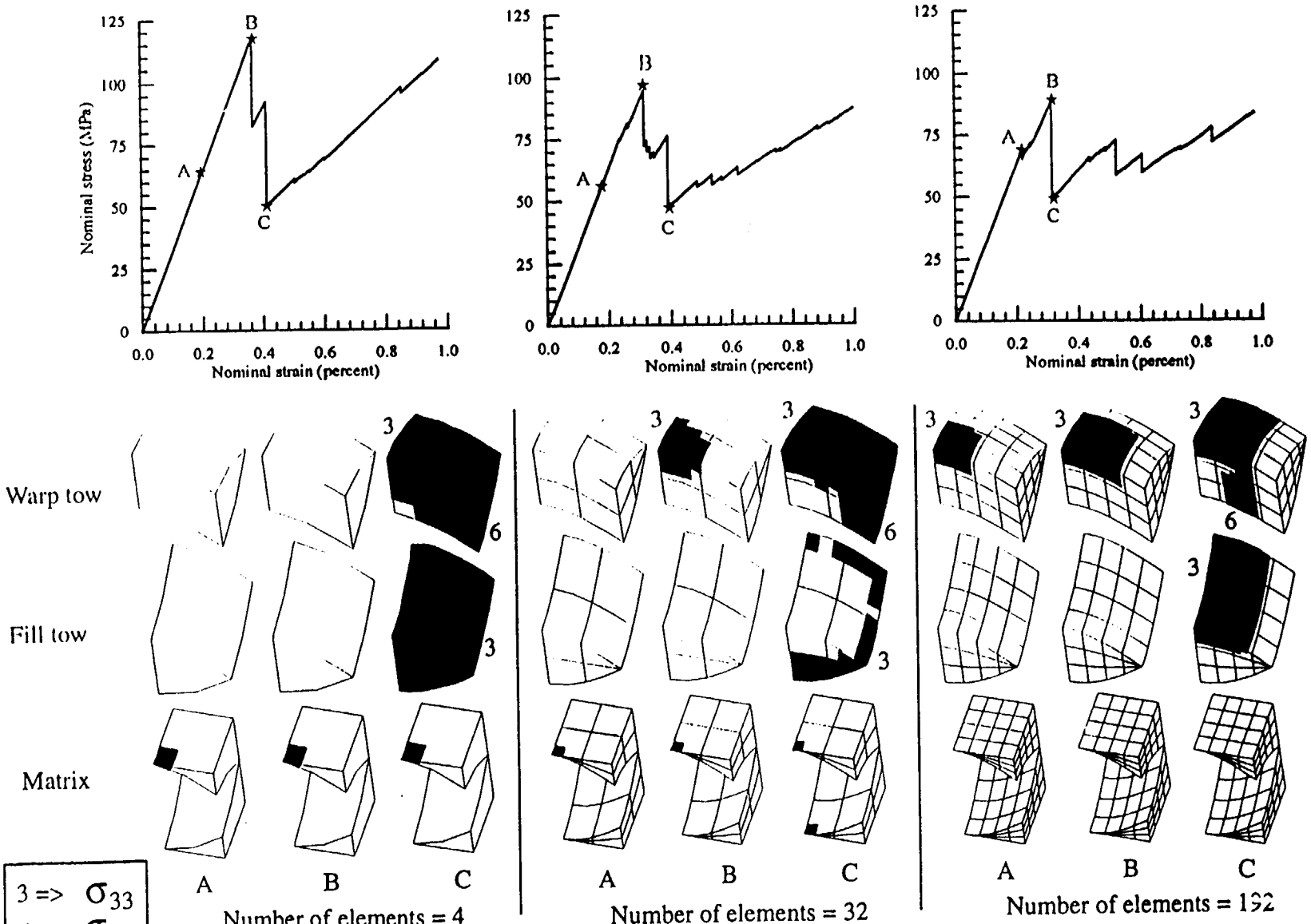

Figure 6 Effect of mesh refinement on damage development for waviness ratio = 1/3. Blackketter discount method was used.

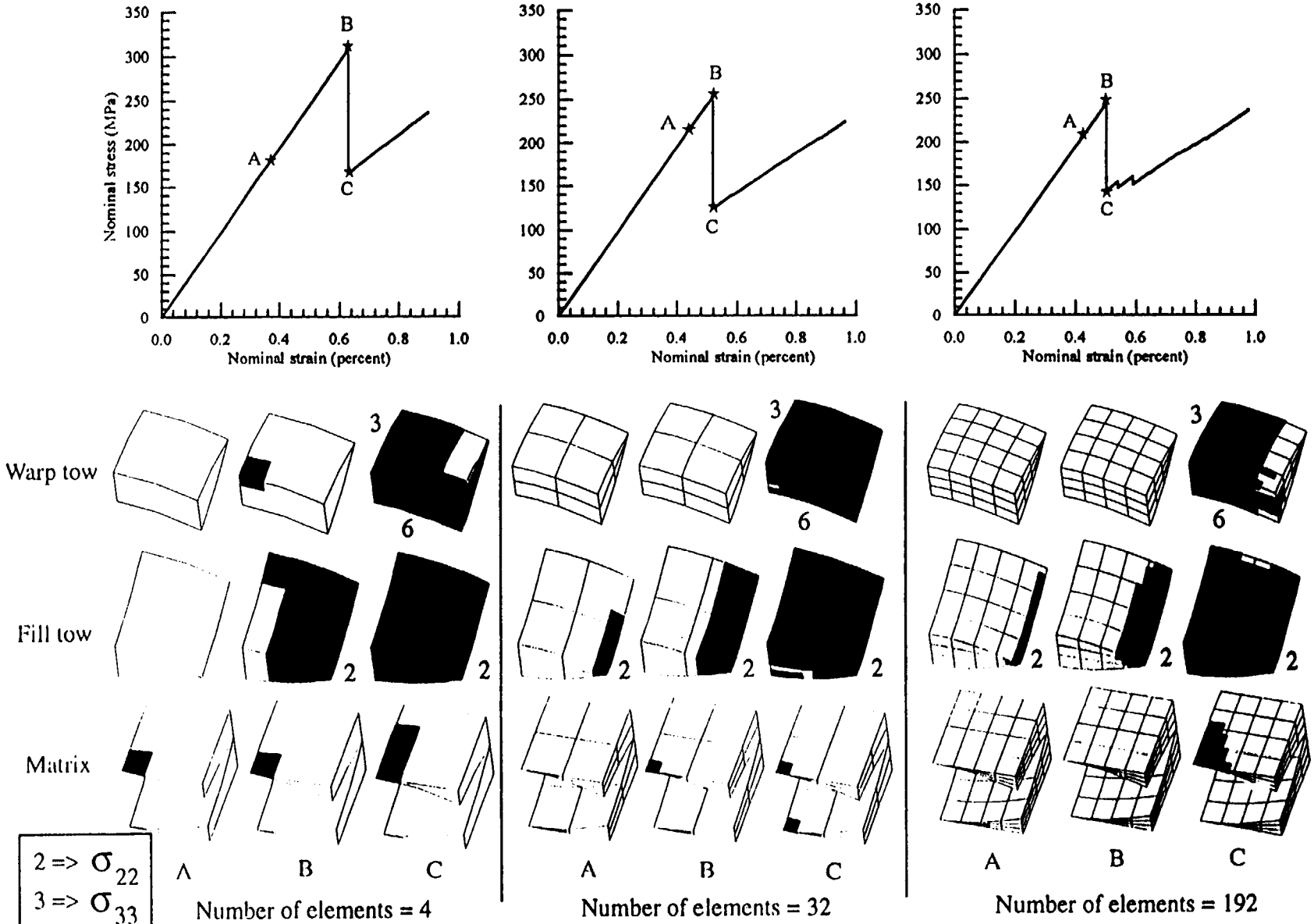

Figure 7 Effect of mesh refinement on damage development for waviness ratio = 1/6 Blackketter discount method was used.

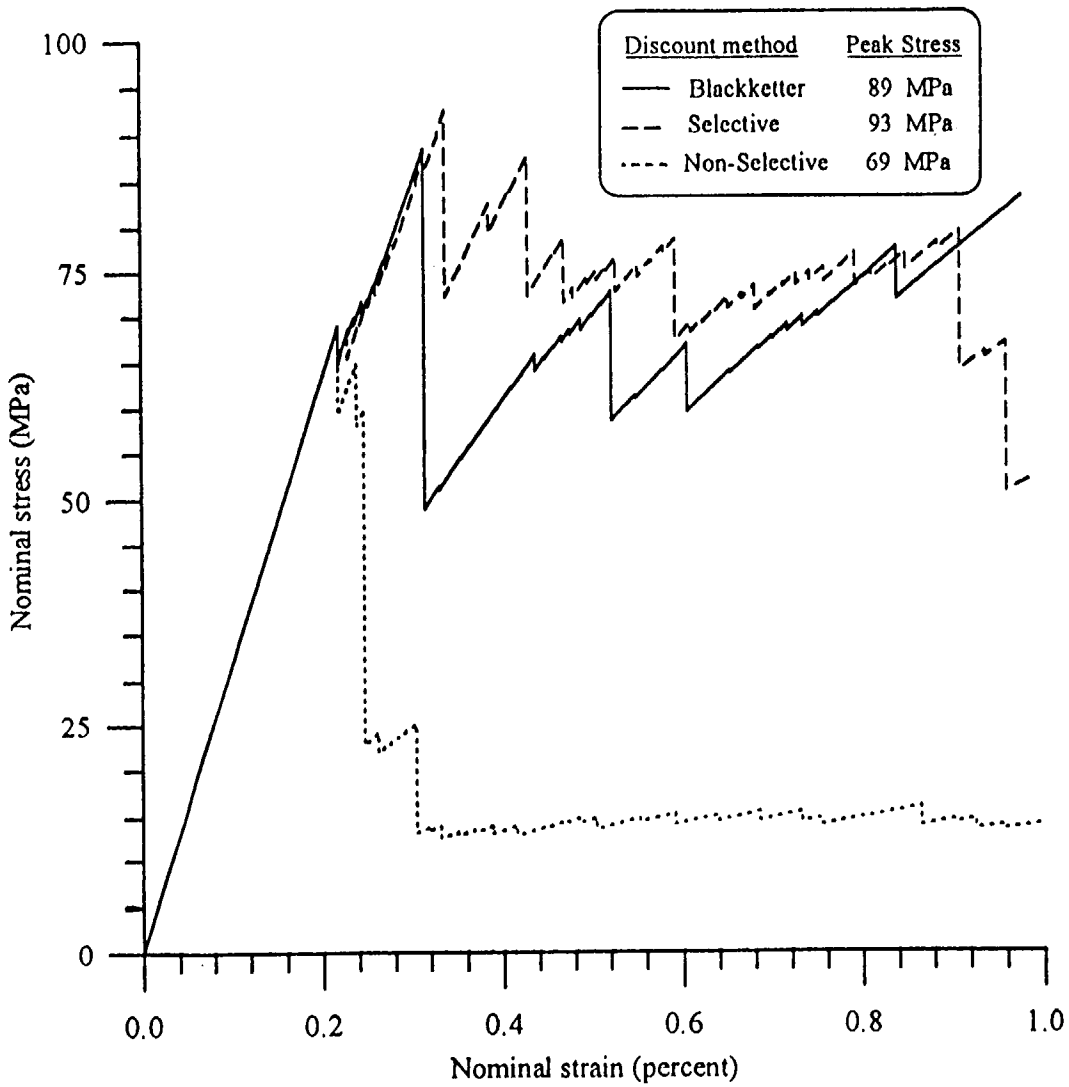

Figure 8 Effect of discount method on nominal stress-strain curve.
Waviness ratio = 1/3. The model had 192 elements and 1049 nodes.

Part II

Chapter: 1

Part II Software Documentation

Stress Analysis of Woven Composites

(SAWC)

Introduction and Abstract

SAWC refers to a collection of three programs which were developed to expedite the study of the failure behaviour of plain weave composites. The programs are a mesh generator (PWMeshGen), a finite element program (Flex94), and a graphical pre- and postprocessor (Plot95).

The primary capability of the software is the generation of solid models of plain weave composites from a few input parameters, the analysis of the solid model, and the display of finite element meshes before and after deformation and stress distributions. Some first order progressive failure capability is also implemented. The finite element code uses a displacement formulation. It includes isoparametric 20-node elements and special "macro" elements which can account for microstructure within a single element.

The input data for the mesh generator is a form, which is generated automatically. The user simply fills in a few blanks in the form with any text editor and then runs the program. The finite element program requires a complex collection of input data. Fortunately, the mesh generator provides most of the data. The plotting program was originally developed using a 2D graphics library and a painter's algorithm to manage hidden line removal. Hardcopy of the display is obtained by writing a PostScript file, which is then printed. Although the program now uses the openGL graphics library (which has built-in hidden line removal), 2D primitives are still used.

The programs are written in a combination of C, C++, and Fortran 77. The programs were developed on an IBM RS/6000 using the AIX (IBM UNIX) operating system version 3.2.5. However, PWMeshGen and Flex94 should port easily to any Unix workstation. The plotting program, Plot95, uses the graphics library openGL and the Motif user interface. The openGL library and Motif user interface is available on major workstations.

This software can be installed on a workststion without root (super user) access.

This manual contains four sections: one section for each program and then a final section which describes installation of the software and sample files.

Listed below are papers which describe the theory and example application of the software.

1993.

Whitcomb, J., Woo, K.: Application of Iterative Global/Local Fini .e Element Analysis Part II - Geometrically Nonlinear Analysis. Communications in Numerical Methods in Engineering. Vol. 9, pp. 757-766, 1993.

Whitcomb, J.D.; Woo, K.; Gundapaneni, S.: Macro Finite Element for Analysis of Textile Composites. Journal of Composite Materials. Vol. 28, pp. 587-681, 1994.

Woo, K. and Whitcomb, J.D.: Macro Finite Element Using Subdomain Integration. Communications in Applied Numerical Methods. Vol. 9, pp. 937-949, 1992.

Whitcomb, J., Woo, K.: Enhanced Direct Stiffness Method for Finite Element of Textile Composites. Accepted for publication in Composite Structures.

Whitcomb, J.; Kondagunta, G.; Woo, K.: Boundary Effects in Woven Composites, accepted for publication in Journal of Composite Materials.

Whitcomb, J. and Srirengan, K., Chapman, C.: Evaluation of Homogenization for Global/Local Stress Analysis of Textile Composites. Presented at theAIAA/ASME/ASCE/AHS/ASC 35th Structures, Structural Dynamics, and Materialsconference, Hilton Head, South Carolina, April 18-20, 1994. Submitted to Journal of Composite Materials.

Whitcomb, J. and Srirengan, K.: Simulation of Progressive Failure in Plain Weave Textile Composites. Proceedings of the International ME'94 Congress and Exposition.

Notice of Restrictions

The Motif interface was developed using AIXwindows Interface Composer. This program generates Motif code which is than compiled and linked with the other parts of the Plot95 program. Appropriate copyright notices for the software generated are shown below.

```
/*
 * COMPONENT_NAME: AIC        AIXwindows Interface Composer
 *
 * ORIGINS: 58
 *
 *
 *              Copyright IBM Corporation 1991, 1993
 *
 *                  All Rights Reserved
 *
 * Permission to use, copy, modify, and distribute this software and its
 * documentation for any purpose and without fee is hereby granted,
 * provided that the above copyright notice appear in all copies and that
 * both that copyright notice and this permission notice appear in
 * supporting documentation, and that the name of IBM not be
```

```
 *  used in advertising or publicity pertaining to distribution of the
 *  software without specific, written prior permission.
 *
 *  IBM DISCLAIMS ALL WARRANTIES WITH REGARD TO THIS SOFTWARE, INCLUDING
 *  ALL IMPLIED WARRANTIES OF MERCHANTABILITY AND FITNESS FOR A PARTICULAR
 *  PURPOSE. IN NO EVENT SHALL IBM BE LIABLE FOR ANY SPECIAL, INDIRECT OR
 *  CONSEQUENTIAL DAMAGES OR ANY DAMAGES WHATSOEVER RESULTING FROM LOSS OF
 *  USE, DATA OR PROFITS, WHETHER IN AN ACTION OF CONTRACT, NEGLIGENCE OR
 *  OTHER TORTIOUS ACTION, ARISING OUT OF OR IN CONNECTION WITH THE USE
 *  OR PERFORMANCE OF THIS SOFTWARE.
 */
/*-----------------------------------------------------------------
 * $Date: 93/04/26 21:05:25 $          $Revision: 2.19 $
 *-----------------------------------------------------------------
 *
 *
 *          Copyright (c) 1992, Visual Edge Software Ltd.
 *
 * ALL RIGHTS RESERVED. Permission to use, copy, modify, and
 * distribute this software and its documentation for any purpose
 * and without fee is hereby granted, provided that the above
 * copyright notice appear in all copies and that both that
 * copyright notice and this permission notice appear in supporting
 * documentation, and that the name of Visual Edge Software not be
 * used in advertising or publicity pertaining to distribution of
 * the software without specific, written prior permission. The year
 * included in the notice is the year of the creation of the work.
 *-----------------------------------------------------------------*/

/*-----------------------------------------------------------------
```

Chapter: 2

User's Manual for PWMeshGen

(Plain Weave Mesh Generator)

A collection of Fortran and C programs were developed to expedite the generation of finite element meshes for plain weave composites. These programs are currently intended to be run under the UNIX operating system. However, only a few changes are required for other operating systems.

The tow path of the plain weave is assumed to be sinusoidal. The user can select between translated and extruded tows (see Ref. 1). Although several programs are required to generate a mesh, an executive program has been provided which orchestrates the transfer of data from one program to the next. Hence, the collection of programs appears to the user to be a single program. The executive is named **PWMeshGen**.

To simplify program operation, the input file is a form. This form contains labels which remind the user of the required data and order of the data. To obtain a copy of the form, simply execute the program "PWForm" with the command line parameter "filename", which will be the name of the generated form. For example, executing the command

PWForm inFile

will generate a file named <inFile>, which is shown in Figure 1. Figure 2 shows a typical finite element mesh with labels which define the terms in the generated form.

When this file is edited, it is critical than none of the form labels be changed, since the labels are used to guide input. Once the form is complete the mesh is generated by executing the command

PWMeshGen inFile

The programs will generate several files, which will be discussed in the next section. Sample data in the sub-directories "Sample3" and "Sample4" on the distribution media include completed forms. The file names for these forms are Samples/Sample3/Input/mesh1 and Samples/Sample4/Input/mesh2.

Warning

Early in the mesh generation process there are duplicate node numbers. One of the tools removes the duplicate node numbers. This tool uses a tolerance to determine whether two points are coincident. This tolerance is hardwired to be .00001. It can be changed by editing the file MeshClass.C in PWMeshGen/MeshToolSource. Line 140 is

#define EPSILON 1e-5

To change the tolerance, simply change this value and recompile.

Output Files:

Several output files are generated. These files are for use with the finite element program Flex94. The following files are generated during a typical execution:

File	Description
new.flex	Main input file for Flex94.
new.sflx	Mesh file for Flex94.
new.as	Element rotation angle file: single angle.
new.am	Element rotation angle file: multiple angle.
mat_list	A material list of the elements.
new.flx	A simple mesh file used for plotting the mesh and determining boundary conditions automatically.
xExtension.mpc	Multipoint constraints for extension in the x direction.
xyShear.mpc	Multipoint constraints for in-plane shearing.
xzShear.mpc	Multipoint constraints for transverse shearing.
ExtSingleConstraints	Constraints for extension.
xyShearConstraints	Constraints for in-plane shearing.
xzShearConstraints	Constraints for transverse shearing.
xExtension.Loads	Loads for extension in the x-direction.
xyShear.Loads	Loads for in-plane shearing.
xzShear.Loads	Loads for transverse shearing.
eighth.flx	A simple mesh file for plotting the 1/8th unit cell.
eighth.am	Element rotation angle file for 1/8th unit cell: multiple angle.
eighth.as	Element rotation angle file for 1/8th unit cell: single angle.

References:

1. Chapman, C. 1993. *Effects of assumed tow architecture on the predicted moduli and stresses in woven composites*, Master thesis, Department of Aerospace Engineering, Texas A&M University.

```
Input File for Mesh Generation Program
------------------------------------------

Thickness of mat:
Waviness ratio:
Tow type:
Tow elements in z-direction:
Primary elements in y-direction:
Resin elements above and below tows:

Execution flow flags: Type yes beside functions to be performed.
      Generate 1/8 unit cell:
      Renumber nodes to reduce profile of stiffness matrix:
-----------------------------------------------------------------
Notes
Tow type:    1=> extruded
             2=> translated

**************End of Input File For Mesh Generator****************
```

Figure 1: Form used to define input for mesh generator.

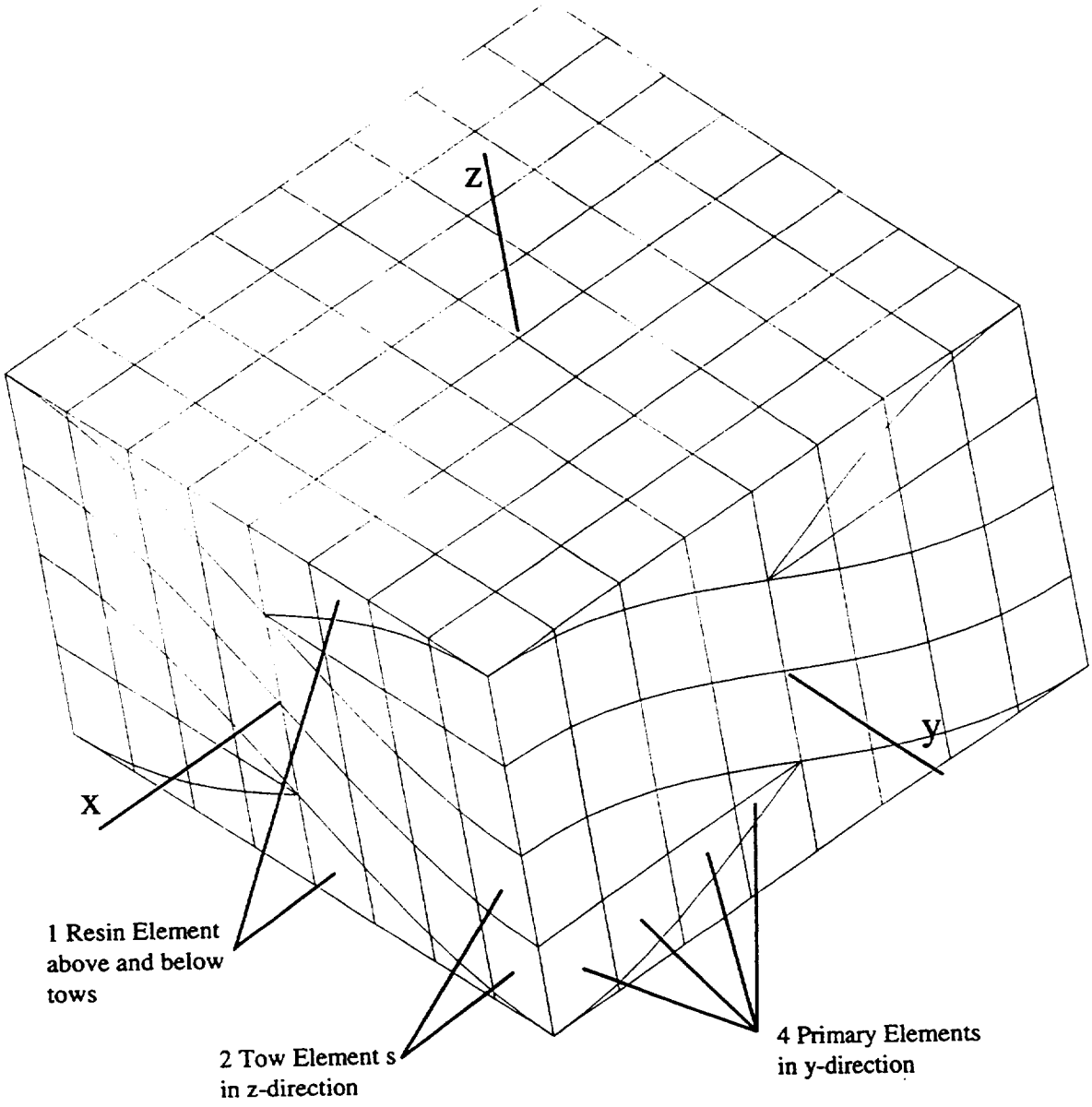

Figure 2: 1/8th unit cell created with PWMeshGen.

Appendix A: Use of output files with Flex94

The files generated using **PWMeshGen** are used in conjunction with the finite element program **Flex94** and the mesh plotting program Plot95. The file new.flex is the main input file for **Flex94**. An example of this file is shown in Figure A1. This example specifies that the mesh new.sflx will be subjected to extension in the x-direction as indicated by lines 6, 26, and 29. Modifications for other load cases are given below:

For in-plane shear, these lines would need to be changed as follows:

6 'xyShearConstraints'
26 'xyShear.mpc'
29 'xyShear.Loads'

For transverse shearing, these lines would need to be changed to:

6 'xzShearConstraints'
26 'xzShear.mpc'
29 'xzShear.Loads'

And finally, for extension in the z direction, the lines would be:

6 'ExtSingleConstraints'
26 'zExtension.mpc'
29 'zExtension.Loads'

Note that ExtSingleConstraints is also used for extension in the x-direction.

```
1     4 3
2     'Title Here'
3     'alternate_input'
4     'new.sflx'
5     'alternate_input'
6     'ExtSingleConstraints'
7     'end_mesh_input'
8     '3d'
9     1
10    206.9e9 5.171e9 5.171e9 .25 .25 .25 2.386e9 2.386e9 2.386e9 0 0 0 0 0 0 0
11    2
12    5.171e9 206.9e9 5.171d9 .00625 .25 .25 2.386e9 2.386e9 2.386e9 0 0 0 0 0
      0 0
13    3
14    3.45e9 3.45e9 3.45e9 .35 .35 .35 1.28e9 1.28e9 1.28e9 0 0 0 0 0 0 0
15    0  'end:T300/5208'
16    'end_material_input'
17    'loop'
18    1 1 1 1
19    2 2 2 1
20    3 3 4 1
21    0 0 0 0
22    'end_pick'
23    'alternate_input'
24    'new.am'
25    'alternate_input'
26    'xExtension.mpc'
27    'end_of_misc_options'
28    'alternate_input'
29    'xExtension.Loads'
30    'end_loads'
31    'end'
```

Figure A1: Typical new.flex file generated with PWMeshGen.

Chapter: 3

FLEX94

User's Manual

Command: fe size

Comments: size = maximum number of terms in global stiffness matrix. If size is omitted, a default size is assigned by the program. The default size is 1500000.

The analysis of an infinite array of unit cells only requires a single mesh. Such analysis is useful for determining homogenized engineering properties and stress (or strain concentrations). Such analysis proceeds much like traditional finite element analyses except that the boundary conditions are fairly complicated. Utilities have been developed to automatically generate the required boundary conditions for various load conditions.

Global/local techniques were developed as part of this research project. There are many possible global/local methods. The ones evaluated used macro elements (Refs. 1-3) in the global mesh and ordinary finite elements in the local mesh. Two types of macro elements are supported: single field (Refs 1, 2) and multi-field (Refs 3). After a global analysis is performed using macro elements, the detailed stress distributions within a weave unit cell are determined using displacements or forces from the global analysis to determine the boundary conditions for the local models, which include details of the weave architecture. The global/local analysis software was not sufficiently automated to release it as part of this software. However, the macro elements are included in the finite element program. Reference 4 discusses one of the more promising procedures evaluated.

The input file for Flex94 can be broken into several blocks which must appear in the following order:

1. Mesh Input
2. Material Properties
3. Macro Element Input (Optional)
4. Miscellaneous Options
5. Loads
6. Macro Element Data
7. Failure Analysis

A description of each block is given in the following sections with an example.

1. Mesh Input

Example:	Description:
'analysis_type' 'LINEAR' 'end_options'	This option allows the user to define the analysis type. 'LINEAR' selects linear analysis. This has to be replaced by 'SELECT' for Selective discount method or by 'NSELECT' for Non-Selective discount method.
43 2 'Small Mesh'	NumberOfElements DegreesOfFreedomPerNode Title - Must be in single quotes.
'alternate_input' *'sml.msh'*	This option allows user to put mesh in another file. Filename must be on the following line. At end of file 'sml.msh', 'standard_input' should be used to return to original file. 'alternate_input' can only be used in the original Flex94 input file (eg. you could not use the command in 'sml.msh')

Example:	Description:
'standard_input'	If 'alternate_input' was used, 'standard_input' would return input to the original input file. 'standard_input' can only occur where a command is appropriate. For example, it could not appear in the middle of reading coordinates.
'coordinates' 102 2 1 -1.5 -1.5 2 -1.5 -1.3 3 -1.3 -1.5 4 -1.1 -1.5 ... 101 1.5 1.3 102 1.5 1.5	Command to signal start of coordinates. NumberOfNodes NumberOfCoordinateDimensions NodeNumber Coordinates
'connectivity' 1 4 1 2 3 4 2 4 2 3 3 6 3 4 4 8 7 6 ... 42 4 97 95 99 100 43 4 100 99 99 101	Command to signal start of connectivity. Element# NumberOfNodesInElement Connectivity Connectivity must be specified in clockwise order for 2D elements. For 20-node 3D elements, the order of the nodes is shown in Figure 1.
'define_element_type' 243 1 43 1 0 0 0 0	Command to start element type definition. ElementType FirstElement LastElement Increment (In this case, elements 1 throught 43 are of type 243). End with four zeroes. The relevant element types are listed below: 243 2D element 300 3D element 851-899 single field 801-849 multi-field

'select_quadrature_order'	Command to start selection of quadrature order for each element.
2 1 43 1	QuadratureOrder FirstElement LastElement Increment
0 0 0 0	End with four zeros. To obtain stresses, a quadrature order of 2 for 2D and 3 for 3D has to be used.
'single_constraints'	Command to set single constraints on individual nodes.
40 1 0	NodeToConstrain ConstraintDof1 ConstraintDof2 ...
41 1 1	1 == Constrain Dof
18 0 1	0 == Don't Constrain Dof
102 1 1	Note: The number of constraints at each node must be equal to the
100 0 1	number of Dof per node which was set at the beginning of the
101 1 0	mesh block. Example shown is for 2 Dof per node.
0 0 0	End with zeros.
'plane'	Command to set constraints on a plane.
1 -1.5 1	idir coord jcon
1 -1.5 2	idir = direction of normal to plane in (x1,x2,x3) space
2 -1.5 2	coord = coordinate of plane
2 -1.5 1	jcon = restraint direction
0 0 0	end with zeros
'end_mesh_input'	exit this input section

2. Material properties

This section defines the material library and which elements have which material properties. Flex94 was designed to handle various types of constitutive definitions (eg. 2D, 3D, properties for a beam, etc.) However, for textile analysis only one option is relevant - '3D'. This option requires the 3D elastic properties to be given as shown below. For 2D analysis the 3D properties which are input are used to determine the 2D properties for plane strain analysis.

Example:	Description:
'3D'	Command to start reading of 3D material properties.
1	Material group number used later in assigning properties to elements.
206.9e9 5.171e9 5.171e9	Young's Moduli (E_{11} E_{22} E_{33})
.25 .25 .25	Poisson's Ratios (ν_{12} ν_{13} ν_{23})
2.386e9 2.386e9 2.386e9	Shear Moduli (G_{12} G_{13} G_{23})
0	Rotation about z-axis (z-axis is out of plane for 2D problems)
0 0 0	(thermal expansion coefficients...not used or implemented)
0 0 0	(moisture expansion coefficients...not used or implemented)
2	Next material group
5.171e9 206.9e9 5.171e9	
.00625 .25 .25	
2.386e9 2.386e9 2.386e9	
0 0 0 0 0 0 0	
3	
3.45e9 3.45e9 3.45e9	
.35 .35 .35	

1.28e9 1.28e9 1.28e9	
0 0 0 0 0 0	
0	Give zero as material group number to end input.
'end_material_input'	End input of material properties
'loop'	Command to start specifing material group.
3 1 43 1	MaterialGroupNumber FirstElement LastElement Increment
1 2 43 4	
1 3 43 4	
0 0 0 0	End with zeroes
'end_pick'	End selection of material properties for elements

Comments: For a mesh consisting of macro elements only, there is no need to input material properties. (It will do no harm, but the data will not be used.) Hence, the following lines are sufficient for the material property section.

```
'end_material_input'
'end_pick'
```

3. Macro Element Input

Most of the data for macro elements will be specified in another file, as described shortly. The following must be included in the main input file if macro elements are being used.

Example:	Description:
'read_macro_mesh'	Command to start reading of macro element mesh.
851	macro element type 851-899: single field 801-849: multi-field
103 95 2	NumberOfNodes NumberOfElements NumberOfDimensions
2	NumberOfDofPerNode
2500 500	length of connectivity array length of coordinate array Minimum requirements are: Connectivity: numberOfElements * (numberOfNodesPerElement + 9)+1 Coordinates: numberOfNodes * numberOfDimensions + 2
12	number of elements in macro element submesh
2	number of degrees of freedom per node in macro element submesh
'title'	
'alternate_input'	
'name'	name of alternate input file *(what is in this file will be described in section "6")*

Repeat above commands of section 3 for each type of macro element to be used.

```
'initmacro'
2                          NumberOfMacroElementTypes
1  2                       List of elements which need to be initialized
```

4. Miscellaneous Options

Element Material Rotation Angle: For the analysis of textile composites, the material properties of the elements making up the tow are the same in the material coordinate system. These properties must be transformed to the global coordinate system. Flex94 allows the user to specify the angular orientation of the elements. For 2D, the user can specify the angle of rotation for an entire element only. For 3D, however, Flex94 also allows the user to specify the angle of rotation for each node in an element. The angle of rotation may be specified using three different commands: 'angles2d', 'angles3d', and 'angles_multiple'. The angles are specified in terms of degrees.

Example:

```
'angles2d'
1  0.00
2  5.17892
3  10.28684
4  15.34983
...
42  -5.17892
43  0.000
```

Description:

```
Command allows the user to specify the angles for a 2d analysis. When
      using this option, angles specify the rotation about the z-axis.
      (Out of plane.) Angles must be specified for all elements in the
      mesh and are positive for a clock-wise rotation.
ElementNumber  RotationAboutZAxis
```

Example:

```
'angles3d'
1  1  0.00
2  2  5.857
3  3  6.449
...
42 1 0.00
43 2 2.48
```

Description:

```
Command allows the user to specify the angle and axis of rotation for 3D
      analysis. Again, the angles must be specified for all elements.
ElementNumber  AxisOfRotation  Angle
```

Example:

```
'angles_multiple'
1  2  20
6.724570
7.294361
...
4.009413
0.000000
2  1  20
```

Description:

```
Command allows the user to specify the angles of rotation for 3d.
ElementNumber  AxisOfRotation  NumberOfAnglesForElement
Angle(1)
Angle(2)
...
Angle(19)
Angle(20)
      Angle(n)  corresponds to the rotation at the nth node specified
```

```
5.877652                    in the connectivity of the element.
2.332992
...
42  1  20  0.000  0.000  0....
43  2  20  2.489  2.476  2.4...
```

It is often more convienient, when specifing the material rotation angles for elements, to use 'alternalte_input' to allow the angles to be kept in another file. When doing this, remember to put 'standard_input' at the end of the file to let Flex94 return to the original input file.

Multipoint Constraints: Another miscellaneous option which Flex94 allows, is the specification of multipoint constraints. When specifying multipoint constraints, the user must specify a master node, slave node, the particular degree of freedom (dof) to constrain, and a difference between the two dof's. The particular dof being constrained (ie. the slave node) cannot have been previously constrained.

It is also possible to apply a mpc such that the displacement of the slave node dof is the opposite that of the master node dof. This is done by putting a minus sign in front of the master node as shown in the following example.

Example:	Description:
'mpc'	Command to start reading of multipoint constraints.
2 1 1 0.000	SlaveNode MasterNode DofToConstrain Difference
3 1 1 0.000	
4 -1 2 0.150	This line constrains Node 4 dof 2 to the negative displacement of Node 1 dof 2 plus a difference of 0.150
100 -1 1 0.000	
101 100 1 0.000	
102 -1 2 0.150	
0 0 0 0	Use four zeros to signal end of multipoint constraints.

Ending Miscellaneous Options: This command must appear at the end of the Miscellaneaous Options section. It is shown below.

Example:	Description:
'end_of_misc_options'	Command to end Miscellaneous Options. (NOT OPTIONAL!)

As stated earlier, it may be more convienient to keep sections of miscellaneous options in another file. This can be done using 'alternate_input' with 'standard_input' as explained in section 1.

5. Loads

Various types of loads can be applied with Flex94. Some of these include the specification of nodal displacements and point forces. All the command options in this section are optional.

'alternate_input' may be used at any time where a command can be accepted. Remember to return to the original input file with 'standard_input'.

Point Forces: Point forces allow the user to specify the nodal force at a node.

Example:	Description:
'point'	Command to start reading of point forces.
1 1e7 1	NodeNumber Force DofNumberForNode
3 2.345e6 2	
...	
87 6.456e8 1	
0 0 0	End reading of point forces with three zeros.

Displacements: Displacements may also be specified at specific degrees of freedom. In the input of the mesh in section 1, constraints can be input. This reduces the actual size of the problem. Specified non-zero displacements are also a type of constraint, but in order to reduce the problem size, the dof must be constrained in the mesh section also.

Example:	Description:
'displacement'	Command to start reading of displacements.
1 3.13e-3 2	NodeNumber Displacement DofNumberForNode
1 .025 1	
2 0.56e-2 2	
87 0.13e-2 1	
102 0.13e-2 1	
0 0 0	End reading of displacements with three zeros.

Plane Displacements: Displacements may be applied to an entire plane in a particular direction. This is known as a plane displacement. This option works in conjunction with setting plane constraints in the mesh input section.

Example:	Description:
'planeDisplacement'	Command to start reading of base displacements.
1 -1.5 .015 2	CoordinateNumber CoordinateValue Displacement Direction
1 -1.5 .010 1	<—This line indicates that on the plane x=-1.5 specify a displacement of
2 -2.0 -.013 2	0.010 in the x-direction.
0 0 0 0	End reading of base displacements with four zeros.

Linearly Varying Displacements on a Plane: Displacements may be applied to an entire plane so that the variation of the specified displacements changes linearly with the value of the coordinates which are parallel to the plane. For example, one may want to specify an x displacement on a plane x=1.5 which varies linearly with y. Displacements are calculated as $d_i = a\ y_i + b$ where a and b are specified by the user and d_i and y_i are the calculated displacement and y coordinate at a specific node on the x=1.5 plane.

Example:	Description:

'linearPlaneDisplacement'	Command to start reading of linearly varying plane displacements.
1 1.5 1 2 .1 -.05	This line specifies that on the plane x_1=1.5, a displacement in the x_1 direction given by $d_i = .1\ x_{2i} - .05$ is being specified at each node i on the plane.
2 -1.5 1 1 .01 -.01	
...	
0 0 0 0 0 0	End reading of linearly varying plane displacements with six zeros.

To end reading of loads, **'end_loads'** must be at the end of the loads section.

6. Seperate Input File For Macro Element Data

Much of this file is identical to the sections described above. Hence, references will be made to the sections above rather than repeating all of the details.

Mesh input block.....refer to Section 1:

Comments:

1. Do not input any restraint information.
2. The nodal coordinates must be normaized coordinates (eg. they must range between -1 and 1.)

Material properties block.....refer to Section 2:

numberOfNodesInMacroElement: The number of nodes in the macro element must be specified. It is not the number of nodes in the submesh.

Miscellaneous options block.....refer to Section 4:

Comments:

1. The material rotation angles for the elements in the submesh is input in this section.
2. Do not apply multipoint constraints to a macro element mesh.

7. Failure Analysis

This section describes the data required for progressive failure analysis.

As described in 'Mesh Input.....section 1,' the analysis type 'LINEAR' has to be replaced with either 'SELECT' or 'NSELECT' option. The option 'SELECT' represents the 'selective discount method' and 'NSELECT' represents the 'Non-Selective discount method.' One additional input file is required. It is named **'strengthdata'.** It contains a list of strength values for each of the material groups used.

Example:	Description:
3	NumberOfMaterialGroups
500 50 50 60 60 60	(tensile strength) $\sigma_{11},\sigma_{22},\sigma_{33}$,(shear strength) $\sigma_{12},\sigma_{13},\sigma_{23}$,
-500 -50 -50	(compressive strength)$\sigma_{11},\sigma_{22},\sigma_{33}$

When progressive failure analysis is performed, the following additional files are created.
'stressstrain' : Data file used to plot 'nominal stress vs nominal strain' curve.

Example:	Description:
1 0.0e6 0.00	ReferenceNumber, NominalStressValue,
2 1.3e6 0.10	NominalStrainValue (percent)
.	
.	

'damagefield': Damage progression sequence is recorded. This file may be used to study the failure mechanism and used for graphical simulation of failure progression.

Example:	Description:
1 1	ElementNumber, MaterialGroupNumber
0 0 1 0 4 3	Each row represents an integration point of the element. Each column
0 0 0 0 0 0	represents a stress component. $\sigma_{11},\sigma_{22},\sigma_{33},\sigma_{12},\sigma_{13},\sigma_{23}$ is the order
6 5 0 0 0 0	the stress components for each row. The numbers 1,4, and 3
.	correspond to the first , fourth and third points on the stress-strain curve.
2 1	
8 7 0 0 0 0	
...	

'fcontour.n' n = 1,2,..., number of points on the stress-strain curve : This file contains the contour data required to plot failure contours for each point on the stress-strain curve. The file format is the same as the stress contours file 'stress'.

References

1. Whitcomb, J.D.; Woo, K.; Gundapaneni, S.: Macro Finite Element for Analysis of Textile Composites. Journal of Composite Materials. Vol. 28, pp. 587-681, 1994.

2. Woo, K. and Whitcomb, J.D.: Macro Finite Element Using Subdomain Integration. Communications in Applied Numerical Methods. Vol. 9, pp. 937-949, 1992.

3. Whitcomb, J., Woo, K.: Enhanced Direct Stiffness Method for Finite Element of Textile Composites. Accepted for publication in Composite Structures.

4. Whitcomb, J. and Srirengan, K.: Evaluation of Homogenization for Global/Local Stress Analysis of Textile Composites. Presented at theAIAA/ASME/ASCE/AHS/ASC 35th Structures,

Structural Dynamics, and Materialsconference, Hilton Head, South Carolina, April 18-20, 1994. Submitted to Journal of Composite Materials.

Chapter: 4

Plot95

User's Manual

Executable: plot95

The program Mesh.app was used in debugging finite element meshes and postprocessing the results from finite element analyses. The program was developed for the IBM RS/6000 workstation using the Motif interface and the openGL graphics library. The program should compile and function properly on other workstations which use Motif and which have the openGL graphics library. However, this is would need to be verified for any particular workststation.

The primary functions of the plotting program are:

1. Plot a finite element mesh.
2. Plot a deformed finite element mesh (ie. with scaled nodal displacements added to original nodal coordinates.)
3. Plot stress contour lines.
4. Plot stress contour bands.

This program was designed to work with the finite element program "Flex94". In brief, the current version of the plotting program supports the following:

Mesh plotting for the following elements

truss
frame
triangular and quadrilateral 2D elements with any number of nodes
20-node hexahedral elements

Contour plotting for the following elements

4 and 8 node quadrilateral elements
20-node hexagonal elements

The following pages describe the use of Plot95. There are two aspects to using the program: preparation of the input files and interaction with the graphical user interface to obtain the type of plot desired. This manual will begin with a discussion of the input files followed by a description of the graphical user interface (GUI).

Input Files

This section describes the following types of input files:

1. Mesh file
2. Nodal displacement file
3. Contour data file

In each case a fragment of a typical input file will be listed and explained. The actuai input data is in small type and the comments are in italics.

Mesh file:

```
1941      384       3                    numberOfNodes  numberOfElements  numberOfDimensions
1   -.75000   -.65625   -.5000           node#  coordinates (for 2D only xy coordinates are needed.)
2   -.65625   -.75000   -.5000
3   -.75000   -.75000   -.5000
4   -.75000   -.65625   -.4951
5   -.75000   -.75000   -.3750
6   -.65625   -.75000   -.4951
...
                                         element#  numberOfNodesPerElement  connectivity
1 20 3 4 11 13 35 32 31 5 6 14 38 34 23 24 27 29 43 40 39 25
2 20 31 32 35 37 112 110 108 33 34 38 111 107 39 40 43 45 120 118 116 41
3 20 11 12 5 53 63 36 35 13 14 54 66 38 27 28 59 61 66 44 43 29
4 20 35 36 63 65 124 114 112 37 38 66 123 111 43 44 67 69 128 122 12 45
5 20 51 52 147 149 159 64 63 53 54 150 ...
...
```

Optional input for mesh file:

```
world                                    input range of screen coordinate system
0.00 0.00                                lowerLeftX lowerLeftY
1.500 1.500                              upperRightX upperRightY
                                         (if left out, program will automatically pick coordinates)

inactive                                 deactivate elements ( elements will not be plotted)
1 64 1                                       first last increment
129 384 1                                    next group to deactivate
0 0 0                                        end option with three zeros

active                                   activate elements
24 32 1
0 0 0

set.colors                               Set Element Colors
5   1   32   1                           colorIndex first last increment
...                                          (0<= colorIndex<12)
...                                          colorIndex corresponds to material group number
0 0 0 0                                      end with four zeros

elementNodalValues                       input contour data (see format in Contour Data File Section)

set.values                               Sets values for each element. Use Shade Elements to view.
3 2                                      numberOfColumnsOfData  selectedColumn
1 2.334  4.566  1.13e9                  total # of columns = numberOfColumnsOfData+1
2 2.567  4.877  1.15e9                        If selectedColumn<0, absolute value of data is input.
...                                          Range is selected automatically.
```

```
fix.values                          Fix Values for each element.  Use Shade Elements to view.
3 2                                 numberOfColumnsOfData   selectedColumn
0 10.5                                  minValue   maxValue
1 2.334  4.566  1.13e9                    If selectedColumn<0, absolute value of data is input
2 2.567  4.877  1.15e9
...
```

Nodal displacement file:

```
  1 -.79272E-24  .13041E-02 -.42810E-22    nodeNum  (u,v,[w]) displacement
  2  .87106E-02 -.97213E-24 -.43845E-22    (w displacement is optional in 2D)
  3 -.12200E-22 -.24332E-23  .10482E-22
  4  .37197E-22  .11482E-02 -.30051E-02
  5  .42536E-22  .13039E-22 -.23021E-01
  6  .83812E-02  .11663E-22 -.36294E-02
  7  .19218E-24  .54321E-02  .13092E-22
  8  .15420E-23  .10875E-01 -.12807E-22
  9 -.14467E-23  .45672E-02 -.52301E-02
 10  .11192E-01  .63668E-02 -.49632E-22
...
```

Contour data file:

This section may be included in the mesh file or as a stand alone file. To include this in the mesh file, the option **elementNodalValues** must be used.

```
(elementNodalValues)                Only include if in the mesh file.
3                                   Number of columns
1                                   Column to be input
fixed                               (These 2 lines explained in Scaling options.)
-4e7  4e7
      1       1                     elementNumber    materialGroupNumber
  .1807296E+08  -.3453916E+06  -.5935107E+08   There is one line of data for each node in each element.
  .1881153E+08   .2379351E+07  -.5971771E+08
...
```

Scaling Options:

A scaling option must be given when the data is read in so that the plotting program will know how to draw contours. The above data uses the **fixed** option which allows the user to specify the minimum value (-4e7 in the above data) and maximum values (4e7) when the data is read in. It is also possible to specify that the program automatically pick the minimum and maximum values when reading in the data. There are several options for doing this. These are **auto, group**, and **active**.

- **auto** tells the program to automatically pick the min. and max. from all of the input data. There is no extra data necessary for this command.

- **group** allows the user to specify that min. and max. value be picked from a specific material group. On the next line, the material group number to scale must be specified.

- **active** allows the program to pick the min. and max. value from all the active elements. No extra data is required for this option.

It is also possible to scale the data after it is read in by changing the Data Range fields in the

bottom right hand corner of the primary panel. However, the data being read in must still have one of the scaling options specified in the file.

Interface

The plotting interface consists of several Motif "widgets" or panels. These are shown in Figures 1 and 2. The widgets shown in Figure 1, the main and redraw widgets, appear when the program is started. These widgets contain a collection of buttons, toggle switches, and text fields. The operation of each is documented below. Figure 2 shows the menu panels. The one labeled "Mesh" is the main panel. The "Mesh" panel is activated by using the mouse to select the main widget (Figure 1) and then clicking the right mouse button. On the IBM one can also press the F10 special function key to bring up the Mesh panel. The others are activated through the "Mesh" panel as indicated by the lines joining the panels. The menus are self-explanatory except for the one labeled "Modify List of Elements to be Plotted". This panel permits one to remove a collection of elements or to add them back. There are three methods provided for identifying the particular elements. These are described below:

1. Modify by Volume: Select elements whose centroids lie within the specified xyz coordinate ranges.
2. Modify by Group Number: Select elements in the specifed group.
3. Modify by Loop List: Select elements "First" to "Last" with an "Increment" or stride. For example, if First, Last, and Increment are 1,10,2, respectively, then the selected elements will be 1,3,5,7,9.

Description of Buttons, Toggles, and Text Fields on Primary Panel:

Redraw	Redraw mesh using current settings.
Zoom In	Zoom in on center portion of plot (magnification = 4x).
Zoom Out	Zoom out (reduction = 4x).
Node Numbers	Label nodes.
Element Numbers	Label elements.
Shade Elements	*Color* element according to the specified color group.
Label Intensity	Label element according to the specified material group.
FontScale	Magnification factor for default font size.
World Coordinates	Range of world coordinates in plotting window.

Rotation	Rotation about z,x, and y axes - in that order followed by incremental rotaion about the z axis. When all angles =0, the z-axis points to the top of the window and the y-axis points to the right side. A right-handed coordinate system is used.
Magnification	Magnification factor to apply to the nodal displacements.
Use Displacements	Click on to plot deformed mesh. Displacements are read in using the menu option Displacements under Document.
AutoWorld	Allows program to automatically specify world coordinates for window based on size of mesh.
To PostScript File	Click on to create PostScript file rather than draw to screen. This function creates a much smaller file than saving with the default print command. Greyscale is always output. By changing one parameter in file, it can be converted to color. (Directions are included in the PostScript file.) Currently, the output file name is "hardwired" to be /tmp/out.ps
Monochrome/Color	Toggles display between color and greyscale.
Contouring	(All options take effect on next ***Redraw***.)
Draw Contours	Click on to draw contours.
Label Contours	Click on to label contour lines if just ***Lines*** selected or draw legend if ***Bands*** are selected.
Lines	Click on to draw contour lines.
Bands	Click on to draw contour bands.
Outline Elements	Click on to draw element bondaries when contouring. Element boundaries are always drawn when contouring is turned off.
Data Range	
Min	Lower limit for contour data.
Max	Upper limit for contour data.

Comments:

Below the Zoom Out button is an unlabeled text field. It is provided to make it convenient to specify a particular zoom level. For example, if the initial (ie. when the mesh file is read) horizontal and vertical ranges are 100 and 200 respectively, specifying a zoom factor of .5 will reduce the ranges to 50 and 100. This will result in a magnified display.

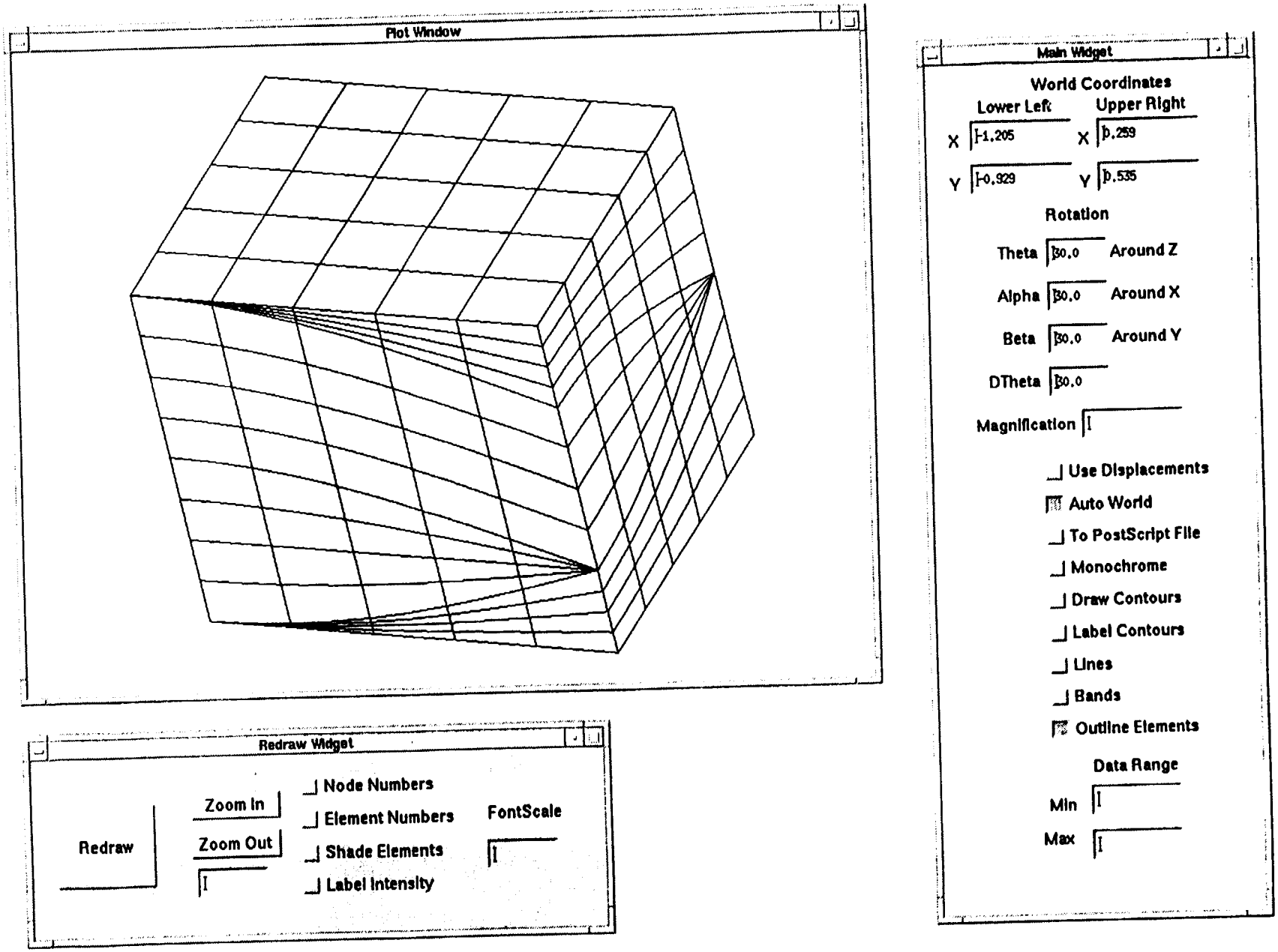

Figure 1 Primary widgets for Plot95.

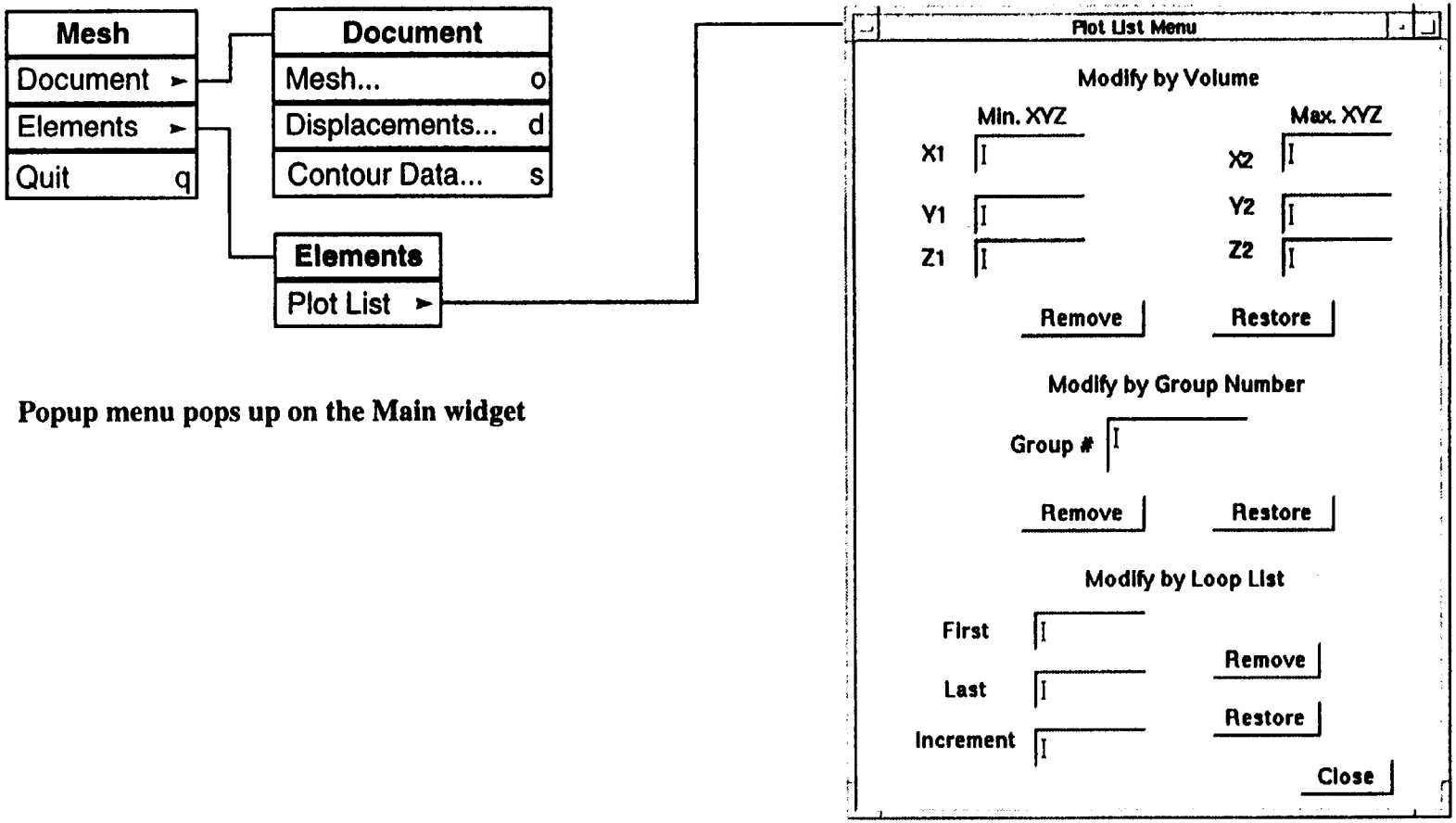

Figure 2 Menu widgets for Plot95

Chapter: 5

Installation of Source Code and Samples

The distribution media contains the following four compressed tar files:

pwmeshge.z
flex94.z
plot95.z
samples.z

After copying these files to a UNIX computer, these files must be renamed as

pwmeshge.Z
flex94.Z
plot95.Z
samples.Z

The files can then be uncompressed using the command

uncompress *

Next the files in each tar file are extracted using the commands

tar -xvf pwmeshge
tar -xvf flex94
tar -xvf plot95
tar -xvf samples

The following four sub-directories are created in the current directory:

PWMeshGen
Flex94
plot95
Samples

Creation of Executables

Change to the directory containing the four sub-directories listed above, then execute the following commands. The words in italics are comments. not commands.

Flex94

cd Flex94/Control
make
The executable is named "fe" and is located in the current directory. It may be moved to any location desired.
cd ..

PWMeshGen

cd PWMeshGen

Change the pathname for PWMESHGEN_DIR in the file makefile.def to the pathname for present working directory.
For example : PWMESHGEN_DIR = /home4jdw/Scratch/sriren4/PWMeshGen
Type the command: pwd to obtain the pathname for the present working directory.

Similarly, change the pathname for PWMESHGEN in the file PWForm to the pathname for present working directory.
For example : PWMESHGEN = /home4jdw/Scratch/sriren4/*PWMeshGen*

make

The executable is named "PWMeshGen" and is located in the current directory. The executable should not be moved.
cd ..

Plot95

cd Plot95
Change the pathname for PLOTTER_DIR in the file makefile.def to the pathname for present working directory.
For example : PLOTTER_DIR = /home4jdw/Scratch/sriren4/Plot95
Type the command: pwd to obtain the pathname for the present working directory.

make all
The executable is named "plot95" and is located in the Plot95 directory.

Sample Input

Input and output files for six problems are included. These are in the subdirectories Sample1 - Sample6. Comments are included in the subdirectories which describe each sample.

REPORT DOCUMENTATION PAGE

Form Approved
OMB No. 0704-0188

1. AGENCY USE ONLY (Leave blank)	2. REPORT DATE	3. REPORT TYPE AND DATES COVERED
	July 1996	Final Contractor Report

4. TITLE AND SUBTITLE

Analysis of New Composite Architectures

5. FUNDING NUMBERS

WU-505-63-5B
G-NAG3-1270

6. AUTHOR(S)

John D. Whitcomb

7. PERFORMING ORGANIZATION NAME(S) AND ADDRESS(ES)

Texas A&M University
College Station, Texas 77843

8. PERFORMING ORGANIZATION REPORT NUMBER

E-10353

9. SPONSORING/MONITORING AGENCY NAME(S) AND ADDRESS(ES)

National Aeronautics and Space Administration
Lewis Research Center
Cleveland, Ohio 44135-3191

10. SPONSORING/MONITORING AGENCY REPORT NUMBER

NASA CR-198506

11. SUPPLEMENTARY NOTES

Project Manager, Christos C. Chamis, Structures Division, NASA Lewis Research Center, organization code 5200, (216) 433-3252.

12a. DISTRIBUTION/AVAILABILITY STATEMENT

Unclassified - Unlimited
Subject Category 24

This publication is available from the NASA Center for AeroSpace Information, (301) 621-0390.

12b. DISTRIBUTION CODE

13. ABSTRACT *(Maximum 200 words)*

Efficient and accurate specialty finite elements methods to analyze textile composites were developed and are described. Textile composites present unique challenges to the analyst because of the large, complex "microstructure". The geometry of the microstructure is difficult to model and it introduces unusual free surface effects. The size of the microstructure complicates the use of traditional homogenization methods. The methods developed constitute considerable progress in addressing the modeling difficulties. The details of the methods and attended results obtained therefrom, are described in the various chapters included in Part I of the report. Specific conclusions and computer codes generated are included in Part II of the report.

14. SUBJECT TERMS

Woven fabrics; Textiles; Carbon fibers; Microstructure; Surface effects; Finite element; Modeling schemes; Approximation techniques; Global; Local methods; Moduli; Displacements; Stresses; Microstresses; Progressive fracture

15. NUMBER OF PAGES

190

16. PRICE CODE

A09

17. SECURITY CLASSIFICATION OF REPORT	18. SECURITY CLASSIFICATION OF THIS PAGE	19. SECURITY CLASSIFICATION OF ABSTRACT	20. LIMITATION OF ABSTRACT
Unclassified	Unclassified	Unclassified	